A Diffuse Reflectance Infra-Red Study of the Alkali Promotion of Copper-Based Catalysts

Kathryn E. Howieson

Degree of Doctor of Philosophy

The University of Edinburgh

1998

Abstract

This study concerns the alkali promotion of $Cu/ZnO/Al_2O_3$ catalysts which are used for the low temperature water-gas shift reaction. Preliminary high pressure microreactor studies revealed that, on addition of the promoter, an enhanced selectivity to the desired products was achieved rather than for by-product methanol formation. Diffuse Reflectance Infra-red Fourier Transform Spectroscopy (DRIFTS) has been employed during adsorption and subsequent temperature programmed desorption (TPD) and temperature programmed reaction (TPR) experiments in order to determine the mode of action of the promoter.

The catalysts were prepared *via* a layered hydrotalcite-type precursor by co-precipitating the mixed metal nitrates with ammonium bicarbonate, thus generating the catalyst alkali free. Promotion was achieved by impregnation with alkali metal salts.

Detailed carbon monoxide adsorption experiments have been used to explore the various parameters in the pre-treatment procedure and their effect on the resultant carbon monoxide stretching band. These studies have also allowed the presence of stepped copper planes to be identified following reduction of the sample, along with partially oxidised copper and a small amount of copper oxide.

Catalysts promoted with potassium to different levels (0.02 to 1 weight %) were studied using carbon monoxide as a probe molecule, where the main observation was a sharp attenuation in the CO stretching frequency intensity, and a site blocking mechanism of the promoter was invoked in explanation. No shift in the CO stretching frequency was observed. Another, more subtle, effect was identified for the support; bicarbonate formation on alumina was hindered while another surface species with a higher desorption temperature dominated. This was suggested as being a

potassium-associated carbonate. Similarly, the effect on the support was seen in analogous carbon dioxide adsorption studies. In addition, the formation of CO following the exposure of the catalysts to CO_2 was found to increase on promotion, and, again, a potassium-associated species, such as a carboxylate, was invoked to explain this.

Adsorption studies using methanol and formic acid indicated that promotion of the catalyst hindered the formation of methoxy and bidentate formate respectively on copper. During TPD, the amount of methoxy desorbed as methanol was increased on promotion, while more was decomposed on the unpromoted sample. The desorption intact of formic acid at slightly lower temperatures in the presence of the promoter suggests that, as for the case of methoxy, the adsorbates were destabilised on promotion. CO_2/H_2 TPR experiments showed that the formation of bidentate formate on copper, which occurred on the unpromoted catalyst, was prevented on promotion. The level of carbon monoxide and water, produced *via* the reverse water-gas shift reaction, was found to continue at a rate comparable to that on the unpromoted sample. This was suggested as being partly due to the enhancement in the conversion of CO_2 to CO found for the CO_2 adsorption studies on promotion.

Declaration

I hereby declare, that the work presented in this thesis is my own, unless otherwise stated.

Kathryn Elizabeth Howieson

May 1998

Acknowledgements

I would like to thank my supervisor, Dr. Gordon McDougall, for his help, and especially for his optimism and approachability. I am grateful to my industrial supervisors, Dr.s Mike Watson and Raymond Hadden at ICI Katalco for their valuable input and interest. I would also like to acknowledge the help of Denise Harrison and Peter Lambert at ICI Katalco for their assistance in the preparation and characterisation of my catalyst.

Special thanks are due to Dr. Ron Brown, who saved the day many times, and to Dr. Ian Harkness, who was always willing to give his time to solve a problem.

Thanks to the Catalysis Group - Ron, Ian, Mark, Lijuan and Richard - for being good company in the lab.

I am also very grateful to Gareth Oakley for doing the XRD experiments and to the mechanical and electrical workshops, the glassblower, Harry Mackenzie and Mike Reilly.

Thanks are due to the EPSRC and ICI Katalco for financial support.

My time at Edinburgh wouldn't have been the same if it were not for the postgrads in the Condensed Matter groups - thanks for the Friday evenings spent in the K.B. bar!

Last, but not least, I would like to thank my family who have always supported and encouraged me in everything I have done, and Ally, who has been with me every step of the way and always knew I could do it when I didn't know myself.

Courses and Conferences Attended

1) ICI Symposium on Catalytic Chemistry - June '95, '96, '97.

2) Summer School in Surface Science - Marseille, June '95
- Copenhagen, June '97

3) Surcat Ecosse Meetings - '95, '96, '97

4) Catalytic Club - Firbush Point Field Centre, May '95, '96.

5) Physical Section Meetings - Firbush Point Field Centre, June '96, '97

6) Rideal Conference - Dundee, March '96

7) Catalysis : Fundamentals and Practice - University of Liverpool, September '96

Contents

List of Figures

List of Tables

Chapter 1 - Introduction

1.1 The Use of Supported Copper Catalysts

Copper/zinc oxide/alumina catalysts play an important role in the modern chemical industry, both for their use in the low temperature water-gas shift reaction and in the methanol synthesis reaction. Their study constitutes an enormous field, with interest from both the industrial and academic communities.

The water-gas shift (WGS) reaction is a very important step in numerous industrial processes, most notably as a route to hydrogen for use in the Haber ammonia synthesis process [1]. The reaction could also be envisaged to play a part in the utilisation of fossil fuel resources in future large-scale industrial processes. For instance, coal gasification may rely on water-gas shift catalysts to upgrade the hydrogen content for down-stream reactions such as methanation or methanol synthesis [2].

Historically, the first report of the WGS reaction was published in 1888 [3], when it was found that on passing carbon monoxide and water vapour over red-hot refractory material, carbon dioxide and hydrogen were produced (reaction 1.1).

$$CO + H_2O \leftrightarrow CO_2 + H_2 \qquad \Delta H = -41.1 \text{ kJ/mol} \qquad \textit{reaction 1.1}$$

It was subsequently discovered in 1912 that, using a catalyst consisting of iron and chromium oxides at 400 - 500 °C, the carbon monoxide in the outlet stream could be reduced to around 2 % of its original value [4]. From 1915 the catalytic WGS reaction was incorporated into the first coal-based ammonia synthesis process [1].

Today, an iron oxide/chromia catalyst is still used in modern ammonia and hydrogen plants but it now forms part of a two-stage WGS process [1]. A high

temperature stage is first carried out over the iron oxide/chromia catalyst at 350 - 450 °C and 1-3 bar partial pressure of carbon monoxide. Although this catalyst is only moderately active, its high selectivity allows the undesirable side reaction of methanation (the formation of methane from CO or CO_2 and H_2) to be avoided. The CO level in the outlet stream is decreased to 2 % of its original value.

The *high temperature* WGS catalyst is limited in its final conversion of carbon monoxide owing to themodynamic considerations - because the WGS reaction is moderately exothermic, its equilibrium constant decreases with temperature. For this reason, a second stage was introduced in the 1960's using copper-based catalysts. These were highly active and could thus be run at 200 - 250 °C and lower CO pressures - the *low temperature* WGS catalyst. Since the thermodynamic equilibrium limitation had been reduced, a higher conversion of carbon monoxide to dioxide was possible (final CO levels of around 0.2 % are attained) [1].

The low temperature (LT) WGS reaction is inextricably linked to the methanol synthesis process, owing to similarities in catalyst composition and the gas mixtures which are reacted over them. The industrial methanol synthesis reaction involves the conversion of $CO/CO_2/H_2$ mixtures to methanol at 220 - 300 °C and at higher pressures than the WGS reaction: about 50 - 100 bar [5]. The catalysts for the two processes vary in the level of copper they contain - an ICI low temperature WGS catalyst has been quoted as containing 33 % Cu, while a methanol synthesis catalyst typically contains 60 % [1].

To understand better the source of activity in the two catalysts, a great deal of interest has focused on trying to identify the active sites and the relationship between the different catalyst components. However, significant disagreement exists for both systems. It has been suggested that a synergy exists between the copper and zinc oxide components of the low temperature WGS catalyst. For instance, Herman *et al.* [6], identified a solid solution of Cu^I in ZnO, and suggested that these species were catalytically active. Conversely, several workers believe that zinc oxide only acts as a

support for the dispersed copper, which is responsible for catalytic activity [2, 7]. The LT-WGS reaction has also been found to be structurally sensitive over polycrystalline and silica supported copper [7, 8].

The situation for the methanol synthesis catalyst is more controversial. Many different hypotheses have been forwarded to explain the origin of activity in the catalysts. It has emerged that the activity is proportional to the copper surface area [9, 10], although some workers still support the suggestion by Klier [11] that Cu^{I} is important [12], in spite of opposition [13]. The role of zinc oxide is less clear, with a possible synergy between copper and zinc oxide being reported by Burch *et al.* [9, 14] where the support is able to store atomic hydrogen. This suggestion also met with opposition [15]. Another suggestion relating to the support by Sizgek *et al.* [16] is that the copper/zinc oxide interface is important in the catalytic activity.

These few examples from the literature are by no means intended as a full discussion of what is known about WGS and methanol synthesis catalysts, especially in the latter case, but they certainly convey the complexity of the systems. Equally, an immense amount of work has been published on the topic of the WGS and methanol synthesis mechanisms, and these will be briefly discussed in Chapters 6 and 7.

1.2 Alkali Promotion

Alkali promotion is a much-studied field from an academic viewpoint, with the aim of elucidating the fundamental interaction between the alkali metal and a transition metal substrate, and also with co-adsorbates such as CO [17]. An additional impetus is found in their application to heterogeneous catalysis; promotion can have a favourable effect on catalytic activity or selectivity [18]. In spite of the huge body of work in both areas, alkali promotion is still not well-understood.

Alkali metals have very low ionisation potentials. When adsorbed on a transition metal surface, their valence s-orbital hybridises with the upper states of the valence band of the substrate metal. As a result, the electrostatic potential around the adsorbed alkali species will be lowered (local work function decrease), while the alkali itself will become partly ionic [17, 19]. The dominating effect of this behaviour is viewed to be a local increase in electron density around the adsorbed alkali induced by the large dipole moment connected with the presence of a positive point charge (the alkali) in front of a continuum of electrons (the substrate) [20, and references therein]. Theoretical calculations have shown the alkali to be $K^{\delta+}$ (in the case of potassium), where δ is "nearly 1" [21].

The question of the "range" of the promotional effect is returned to often. While early studies [22] suggested the evidence of a long-range, "through metal" type of interaction, this has been refuted more recently, with the suggestion that short-range, purely electrostatic interactions dominate. For instance, Lang *et al.* [19] have calculated the electrostatic potential around a potassium atom on a simulated metal surface and concluded that the positive potassium is screened by electron density just below the surface of the substrate; that is, the promoter effect is highly local and limited to the adjacent adsorption site only. This idea has been confirmed by Janssens *et al.* [23] who found that a theoretical model of the electrostatic potential caused by an ordered network of dipoles agreed with experimental measurements of the electrostatic surface potential of a potassium promoted rhodium (111) surface. Thus, they postulated that both the short and long range promoter effect of potassium were of purely electrostatic origin and that effects through the substrate associated with charge donated by potassium to the substrate metal did not need to be invoked at all.

Overall, numerous effects have been observed experimentally following alkali promotion [17]. Many studies involve CO co-adsorption, and will be discussed at length in Chapter 5. However, some commonly reported interpretations are given below, as summarised by Uner *et al.* [24]:

- active metal site blocking for chemisorption [25]
- electron donation to or from the metal [22]
- direct chemical interactions between adsorbate and the promoter [26]
- through space interactions (e.g. electrostatic) [23]
- alkali induced surface reconstruction [27]

With regard to the variety of observations in the literature, Bonzel [17] has commented that no unified description of the alkali metal-molecule complex can be given, and this is unsurprising bearing in mind the different strengths of interaction between substrate and molecule possible, even before an alkali is introduced to the picture.

Alkali salt promoters are used in several industrial processes [18], where it is found that they can often assist the dissociation of certain molecules. For instance, in the ammonia synthesis process, alkali promotion of the iron catalyst results in a three-fold increase in catalytic activity, in spite of a decrease in surface area of the catalyst by two, and this is due to the enhanced dissociation of N_2 [28]. Similarly, the selectivity of the Fischer-Tropsch reaction [29] is enhanced by the increased dissociation of CO in the presence of an alkali. As a final example, although not used industrially, surface science studies have shown that promotion with an alkali metal can enhance the activity of the water-gas shift reaction over copper, and this has been partly attributed to an increased rate of dissociation of water [30].

The value of using surface science studies on alkali promotion to extract information about industrial processes has, however, been questioned [24] as a result of the discrepancy between the state of the alkali in the two different studies. Usually (but not always), the alkali will start off as a zerovalent atom evaporated onto the substrate in surface science studies and, as discussed above, often a strong electronic interaction between the metal and the alkali is invoked as being responsible for the promoter effect [17]. In the case of industrial catalysts, the alkali will be in the form of a compound or complex: consequently a drastic reduction to nearly zero of the

electron density available for donation from the alkali to the metal occurs. The polarizing effect of the positive charge which is screened by the counter-ion will also be significantly reduced [20]. Uner *et al.* [24] also suggested that even adsorbate-induced restructuring will not occur in the presence of the alkali compound, because this has been suggested to occur with zero valent alkalis owing to their ability to increase the density of states at the Fermi level [31]. Finally, surface science studies do not allow for the participation of the support, e.g. Uner *et al.* [24] found in a study of silica supported ruthenium that the alkali promoter was partitioned between the metal and support.

Much debate also surrounds the nature of the counter-ion under reaction conditions, and this topic is addressed in the introduction to Chapter 3.

1.3 Applying Infra-Red Spectroscopy to Catalysis

The performance of a heterogeneous catalyst is dictated by events at the gas-solid interface, and infra-red spectroscopy has proven to be a sensitive and particularly informative tool in this application. In fact, it has even been pronounced "by far the most useful single technique for the analysis of surface layers on solids" [32]. It is able to characterise the composition and structure of surface compounds, give information on the nature of bonds formed between adsorbed molecules and the surface, and using probe molecules such as CO and NO can investigate the existence of different types of active surface centre or monitor catalyst morphology [32]. Of particular importance is the scope for infra-red spectroscopy to be used as an *in-situ* probe in catalytic studies; that is, it can be utilised under reaction conditions [33]. The versatility of the technique is also attractive - it can be applied with relative ease to a uniquely wide variety of substrates from precisely defined metal single crystals to complex industrial catalysts, under a wide range of temperatures and pressures.

Eischens and co-workers [34-36] first demonstrated the usefulness of infra-red spectroscopy as a surface sensitive method in the 1950's with adsorption studies on supported metal catalysts. Transmission infra-red spectroscopy of pressed discs of the samples were carried out, and this method is still used widely today in spite of disadvantages:

1) the accessible spectral range is limited by the transparency of the support, and
2) the use of pressed discs limits the diffusion rate of reactants and products, making *in-situ* kinetic studies problematic.

Alternatively, using Diffuse Reflectance Infra-red Fourier Transform Spectroscopy (DRIFTS), catalyst powders can be studied directly without the need for pressed discs [37, 38]. This results in an increased area of contact of the adsorbent with the gas, and a higher rate of diffusion through the sample. In addition, since transmission through the sample is not sought (Fig 1.1(a)), dark coloured samples can be studied. As the name suggests, DRIFTS makes use of infra-red radiation reflected from the sample. The acronym "DRIFTS" was first coined by Fuller and Griffiths in 1978 [39], when they reported an improvement in the signal to noise ratio and resolution by using Fourier Transform IR.

Two types of reflection occur from a sample - from the topmost layer, where the angle of incidence equals the angle of reflection, *Frensel* or *specular* reflection takes place. The infra-red beam interacts only once with the surface and contains little information. Particles in the bulk can also participate; particles oriented parallel to the surface produce *regular* Frensel and those whose surfaces are not parallel with the sample surface generate *diffuse* Frensel.

Diffuse reflectance results from the reflection of light from matt surfaces. Radiation is considered to pass into the bulk of the material and undergo reflection, refraction and absorption to varying degrees, before re-emerging from the surface. Radiation interacts more than once with the powder and after interaction is distributed isotropically in all directions. For most materials, both specular and diffuse reflectance

occur. Fig. 1.1 highlights the basic difference in the interaction of infra-red radiation between transmission and diffuse reflectance experiments.

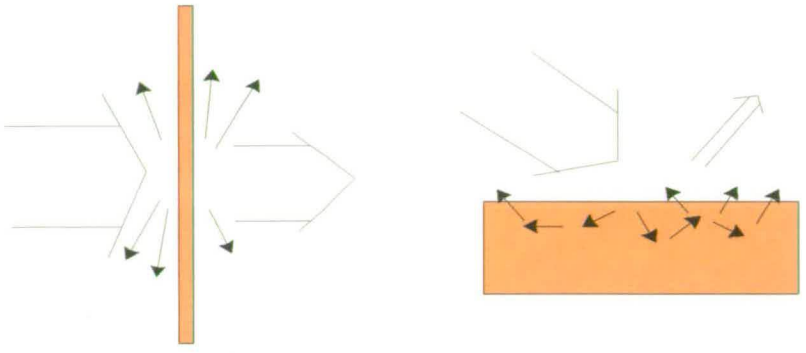

(a) (b)

Fig. 1.1. *The interaction of infra-red radiation during (a) a transmission, and (b) a diffuse reflectance experiment.*

The main disadvantage with DRIFTS is found with increasing absorptivity of the substrate; diffuse reflectance is then minimal and specular reflection can be substantial. In these regions, it can appear that the reflectance of the sample is high, but as radiation does not even penetrate the sample it is very unlikely that the true absorption bands will be observed [38].

An additional advantage of using infra-red spectroscopy for the study of heterogeneous catalysts is the opportunity to use reference spectra of model systems such as inorganic clusters and, more recently, surface science studies to aid spectral assignment. Reflection-Absorption Infra-Red Spectroscopy (RAIRS) [40, and references therein] considers the reflected electromagnetic radiation from an extended metal surface, which is usually in the form of a precisely-defined single crystal, and often under ultra-high vacuum conditions. The technique was utilised extensively by Pritchard and co-workers [41] from the 1970's onwards, and is subject to the *metal surface selection rule* (MSSR), which imposes the restriction where only vibrations giving a dipole change perpendicular to the metal surface will be infra-red active [42]. In 1975, Pritchard *et al.* [41] published work which demonstrated the applicability of

RAIRS results as models for the assignment of transmission spectra from supported systems. It was subsequently shown that the MSSR also applied to spectra of species adsorbed on metal particles with a diameter larger than 2 nm [43].

However, care must be taken when making direct comparisons between, say RAIRS and DRIFTS experiments, owing to the so-called *material* and *pressure* gaps. That is, experiments carried out on single crystals do not account for any support, crystallinity or particle size effects, while RAIRS experiments carried out under ultra-high vacuum may hold little relevance for an industrial process carried out at very high pressures. The latter problem has been addressed by the advent of medium and high pressure RAIRS experiments, which have been successfully carried out, mainly with CO adsorption [44, 45].

1.4 Aim of This Work

Environmental objectives call for catalytic processes with much higher conversion and better selectivities [46]. An enhancement in selectivity is also desirable from a purely economic standpoint, since the need for by-product removal from outlet streams can be reduced. As discussed above, alkali promoters have been shown to have a favourable effect on the action of industrial catalysts. The purpose of this project was to elucidate the impact of alkali promoters on copper-based catalysts, with particular emphasis placed on the effect on activity and selectivity for the water-gas shift reaction.

The value of infra-red spectroscopy, and in particular DRIFTS, as a tool to study catalysts *in-situ* has also been illustrated above. Another consideration in the study of supported catalysts is that, if academic studies are to be of value to the catalytic community, it is imperative that the experimental conditions and catalyst compositions are relevant [46], since small variations in, say, catalyst composition, can lead to very different product distributions. In studying a catalyst close in

composition to those used industrially [1], and by employing an environmental cell in conjunction with DRIFTS, it is hoped that this has been achieved here.

The thesis can be loosely considered as comprising two sections:

1) Chapters 2 - 4 set the scene for the alkali promotion - DRIFTS studies. Chapter 2 contains the experimental details for the DRIFTS experiments, while Chapter 3 covers the preparation and characterisation of the catalyst, including micro-reactor studies which look at the effect of alkali promotion on the catalysts' performance in the water-gas shift reaction. Chapter 4 explores the effect of reduction on the unpromoted catalyst and determines the state of the copper component using CO as a probe molecule.

2) Chapters 5 - 8 aim to investigate the effect of alkali promotion on the catalyst during adsorption studies. Chapters 5 and 6 concern the effect of alkali promotion on CO and CO_2 adsorption, and methanol and formic acid adsorption, respectively. Chapter 7 aims to elucidate the action of the promoter under conditions more akin to those in an industrial system by carrying out a temperature programmed reaction with a CO_2/H_2 mixture. Finally, Chapter 8 pulls together the results concerning the effect of alkali promotion on the catalyst in order to gain a broader picture.

Chapter 2 - Diffuse Reflectance Infra-red Fourier Transform Spectroscopy (DRIFTS)

Investigations were made whereby the adsorption and subsequent temperature programmed desorption of gases could be carried out. Surface species were monitored using DRIFTS, and species in the gas phase were followed using mass spectrometry. In this chapter, the experimental set-up will first be described, followed by the procedure employed during typical experiments.

2.1 - Experimental Set-Up

A schematic diagram showing the DRIFTS apparatus in relation to the gas handling facilities and the mass spectrometer can be found in Fig. 2.1. Briefly, the DRIFTS environmental cell sits inside the sample compartment of the spectrometer, allowing spectra to be scanned when required. The sample inside the cell may be heated. Reduction and carrier gases are passed over the sample at measured flowrates. Adsorbate gases are introduced into the carrier gas *via* a glass vacuum line. Post-reaction analysis is carried out by bleeding a fraction of the outlet carrier gas into the mass spectrometer. Each component of the set-up will now be discussed in turn.

2.1.1 - Fourier Transform Infra-Red (FTIR) Spectrometer

The use of an FTIR spectrometer, as opposed to a dispersive instrument [47], is key in the application of diffuse reflectance experiments. Signals of very low intensity must be detected, and the greater throughput achievable with an FTIR spectrometer

makes this possible ("Jacquinot" advantage). Aside from this and the improved resolution obtainable with an FTIR instrument, another major advantage is that transient species formed during chemical reactions can be observed, and this could be invaluable in the study of heterogeneous catalysis. This advantage ("Fellgett" advantage) arises because data from all the spectral frequencies are measured simultaneously, in contrast to a dispersive instrument, leading to a reduction in measurement time.

Spectra were recorded during this study on a *BioRad FTS-6000* [48] (shown schematically in Fig 2.2) with data storage and manipulation on a P.C.. The FTS-6000 optical bench contained a Michelson interferometer with a beam splitter - a thin germanium film supported by KBr plates. The moving mirror ran on an air bearing, which was supplied with dry air from a compressor, providing almost frictionless movement. The ceramic source was water cooled and a HeNe laser was used to calibrate the infrared beam and to facilitate a high degree of precision in frequency assignment. An MCT (mercury cadmium telluride) photoconductive infrared detector was used which was liquid nitrogen cooled. This is a commonly used detector which is sensitive for mid-infrared and is capable of monitoring the spectral range 4000-700cm^{-1}.

The main compartment of the spectrometer was dry air purged constantly at a rate of about 4.5 litre/min, minimising interference from atmospheric water vapour as much as possible apart from the 1.5 cm pathlength of the environmental cell (discussed below). The sample compartment could be isolated from the rest of the spectrometer by means of shutters. A customised cover with an additional inlet from the main purge line fitted over the sample compartment and thus allowed purging to be carried out more quickly, prior to experiments.

Spectra were scanned at a speed of 20 kHz and at 4 cm^{-1} resolution. The method used during experiments to obtain spectra will be given below in the Experimental Procedure, but the spectrometer was essentially operated in two modes:

1) *Rapid Data Collection* - used when changes were not expected with time. Interferograms were co-added over a period of time and a single spectrum was produced, and

2) *Kinetics Data Collection* - spectra collected as a function of time as processes occurred. A set of many spectra was produced. These could be examined and manipulated individually or as a set. In practice, a few scans were co-added into a scanset, which was a single spectrum, then multiple scansets were collected into a document. In this mode, the software (*Win-IR Pro*) made it possible to construct "functional group chromatogram"s, where the absorbance in a region was tracked with respect to time.

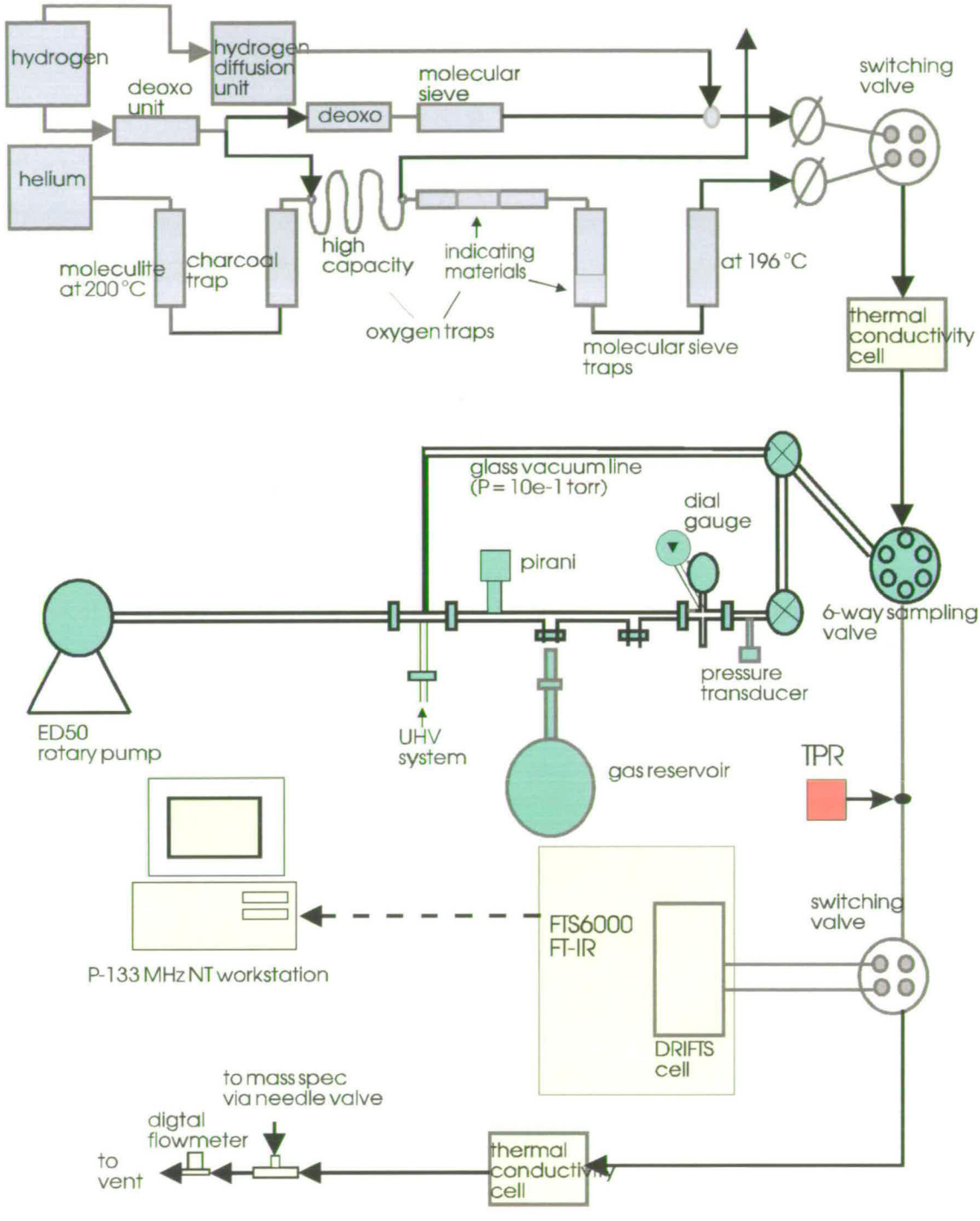

Fig. 2.1. *DRIFTS set-up: top section (purple) represents gas handling of the reduction and carrier gases, central section (green) the introduction of adsorbate gases and the lower section (yellow) DRIFTS and mass spectral analysis. "TPR" denotes an additional set of apparatus which is detailed later, in Fig. 2.5.*

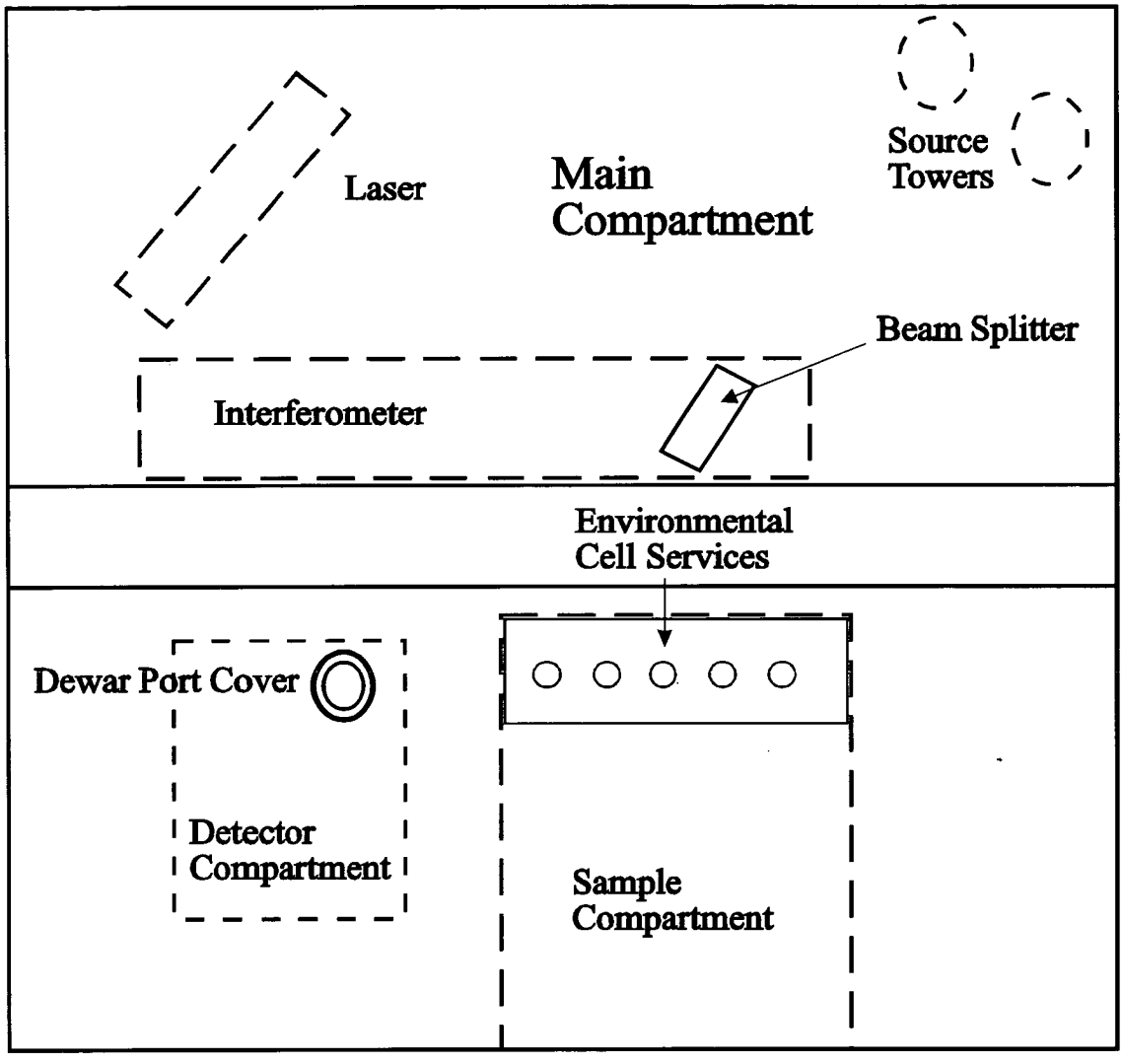

Fig. 2.2. *A schematic diagram of the optical bench of the Bio-Rad FTS-6000*

2.1.2 - The DRIFTS Optics

A *SpectraTech* DRIFTS accessory [49] was used to maximise the collection of diffuse reflectance. It was located by posts which fitted into mounting holes in the baseplate of the optical bench sample compartment. The optics could be easily manipulated whilst inside the compartment to maximise the response signal (Fig. 2.3).

2.1.3 - The Environmental Cell

Fig. 2.4 represents the two constituent parts of the modified-*SpectraTech* environmental cell. The cup at the top of the post (3 mm deep, 10 mm in diameter) was filled with catalyst powder and levelled off. A spring-mounted arm allowed the cell to be raised and lowered with respect to the optics in order to attain the maximum signal intensity.

The cell was isolated from the ambient spectrometer by the stainless steel cap fitted with two CaF_2 windows. These were sealed with Kalrez™ O-rings and steel clamping plates, and the base of the cap was sealed with a large Viton™ O-ring which was protected from the temperature extremes of the heater by a cooling system. The sample was heated *via* the heating element within the post, which was controlled by a programmable in-house-built power supply. A maximum catalyst temperature of 300 °C was used for routine use, although 400 °C could be reached if necessary, the upper temperature being limited by the O-rings and windows. Catalyst temperatures were measured with a 0.5 mm steel sheathed chromel-alumel thermocouple which entered the cell through a hole in the steel cap and sat about 1 mm into the catalyst bed. During some early experiments, a 1 mm chromel-alumel thermocouple was used, and this is discussed where it is of relevance in Chapter 4. A lag of about 50 °C* between the heating post and the sample was observed, and this has been reported in previous studies [50]. In addition to this, problems were encountered during this

study with the reproducible recording of the sample, i.e. the recorded temperature was very dependent upon the position of the thermocouple within the catalyst bed. This topic will be returned to in later chapters.

Within the cell, gases could be passed over the sample - there were three outlets for gas dosing - one inlet, one outlet, and one which was blocked off (Fig. 2.4).

2.1.4 - Mass Spectrometry

Analysis of the gas exiting from the DRIFTS cell was carried out using a P.C.-controlled *VG-Monitorr* quadrupole mass spectrometer (see Fig. 2.1). A jet-separator was fitted and this was constantly pumped to $\leq 5 \times 10^{-2}$ Torr.

2.1.5 - Gas Handling

To ensure the highest possible purity of the carrier and reducing gases (helium** and hydrogen respectively) they were passed through the following set of traps in the sequence shown:

Helium:

- Moleculite™ trap at 200 °C (to remove CO)
- activated charcoal at ambient (to remove hydrocarbons)
- high capacity oxygen trap at ambient temperature
- indicating oxygen trap at ambient temperature
- molecular sieve at ambient temperature with indicator
- molecular sieve at -196 °C

---

* Temperatures will be quoted in °C throughout this thesis.
** The purity and suppliers of gases are listed in Appendix A

Hydrogen:

- deoxo unit
- two molecular sieve traps at ambient

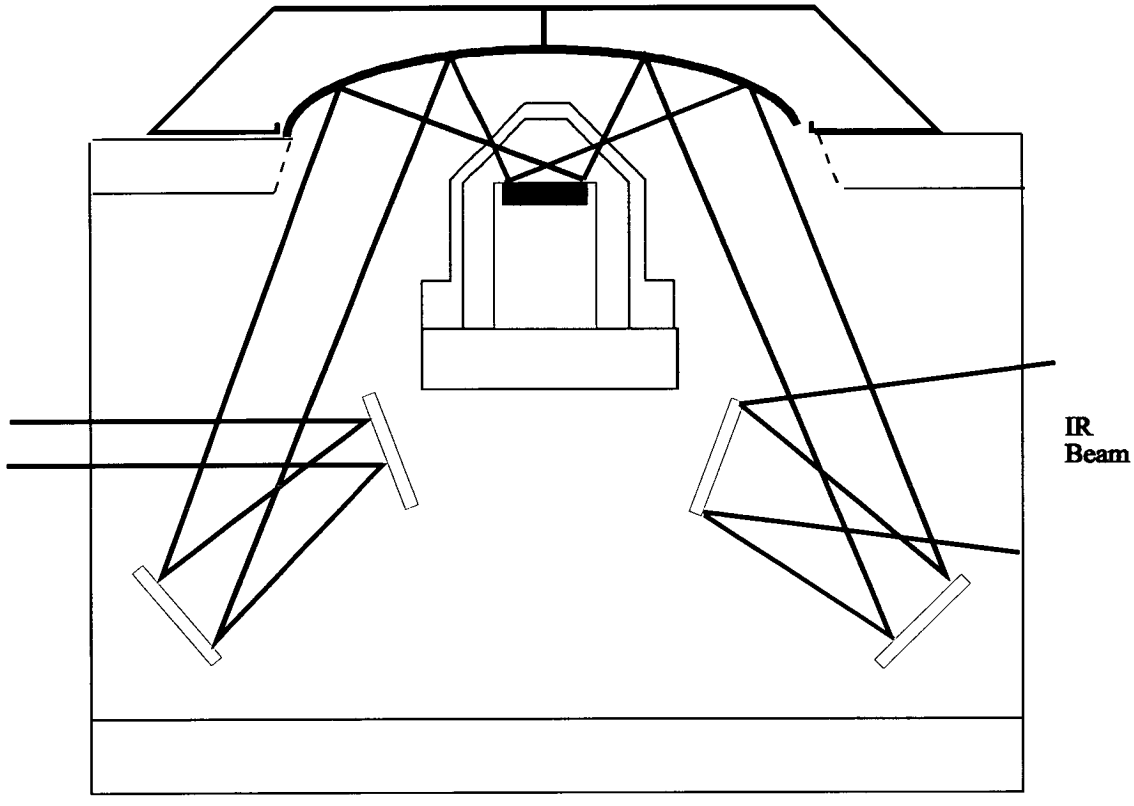

Fig. 2.3. *Schematic diagram of the Spectra-Tech DRIFTS Accessory*

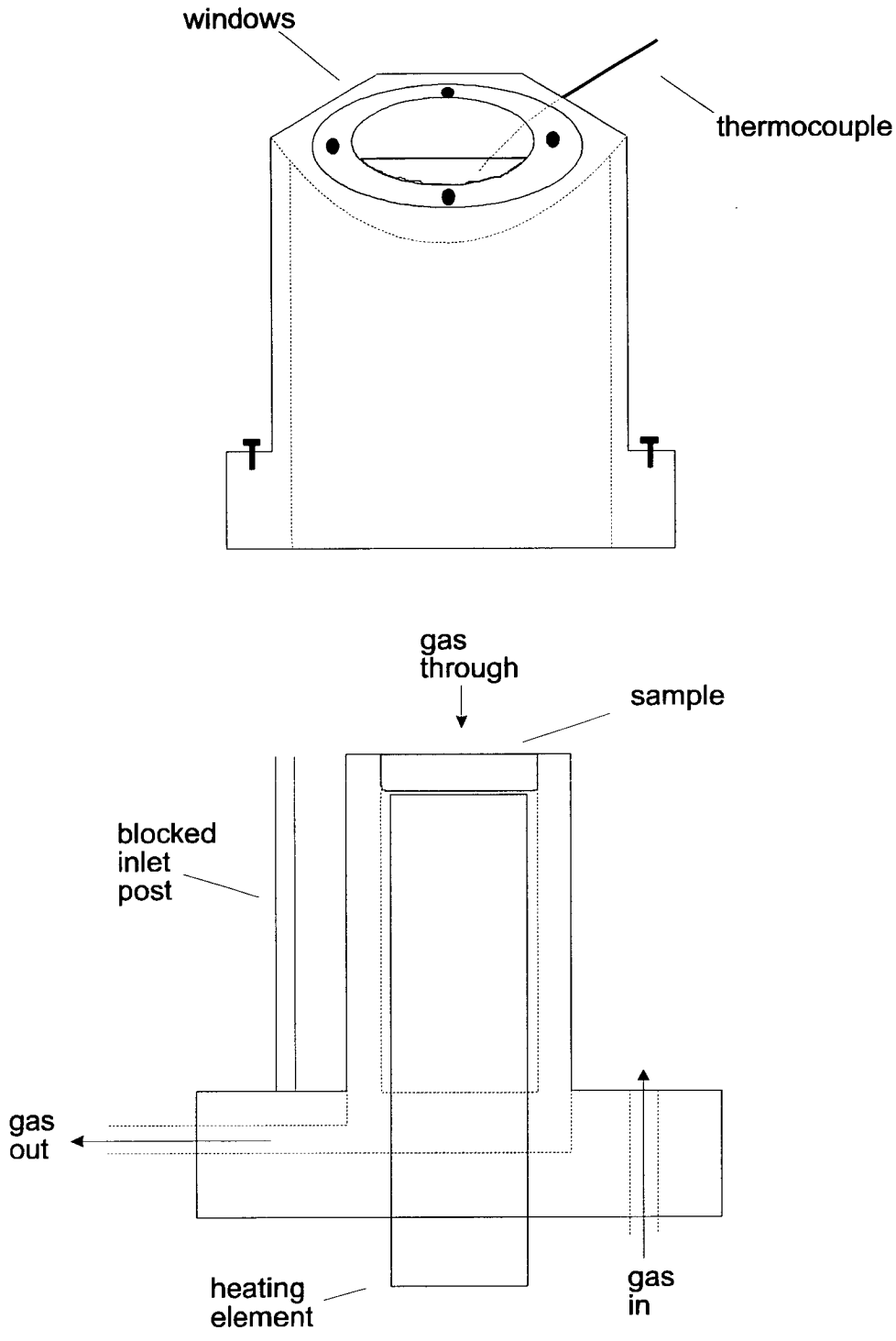

Fig. 2.4. *Detail of the environmental cell (upper: steel cap, lower: sample post)*

2.2 - Experimental Procedure

2.2.1 - Pre-treatment

The pre-calcined catalyst (about 80 mg) was gently crushed and sieved (to "100 mesh"). It was then put through a reduction procedure in order to activate it before the adsorption of reactant gases. Chapter 4 considers the effect of reduction on the catalyst, and this will not be discussed here. The standard pre-treatment which was eventually established is, however, as follows: 100 % hydrogen at a flowrate of 50 cm^3/min was passed over the catalyst. A temperature ramp was applied from room temperature to 140 °C at + 10 °C/min, where the temperature was held for 1 h and 10 min. Following this, the ramp was continued but at + 1.5 °C/min to 230 °C where the temperature was held for 2 h. The sample was degassed under helium at 20 cm^3/min, 230 °C for 30 min, then taken to 300 °C at + 7.0 °C/min and held for 10 min. Gases within the cell were at approximately atmospheric pressure.

The sample compartment cover was not put into place until degassing had commenced in order to prevent overheating of the DRIFTS cell. Once in place, purging of the sample compartment was allowed to proceed for at least 1.5 h before experiments began, at which point bands due to the miscancellation of atmospheric water were at a low level.

2.2.2 - Pulse Experiment

The glass line was pumped to $\leq 1 \times 10^{-1}$ Torr (Fig. 2.1). CO_2, methanol vapour and formic acid vapour were purified by a number of freeze-pump-thaw cycles before use using a cold finger attached to the glass line. CO was used as received. The gas was then introduced from the glass vacuum line into a 0.2 cm^3 sample loop which had also been evacuated. The pressure of the gas was measured using a pressure transducer.

The turning of a Carle valve directed it from the sample loop into the helium carrier gas and then over the sample. Pulses were introduced every 5 min at successively higher pressures. As a convenient experimental quantity, the pressure of gas exposed to the sample is quoted in Chapters 5 and 6, but the equivalent number of moles to which this corresponds for each pressure is expressed in Table 2.1.

Table 2.1. *Equivalent number of moles for pulses introduced from the sample loop*

Pressure in Sample Loop (Torr)	Equivalent No. μmol
20	0.22
50	0.54
100	1.08
150	1.61
200	2.15

A standard background spectrum (200 scans, resolution 4 cm^{-1}) was recorded after pre-treatment before each pulse experiment at room temperature and subsequent spectra (100 scans, resolution 4 cm^{-1}) were ratioed against this to leave only features due to the adsorbed species. All spectra are expressed as "absorbance". It was determined early on in the project using a thermal conductivity detector that any unadsorbed gas phase species from the pulse had a residence time in the environmental cell of 3 min. Thus, spectra were scanned 3 min after each pulse had been introduced, and recorded only surface species or gas phase species from reaction with the surface.

The experiment was also monitored simultaneously using the mass spectrometer by bleeding a portion of the product gas stream into the instrument *via* the jet-separator after it had passed over the catalyst . Any CO (*m/e* 28) observed in conjunction with CO_2 (*m/e* 44) was corrected for the fragmentation of CO_2 in the mass spectrometer, i.e. $CO_{(genuine)} = (CO_{(observed)}) - (0.11 \times CO_{2(observed)})$. The fragmentation patterns of methanol and formic acid were investigated prior to their adsorption in order to facilitate mass spectrum interpretation.

Calibration of the mass spectrometer was attempted as follows: pulses of a known number of moles of gas were passed through the DRIFTS cell in the absence of a sample, while monitoring with the mass spectrometer. The integrated area of the resulting peaks (in arbitrary units, a.u.) was found and related back to the number of moles in each pulse. When applying the relationship of x (a.u.) $\equiv y$ (no. moles), to data from DRIFTS experiments, it was found that the number of moles of gas detected during the experiment always far exceeded the number of moles that the catalyst had been exposed to. This was traced to the sampling rate of the mass spectrometer - during the calibration pulses, the peak widths registered by the mass spectrometer were narrow, because the pulse passed through the cell very quickly in the absence of the catalyst, and each pulse was composed on average of only three data points. In the presence of a sample, peaks were broader, even for the same quantity of gas.

Therefore, results are usually quoted simply as "a.u.", and reliable comparisons can still be made between experiments. In the case of the experiments in Chapter 5, however, a calibration *was* undertaken - although the use of the units "μmol" may be somewhat arbitrary the amounts of CO and CO_2 detected are at least weighted relative to each other, thus taking into account their relative sensitivities in the mass spectrometer.

2.2.3 - Temperature Programmed Desorption (TPD)

The temperature of the sample was raised in flowing helium from room temperature (25 °C ± 3) at + 20 °C/min to 300 °C and spectra were recorded in Kinetics mode (time resolution - 10 s). The temperature was then held at 300 °C for 10 min before being allowed to return to room temperature. Once again, gas phase species were monitored using the mass spectrometer.

Subsequently, spectra were extracted from the Kinetics file at set time intervals. Functional group chromatograms were constructed by monitoring the intensity of specific bands over the course of the TPD.

2.2.4 - Temperature Programmed Reaction (TPR)

The TPR experiment in chapter 7 was carried out in a similar manner to the TPD experiments described above, except that a flowing gas mixture was used (CO_2/H_2) and a different temperature ramp was applied (detailed in chapter 7). Hydrogen was purified using a Johnson Matthey Hydrogen Diffusion Unit at 300 °C. The gases were mixed prior to flowing over the sample, as shown in Fig. 2.5.

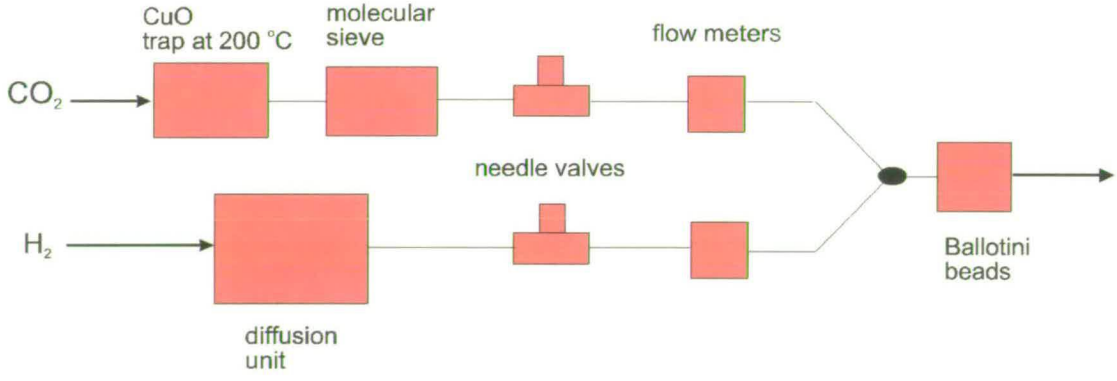

Fig. 2.5. *TPR set-up for the preparation of the CO_2/H_2 mixture (positioned as shown by "TPR" in Fig. 2.1)*

Chapter 3 - Catalyst Preparation and Characterisation

3.1 - Introduction

Catalysts have been prepared during this study *via* a layered hydrotalcite-type precursor. Hydrotalcites have been shown to decompose to produce oxides which, following reduction, possess important catalytic qualities such as a high metallic dispersion and good particle stability against sintering [51, 52, 53]. The structure formed synthetically is isomorphous with the naturally occurring mineral, $Mg_6Al_2(OH)_{16}CO_3.4H_2O$, where positively charged brucite-like layers, $(Mg_6Al_2(OH)_{16})^{2+}$, alternate with disordered negatively charged interlayers, $(CO_3.4H_2O)^{2-}$. In this case, Cu^{2+} and Zn^{2+} will substitute the Mg^{2+} ions.

A modification of a preparation method by Trifiro and co-workers [53] has been used, involving the co-precipitation of copper, zinc and aluminium nitrates with ammonium bicarbonate, thus generating the catalyst alkali free. They identified the importance of ensuring the following ratios: (Cu+Zn)/Al = 3 and Cu/Zn = 1, in order to obtain the hydrotalcite pure. When these conditions were satisfied, the hydrotalcite was the prevalent structure in the precipitate, and thermal decomposition, followed by reduction, resulted in the formation of smaller copper crystallites than those from other precursors. It was also shown [53] that catalysts produced *via* the hydrotalcite route had a higher catalytic activity for the methanol synthesis reaction than those originating from a malalchite precursor

Following preparation and calcination, the catalysts were promoted with alkali salts using a standard impregnation method. As discussed in the introduction to this thesis, the exact nature of the alkali counter-ion in a supported catalyst under reaction

conditions is debatable, [20, 29] and depends strongly on the thermal history and gaseous environment [54]. However, it has also been suggested that although the catalytic promoter action of the alkali varies slightly with the anion, the principal effect is due to the cation [54].

While bearing this concept in mind, it is still interesting to consider reports so far on the nature of the alkali compounds/complexes present under reaction conditions. Schloegl [20] used a thermodynamic argument to highlight the improbability of finding an alkali metal in a practical catalytic system (reaction 3.1). Similarly, he argued that KOH is the most thermodynamically stable form of potassium oxide compound in the absence of carbon dioxide (e.g. reaction 3.2). The reduction of potassium oxides or hydroxides were said to require "very drastic conditions", and would be stable to chemical reduction up to about 580 °C.

$$K + 0.5O_2 + 0.5H_2 \rightarrow KOH \qquad \Delta H = -428 \text{ kJ/mol} \qquad \textit{reaction 3.1}$$

$$K_2O + H_2O \rightarrow 2KOH \qquad \Delta H = -87.5 \text{ kJ/mol} \qquad \textit{reaction 3.2}$$

Dwyer, on the other hand [29], reported that while the decomposition of potassium carbonate was unlikely in terms of bulk thermochemical properties (reactions 3.3 - 3.5, $\Delta G°(327\ °C)$), on reduction of a K_2CO_3-promoted iron powder catalyst, the carbonate was totally decomposed to a "KO" species, as detected using x-ray photoelectron spectroscopy (XPS). The exact chemical nature of the adsorbed potassium phase was unclear, but it was suggested that oxygen could have been in the form of a hydroxyl or simply an adsorbed oxygen anion.

$$K_2CO_3 \rightarrow K_2O + CO_2 \qquad \Delta G° = +301 \text{ kJ/mol} \qquad \textit{reaction 3.3}$$

$$K_2CO_3 + H_2 \rightarrow KOH + CO \qquad \Delta G° = +142 \text{ kJ/mol} \qquad \textit{reaction 3.4}$$

$$K_2CO_3 + H_2O \rightarrow KOH + CO_2 \qquad \Delta G° = +130 \text{ kJ/mol} \qquad \textit{reaction 3.5}$$

In view of the fact that bulk K_2CO_3 is stable as a molten salt and only decomposes at temperatures well above its melting point (891 °C), and considering reactions 3.3 - 3.5, Dwyer [29] proposed that the surface phase formed during reduction must have been stabilised considerably by its interaction with the metallic substrate, such that its free energy of formation (ΔG) was more negative than for the bulk phases. He also found that the "KO" surface complex was stable under CO_2 gas until pressures in excess of 2 bar, whereupon K_2CO_3 was re-formed. This result was given as evidence for the stability of the "KO" phase and it was thus suggested as being the "working form" of the alkali promoter under reaction conditions.

Additional XPS studies of promoted iron foil and Pt(100) by Bonzel and Krebs [54] showed that regardless of the original promoter compound (KNO_3, KOH or K_2CO_3), partial decomposition to a potassium oxide of unknown stoichiometry ocurred on heating (K_2O_2 or KO_2). Reduction of the decomposed (or even the as-prepared) K-compound always led to KOH formation. Therefore, neglecting any additional reaction with the catalyst support (and this will be discussed in Chapter 5), it appears that the promoter will be in the form of a "KO" surface species following reduction, which is most likely to be KOH.

3.2 - Preparation Routes

The preparation route was varied slightly to produce the catalyst by two similar methods in an attempt to optimise the copper surface area for the DRIFTS experiments. These will be termed *Catalyst 1* and *Catalyst 2*.

Catalyst 1: "Forward Batch" Co-precipitation

2 litres of a mixed metal nitrate solution (0.77 moldm^{-3} $Cu(NO_3)_2.3H_2O$, 0.77 moldm^{-3} $Zn(NO_3)_2.6H_2O$, 0.97 moldm^{-3} $Al(NO_3)_3.9H_2O$) was prepared and heated to 60 °C. According to the set-up in Fig. 3.1, 5.1 litres of aqueous ammonium bicarbonate, also at 60 °C, was added in portions using a peristaltic pump over a period of 25 min until the solution had increased in pH from its original value of 2.6 to the range 6.3 - 6.5. The resulting sky-blue precipitate was aged at pH 6.3 - 6.5 for 30 min and then the mother-liquor was removed by filtering under vacuum. The filtercake was re-slurried in 6 litres of warm distilled water, before once again being filtered and washed with warm water. This re-slurrying/filtering/washing process was continued until the conductivity of the filtrate was below 200 μS - eventually the filtercake had been washed with 20 litres of water.

The filtercake was then dried at 110 °C for 22 h to produce a light blue catalyst precursor which was calcined at 300 °C for 6 h, resulting in a dark green solid.

Catalyst 2: "Constant-pH Batch" Co-precipitation

This preparation was carried out in an identical fashion to that for *Catalyst 1*, except that the mixed metal nitrate solution and aqueous ammonium bicarbonate were added simultaneously to an empty vessel in a controlled manner over the course of 18 min, using peristaltic pumps (Fig. 3.2). Thus, the pH of the precipitate was maintained in the range 6.3-6.5 throughout. Difficulty was encountered in trying to remove the mother liquor by filtering, such that the filtercake was eventually divided between two funnels. In total, 42 litres of water were used to wash the solid.

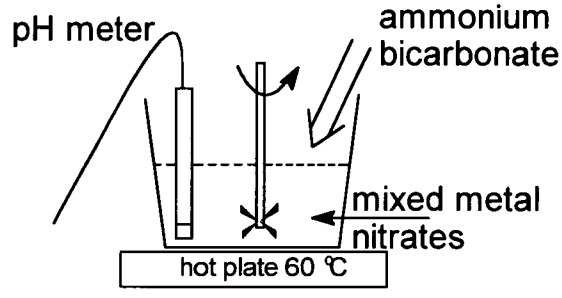

Fig. 3.1. *Experimental set-up for the preparation of the Catalyst 1 precursor via a "forward batch" co-precipitation method*

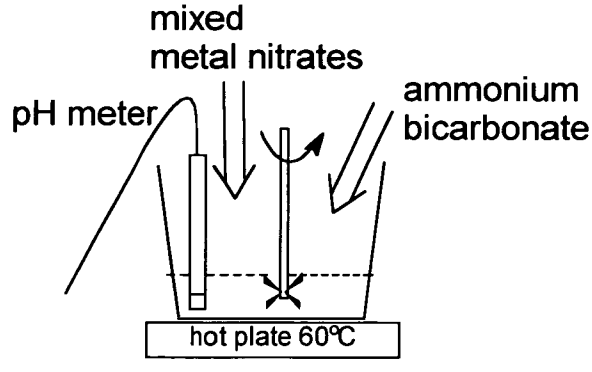

Fig. 3.2. *Experimental set-up for the preparation of the Catalyst 2 precursor via a "constant pH batch" co-precipitation method*

3.3 - Characterisation of the Unpromoted Catalysts

Unpromoted *Catalyst 1* and *Catalyst 2* and their respective precursors were characterised in the following manner:

- powder x-ray diffraction (PXRD) of the precursors at room temperature and during calcination
- thermogravimetric analysis (TGA) during calcination of the precursors
- elemental analysis of the calcined samples
- copper surface area of the calcined samples by reactive frontal chromatography (RFC)

3.3.1 - Powder X-Ray Diffraction

3.3.1.1 - At Room Temperature

The presence of the hydrotalcite structure in the catalyst precursors was first verified by the X-ray Diffraction Group at ICI Katalco using PXRD. Patterns were recorded on a Philips Diffractometer *D1*, and comparisons were made with the *JCPDS* database. The result was subsequently repeated at The University of Edinburgh, again using PXRD, recorded on a Philips Powder Diffractometer *PW 1730* (40 kV, 30 mA) with a copper K_α x-ray source at 1.54 Å. The patterns recorded at room temperature for the *Catalyst 1* and *Catalyst 2* precursors are shown in Fig. 3.3 and Fig. 3.4 respectively, where it can be seen that both contained a major phase of a hydrotalcite-type structure similar to $Cu_3Zn_3Al_2(OH)16CO_3.4H_2O$ (JCPDS No. 37-629). This phase is typified by an intense feature at 2θ 11.9°, but the other peaks due to it are marked in Fig. 3.4. On comparison of the two patterns, it will be noticed that the "constant pH batch" route precursor (*Catalyst* 2) is predominantly hydrotalcite, while the "forward pH batch" (*Catalyst* 1) precursor also contains another phase; the most intense feature is seen at 13.8° and the other features are broad and low in intensity. The identity of this phase is uncertain, but it is most likely to be a zinc-containing

(JCPDS No. 11-287) matches closely. The formation of this species probably results from the fact that at low pH values, all of the copper and some zinc will have co-precipitated to give the expected hydrotalcite. However, since zinc is not expected to fully precipitate until around pH 6.5, as this pH was approached, the solution would have been very rich in zinc. Therefore, a zinc-rich phase was formed. Trifiro and co-workers [55] have observed the formation of hydrozincite ($Zn_5(CO_3)_2(OH)_6$) where (Cu+Zn)/Al > 3, and this condition would be satisfied in a zinc-rich solution. Finally, amorphous material is also present in this sample, as shown by broad peaks.

The sharp peaks in the diffraction pattern of the *Catalyst 2* precursor indicate the presence of a more crystalline, less amorphous species. Another phase also exists in this sample, and the exact nature of this species is uncertain. It could be due to a Zn-Al hydroxide type phase, but one which is different from the zinc rich phase seen in the *Catalyst 1* precursor, in spite of the presence of the most intense feature also occurring at 13.8°.

3.3.1.2 - During Calcination

The effect of calcination on the precursors was studied (Fig.s 3.5 and 3.6) using *hot-stage* PXRD at The University of Edinburgh with an Anton Paar *XRK 900* reaction chamber. The temperature of the sample was ramped under air from 25 to 300 °C in 25 °C steps, but in 5 °C steps between 90 and 130 °C. The sample was allowed to stabilise at each step for 30 min, followed by 60 min data acquisition. An average heating rate between steps of + 250 °C/min was used, except between 90 and 130 °C, where + 50 °C/min was used. It was found by monitoring the peak at 2θ 11.9° (illustrated in Fig. 3.7 for the *Catalyst 2* precursor) that the hydrotalcite structure was decomposed by 130 °C. An amorphous oxide remained at 300 °C for both samples, as indicated by the development of a single broad XRD peak at 2θ 36°. These results agree with those of Trifiro and co-workers [55].

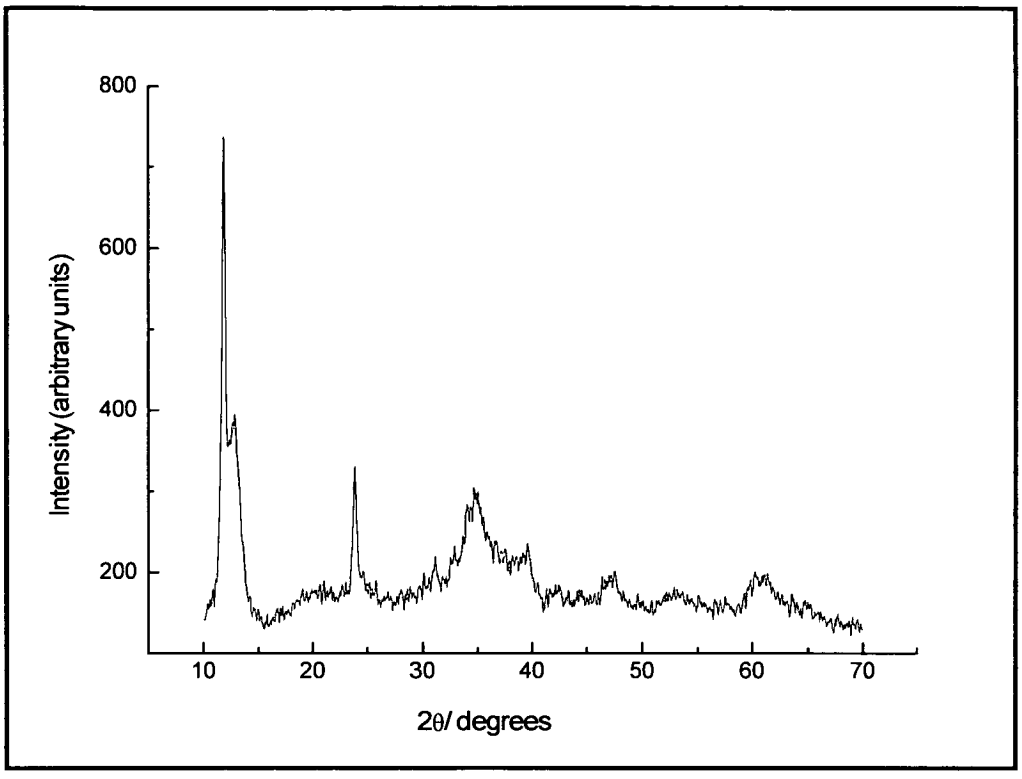

Fig. 3.3. *Powder diffraction pattern showing the presence of hydrotalcite structure in the Catalyst 1 precursor at room temperature*

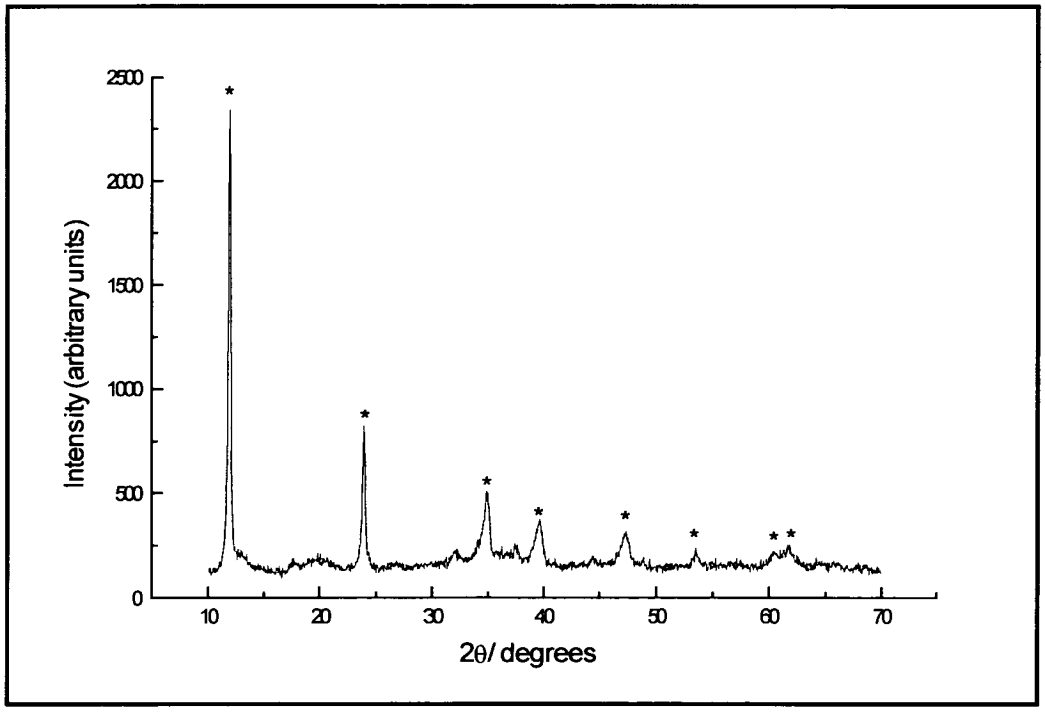

Fig. 3.4. *Powder diffraction pattern showing the presence of hydrotalcite structure (marked - *) in the Catalyst 2 precursor at room temperature*

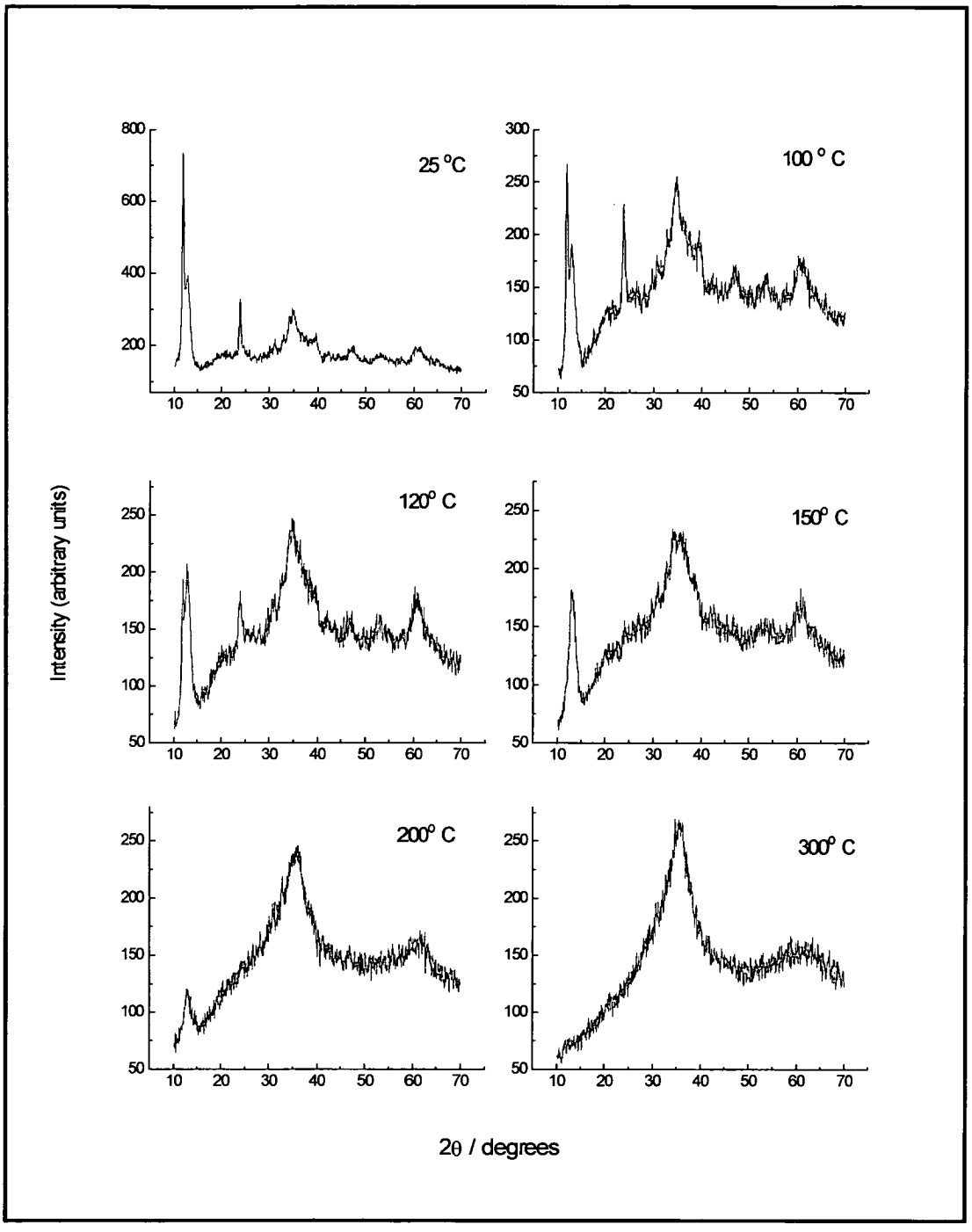

Fig. 3.5. *Hot stage PXRD pattern of Catalyst 1 precursor.*

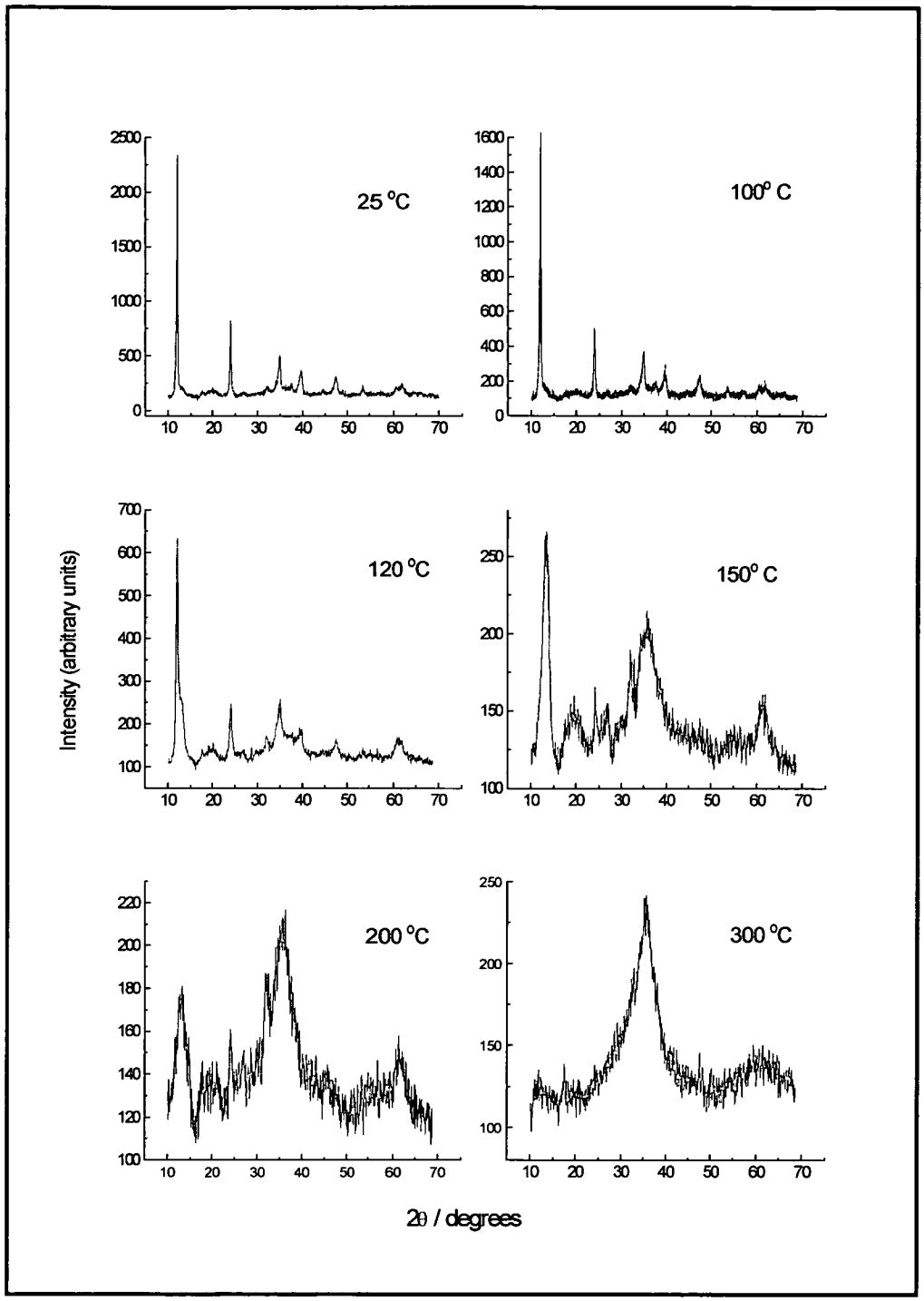

Fig. 3.6. *Hot stage PXRD pattern of Catalyst 2 precursor.*

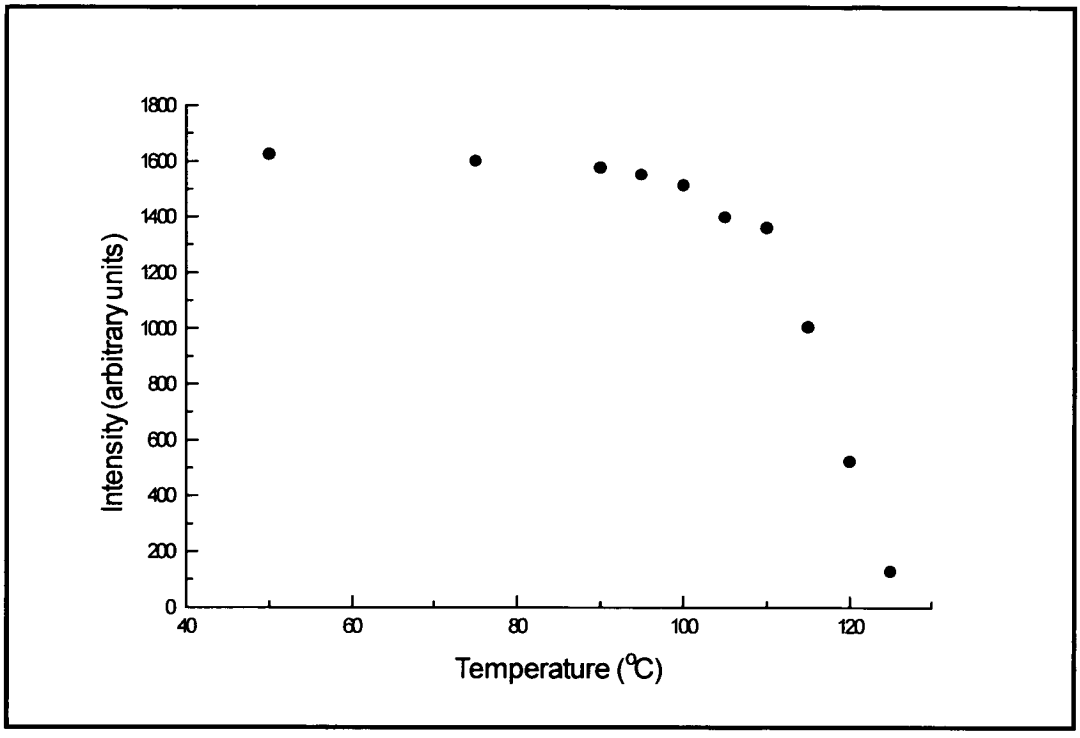

Fig. 3.7. *Decrease in intensity of peak at $2\theta = 11.9^{o}$ with respect to temperature for Catalyst 2 precursor.*

3.3.2 - Calcination followed by Thermal Gravimetric Analysis (TGA)

The decomposition of the catalyst precursor was also followed with TGA by monitoring the loss in the mass of the sample during a heating ramp using a Stanton Redcroft *TG-760* interfaced to a P.C.. 10 mg of each sample was heated at a rate of + 10 °C/min in flowing air from room temperature to 400 °C. Differential Thermal Analysis (DTA) was carried out using alumina as a reference - thus, the endo/exothermicity of processes was assessed by finding the difference in temperature between the sample and reference (ΔT).

Fig. 3.8 and 3.9 illustrate the changes occurring on heating the *Catalyst 1* and *Catalyst 2* precursors, respectively. A small shoulder is seen for the *Catalyst 1* precursor at 70 °C, which is probably due to the loss of adsorbed water. Although there is the possibility of a very small feature at low temperature also for *Catalyst 2*, it

is clear that this sample is drier. Two major endothermic events are recorded for each sample. One starts at low temperature and peaks sharply at 156 and 168 °C respectively. This can be attributed to the loss of water of crystallisation [50, 53, 56]. The slight difference between the two values could be due to a slight difference in the level of crystallinity [50]. A greater amount of water was also lost from *Catalyst 2* at this temperature, which could perhaps be attributed to a higher level of hydrotalcite in this sample. The broader feature seen peaking at 275 and 309 °C respectively is due to the decomposition of the precursors to oxides, with the irreversible loss of structural water and carbon dioxide[50, 53, 55]. A larger shift is observed between the two samples for this peak; this difference could be due to the presence of a zinc-rich phase in *Catalyst 1* - hydrozincite has been previously shown to peak at 280 °C [56] - and thus the peak would appear overall at a lower temperature.

Overall, the TGA results support the PXRD findings that *Catalyst 1* is less pure in terms of the hydrotalcite structure, and that the level of crystallinity differs between the two samples.

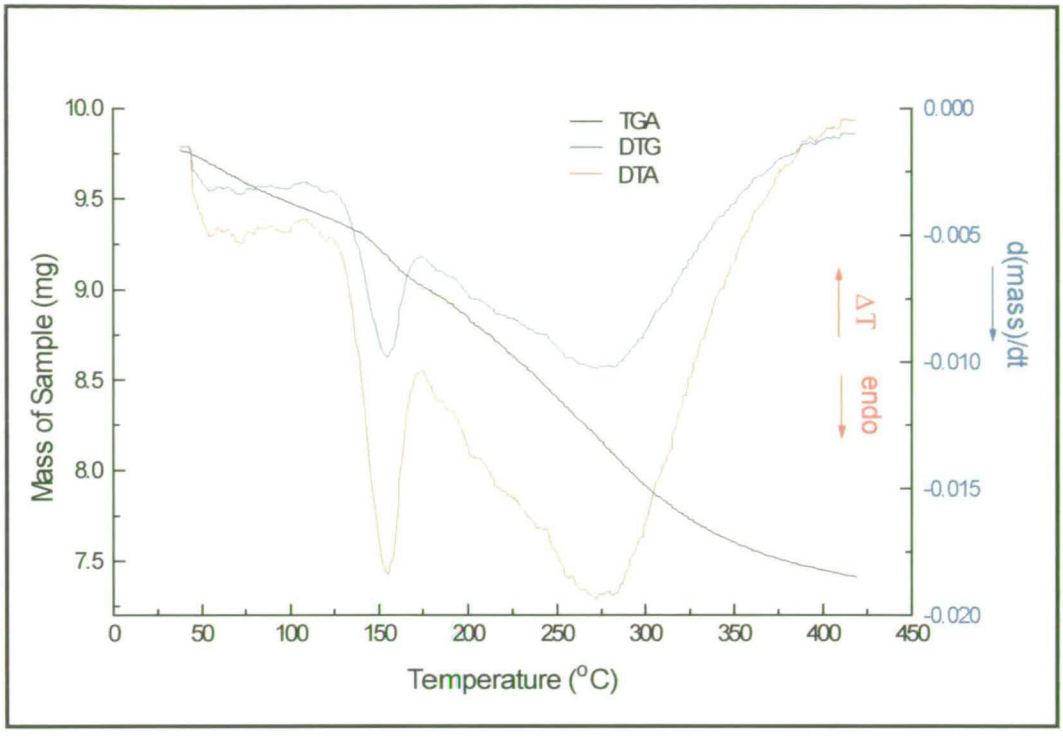

Fig. 3.8. *Themal analysis for the Catalyst 1 precursor. N.B. The DTA trace is scaled arbitrarily.*

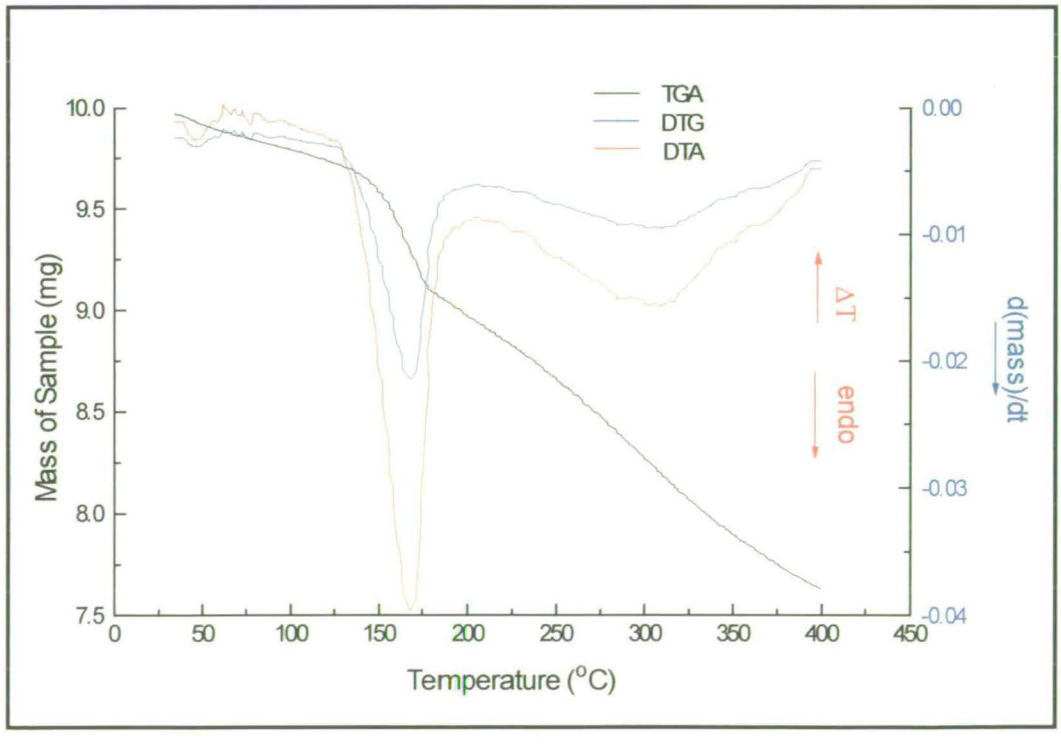

Fig. 3.9. *Themal analysis for the Catalyst 2 precursor. N.B. The DTA trace is scaled arbitrarily.*

3.3.3 - Elemental Analysis of Calcined Catalysts

Elemental analysis was carried out by the Characterisation and Physical Science Group at ICI Katalco using X-ray Fluorescence. The compositions for *Catalyst 1* and *Catalyst 2* are shown in Table 3.1, expressed on a (% weight)/(catalyst weight) basis of the metal oxides. The measurements are also expressed on a "loss free" basis, i.e. corrected for heating to constant mass at 900 °C, which removes any problems such as varying amounts of adsorbed water. Thus, it is observed that the ratio of $CuO:ZnO:Al_2O_3$ is in good agreement with the anticipated values and is virtually unchanged for the two preparation routes used.

Table 3.1. *Elemental analysis of calcined Catalyst 1 and 2.*

Component	Wt % of Component		
	Expected	*Catalyst 1*	*Catalyst 2*
CuO	41	40	40
ZnO	42	41	42
Al_2O_3	17	18	18

3.3.4 - Copper Surface Area of Calcined Catalysts

The copper surface area of *Catalyst 1* and *Catalyst 2* was determined at ICI Katalco by reactive frontal chromatography (RFC), which has been described previously [57]. Briefly, the technique relies on the decomposition of N_2O over copper metal at 60 °C, according to reaction 3.6. N_2 is produced in an amount equivalent to the number of oxygen atoms on the copper surface. The values given in Table 3.2 (given per g of catalyst in the reduced state) show that *Catalyst 1* has a higher copper area than *Catalyst 2*.

$$N_2O_{(g)} + 2Cu_{(s)} \rightarrow N_{2(g)} + (Cu-O-Cu)_{(s)} \qquad \textit{reaction 3.6}$$

Table 3.2. *Copper surface area of Catalyst 1 and 2, (± 5 %).*

Sample	Copper Surface Area (m^2g^{-1})
Catalyst 1	19
Catalyst 2	15

3.4 - Promotion

Initial DRIFTS experiments (Chapter 4) revealed that the slight difference between the precursors of *Catalyst 1* and *Catalyst 2* had little effect on the spectra following CO adsorption on the (reduced) calcined samples, apart from an increased CO uptake on *Catalyst 1,* probably owing to its higher copper surface area. In view of this enhanced uptake and the obvious implications for signal to noise ratios in infra-red spectroscopy, *Catalyst 1* was chosen to be promoted to different levels of potassium carbonate at The University of Edinburgh, for subsequent study by DRIFTS.

Prior to this, however, the promotion method was established using *Catalyst 2* at ICI Katalco, where samples were promoted to a common mole % with the salts of different alkalis and then characterised in the following ways:

- the level of alkali was determined by Inductively Coupled Plasma Mass Spectrometry (ICP-MS) [58]. The sample was first digested into liquid form and then analysed relative to a calibration graph constructed using known elemental standards.
- the copper surface area was determined using RFC, as described in section 3.3.4.

To compliment these studies, the total surface area of *Catalyst 2* and that promoted with potassium carbonate was determined at The University of Edinburgh by using a standard BET method with nitrogen adsorption at -196 °C.

To establish the effect of promotion on *Catalyst 2* under typical water-gas shift reaction conditions, catalyst activities were measured at ICI Katalco using a multitube flow microreactor system. Measurements were made on small catalyst

particles (0.6-1.0 mm) to eliminate any diffusion limitations. After reduction, catalyst performance was measured at an operating pressure of 25 bar, a temperature of 217 °C, and using a mixed $CO/CO_2/H_2/H_2O$ feed with a steam:gas ratio of 0.5 (i.e. $H_2O:(CO+CO_2+H_2)$). CO conversion data was determined by on-line infra-red analysis. All catalyst activities were measured relative to a "standard" low temperature WGS catalyst. Methanol levels in the condensate were determined by gas chromatography and again ratioed to that of a standard catalyst.

3.4.1 - Promotion Procedure

It was intended to promote *Catalyst 2* with a common mole % of each alkali; 2.12 x 10^{-4} moles alkali/g catalyst which is equivalent to a final level on the sample of 1 wt % K_2O, i.e. promotion with other alkali salts will change the wt % value according to the alkali molecular weight. The calcined catalysts were promoted with sodium, potassium and caesium carbonates, and lithium nitrate (owing to the low solubility of lithium carbonate) by impregnation according to the following method: "water pick-up" - the amount of water taken up by the dry, calcined catalyst - was first determined by soaking a quantity of the catalyst in water for 20 min. Using this information, the concentration of alkali salt solution needed to promote the catalyst to the required level was prepared (e.g. in this case 0.078 mol dm^{-3} for potassium carbonate). Enough of this solution was added to the calcined catalyst while mixing to produce a thick paste with a slight excess of solution. This paste was soaked for 20 min then dried at 110 °C for 6 h followed by recalcination at 300 °C for 1.5 h.

Table 3.3 presents the final wt % values for the different alkali metal salts, where it can be seen that levels are largely as expected apart from for lithium oxide. After the percentage of alkali present was measured by ICP-MS, this value was then converted to the wt % that would result if the alkali was present as its oxide, M_2O (by convention at ICI Katalco). The intention is not to indicate that the alkalis are present as oxides, though.

Table 3.3. *Alkali levels on Catalyst 2, according to ICP-MS (± 4 %).*

Alkali	Expected wt %	Actual wt %
Li_2O	0.36	0.14
Na_2O	0.75	0.80
K_2O	1.16	1.26
Cs_2O	3.45	3.38

As mentioned in section 3.4, this promotion procedure was also followed at The University of Edinburgh for *Catalyst 1*, but this time only potassium carbonate was used as a promoter, and instead the level of promotion was varied: catalysts with a final wt % of promoter of 0.02, 0.05, 0.2 and 1 were prepared (again, on a loss free basis, as discussed in section 3.3.3). Since the above method was followed exactly, only the 1 wt % catalyst was analysed at ICI Katalco to confirm the accuracy of the method, and the level was found to be 0.98 %. The potential coverage of potassium on copper was calculated for the 1 wt % sample to be approximately 1.2 of a monolayer, assuming spherical atoms, that all the potassium is located on the copper component of the sample, and that it is evenly "spread" and not in the form of 3-dimensional clusters or islands. It is appreciated that some of these assumptions are unlikely, so this value is only intended to give an impression of the level of alkali present.

It seems worthwhile, at this point, to make it clear that during the remainder of this thesis, where the promotion of supported catalysts is being considered, the terms "alkali" and "alkali ion" will be used interchangeably for the sake of brevity: that is, it is appreciated that the promoter will be in the form of an ion.

3.4.2 - The Effects of Promotion

The effects of promotion on *Catalyst 2* in terms of copper surface area, total surface area, relative activity for the WGS reaction, and relative methanol level in the condensate can be seen in Table 3.4. In the last row, "selectivity", represents the ratio of the relative methanol level to the relative WGS activity, which is a more meaningful quantity when such a large decrease in activity is seen on promotion. Essentially, a decrease in this value represents a relative decrease in the selectivity of the reaction towards methanol. These data, apart from total surface area, are also shown graphically in Fig. 3.10.

Table 3.4. *The effect of different alkali carbonates on Catalyst 2.*

Analysis	none	Li	Na	K	Cs
Copper Surface Area (m^2g^{-1}) (RFC)	14.6	12.3	9.80	8.91	7.72
Total Surface Area (m^2g^{-1}) (BET)	141	-	-	72	-
Relative Activity	1.11	0.53	0.39	0.48	0.52
Relative Methanol Level	1.08	0.51	0.21	0.19	0.11
Selectivity	0.97	0.96	0.54	0.40	0.21

A loss in copper surface area is observed on promotion (between around 15 and 50 % depending on the alkali). BET total surface area measurements show a similar trend, dropping from 141 to 72 m^2g^{-1} in the case of potassium promotion. In line with these results, a decrease in WGS activity is also seen, which is anticipated. However, a favourable increase in selectivity for the WGS reaction is observed on promotion, compared to the undesirable methanol forming reaction. This effect is greatest for K and Cs. The maximum promotional effect of K, followed by Cs, has been observed previously in a study on the enhancement of CO hydrogenation over unsupported copper [59]. Lang *et al.* [19] have, in a theoretical study, rationalised similar observations in surface science studies in terms an electronic effect; while the amount of charge transferred to the metal substrate by various alkali metals is similar, the distance over which charge is transferred is larger for the heavier ones. Just how

relevant this is for the case of supported catalysts in the presence of an alkali *ion* is debatable, however.

The topic of how the promoter achieves its results will be taken no further in this chapter: the purpose of these studies was to illustrate the effect of alkali promotion on the selectivity of the catalyst in the context of reaction conditions. This has been achieved, and the elucidation of the actual role of the promoter will be undertaken by DRIFTS.

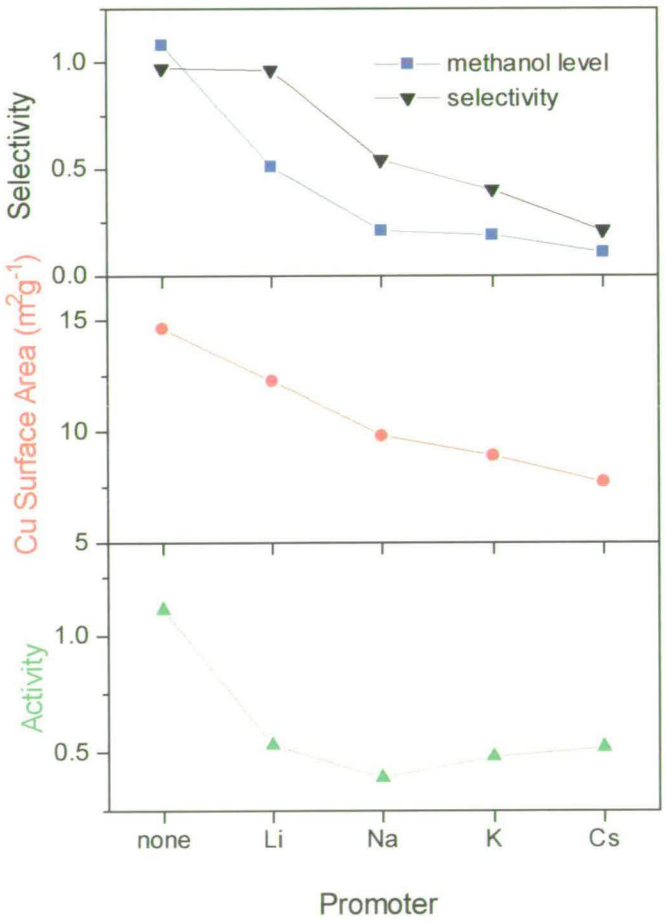

Fig. 3.10. *The effect of different alkali carbonates on the copper surface area, relative activity for the WGS reaction, relative methanol level in the condensate, and selectivity towards methanol formation for Catalyst 2.*

3.5 - Preliminary DRIFTS Experiments - Nature of the Catalyst

In order to understand better the characteristics of the catalyst under study before DRIFTS adsorption experiments are discussed, the response of the single beam spectrum to a change in different parameters will be considered.

Some standard single beam spectra following reduction of *Catalyst 1* can be seen in Fig. 3.11. The overall shape of the spectrum is due to the spectrum of the source modified by the transmission characteristics of the beamsplitter and the response characteristics of the detector. This profile is then modified further by the absorbance due to the sample: a broad feature centred at about 3760 cm^{-1} suggests that the sample is not completely dry, while apparent noise in this region and another two areas either side of about 1600 cm^{-1} are due to the rotational-fine structure of atmospheric water. Bands around 2900 cm^{-1}, indicative of C-H stretching vibrations, are due to hydrocarbons, most likely as a result of small amounts of contaminating grease on the DRIFTS cell windows or spectrometer optics. A doublet with bands at 2360 and 2338 cm^{-1} can be assigned to atmospheric CO_2 in the spectrometer. The frequency limit below which no information can be obtained is dictated by the position at which intense metal-oxygen absorption bands occur - in this case, the "cut-off" is at about 960 cm^{-1}.

The two intense features positioned at 1550 and 1407 cm^{-1} and a possible weak shoulder at 1070 cm^{-1} are likely to be due to some vibration of the bulk solid. Similar bands have been attributed to carbonates, following the calcination of synthetic Mg-Al hydrotalcites [51]. During that study, intense bands were still seen at 1518 and 1383 cm^{-1} even after calcination at 800 °C.

Another important observation from Fig. 3.11 is that the overall intensity of the single beam spectrum increases with time. This was most pronounced initially, and its effects were minimised by allowing the catalyst to sit at room temperature for at

least 1.5 h while the spectrometer was being purged. However, even then this effect caused problems which resulted from the continually changing baseline relative to the background recorded at the start of an experiment. On ratio-ing a spectrum taken during the experiment against the background taken before the experiment, especially intense features were accentuated which lead to miscancellation. This is illustrated in Fig. 3.12 where single beam spectra were scanned every 4 min while helium was passed over the catalyst and ratioed against a background spectrum taken at 0 min. It is suggested that this behaviour could be due to changes in packing of the catalyst in the flowing gas; as the gas stream is changed from 50 cm^3/min hydrogen to 20 cm^3/min helium, it could conceivably take some time for the catalyst particles to adjust into their ideal positions, over which time the resulting single beam would vary.

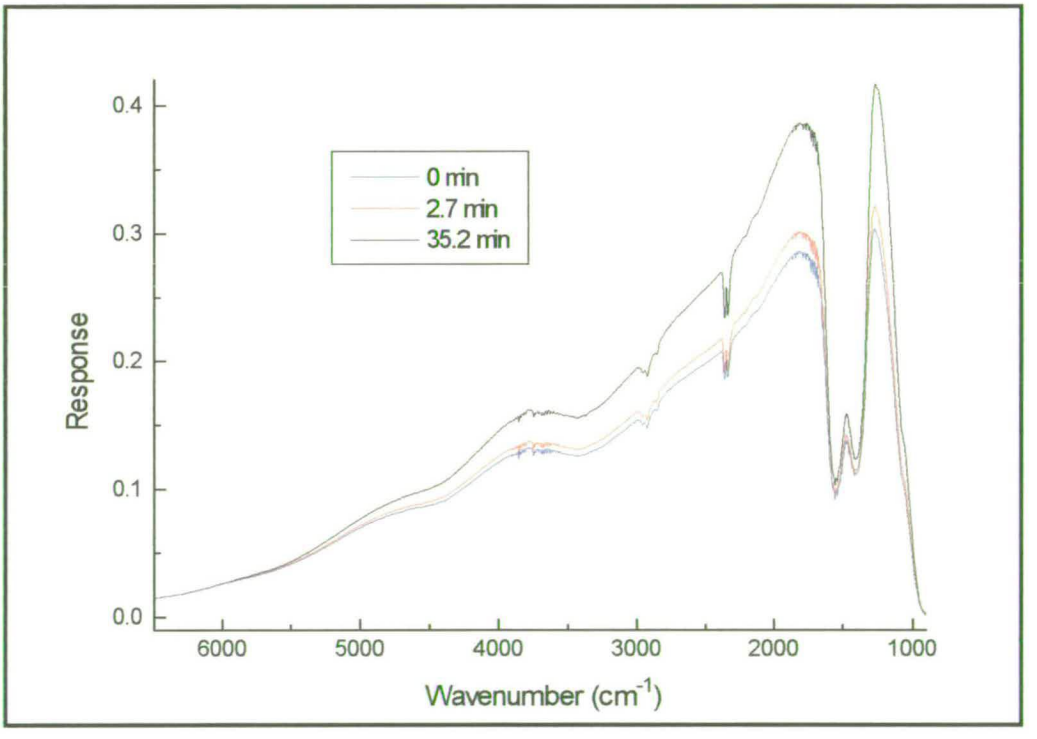

Fig. 3.11. *Typical single beam spectra for unpromoted Catalyst 1- variation in signal intensity with respect to time at room temperature.*

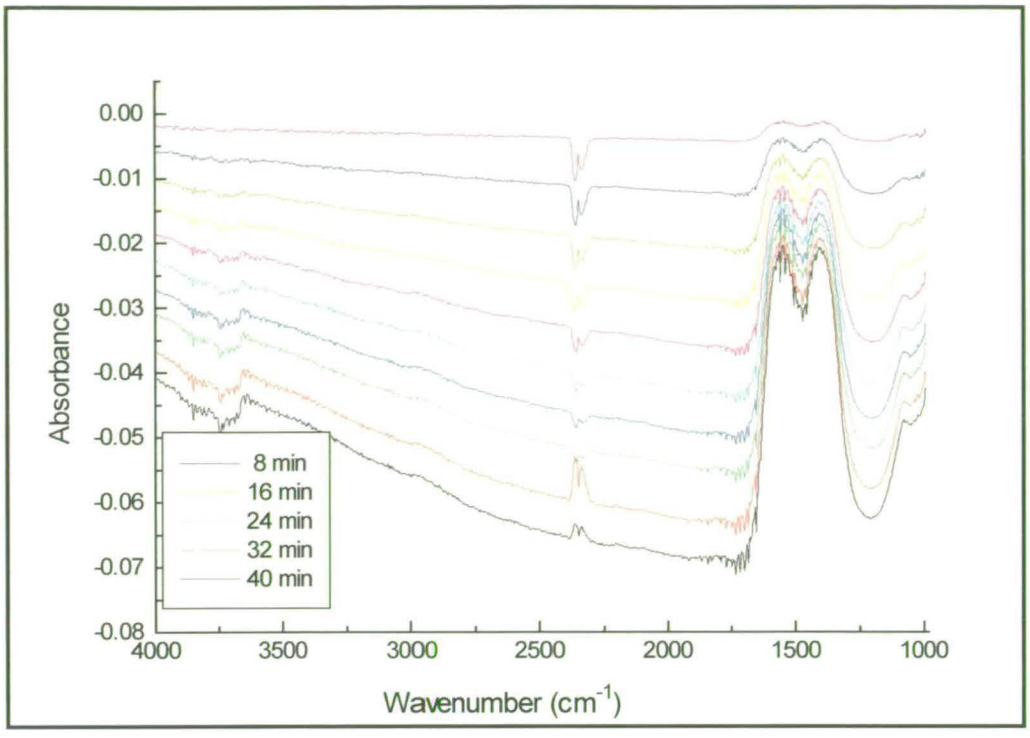

Fig. 3.12. *Build-up of "miscancellation features" for Catalyst 1 under flowing helium. Spectra were scanned every 4 min and ratioed against a background taken at time = 0 min.*

Fig. 3.13 illustrates the effect of temperature on the single beam profile. An initial increase in the intensity is seen at room temperature, followed by a decrease at high temperature of 47 % which could be as a result of a physical change in the sample (e.g. a loss in surface area due to sintering). However, on inspection of a spectrum taken at room temperature subsequent to TPD, a decrease in the overall intensity of the single beam spectrum of only 10 % was seen. Therefore, an alternative explanation must be proposed for the remaining decrease at high temperature: it has been observed previously that as the temperature of the sample post is raised, at high temperatures infra-red radiation emitted from it can be detected by the MCT detector. Hamadeh *et al.* [60] has suggested that this can decrease the amplitude of the original interferogram by up to 50 % at 300 °C. Marshall has found the decrease to be closer to 25 % in a study using the same DRIFTS cell as that in this study [50], but with a different spectrometer (*Digilab FTS-40*). Thus, it appears that either the *FTS-6000* used in this study was more sensitive to infra-red radiation emitted by the hot sample

post, or that, more likely, the original signal from the sample in Marshall's study was more intense, meaning that radiation from the sample post had less impact overall.

The decrease in single beam intensity with increasing temperature has been found to cause problems during temperature programmed desorption experiments. Intense negative features at the same position as those seen as a result of flowing helium in Fig. 3.12 are observed to grow in, as well as a sharply sloping negative baseline at low wavenumber. The origin of these miscancellation features can be appreciated by imagining the result of ratio-ing the spectrum taken at 308 °C in Fig. 3.13 against one taken at room temperature as a background.

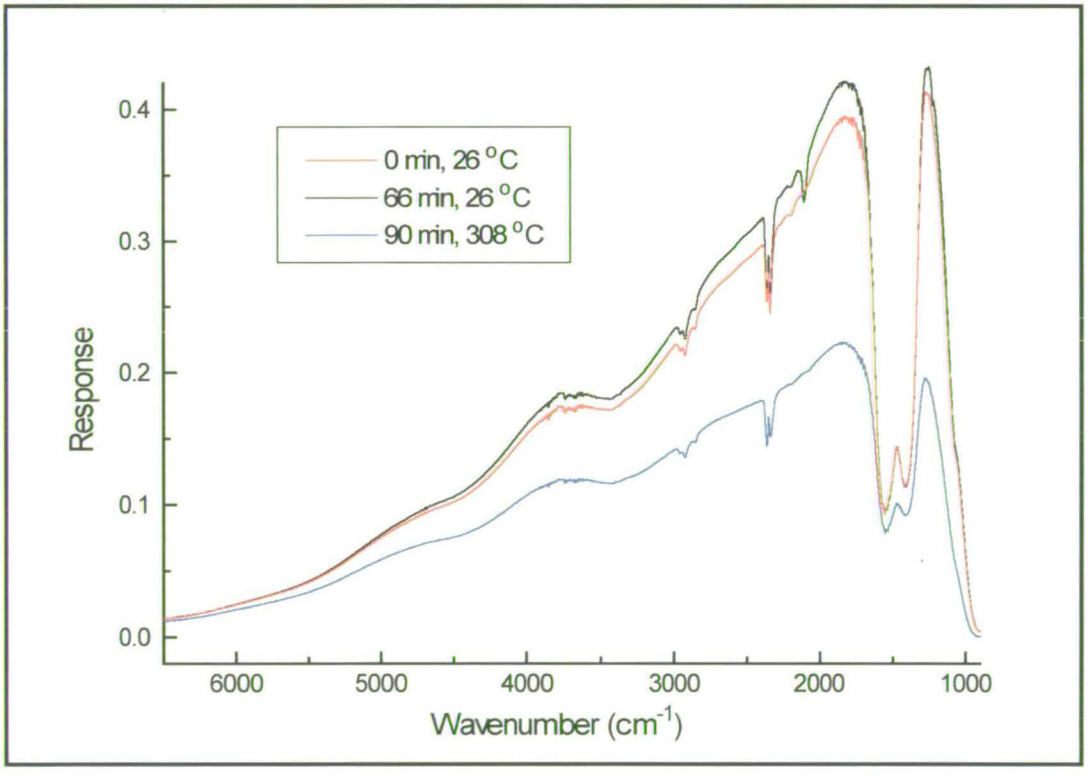

Fig. 3.13. *Variation in the single beam spectrum with respect to temperature for Catalyst 1 during a TPD experiment.*

Finally, the effect of promotion on the single beam spectrum is shown in Fig. 3.14, where it is clear that the intensity for the promoted sample is less than that for the unpromoted. Implicit in this finding is that the physical nature of the catalyst has

been changed on promotion, and this is also borne out by a slight change in the cut-off frequency for the two samples and the variation in their physical appearance - the calcined promoted sample is more "granular"-looking. The decrease in single beam intensity could originate in the way the infra-red radiation is interacting with the promoted sample. It is possible that, on promotion, the sample becomes more absorbing of radiation, and as a result less is diffusely reflected and specular reflectance becomes more important.

Throughout the DRIFTS experiments in this study, it was found that the signal to noise ratio was inferior for the promoted sample, owing to the decreased signal initially. Miscancellation features were often less severe than for the unpromoted catalyst, which could either be as a result of a change in the way the sample adjusts in the varying gas flowrate or simply as a result of the ratio of one low signal against another leading to smaller miscancellation features.

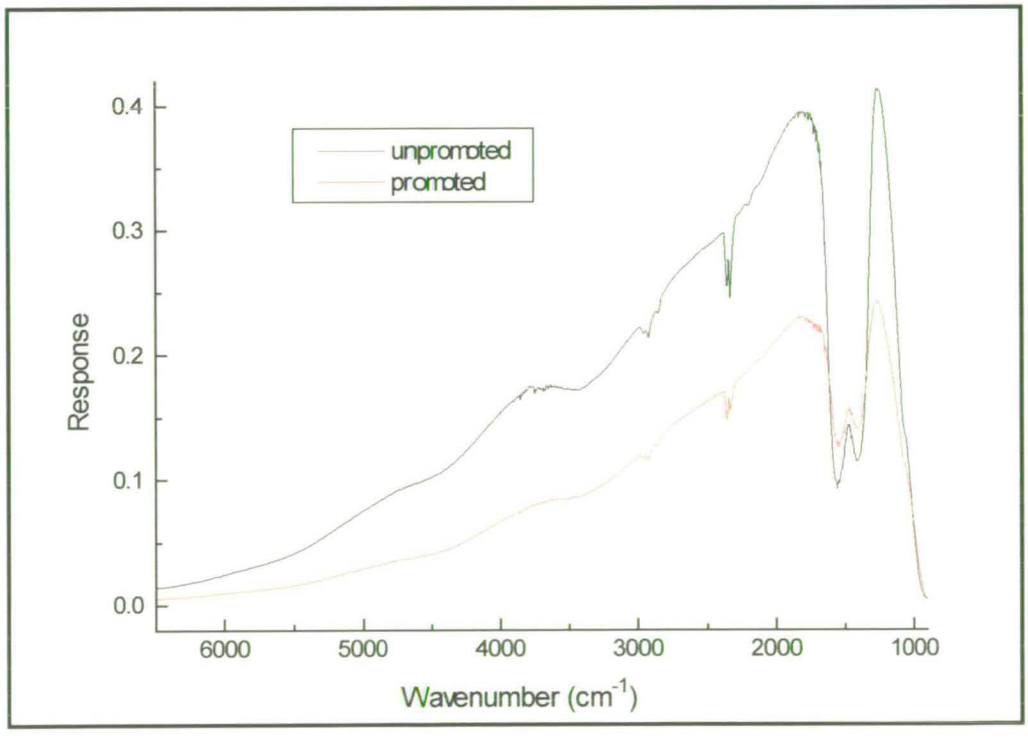

Fig. 3.14. *Effect of promotion on the single beam spectrum*

Chapter 4 - Determination of the Degree of Catalyst Reduction Using CO Adsorption

4.1 - Introduction

Extensive investigations have been made during this study using CO as a probe molecule. In this chapter, the degree of catalyst reduction will be investigated by examining the CO-Cu interaction following CO adsorption. Characterisation of the type of copper planes present in the catalyst will be attempted, drawing comparisons with the wealth of information in the literature on CO adsorption on copper single crystals and other supported catalysts. This study is also valuable because CO takes part in the WGS reaction.

As was detailed in Chapter 2, prior to adsorption experiments, the catalyst was "activated"; the purpose of such a procedure is to reduce the copper component to Cu^0, thus making it active for the adsorption of the probe molecule (e.g. CO). Bowker *et al.* have reported the difficulty of completely reducing the copper component of $Cu/ZnO/Al_2O_3$-type catalysts [61]. Indeed, early on in this study, difficulty was experienced in obtaining a completely reduced catalyst. In addition to this, copper catalysts are known to be susceptible towards thermal sintering, whereby an agglomeration of crystallites occurs leading to a severely reduced copper area and activity [1]. This occurs as a consequence of the exothermicity of the reduction process (reaction 4.1) coupled with the relatively high copper loading in the catalysts.

$$CuO + H_2 \rightarrow Cu + H_2O \qquad \Delta H = -80.8 \text{ kJ/mol} \qquad \textit{reaction 4.1}$$

In view of the temperamental nature of the catalyst, an exploratory study was undertaken in order to optimise the pre-treatment conditions - i.e. to determine those which would ideally generate a completely reduced sample with no loss in copper surface area. It must be stressed at this point that the study presented below is not fully systematic - nor was it intended to be so. To a certain extent, obvious trends became apparent through experience, forgoing the need to carry out all the combinations of the various parameters involved in the reduction method, which are listed below:

- reduction gas composition (e.g. 2 % H_2/N_2 or 100 % H_2)
- gas flowrate,
- rate of temperature ramp,
- length of time at T_{max} (usually 230 °C),
- optional degassing at high temperature (300 °C)

The study presented below builds up a picture of the nature of the catalyst's copper component and the way it responds to changes in pre-treatment conditions. To aid the assignment of spectra resulting from CO adsorption, a summary of the literature in the area is first presented, and this information is collated in Table 4.1.

4.1.1 - The Metal-CO Interaction

The chemisorption of CO on metals has been interpreted with reference to metal carbonyl compounds for many years [e.g. 34-36] and has been discussed at length by Little [62]. In accordance with the traditional description for the bonding in such compounds, CO bonds to a metal surface *via* a σ-bond between the filled CO 5σ-orbital and unfilled metal d-orbitals. The metal then "back-donates" from filled d-orbitals to the vacant CO 2π*-orbital, as shown schematically in Fig. 4.1. The latter interaction decreases the strength of the C-O bond and thus shifts the frequency of the υ_{CO} stretching vibration downwards relative to the value for gaseous CO, 2143 cm^{-1}.

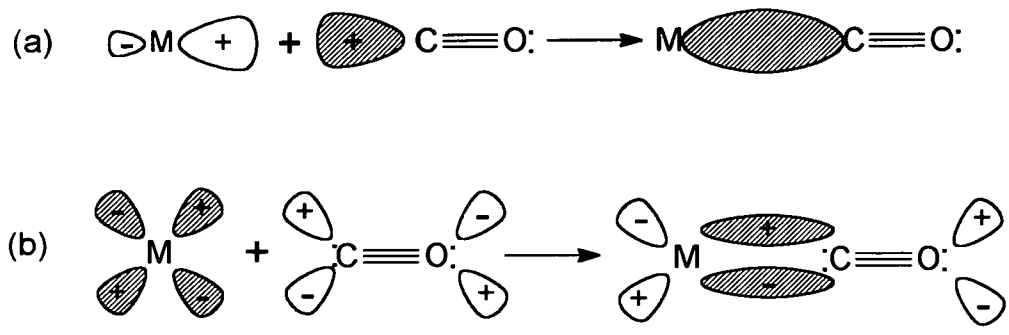

Fig. 4.1. *Schematic diagram illustrating the interaction of CO with a metal surface, where (a) depicts the formation of a σ-bond and (b) illustrates the formation of a π-bond. Shaded regions represent filled orbitals.*

In 1978, Sheppard and Nguyen comprehensively reviewed the information to date on the chemisorption of CO on the surfaces of metal catalysts, as studied by infra-red spectroscopy [40]. They developed a general strategy for the interpretation of the arising infra-red absorption bands - the region from 2200 to about 2130 cm^{-1} could, they believed, be assigned to CO adsorbed on incompletely reduced salts, or metals that had become oxidised. The region from about 2130 to 2000 cm^{-1} could be attributed to CO adsorbed linearly on the metal surface, i.e. bonding with one metal at an on-top site, while the regions from 2000 to about 1880 cm^{-1}, and 1880 to 1650 cm^{-1} were assigned to CO bridging two or three metal atoms, respectively. They remarked, however, that these regions were only an approximate guideline; for instance, in the case of linearly adsorbed CO, the group IB metals Cu, Ag and Au gave bands at considerably higher frequencies than the group VIII metals.

4.1.2 - Infra-Red Studies of CO Adsorption on Copper

Sheppard and Nguyen's review [40], which included a comparison between results on copper single crystals, films and supported metal particles, concluded that copper invariably gave rise to linearly adsorbed CO.

Much of their data came from work by Pritchard *et al.* in 1975 [41], who used RAIRS of single crystals to gain reference data for the interpretation of transmission infra-red spectra on more complex systems such as supported metal particles. They obtained CO stretching bands at saturation coverage and -196 °C for low index crystals as follows: Cu(100) at 2088 cm^{-1}, Cu(111) at 2070 cm^{-1}, and Cu(110) at 2094 cm^{-1}. Unlike the (100) and (111) planes, which had only one band at low coverage, the (110) plane had two, at 2088 and 2104 cm^{-1} which blended together to form one at higher coverage. The same results for this plane were found at -78 °C. Fig. 4.2 illustrates the crystal structures for the (110), (100) and (111) face-centred cubic (fcc) surfaces.

Pritchard *et al.* [41] also studied the high index planes (211), (311) and (755) at -196 °C, which can be thought of as 3-, 1-, and 6-atom rows, respectively, of the (111) type, forming terraces separated by 1-atom steps of the (100) type. The (755) plane is given as an example in Fig. 4.3. For the (211) face, at low coverages two distinct bands were seen at 2095 and 2109 cm^{-1} which blended together to form a band at 2100 cm^{-1}. A second stage was seen, whereupon, at saturation, a symmetric narrow band at 2110 cm^{-1} was formed. Likewise, for the (311) plane, two bands were observed at low coverage, this time at 2093 and 2109 cm^{-1}. On increasing coverage, the two bands grew closer together, but were still distinct from one another at saturation, with frequencies of 2093 and 2103 cm^{-1}. For the (755) plane, a main band (2112 cm^{-1}) was accompanied by a weak side band (2093 cm^{-1}) at low coverage. At saturation the main band had shifted to 2106 cm^{-1} while the side band, found now at 2073 cm^{-1}, was very weak indeed.

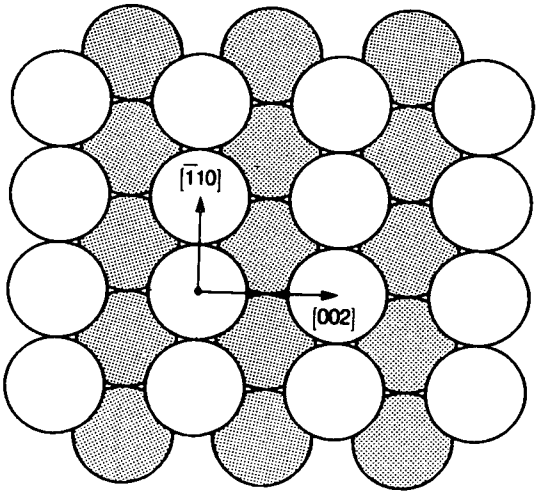

fcc (110)

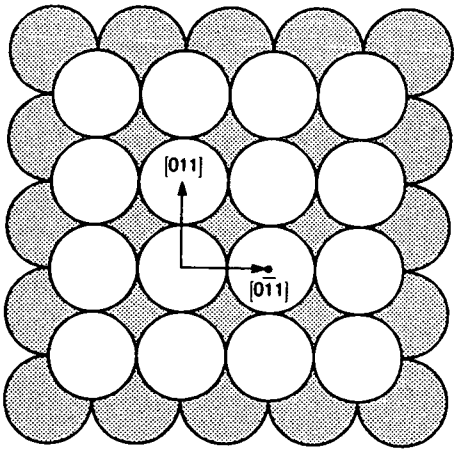

fcc (100)

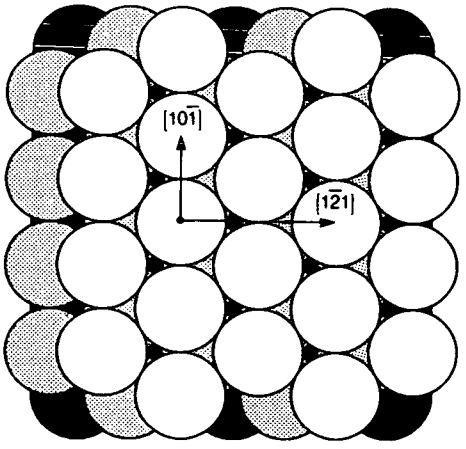

fcc (111)

Fig. 4.2. *Top and side views of the face-centred cubic crystal surfaces: (a) (110), (b) (100), and (c) (111), taken from reference [63].*

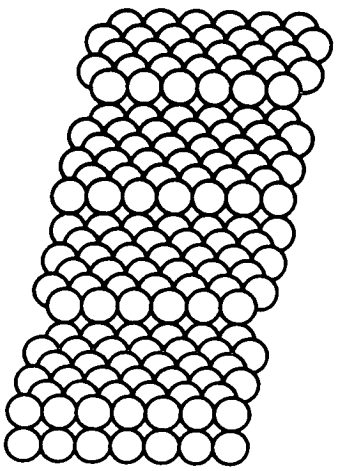

Fig. 4.3. *The (755) surface for a face-centred cubic crystal taken from reference [63]*

As shown by Pritchard *et al.* above, the weak chemisorption of CO by copper is reversible on evacuation at room temperature, and therefore, their experiments were carried out at -196 °C. More recently, it has been possible to carry out RAIRS experiments at higher pressures of CO and at room temperature. One such study, also by Pritchard and co-workers, [45] made a comparison of the adsorption of CO on Cu(100) at -153 °C under ultra-high vacuum (UHV) conditions with that at 27 °C at about 20 Torr of CO, which resulted in a shift of the CO stretching band from 2086 to 2076 cm^{-1}. These type of experiments go some way to bridging the "pressure gap" which was discussed in Chapter 1.

On applying their results for copper single crystals to supported metals Pritchard *et al.* [41] revealed effects which correlated with copper loading, support and reduction conditions. A Cu/SiO_2 sample was studied: for a 5% Cu loaded sample, a peak centred at 2113 cm^{-1} was seen after reduction at 140 °C, while after reduction at 350 °C, the peak shifted to 2103 cm^{-1}. Similarly for a 10% Cu loaded sample, a peak centred at 2220 cm^{-1} was seen after reduction at 140 °C, while after reduction at 350 °C, the peak shifted to 2105 cm^{-1}. A slight difference in peak frequency was noted for a 5% Cu/Al_2O_3 sample; a shift from 2124 to 2108 cm^{-1} was seen on increasing the reduction temperature. However for magnesia supported samples, quite

different results were obtained. Samples were already reduced by 140 °C, and the CO stretching frequency was found to be much lower than for other samples - 2081 cm^{-1}. Thus, it can be concluded from this study that an increase in reduction temperature results in a shift in CO stretching frequency to a lower wavenumber and an increase in copper loading results in a slight increase in wavenumber. While using silica and alumina as supports yields similar results, magnesia as a support appears to lower the CO frequency markedly. Finally, they concluded that there seems to be a distinct lack of low index planes present in the supported samples, apart from that supported on magnesia; this difference was attributed to magnesia's ability to promote epitaxial growth of the low index orientated copper planes. It was assumed that, while the results do not necessarily prove that any particular high index plane was present on the supported metals, it is likely that a wide variety of step frequencies (terrace widths) and orientations may be involved.

Results reported for studies on evaporated copper films by Pritchard *et al.* [41] form a valuable link between the single crystal and supported metal experiments. The reflection-absorption experiments carried out on polycrystalline copper deposited on different subtrates (glass, alumina and oxidised magnesium) found CO stretching frequencies which mirrored those found for the supported samples (2102, 2106 and 2079-2085 cm^{-1} respectively for the different substrates), suggesting the abundance of low index planes in the presence of the magnesia substrate and virtual absence in the other samples. Overall, they felt that their results were a justification of the use of reflection-absorption spectra from single crystals in the analysis of transmission spectra from supported metals.

The results found on films and supported catalysts in Sheppard and Nguyen's review generally echo those found by Pritchard. On evaporated copper films, they found a band centred on average at 2104 $\pm$ 2 cm^{-1} and noted again that this was a "high index-like" frequency. One particular study therein [64] commented how, on exposure to O_2, the main band at 2103 cm^{-1} on the clean film shifted to 2113 cm^{-1}, while a second band grew in at 2135 cm^{-1}. The general view for supported metal

samples in the review is that results are numerous, and the CO bands observed are variable in wavenumber. It was found that values at around 2120 cm^{-1} are typical of less well-reduced samples, and that more complete reduction gives frequencies in the region of 2110-2100 cm^{-1}, with a mean value of 2105 cm^{-1}. Bands below 2100 cm^{-1} were uncommon but typical of methods where very high reduction temperatures had been used, and of samples supported on magnesia, as mentioned above. Bands between 2140-2110 cm^{-1} were believed to be due to partially oxidised copper, for instance Pearce [65] assigned a band at 2130 cm^{-1} as being due to CO on Cu_2O and one at 2215 cm^{-1} to CuO.

Since the publication of Sheppard and Nguyen's review, several other studies have been published on the adsorption of CO on copper, with a view to determining the nature of the copper planes present, the effect of reduction conditions on the final spectrum, and the effect of the support. Indeed, in 1980 de Jong *et al.* [66] studied Cu/SiO_2 samples with the aim of "discriminating between the influence of the surface structure of the metal particles and the degree of reduction". They found that the position of the CO stretching frequency was very sensitive to the preparation route and pre-treatment conditions of the catalyst. However, conversely to the results discussed so far they found that one catalyst showed a peak which shifted from 2104 to 2139 cm^{-1} on prolonged reduction. By comparison with work by Moskovits and Hulse [67], they attributed this, not to the degree of reduction, but to the presence of CO bonded to an isolated Cu atom or a Cu atom strongly interacting only with a small number of other Cu atoms. They believed this could occur because of the presence of small, spherical Cu crystallites in their samples which could expose surfaces with many protruding Cu atoms or small clusters of Cu atoms. This species, found at 2139 cm^{-1}, is apparently thermodynamically preferred and is converted on prolonged reduction from a structure with more extended stepped surfaces i.e. the kinetically established species, flat crystallites (2104 cm^{-1}). Another catalyst prepared *via* a different route showed a shift from 2146 to 2129 cm^{-1}, again on severe reduction. This was put down to the formation of large copper particles *via* sintering.

Bocuzzi *et al.* [68], in a study of Cu/ZnO, returned to the proposal from Pritchard *et al.* of the relationship between the CO stretching frequency and the degree of reduction of the catalyst. Bands at 2098 and 2070 cm^{-1} were found on exposure of the reduced catalyst to CO at 27 °C and were assigned as being due to CO adsorbed on stepped close-packed sites, and open, corner or edge sites, respectively. These bands shifted to 2116 and 2143 cm^{-1} respectively when the reduced sample was first oxidised with O_2 before CO exposure, and this was attributed to the copper species being directly bonded to adsorbed oxygen. They did not, however, specify what oxidation state the copper was then in. Another band seen on a less well-reduced catalyst at -196 °C at 2172 cm^{-1} was attributed to a carbonyl species on a cationic site, specifically Cu^{2+}.

In another study of a Cu/SiO_2 sample, Kohler *et al.* [69] looked at the effects of reduction on the ensuing CO spectrum. On an "unreduced" sample they found bands at 2127-2132 and 2199 cm^{-1}, which they interpreted as being due to CO adsorbed on small CuO particles, and CO on isolated Cu^{2+} ions incorporated in the silica surface, respectively. A band was observed at 2090-2113 cm^{-1} on the reduced sample, which was attributed to CO adsorbed on very small metal clusters (1-5 nm) and was dependent upon surface coverage and copper loading. They suggested that the observed range from 2090 to 2113 cm^{-1} indicated the presence of steps and terraces similar to low index Cu planes in very small particles (1-2 nm) and the presence of similar higher index planes on larger clusters (2-5 nm). A band at 2175 cm^{-1} which was unaffected by copper loading was assumed to be due to CO bound to isolated Cu^{+} ions.

In addition to the many studies on supported copper in the literature, there is also a wealth of information regarding the adsorption of CO on copper oxide samples. This might be expected to clarify the confusion around the oxidation state of the copper when it is not fully reduced. For instance, London and Bell [70] attributed a band at 2140 cm^{-1} to CO adsorbed on CuO in a study of CuO/SiO_2. A study by de Jong *et al.* [71] dealing with the room temperature adsorption of CO on CuO/SiO_2,

found bands at 2136 and 2204 cm^{-1} which were ascribed to CO on CuO and CO on isolated Cu^{2+} incorporated in the SiO_2 surface, respectively.

Hierl *et al.* [72] studied the reduction behaviour of calcined CuO/Al_2O_3 samples. Copper aluminate was formed by high temperature calcination (800 °C, 15 h). On an unreduced sample, bands observed at 2118 and 2135 cm^{-1} were assigned to CO bound to coordinatively unsaturated Cu^{2+} in the aluminate surface, in tetrahedral and octahedral sites respectively. On heating under vacuum, bands at 2125 and 2170 cm^{-1} formed, assigned as being due to CO coordinated to Cu^{+} in the form of disperse Cu_2O supported on Al_2O_3 and $Cu\text{-}CO^{+}$, respectively, the latter being easily removed on evacuation. Reduction in hydrogen resulted in the appearance of a band at 2097 cm^{-1}, attributed to CO on copper metal. The 2118 and 2135 cm^{-1} bands remained, although at a decreased intensity, indicating that the sample was not completely reduced.

A study carried out by Hollins and Pritchard [73] looked at the adsorption of CO on oxidised copper single crystals. An oxidised Cu(111) crystal showed bands at 2100 and 2117 cm^{-1} at low coverage of CO. At saturation, the main band shifted to 2115 cm^{-1} while the low frequency band had become merely a shoulder. These features were explained by the presence of copper atoms not bonded directly to oxygen - consequently their frequencies were little changed from the reduced samples. The doublet structure was explained by the presence of nothing more specific than "two slightly different sites on the surface". A third very weak feature was also evident at high coverages, at 2140 cm^{-1}. Oxidised Cu(110) was studied (O(2 x 1) surface). A similar feature to the Cu(111) low frequency band was seen at 2100 cm^{-1}, but a main band was exhibited at 2140 cm^{-1}, this time with high intensity. Thus, this band was attributed to the oxidation of copper which was previously in a stepped site (Cu(110) being considered as an extreme form of a stepped surface and Cu(111) assumed as having several steps or defects prior to oxidation).

There are many more examples of related work in the literature [e.g. 74, 75] and most recently by Millar *et al.* [76, 77], which, arguably, add little more to the emerging pattern. It can be seen, however, as Sheppard and Nguyen commented [40], that results reported are diverse. The results presented especially show a wide number of frequencies for the Cu^{+} and Cu^{2+} species, and interpretations thereof are varied. Many studies do not even specify the oxidation state of the oxidised copper. Findings are collated in Table 4.1, below, starting with single crystal reference data, followed by films and then supported metals.

Table 4.1. *Selected infra-red results from the literature for CO adsorbed on copper.*

System	Frequency at Saturation (cm^{-1})	Species to Which CO Adsorbed	Ref.	Comment
Cu(100)	2088	-	[41]	
Cu(111)	2070	-	[41]	
Cu(110)	2094	-	[41]	
Cu(211)	2110	-	[41]	
Cu(311)	2093, 2103	-	[41]	
Cu(755)	2073, 2106	-	[41]	
oxidised Cu(111)	2115	Cu not bonded directly to oxygen	[73]	
oxidised Cu(110)	2110	Cu not bonded directly to oxygen	[73]	
	2140	oxidised "stepped site"	[73]	
Cu film	2103	-	[64]	
	2113, 2135	"copper oxide"	[64]	on exposure to O_2
Cu films on -glass	2102	high index plane	[41]	
-alumina	2106	high index plane	[41]	
-oxidised Mg	2079-2085	low index plane	[41]	
5% Cu/SiO_2	2113 2103	high index planes	[41]	reduction at: 140 °C reduction at: 350 °C
10% Cu/SiO_2	2220 2105	high index planes	[41]	reduction at: 140 °C reduction at: 350 °C

Table 4.1. *Continued...*

System	Frequency at Saturation (cm^{-1})	Species to which CO Adsorbed	ref.	Comment
5% Cu/Al_2O_3	2124 2108	high index planes high index planes	[41]	reduction at: 140 °C reduction at: 350 °C
Cu/MgO	2081	low index planes	[41]	reduction at: 140 °C
CuO/SiO_2	2140	CuO	[70]	
Cu/SiO_2	2104 2139	flat crystallites small, spherical crystallites	[66]	prolonged reduction
	2129	sintered large particles	[66]	severe reduction
Cu/ZnO	2070 2098	open, corner or edge sites stepped close packed sites	[68]	
	2143 2116	open, corner or edge sites stepped close packed sites	[68]	on exposure to O_2 "
	2172	Cu^{2+}	[68]	"unfinished reduction"
Cu/SiO_2	2127-2132 2199	small CuO particles Cu^{2+} incorporated into SiO_2 surface	[69]	"unreduced sample"
	2090-2113 2175	very small Cu clusters Cu^{+}	[69]	"reduced sample"
CuO/SiO_2	2136 2204	CuO isolated Cu^{2+} in SiO_2 surface	[71]	
CuO/Al_2O_3	2118 2135	Cu^{2+} in aluminate surface "	[72]	"unreduced"
	2125 2170	Cu_2O on Al_2O_3 $Cu\text{-}CO^{+}$	[72]	reduced under vacuum
	2097 2118 2135	Cu^{0}-CO Cu^{2+} in aluminate surface "	[72]	H_2 reduction -sample incompletely reduced

4.2 - CO Adsorption Experiments

Experiments are presented below in groups which investigate the effect of varying the pre-treatment parameters discussed in section 4.1. DRIFTS pulse experiments were carried out using CO as an adsorbate, as detailed in Chapter 2. In every case the sample was reduced under hydrogen and degassed under helium. The details of each set of pre-treatment conditions is given in Tables 4.2 - 4.5. Room temperature (r.t.) can be taken as 25 ± 3 °C.

Final spectra taken at saturation are shown (Fig. 4.4, 4.5, 4.7, 4.8, and 4.9), and each set of spectra is annotated with the total amount of CO to which the samples were exposed. Both *Catalyst 1* and *Catalyst 2* were used, and it was shown in Chapter 3 that although the precursors to these varied slightly, the main difference between the resulting mixed oxides was a slightly higher copper surface area for *Catalyst 1*. Likewise, the only difference between the two samples as determined by the infra-red spectra recorded following CO adsorption was a slightly more intense CO stretching band for *Catalyst 1*.

Results

Example 1: Varying the H_2 Concentration in the Reduction Gas and the Gas Flowrate

Fig. 4.4 shows the effects of changing from a 100% H_2 reduction gas to a 5% H_2/Ar mixture for *Catalyst 1*. It was not possible to maintain a high flowrate with the dilute gas, although the reason for this is unclear. Thus, there is also a change in flowrate between the two experiments. The experimental conditions are shown in Table 4.2.

Table 4.2. *Conditions of pre-treatment for experiments in Example 1.*

Example	Catalyst	Reduction Gas and Flowrate	Reduction Procedure
1a	1	100% H_2 at 30 cm^3/min	Ramped at +8.3 °C/min from r.t. to 240 °C, and held for 3 h. Degassed at 240 °C for 30 min.
1b	1	5% H_2/Ar at 10 cm^3/min	Ramped at +8.0 °C/min from r.t. to 240 °C, and held for 3 h. Degassed at 240 °C for 30 min.

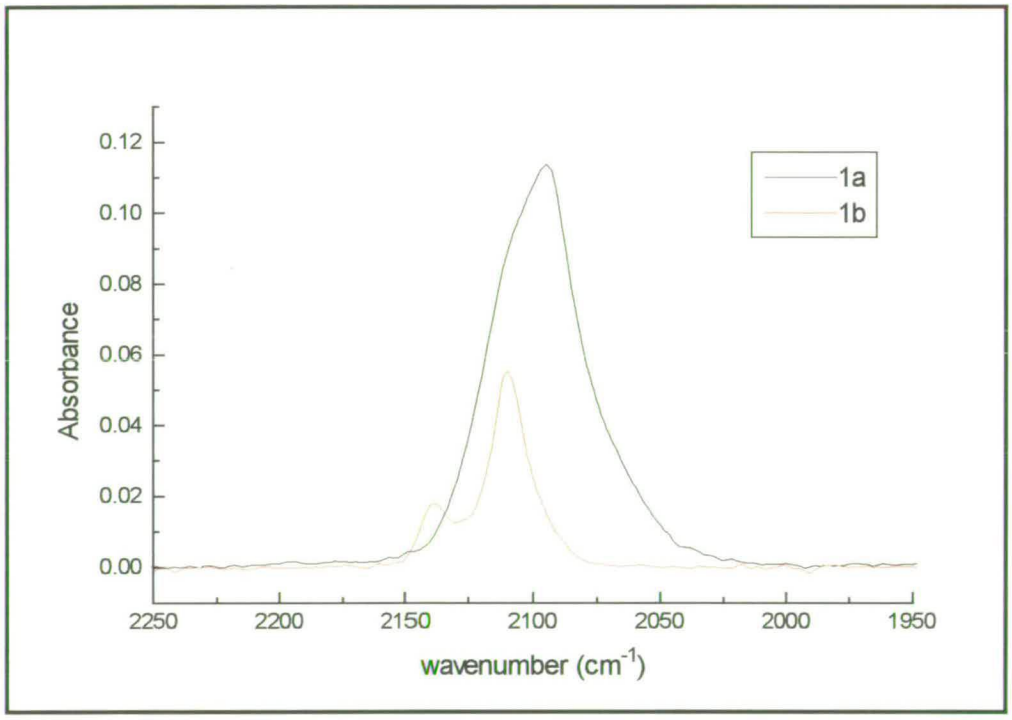

Fig. 4.4. *Example 1 showing effect of a change in the H_2 concentration of reduction gas and gas flowrate on the CO stretching band. Total exposure of CO: 13.4 μmol*

Spectrum 1a in Fig. 4.4, where the sample was subjected to reduction under 100% H_2 and a relatively fast temperature ramp, shows a CO stretching band with maximum absorbance of 0.114 at 2095 cm^{-1}. The band also possesses an asymmetry which could be due to a shoulder at around 2110 cm^{-1}. The FWHM (full width at half maximum) of the band envelope is 40 cm^{-1}.

Spectrum 1b in Fig. 4.4, for which the catalyst was subjected to milder conditions (a dilute reduction gas), has a CO stretching frequency with two maxima - a main band at 2110 cm^{-1} (absorbance 0.0552, FWHM 18cm^{-1}) and a smaller one at 2139 cm^{-1} (absorbance 0.0176)

Example 2: Varying the H_2 Concentration in the Reduction Gas using a Slower Temperature Ramp.

Fig. 4.5 shows the effects of a change in the hydrogen concentration of the reduction gas at a slower temperature ramp than for Example 1. The experimental conditions for the two experiments, where *Catalyst 2* was studied, are shown in Table 4.3.

Table 4.3. *Conditions of pre-treatment for experiments in Example 2.*

Example	Catalyst	Reduction Gas and Flowrate	Reduction Procedure
2a	2	100% H_2 at 50 cm^3/min	Ramped at +6.0 °C/min from r.t. to 140 °C, to 230 °C at +0.8 °C/min, then held for 2 h. Degassed at 230 °C for 30 min.
2b	2	2% H_2/N_2 at 50 cm^3/min	Ramped at +6.8 °C/min from r.t. to 140 °C, to 230 °C at +0.9 °C/min, then held for 2 h. Degassed at 230 °C for 30 min.

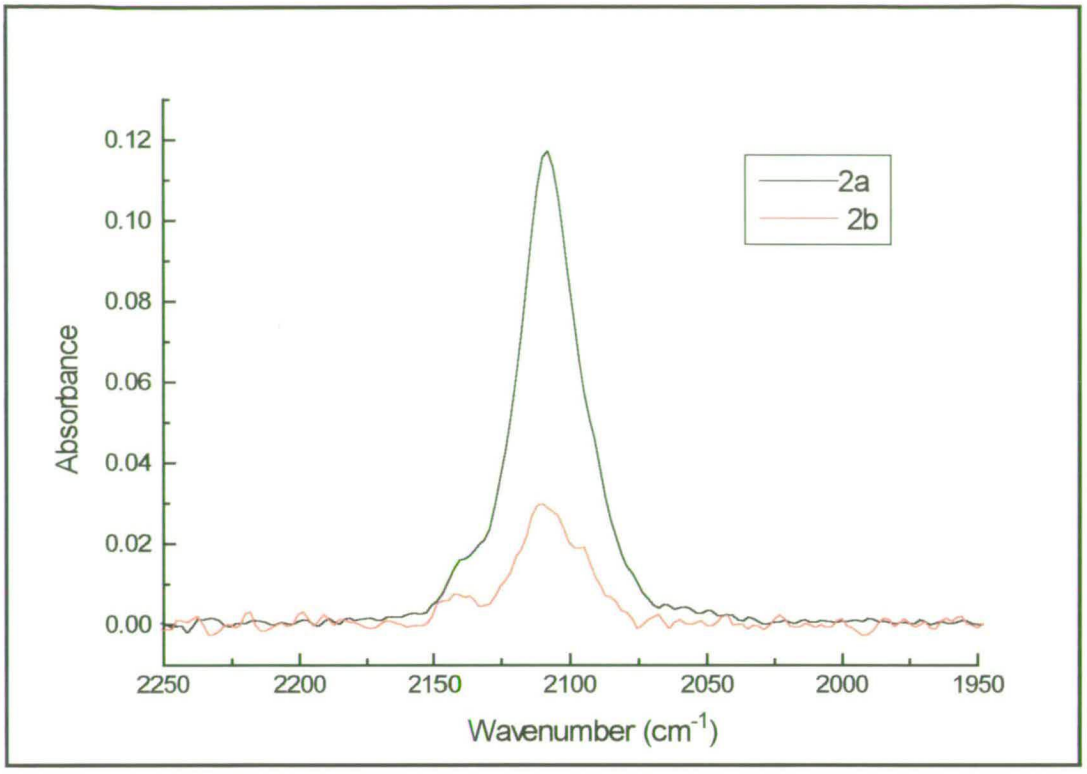

Fig. 4.5. *Example 2 showing the effect of a change in the H_2 concentration of reduction gas on the CO stretching band, at slower temperature ramps. Total exposure of CO: 6.45 μmol.*

Example 2a for *Catalyst 2* (Fig. 4.5) is similar in conditions to Example 1a for *Catalyst 1*, except that in this case the flowrate of hydrogen was higher and the temperature ramp more gentle. The CO stretching region shows a maximum absorbance of 0.117 at 2108 cm^{-1} with a shoulder at 2139 cm^{-1}. There is possibly another very weak shoulder at 2094 cm^{-1}. The FWHM for the main peak is 25 cm^{-1}.

Example 2b (Fig. 4.5) differs from 2a in that a dilute reduction gas was used - 2% H_2/N_2. This time the CO stretching band is much weaker, with a maximum absorbance of 0.0298 at 2110 cm^{-1}. A shoulder is seen at about 2141 cm^{-1} and there is possibly another at 2095 cm^{-1}, but the high level of noise makes it difficult to be certain. The FWHM is 29 cm^{-1}.

Example 3: Effect of a Higher Temperature Degas

During the study of the reduction conditions, it was found by looking at the single beam spectrum of the catalyst that some adsorbed CO existed after catalyst pre-treatment and prior to the CO pulse experiment. It was not possible to ascertain the origin of this preadsorbed CO but it was found that it could be easily removed by an additional degassing period under helium at 300 °C. The preadsorbed CO can be seen desorbing from the catalyst surface in the single beam spectra in Fig. 4.6. The catalyst was degassed at 230 °C for 20 min, then ramped up in temperature gradually to 300 °C, where it was held for 10 min before being allowed to cool back to room temperature. The band at 2089 cm^{-1} present after 20 min degassing at 230 °C gradually decreased in intensity with increasing temperature, and was negligible in size after 10 min at 300 °C. A small amount of adsorbed CO returned at room temperature, as shown by a band at 2100 °C (black spectrum in Fig. 4.6).

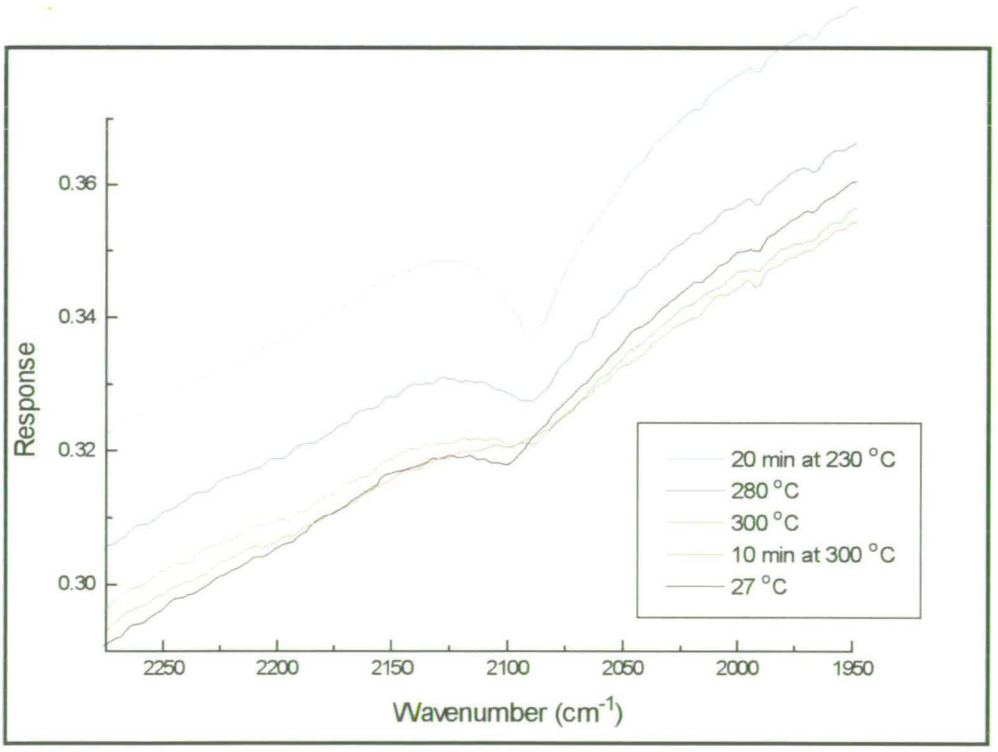

Fig. 4.6. *Removal of preadsorbed CO by degassing in helium at 300 °C.*

Fig. 4.7 shows the effect of this higher temperature degas on the CO spectrum following the pulse experiment. The experimental conditions for the two experiments, where *Catalyst 2* was studied, are shown in Table 4.4. Apart from a difference in the speed of the first temperature ramp (i.e. that to 140 °C), the main difference between the two experiments is the introduction of the high temperature degassing in Example 3b.

Table 4.4. *Conditions of pre-treatment for experiments in Example 3.*

Example	Catalyst	Reduction Gas and Flowrate	Reduction Procedure
3a	2	100% H_2 at 50 cm^3/min	Ramped at +9.6 °C/min from r.t. to 140 °C, then at +0.8 °C/min to 230 °C and held for 2 h. Degassed at 230 °C for 30 min.
3b	2	100% H_2 at 50 cm^3/min	Ramped at +5.2 °C/min from r.t. to 140 °C at, then at +1.3 °C/min to 230 °C and held for 2 h. Degassed at 230 °C for 20 min then to 300 °C at +7.0 °C/min and held for 10 min.

Spectrum 3a (Fig. 4.7), where the sample was reduced under conditions very similar to those for Example 2a, shows a band peaking at 2114 cm^{-1}, absorbance 0.171. A small shoulder is also evident at 2139 cm^{-1}. The FWHM of the main band envelope is 26 cm^{-1}.

Example 3b (Fig. 4.7), which involved degassing at 300 °C, exhibits a band whose maximum absorbance of 0.175 peaks at 2112 cm^{-1} and a prominent shoulder at 2139 cm^{-1}. The FWHM of the main band envelope is 24 cm^{-1}.

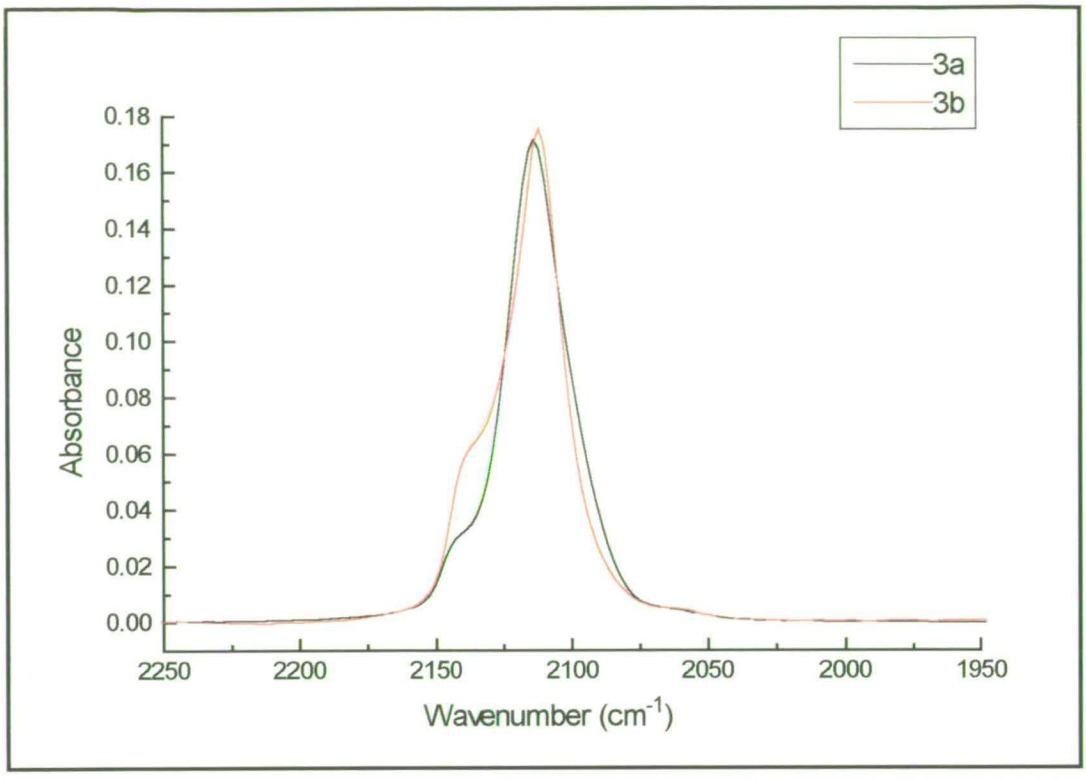

Fig. 4.7. *Example 3 showing effect on the CO stretching band of an additional degas at 300 °C. Total exposure of CO:11.0 μmol.*

Example 4: Final Steps Taken To Determine "Ideal" Conditions For Reduction

Fig. 4.8 shows the spectra in the CO stretching region for three experiments. The conditions for the three experiments, where *Catalyst 1* is studied, are shown in Table 4.5.

Spectrum 4a in Fig. 4.8, where the sample was subjected to reduction under 100% H_2 but a gentle temperature ramp, shows a band peaking at 2112 cm^{-1}, absorbance 0.223. An accompanying shoulder is also evident at 2139 cm^{-1}. The FWHM of the main band envelope is 27 cm^{-1}.

In addition to a slightly more harsh reduction regime, Example 4b's main experimental difference from 4a is the introduction of a new thermocouple (diameter

0.5 instead of 1 mm). This spectrum exhibits a band whose maximum absorbance of 0.0560 peaks at 2094 cm^{-1}. A smaller, but prominent, absorbance can also be seen at 2112 cm^{-1}. The FWHM of the band envelope is 51 cm^{-1}. Finally, Example 4c (Fig. 4.8), which represents conditions similar to those in 4b but with an altered thermocouple position, exhibits a main band at 2114 cm^{-1} with an absorbance of 0.0951 and FWHM of 36 cm^{-1}.

Table 4.5. *Conditions for pre-treatment for experiments in Example 4.*

Example	Catalyst	Reduction Gas and Flowrate	Reduction Procedure
4a	1	100% H_2 at 50 cm^3/min	Ramped at +5.0 °C/min from r.t. to 140 °C and held for 30 min, then to 230 °C at +1.0 °C/min and held for 2 h Degassed at 230 °C for 20 min, then to 300 °C at +7.0 °C/min and held for 10 min.
4b	1	100% H_2 at 50 cm^3/min	Ramped at +6.8 °C/min from r.t. to 140 °C and held for 30 min, then to 230 °C at +1.2 °C/min and held for 2.5h. Degassed at 230 °C for 30 min, then to 300 °C at +7.0 °C/min and held for 10 min. 0.5 mm thermocouple used to measure sample temperature.
4c	1	100% H_2 at 50 cm^3/min	Ramped at +9.6 °C/min from r.t. to 140 °C and held for 1h 10min, then to 230 °C at +1.3 °C/min for 2h Degassed at 230 °C for 30 min, then to 300 °C at +7.0 °C/min and held for 10 min. Thermocouple inserted deeper into sample surface.

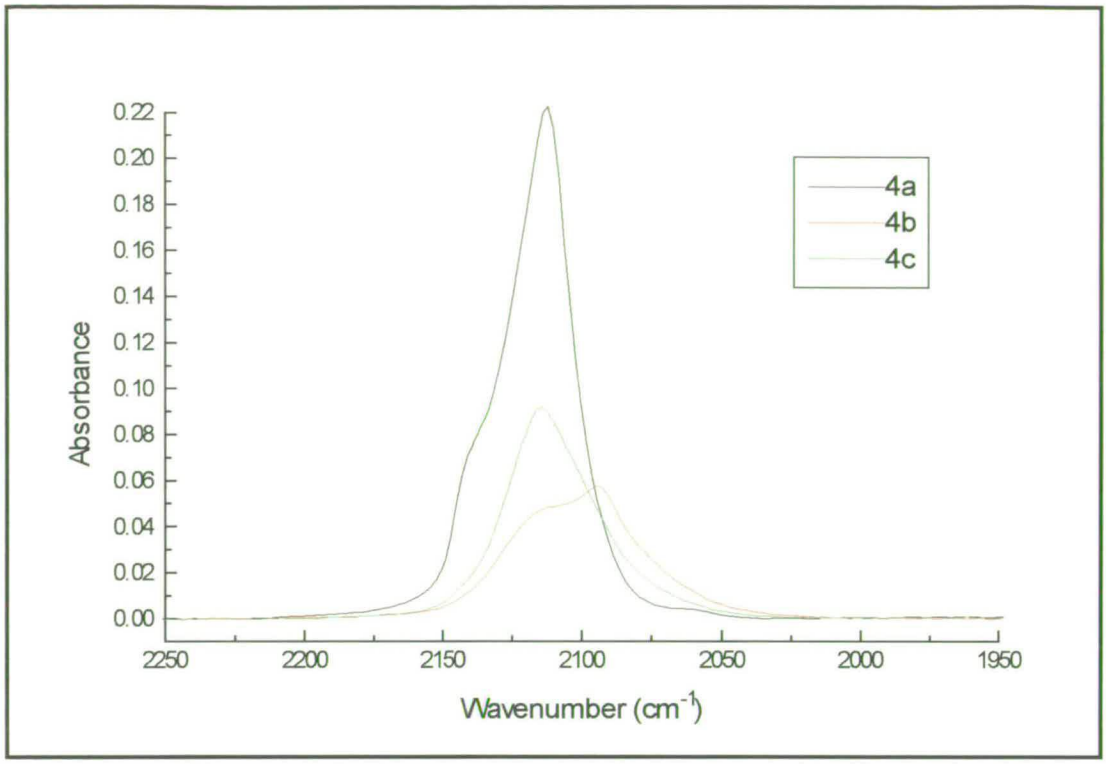

Fig. 4.8. *Example 4 showing final steps taken towards determining "ideal" conditions for reduction. Total CO exposure: 11.0 μmol.*

Example 5: Degree of Reduction of the Catalyst from Section 5.3 Onwards

As shown in Example 4, the catalyst was very susceptible to minor changes in experimental set-up, and in particular to the thermocouple position within the catalyst bed. As a result, it was not always possible to maintain consistency between sets of experiments, since often, after periods away from the DRIFTS system, the set-up had been altered by other workers. This problem was tackled by carrying out experiments using CO as a probe molecule at the start of each set of experiments and thus defining the state of the copper. Using this method, it was found that after the experiments in section 5.2 in Chapter 5 had been carried out, conditions had changed slightly, and so the example given below defines the state of the copper component of the catalyst from section 5.3 onwards. CO probe experiments carried out periodically *within* sets of experiments, allowed consistency to be confirmed.

Despite the limitations mentioned above, the differences between sets of experiments are not so great that trends would be masked, thus still allowing comparisons to be made between sets.

Fig. 4.9 shows Example 5, where identical pre-treatment conditions were used to Example 4c. A single band at 2093 cm^{-1} was seen with an intensity of 0.0445 and a FWHM of 41 cm^{-1}.

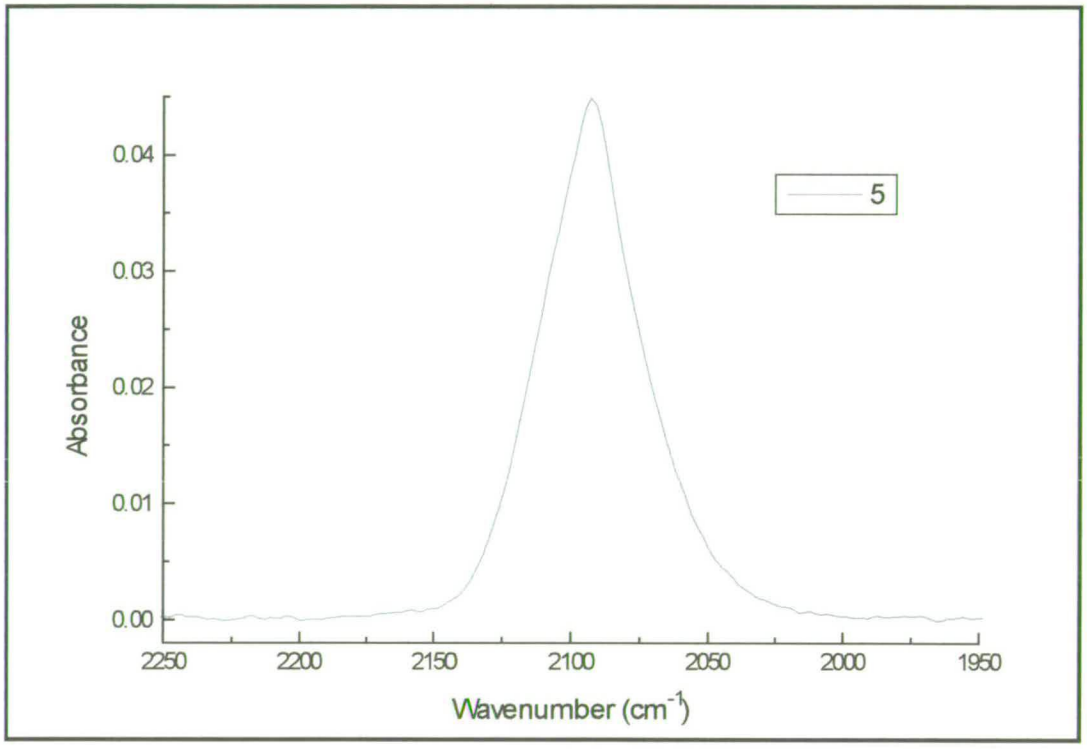

Fig. 4.9. *Example 5 showing CO pulse experiment to determine the state of the catalyst for section 5.3 and Chapters 6 and 7. Total CO exposure: 11.0 μmol.*

Discussion

The results reported in this section allows the effects of pre-treatment conditions on adsorbed CO in a pulse experiment to be elucidated. Example 1 highlights the effects of altering the reduction gas and gas flowrate on *Catalyst 1*. An immediate comment which can be made for Example 1a is that it possesses a broad CO band, with a FWHM of 40 cm^{-1}. This observation points towards the possible sintering of the copper particles leading to a loss in definition of the metal crystal planes [1]. However, a low copper surface area would also be expected on sintering while the absorbance of the main band found in the experiment (0.114) is relatively intense.

According to the literature discussed in the introduction, the main band for Example 1a, positioned at 2095 cm^{-1}, could be assigned to linearly adsorbed CO on Cu(110) planes, which show two bands at low coverage (2088 and 2104 cm^{-1}) and one on saturation, at 2094 cm^{-1} [41]. Alternatively, this band may show the existence of high index planes. Cu(211) shows two bands at low coverage (2095 and 2109 cm^{-1}) which blend together to form one at saturation (2110 cm^{-1}) while Cu(311) shows two bands at low coverage (2093 and 2109 cm^{-1}) which shift at saturation (2093 and 2103 cm^{-1}) [41].

The frequency of the main band at 2095 cm^{-1} along with the possibility of a shoulder at 2110 cm^{-1} are very similar to the frequencies observed for Cu(211) at low coverage, but not at high coverage. Another explanation for the origin of bands at approximately 2095 and 2110 cm^{-1} has been suggested by several authors. Tompkins and Greenler [64] found that, on exposing a copper film to O_2, the CO band shifted from 2103 to 2113 cm^{-1} (along with the generation of an additional band at 2135 cm^{-1}). Bocuzzi *et al.* [68] found a similar shift from 2098 to 2116 cm^{-1} for a Cu/ZnO sample on oxidation and Pritchard and Hollins [73] saw a shift for an Cu(110) single crystal from 2094 to 2105-2110 cm^{-1} at low coverages of oxygen, and attributed a similar band at 2115 cm^{-1} on oxidised Cu(111) to "copper not bonded directly to oxygen".

Thus, it appears that for the sample in Example 1a, a mixture of partially oxidised copper, $Cu^{\delta+}$, (or copper with Cu-O or oxide from the support as its next-nearest neighbour) and completely reduced copper species exist. Additionally, while it is difficult to specify exactly which copper plane is present, it seems likely it is a stepped plane, which encompasses Cu(110) as well as high index planes. A mixture of planes with different step densities probably exist. The lack of structure to the band also suggests poorly defined faces, while the band width which encompasses contributions from 2150 to 2040 cm^{-1} again suggests a mixture of different planes.

It could be concluded from Example 1a that the reduction conditions used (100% H_2 with a relatively fast ramp) were too harsh, resulting in a broad band with little definition. Although the copper surface area does not appear to have been decreased greatly by the reduction conditions used as compared with other experiments, it is desirable to have well defined crystal planes which can be easily identified. It would then be easier to link future observations to structural factors.

In view of this, Example 1b involved the reduction of *Catalyst 1* under milder conditions; a 5% H_2/Ar mixture was used with a lower flowrate. Overall, a lower band intensity is observed than in Example 1a. Two definite features can be seen, at 2139 and 2110 cm^{-1}. The latter band could perhaps be attributed to the presence of Cu(211). However, the new reduction conditions are expected to be less reducing, and indeed, it appears that this is so. The absence of the band at 2095 cm^{-1} along with the new band at 2139 cm^{-1} are consistent with the sample in Example 1b being more oxidised than that in 1a.

As discussed in the introduction, a band at around 2139 cm^{-1} has often been observed, [65, 68-71], and while it is agreed that this can be attributed to copper oxide [65, 68-70] there is disagreement as to the oxidation state of the copper. In this case, it seems most likely that the band can be assigned to copper (I) oxide, bearing in mind that the sample will be reasonably reduced having spent so long under hydrogen. However, it is not possible to be certain, so hereafter the species will be referred to

simply as "copper oxide". Another study [71] found that a band at 2104 cm^{-1} shifted to 2139 cm^{-1} on prolonged reduction, which was attributed to the generation of small, spherical crystallites from flat crystallites. This seems unlikely to be the case here, as no band at 2139 cm^{-1} was observed for Example 1a, where reduction conditions were more severe.

Another difference observed on going from Example 1a to 1b is that although the sample was less reduced, it also appeared to adsorb less CO, as shown by weaker CO stretching bands. This could be due to the fact that some sintering of the copper metal particles may still have been occurring. The low flowrate of reduction gas in Example 1b could be responsible for this - it will be less efficient at the removal of heat produced during the exothermic reduction process (reaction 4.1). In addition to this, the efficiency of heat dissipation is likely to decrease on going from the 100 % H_2 reduction gas (1a) to the 5 % H_2/Ar mixture (1b) because the heat capacity of hydrogen is higher than that of argon [78].

Example 1 illustrates the importance of treating the catalyst gently during reduction. With this in mind, Example 2a investigated the effect on *Catalyst 2* of using a slower temperature ramp, whilst maintaining a high flowrate of the reduction gas. The temperature ramp was left unchanged up to 140 °C and was then decreased in rate up to 230 °C, since it has been found through experience at ICI Katalco that the greatest susceptibility to sintering occurs at high temperature. The catalyst was maintained in reducing conditions at T_{max} for a longer period in order to attain complete reduction of the copper.

Example 2a shows a narrow band at 2108 with a shoulder at 2139 cm^{-1}, suggesting that once again complete reduction of the metal had not been achieved. However, the narrowness of the band (FWHM = 25 cm^{-1}) and its intensity - absorbance 0.117 compared with 0.114 for Example 1a, in spite of 2a's slightly decreased copper surface area as determined by reactive frontal chromatography of 15 compared with 19 m^2/g - suggest a well-defined, un-sintered surface.

Alternatively, it is possible that the dominance of the band at 2108 cm^{-1} and absence of 2095 cm^{-1} shows that under certain circumstances, certain faces predominate, e.g. Cu (211) *versus* Cu(110). However, bearing in mind that reduction conditions are being varied between experiments, it is most likely that degree of reduction is the determining factor for band position.

On moving to a more dilute reduction gas (2% H_2/N_2 - Example 2b), a weak, broad absorbance (0.0298, band envelope FWHM = 29 cm^{-1}) was observed at 2110 cm^{-1}, with an accompanying prominent shoulder at 2141 cm^{-1}. Hence, nothing was gained in terms of degree of reduction, uptake of CO or sharpness of the resulting bands. This supports the conclusions suggested above of the importance of not just a high flowrate of reduction gas, but a high flowrate of *hydrogen*, most probably as a result of its superior efficiency of heat dissipation. Overall, Example 2 also shows the importance of a gentle temperature ramp above about 140 °C, in order to maintain well-defined crystal faces. Finally, it demonstrates once again the difficulty of achieving complete reduction of the supported copper.

Example 3 investigated the effect on *Catalyst 2* of removing preadsorbed CO from the catalyst prior to the CO pulse experiment. The spectra shown in Fig. 4.7 do not exhibit any striking differences between Examples 3a (absorbance 0.171, FWHM 26%) and 3b (absorbance 0.175, FWHM 24%) within the level of noise. It is also possible that dipole coupling could be in existence, making comparisons of the band intensities difficult [79]. However, the loss of the preadsorbed CO is well illustrated in Fig. 4.6, and it is expected that its removal could become more important when quantifying the amount of CO evolved during thermal desorption by a technique such as mass spectrometry. The shift in frequency of the preadsorbed CO band from 2089 cm^{-1} at 300 °C to 2100 cm^{-1} at room temperature may indicate that the catalyst becomes less reduced as it cools, e.g. by adsorbing oxygen impurities from the helium stream.

Example 4 illustrates the final stages taken towards establishing a "standard" pre-treatment regime to be used throughout the rest of this thesis for *Catalyst 1*. The most intense CO band found so far is obtained for Example 4a - an absorbance of 0.223 at 2112 cm^{-1} with a FWHM of 27 cm^{-1}. The intensity of this CO band is 30% greater than that in Example 3b, which is most likely due to the difference in copper surface area between *Catalysts 1* and *2*, which is about 30%. The other main difference between the two experiments is that 4a was held at 140 °C for 30 min during reduction before being ramped to higher temperatures, again to prevent sintering. It is conceivable that this, too, may have made some contribution to the increased uptake of CO.

Drastic effects are seen in Example 4b, where the thermocouple was replaced with the thinner one described in Chapter 2. The sample appears to be more thoroughly reduced - no band at 2139 cm^{-1} is observed, and the main band is at 2094 cm^{-1}, with a prominent shoulder at 2112 cm^{-1}, reminiscent of the frequencies observed in Example 1a. The FWHM of the band envelope (51 cm^{-1}) is even greater than in 1a, although the two species are clearly overlapping. These findings, along with the small intensity of the band (0.0560), point towards a catalyst which has been reduced too harshly. Since a high flow of 100% H_2 was maintained throughout the reduction, the fault must lie with the temperature ramp. Indeed, on examination of the new thermocouple, it was noticed that it was not embedded as deeply into the catalyst surface as the original thermocouple. A temperature differential between the bottom and top of the catalyst bed (about 2 mm depth) of around 50 °C had already been recognised [50], and it was appreciated at this point, the importance of thermocouple position. If the thermocouple is only just in contact with the surface of the bed, it will measure a lower temperature than if it is at the centre of the bed, and as a result the overall mass of catalyst will mistakenly be ramped to a higher temperature.

In order to correct this problem, the thermocouple was returned to the original thermocouple's position - at the centre of the bed, where the average catalyst temperature would be measured. Example 4c reflects this situation, where a

moderately intense band (absorbance 0.0951, FWHM = 36 cm^{-1}) at 2114 cm^{-1} was observed, with little or no absorbance at either 2139 or 2094 cm^{-1}.

As mentioned in the Results section, Example 5 illustrated the sensitivity of the catalyst to minor changes in experimental set-up. The pre-treatment conditions were identical to those for Example 4c, so should have given an identical result. Instead, the dominant species in the spectrum was found to be CO adsorbed on the fully reduced stepped planes of copper (2093 cm^{-1}) with only a minor contribution from the species at 2112 cm^{-1}. No band was observed at 2140 cm^{-1}, revealing the absence of copper oxide, and thus showing that the sample was better reduced than that of Example 4c. The decreased uptake of CO in this case (maximum absorbance of 0.0445 compared with 0.0951) could suggest that some sintering has occurred perhaps owing to the catalyst being taken to too high a temperature. Overall, these results suggest the thermocouple position as being responsible for the difference between the two spectra.

These final results highlight the temperamental nature of the catalyst system under study. Much effort was poured into fine-tuning the pre-treatment conditions in order to obtain the optimum spectrum, but this has been shown to be a difficult task. Eventually, compromises were necessary; reproducibility (as opposed to maximum CO uptake or a completely reduced catalyst) was accepted as being the most important factor and this was tested at the start of each set of experiments using CO as a probe molecule. As already discussed, reproducibility could not be assumed *between* sets of experiments.

In summary, the work in this chapter has, first, established the difficulty in studying the $Cu/ZnO/Al_2O_3$ system with DRIFTS, and ascertained the effects of the pre-treatment conditions. It was found that the reduction of the catalyst with a high flowrate of 100% H_2 with a gentle temperature ramp to 140 °C resulted in well-defined CO bands of a reasonable intensity. It was found necessary to degas at 300 °C

for a short period to remove pre-adsorbed CO. The thermocouple position in the bed of catalyst was found to be critical.

Second, the state of the copper component of the catalyst has been investigated. It was suggested in the discussion of Examples 1 and 2 that the variation in acquired spectra between experiments could be due to:

1) certain conditions encouraging the formation of certain crystal planes: more reducing conditions result in spectra which resemble Cu(110) or (311), while less reduced spectra are more similar to Cu(211), or
2) the degree of reduction of the sample, where 2095 cm^{-1} represents fully reduced copper, 2112 cm^{-1} is due to partly oxidised copper (e.g. $Cu^{\delta+}$ or copper with Cu^{n+} as its next-nearest neighbour), and 2140 cm^{-1} to copper oxide.

The second suggestion now seems most likely, in the light of the other experiments discussed, as the peak positions vary by only about +/- 2 cm^{-1} between spectra and this is likely to be due to changes in coverage. The largest difference between spectra is the change in distribution of the species.

Other supported copper studies, along with the comparison of the frequencies in this study with single crystal data, suggest that in this case stepped planes of copper exist, and probably a variety of these. Additionally, Hollins and Pritchard [73] attribute their band at 2140 cm^{-1} to the oxidation of copper previously in a stepped site, where they are considering Cu(110) as an extreme form of a stepped surface.

Chapter 5 - The Effect of Alkali Promotion on CO and CO_2 Adsorption

5.1 - Introduction

The interaction of carbon monoxide with copper has been discussed in Chapter 4 with a view to determining the degree of reduction of the catalyst surface. In this chapter, the effect of alkali promotion on adsorption at the surface will be studied - both the impact on the interaction of CO with copper itself and with the support (in the form of carbonate-type species) will be considered. The effect on CO adsorption of varying the level of alkali promotion will also be discussed.

The adsorption of carbon dioxide will be considered, with the aim of obtaining more information about the effect of the alkali promoter. In addition to participating in the WGS reaction, CO_2 has also been shown to be the source of "carbon" in the methanol synthesis reaction over copper-based catalysts [e.g. 80-82]. Thus, the study of its adsorption is of particular value.

Work already published in the literature which is relevant to the topic of this chapter will be briefly summarised below.

5.1.1 - Alkali Metal - CO Coadsorption

The general effects of alkali promotion were considered in Chapter 1. Many workers have investigated the promotional effect by studying the coadsorption of alkali metals with CO, largely on single crystals, using vibrational spectroscopy - either RAIRS, which was also mentioned in Chapter 1, or HREELS (High Resolution Electron

Energy Loss Spectroscopy), which for the purpose of this introduction can be considered to give comparable information to RAIRS.

Typically, a red shift in the CO stretching frequency on promotion is anticipated in vibrational studies, which can be explained in a simplistic way by the following: an interaction between the alkali metal valence state and transition metal conduction band would result in an increase in backdonation to the CO $2\pi^*$ orbital with the accompanying red shift in CO stretching frequency. In reality, however, the exact mechanism of promotion is not clear, even though alkali metal-CO co-adsorption is a much studied field.

Observations have been made pertaining to the range of the alkali promotion. The predominant interaction may be a long-range, indirect interaction which could be mediated by the substrate, as proposed by Crowell and Somorjai [22] in a HREELS study of potassium-promoted Rh(111). Alternatively, a short range interaction may predominate where direct interaction exists between coadsorbates, and this usually leads to a larger red shift than the long range effect. For instance, Whitman and Ho [25] investigated the room temperature adsorption of CO and low coverages of K on Ni(110) with HREELS, and saw two distinct CO species coexisting - a strongly perturbed species with a higher thermal desorption temperature and a CO stretching frequency more than 300 cm^{-1} lower than for the clean surface, and a very weakly perturbed species that behaved in nearly identical fashion to CO adsorbed on the clean surface. The former result was attributed to ordered surface structures of fixed alkali:CO stoichiometry.

The formation of complexes between the alkali and CO have also been observed. Lackey *et al.* [83] found that the CO stretching frequency was shifted from 2090 cm^{-1} on a clean surface to coverage-dependant bands in the region of 1200 to 1600 cm^{-1} in the presence of coadsorbed potassium in a HREELS study of Cu(110). An explanation for this was given in the form of a local interaction of the alkali, where complexes with empirical formulae $K_{m/2}C_qO_q(ad)$ were formed (where q=2 or 4).

Complexes have also been suggested for similar studies on Pt(111) [84] and Ni(111) [85].

More recently, studies have been published which highlight the complexity of alkali promoted systems. For instance, Dubois *et al.* [86] found at least seven different C-O vibrational modes in a study of Cu(100) by HREELS with various potassium precoverages, as many as five of which were observed simultaneously. Although they could draw no solid conclusions as to the formation of $(CO)_n$-K polyhedral complexes, they believed that their results suggested their existence.

There are fewer examples in the literature of alkali promoted supported metal catalysts. As was discussed in Chapter 1, limitations exist when comparing the alkali metal promotion of single crystals with the alkali salt promotion of supported catalysts. The red shift is expected to be smaller, and additional interactions might also be expected as a result of the support. Nevertheless, Marshall, studying Ni/Al_2O_3 catalysts promoted with potassium carbonate by DRIFTS, found long range effects showing red shifts of up to 125 cm^{-1} which depended on the original mode of bonding on the unpromoted sample (e.g. linear or bridged CO) [50]. Short range effects in the form of potassium carboxylate or carbonate-type compounds were also observed in the region below 1650 cm^{-1}.

Another example from the literature of a supported system is the study by Millar *et al.* [87] of Cu/SiO_2 promoted with potassium acetate. In this case, only a 10 cm^{-1} red shift was observed for each CO stretching frequency for both calcined and reduced catalysts. However, in spite of this shift the strength of the Cu-CO bond was decreased, as determined by desorption studies. A model for the red shift developed by Heskett *et al.* [88] was invoked; they suggested that the presence of potassium atoms near CO molecules can induce a significant interaction between the potassium and the 1π orbitals of CO. This is assumed to produce a transfer of charge to potassium and the resultant perturbation of the 1π orbitals of CO leads to a weakening of the C-O bond. The study also revealed features at 1510 and 1366 cm^{-1}

which they attributed to a carboxylate species stabilised on the copper component by added potassium, while rejecting the suggestion of Lackey *et al.* [83] of K-CO complexes existing in their case.

5.1.2 - The Interaction of Carbon Dioxide with Copper

The interaction of CO_2 with metals has received little attention compared with their interaction with CO, and is incompletely understood. It is clear that in general CO_2 dissociatively adsorbs on most transition metals [89] while it reacts with surface oxygen to form carbonate-type compounds on noble metals such as silver [90] and some transition metals under special conditions (e.g. nickel at low temperature with the coadsorption of oxygen [91]). However, the situation for copper is more controversial.

The question of whether CO_2 dissociatively adsorbs on copper is important from the standpoint of both the methanol synthesis reaction, where the working catalyst has been found to be partially covered in oxygen and its coverage is highly dependent on the CO_2-CO ratio used [92], and also the WGS reaction, where in the reverse direction, the dissociation of CO_2 has been proposed as a step in the redox mechanism [93, 94].

It has been found that there is very little dissociation of CO_2 on Cu(111) [95]. Nakamura *et al.* [93] have also shown that at temperatures up to -23 °C, no CO_2 dissociation was observed on Cu(110) under UHV conditions, but the extent of dissociation was increased at higher pressures. In contrast, Wachs and Madix [96] reported that more than 99% of the adsorbed CO_2 on Cu(110) dissociated after exposure at -93 °C, although they did not go into detail about their experimental conditions. Other workers have reported the dissociation of CO_2 at higher temperatures over single crystals [97, 98]. Schneider and Hirschwald [97] found "nearly 100%" dissociation of CO_2 on oxygen-free Cu(110) during thermal

desorption, following adsorption at low temperature and pressure. Only about 0.3% of a monolayer of CO_2 was adsorbed molecularly. However, sub-monolayer coverages of oxygen on the copper stimulated molecular CO_2 adsorption and possibly gave rise to the formation of activated CO_2^- or CO_3^- species which could act as precursors to formate. Copperthwaite *et al.* [99] also found evidence for physisorbed CO_2 and CO_2^- on oxygen containing Cu(211) and polycrystalline copper following the low temperature adsorption of CO_2.

In a study by Hadden *et al.* [100] on the interactions of CO_2 with copper powder, it was found that the CO_2 adsorbed only weakly on a clean surface at 25 °C; this state acted as a precursor, which on activation, produced adsorbed CO and surface oxygen. The resulting copper surface was found to adsorb CO_2 more strongly, yielding a state which, it was suggested, could be hydrogenated to produce formate and then methanol.

Studies on copper supported catalysts have also seen evidence suggesting dissociative adsorption. [101-103]. Millar *et al.* [101] suggested the requirement of stepped copper surfaces in order for CO_2 dissociation to occur and found that additional CO_2 then interacted with surface oxygen to produce a symmetric carbonate species. The structural sensitivity of the CO_2 dissociation reaction has been further highlighted by Fu and Somorjai [104], who found that while no dissociation occurred at low temperature over Cu(110), it did occur even below 10^{-7} bar on Cu(311).

5.1.2.1 - The Effect of Alkali Promotion on CO_2 Adsorption

The coadsorption of CO_2 with alkali metals has not been as widely studied as CO, but nevertheless several effects have been established. Rodriguez *et al.* [105] have shown that the caesium promotion of a Cu(110) crystal drastically influenced the adsorption and reactivity of CO_2, where they were unable to react any measurable amount of CO_2 on a clean sample. Following the coadsorption of CO_2 with Cs, they detected the thermal desorption of CO_2 in the temperature ranges -160 to -100 °C and 230 to

430 °C. The high temperature desorption state was attributed to the thermal cracking of $Cs.nCO_{3(a)}$ complexes according to reaction 5.1, where n is approximately 1, which had formed on the surface already at -160 °C, (reaction 5.2). The low temperature desorption was attributed to the desorption of weakly adsorbed CO_2 molecules.

$$Cs.nCO_{3(a)} \rightarrow Cs_{(a)} + nCO_{2(g)} + nO_{(a)} \qquad \textit{reaction 5.1}$$

$$2nCO_{2(g)} + Cs_{(a)} \rightarrow nCO_{(a)} + Cs.nCO_{3(a)} \qquad \textit{reaction 5.2}$$

Thomsen *et al.* [106] showed how the low sticking probability of CO_2 on Cu(110) (found by Rasmussen *et al.* to be 7.5 x 10^{-12} at 990 mbar and 227 °C [98]) could be increased by the addition of potassium. This was attributed to the activation of the CO_2 molecule by charge transfer from the alkali metal, which lowered the work function considerably. An enhanced amount of both physisorbed and chemisorbed CO_2 was obtained at -160 °C in the presence of the alkali. On heating, they detected the desorption of CO according to a similar mechanism to Rodriguez *et al.* (reaction 5.3). The carbonate species was found to decompose between 180 and 280 °C (reaction 5.4).

$$2CO_2^- \rightarrow CO_3^{2-} + CO_{(a)} \qquad \textit{reaction 5.3}$$

$$CO_3 \rightarrow CO_2 + O \qquad \textit{reaction 5.4}$$

Similar results have been observed for other metals. Solymosi and Bugyi [107] studied the adsorption of CO_2 on a potassium-promoted Rh(111) surface and found that whereas for the clean surface CO_2 was only weakly and non-dissociatively adsorbed, on addition of potassium, the rate of adsorption was increased, the formation of a strongly bonded CO_2 species was induced, and the dissociation of CO_2 was initiated. According to thermal desorption experiments, potassium was also found to be stabilised in the presence of CO_2. This mutual stabilisation was attributed to a direct interaction between CO_2 and K and to the formation of a carbonate-like

species. Solymosi and Berko [108] reported a similar range of effects for CO_2 adsorbed on a potassium-promoted Pd(100) surface.

5.1.3 - The Interaction of Carbon Oxides with Oxide Supports

The study of CO_2 adsorption on supported copper is further complicated by the chemical behaviour of the support (e.g. ZnO or Al_2O_3) towards CO_2. CO has been shown to react in a similar way because it is easily converted to CO_2 as soon as it comes into contact with the metal oxide [109, 110]. In the case of an alumina sample, CO_2 is formed in two ways [110]:

1) disproportionation - $2CO_{(g)} \rightarrow C_{(s)} + CO_{2(g)}$ *reaction 5.5*

2) oxidation - $CO_{(g)} + O_{(a)} \rightarrow CO_{2(g)}$ *reaction 5.6*

Both methods 1 and 2 have been found to operate, but the Boudouart reaction (1) occurs more slowly. Thus, instantaneous CO_2 formation is thought to occur from the surface oxidation reaction. As a result, adsorbates formed after contact with CO are similar to those formed from CO_2, but the features in resulting spectra are less reproducible and weaker [111, 112].

The adsorption of carbon oxides on metal oxide surfaces can occur at surface oxide species and surface hydroxyl groups. The resulting adsorbates are commonly of the carbonate-type structure, which can be observed in the 1700 - 1000 cm^{-1} range of the infra-red spectrum. Original studies based their spectral interpretations on analogy with the spectra of bulk compounds [62]. Interactions can also occur with coordinatively unsaturated cations, and, although the exact nature of the adsorbed species have not been conclusively established, the resulting infra-red bands are seen between 2200 - 2140 cm^{-1} [32, 62].

Busca and Lorenzelli [113] have reviewed the field of CO and CO_2 adsorption on oxides. They commented on the difficulty in interpreting spectra owing to the wide range of conditions under which experiments had been carried out and the opportunity for broad, overlapping bands. Nevertheless, the review successfully compared the infra-red frequencies found in different studies for surface compounds commonly formed from CO and CO_2 (shown below in Fig. 5.1) with values obtained for inorganic and organometallic compounds. Conclusions were made as to the expected frequencies for each group and to their thermal stabilities.

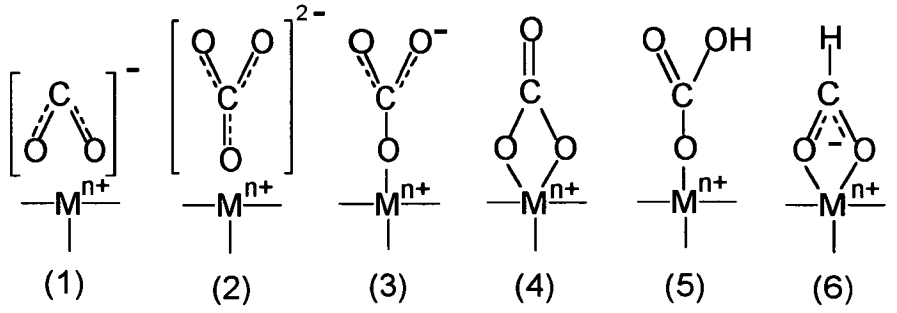

Fig. 5.1. *Examples of surface compounds commonly formed on metal oxides from CO and CO_2: (1) carboxylate, (2) uncoordinated carbonate, (3) unidentate carbonate, (4) bidentate carbonate, (5) bicarbonate, and (6) bidentate formate.*

A large number of individual infra-red studies have been carried out, particularly on alumina [e.g. 110, 112, 114-116]. Although several different surface species have been observed (e.g. physisorbed CO_2, bidentate and unidentate carbonates), the formation of a bicarbonate species from the interaction of CO_2 with surface hydroxyl groups (Fig. 5.2), has been discussed at length, and its infra-red bands are now fairly well-recognised. Initially, however, there was some disagreement as to the assignment of the bicarbonate peaks but eventually differences in spectra were shown to be dependent on the extent of surface hydroxylation, which is a function of the pre-treatment conditions. More reproducible results were obtained using CO_2 rather than CO as an adsorbate, and results were less dependent on the pre-treatment conditions.

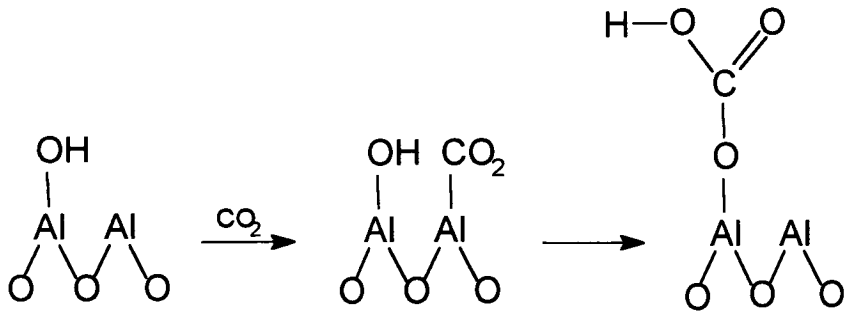

Fig. 5.2. *The formation of bicarbonate from CO_2 on alumina [112].*

Infra-red data on surface carbonates, which are formed form the interaction of CO_2 with surface oxide species (e.g. Fig. 5.3) are less conclusive [113]. In addition, different results can also be obtained due to variations in pre-treatment conditions. For instance, the formation of carbonate species occurs from CO in some studies, while no reactive adsorption is observed under other conditions.

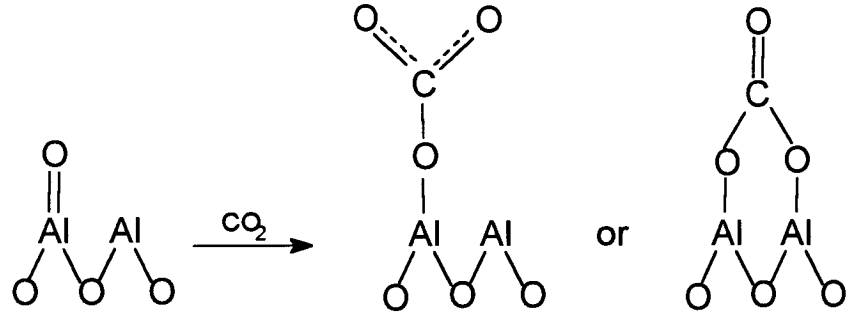

Fig. 5.3. *The formation of carbonate (unidentate and bidentate) from CO_2 on alumina [112].*

The adsorption of carbon oxides on other metal oxides has not been as well defined as for alumina. Lavalley and co-workers [117] have commented on the complicated nature of the spectra obtained following the adsorption of CO_2 on zinc oxide. However, they were still able to identify bidentate and polydentate carbonates, bicarbonates and linear CO_2 species on the surface [117, 118].

The interaction of supports such as alumina with alkali metals are also reported in the literature. For instance, on the basis of hydroxyl stretching frequencies in the 3600 cm^{-1} region and the work of Stork and Pott [119], Krupay and Amenomiya [111] have determined the effect of potassium on the alumina surface as being due to the exchange of hydroxyl groups with K^+ to form O^-K^+. They have also shown spectroscopically that CO will adsorb in small quantities on alumina at room temperature and on the addition of potassium, new bands appear below 1600 cm^{-1}. These are attributed to bidentate carbonate and carboxylate species, both associated with the potassium ion. Furthermore, they observed that the number of exchangeable oxygen atoms in alumina is increased in the presence of potassium and that their reactivity is increased. As a result, more oxygen atoms are available to form carbonate-type species, and there is a reduction in the difference in the rate of exchange between CO and alumina and CO_2 and alumina.

5.2 - The Adsorption of Carbon Monoxide

CO was pulsed onto the sample *via* the helium carrier gas, as described in Chapter 2; successively higher pressures of CO were introduced from the sample loop in the sequence 20, 50, 50, 100, 100, 150, 150, 200, and 200 Torr, so that the total exposure was eventually 1020 Torr. Simultaneously, DRIFTS was used to monitor for adsorbed species, and the mass spectrometer for species in the gas phase. A temperature programmed desorption was subsequently carried out. The unpromoted catalyst will be discussed first, followed by the 1 wt% potassium-promoted catalyst.

5.2.1 - Unpromoted Catalyst

5.2.1.1 - Pulse Experiment

Results

The pre-treatment conditions for the experiments discussed in this section are defined by Example 4c in Chapter 4. Fig. 5.4 shows the effects of pulsing the unpromoted catalyst with CO to successively higher pressures, and the results given below are in terms of the total pressure of CO dosed. Table 2.1 in Chapter 2 showed the equivalent number of moles of gas dosed for each pressure in the sample loop.

After the first pulse (20 Torr), a main band at 2112 cm^{-1} was seen which was accompanied by a shoulder at 2102 cm^{-1} and a small peak at 2145 cm^{-1}. These continued to grow until a total of 320 Torr had been pulsed, when the shoulder at 2102 cm^{-1} started to die away, as did the highest frequency band which also shifted slightly down to 2143 cm^{-1}. The main band was shifted to 2114 cm^{-1}. By 470 Torr of CO, all that remained of the 2102 shoulder was a slight asymmetry to the main band, while the small band at 2143 cm^{-1} continued to shrink, and both have disappeared by

820 Torr. Finally, a single band at 2114 cm^{-1} with an absorbance of 0.0915 and a FWHM of 36 cm^{-1} is seen at saturation.

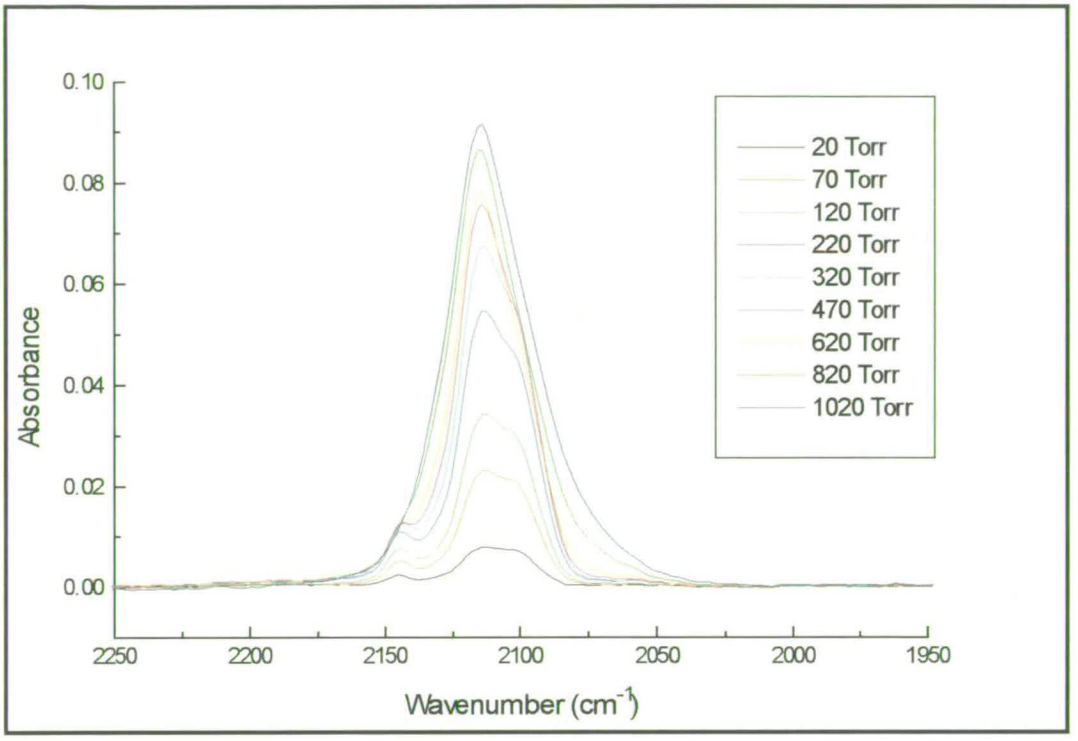

Fig. 5.4. *CO pulse experiment for the unpromoted sample. Total CO exposure = 1020 Torr.*

The other area of interest following CO adsorption is that below 1700 cm^{-1}. Fig. 5.5 shows the build-up of bands in this region on pulsing with CO to successively higher pressure.

Difficulties in assigning the species present in the region between 1550 and 1400 cm^{-1} were encountered owing to the problems of miscancellation which were discussed in Chapter 3. Usually these miscancellation features became more prominent with time but surprisingly in this experiment, after an initial increase, they then decreased towards the end of the experiment allowing adsorption features to be seen more clearly. Bands were seen in the final spectrum at 1650, 1323, 1227 and 1045 cm^{-1}. The sharpest feature was that at 1227 cm^{-1}, which was well away from the miscancellation region, and this peak increased with increasing pressure of pulse. A

band at 1418 cm^{-1} was poorly resolved, but was observed in other experiments carried out on the same sample where miscancellation was less evident. This band is probably present in the final spectrum. Finally, a weak but sharp band was observed at 3620 cm^{-1} superimposed over a very broad feature (shown in Fig. 5.6 following the final pulse).

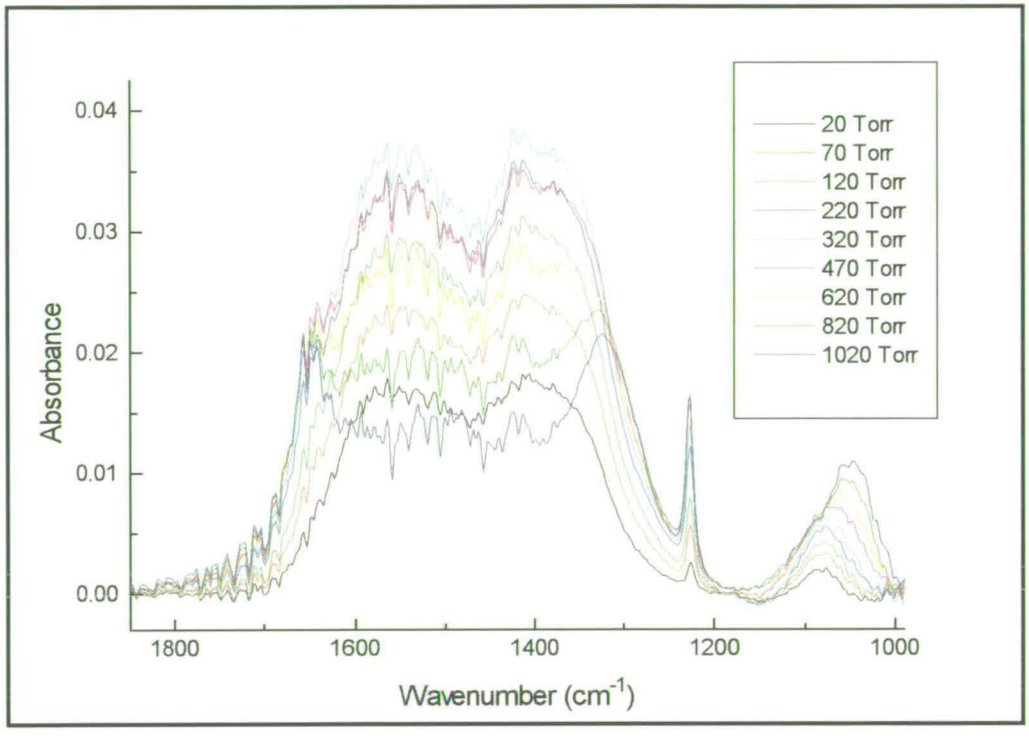

Fig. 5.5. *CO pulse experiment for unpromoted Catalyst 1 - 1850-980 cm^{-1} region.*

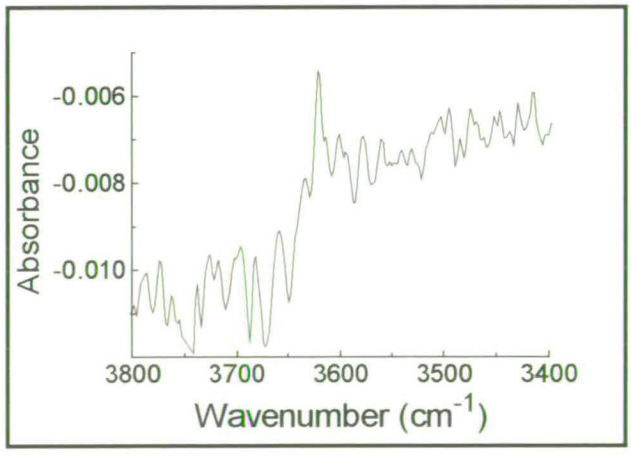

Fig. 5.6. *Band at 3620 cm^{-1}, shown following final pulse of CO on unpromoted catalyst.*

In order to aid easier interpretation of this region, an identical experiment was carried out on a γ-alumina sample. Pre-treatment conditions were as for the example above, and the final spectrum, again for a total exposure of 1020 Torr of CO, is shown in Fig. 5.7. Bands were seen at 1651, 1437 and 1229 cm^{-1}, as well as a single, sharp band which was seen at 3622 cm^{-1} (Fig 5.8). Generally, each band was sharper and more intense than those for the supported catalyst, which reflects the amorphous nature of the mixed-oxide sample resulting from its preparation *via* the co-precipitation route. The cut-off for the γ-alumina was at 1145 cm^{-1} compared with 970 cm^{-1} for the supported catalyst which results from the influence of the zinc oxide component.

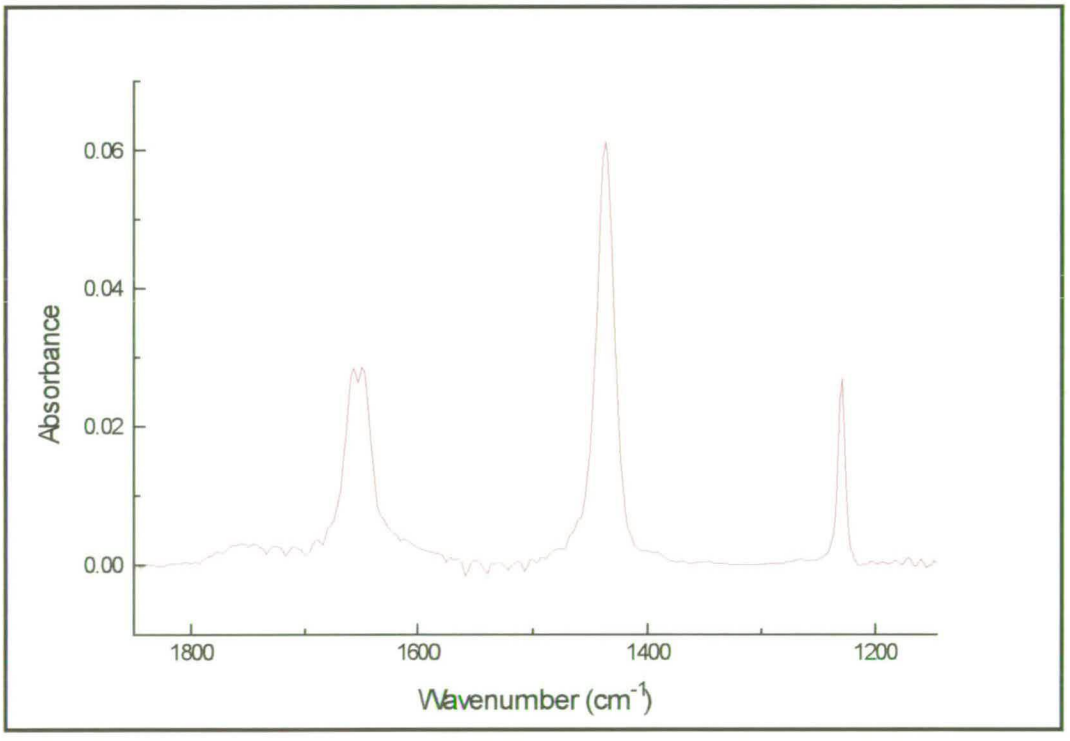

Fig. 5.7. *CO pulse experiment for a γ-alumina sample - final spectrum. Total exposure of CO: 1020 Torr.*

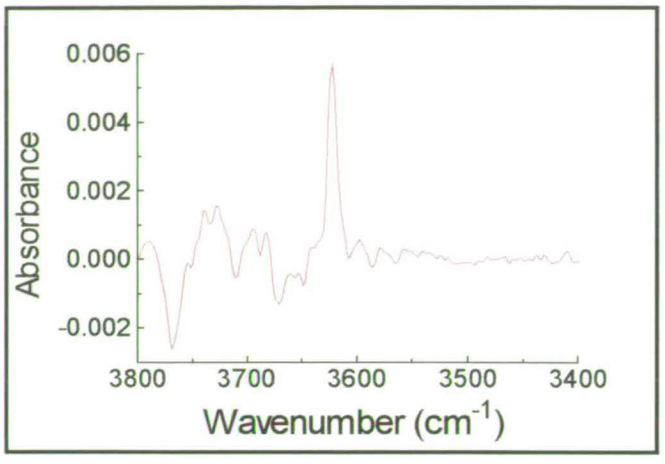

Fig. 5.8. *Band at 3620 cm^{-1}, shown following final pulse of CO on γ-alumina sample.*

In addition to this infra-red information, the mass spectrometer detected excess CO (i.e. that not adsorbed from the incoming pulse) and evolved CO_2, as shown in Fig. 5.9.

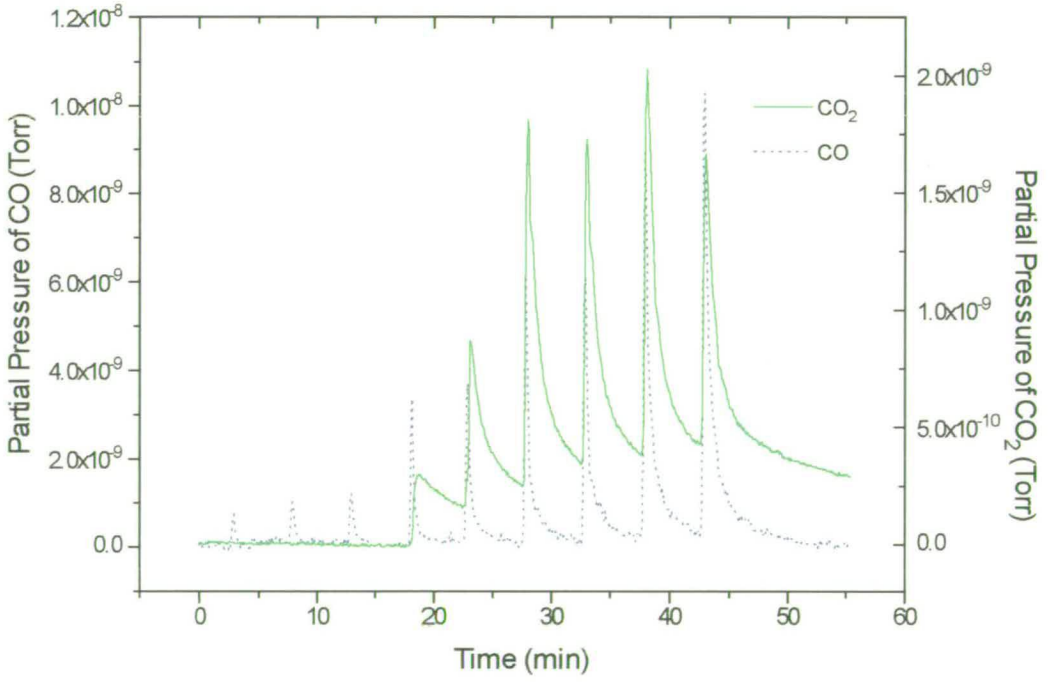

Fig. 5.9. *Gas phase CO and CO_2 observed by the mass spectrometer during the CO pulse experiment for the unpromoted sample*

A calibration relationship between the amount of CO introduced *via* the sample loop and the resultant pressure seen by the mass spectrometer was established by conducting a "blank" experiment (i.e. with no catalyst in the cell). Following integration of the mass spectrometer traces in Fig. 5.9, the amounts of unadsorbed CO ($CO_{(unadsorbed)}$) and CO_2 produced on exposure of the surface to CO ($CO_{2(reaction)}$) were thus calculated to be 21 and 51 μmol, respectively. A Gaussian fit was used in the integration of the $CO_{2(reaction)}$ trace. This allowed the trace to be extrapolated to the baseline, since CO_2 was still being evolved after data acquisition had ceased.

Discussion

The spectra in Fig. 5.4 can be explained according to the reasoning in Chapter 4. The band at 2102 cm^{-1} can be assigned to CO linearly adsorbed on a stepped plane of Cu^0 [41], while that at 2114 cm^{-1} suggests CO adsorbed on either $Cu^{\delta+}$ or Cu^0 with Cu^{n+} as its next nearest neighbour [64, 68]. These species are accompanied by a small amount of CO adsorbed on copper oxide, as shown by a band at 2143 cm^{-1} [68, 70, 75]. The oxidation state of the oxidised copper is unclear, and this was discussed in Chapter 4. Overall it can be said that the copper component of the sample is not completely reduced.

The other main area of interest on the infra-red spectrum following CO adsorption is that between 1700 and 1000 cm^{-1}. There are a series of bands in this region, but as commented on in the introduction to this chapter, they are difficult to interpret due to the overlapping of broad features. Moreover, the miscancellation features present in Fig. 5.5 obscure important areas and make assignment of the bands even more difficult. However, sharp bands in the final spectrum can be seen at 1650 and 1227 cm^{-1}, which can be assigned to bicarbonate on alumina. Parkyns commented [114] on the ease with which bands due to bicarbonate species adsorbed on alumina could be differentiated from other species owing to their relative sharpness. He observed bands at 1640 and 1233 cm^{-1}, as well as additional features at 3605, 1480

cm^{-1}, following adsorption of CO on alumina and attributed them to a bicarbonate species [110]. As illustrated by Fig. 5.2 in the introduction to this chapter, this bicarbonate species was thought to occur as a result of the interaction of CO_2 with surface hydroxyl groups.

Instantaneous CO_2 formation is thought to occur from the surface oxidation of CO by "oxidising centres" on the alumina surface, as described by Parkyns [110] and shown by reaction 5.6. The copper component of the catalyst in the present study has also been shown to be incompletely reduced, and this could be another source of oxygen to oxidise CO. As anticipated, the mass spectrometer trace in Fig. 5.9 shows the evolution of CO_2 on the exposure of the catalyst to CO. It is unclear why CO_2 formation commences only once the fourth pulse of CO has been introduced, since no new bands are observed in the infra-red spectrum at this point. It is possible that a certain coverage of CO is required on the surface before CO_2 is evolved.

The remaining two bands observed by Parkyns will now be considered. A weak, but sharp, band was observed at 3620 cm^{-1} in this study, which can be assumed to be the υ_{OH} mode which was seen at 3605 cm^{-1} in Parkyns' work. The broad feature over which this band was superimposed can be attributed to hydrogen-bonded surface hydroxyl groups. The assignment of the remaining band is less straight-forward, as it deviates by more than 60 cm^{-1} from the frequency of Parkyns' band at 1480 cm^{-1}. Miscancellation features make it difficult to say for certain that the band is at 1418 cm^{-1}, but generally in other spectra where this problem was less severe the band was found between 1427 - 1418 cm^{-1}. To assign this band, the experiment illustrated in Figs. 5.7 and 5.8 should be considered. This concerned the adsorption of CO on an alumina sample, which had undergone identical pre-treatment conditions to the $Cu/ZnO/Al_2O_3$ sample under question. The final spectrum from this experiment exhibited bands at 3622, 1651, 1437 and 1229 cm^{-1}, which reflect the results being discussed, and removes any doubt surrounding the band at 1418 cm^{-1}.

The difference between the results found here and those of Parkyns are evidence for the variation in the bicarbonate band with the extent of surface hydroxylation, which is a function of the pre-treatment conditions. Parkyns showed [112] that on going from degassing an alumina sample at 400 °C to 800 °C, the resulting CO_2 adsorption spectra showed bands at 1640, 1480, and 1233 cm^{-1}, and 1653, 1449 and 1232 cm^{-1} respectively. In addition, the fact that similar bands were obtained during this study for a sample of γ-alumina and the alumina component in a mixed oxide catalyst produced *via* a co-precipitation route reinforces the suggestion in the literature [114] that the pre-treatment conditions have far more bearing upon the resulting spectrum than does the solid phase of the alumina.

Thus, it is clear that bicarbonate species are present on the alumina support of the catalyst. Neither of the other remaining bands (seen clearly at 1323 and 1045 cm^{-1}) match those reported in the literature for adsorbates on the surface of alumina, and the experiment carried out in this study on γ-alumina revealed no other bands. The interaction of CO with reduced [69] and oxidised [70, 76, 120] supported copper has been shown to result in the formation of carbonate-type species on copper, but none of the frequencies of the infra-red bands corresponded to those found in this study.

The remaining component of the catalyst, zinc oxide, has been studied by Lavalley and co-workers [117, 118], as discussed in the introduction to this chapter. They found evidence for the presence of bidentate carbonates adsorbed on the zinc oxide surface after CO_2 adsorption, as shown by bands at 1595, 1339, and 1000 cm^{-1}. The second two of these bands fit well with those seen at 1323 and 1045 cm^{-1} on the $Cu/ZnO/Al_2O_3$ sample. It is probable that the third band, at 1595 cm^{-1}, is unresolved from the bicarbonate band at 1650 cm^{-1}. Although Lavalley and co-workers did observe the formation of a bicarbonate species on zinc oxide which showed bands similar to the species on alumina, the formation only occurred when fairly high pressures of CO_2 were used, or when the sample was pre-treated with water prior to CO_2 adsorption [117].

The band assignments are summarised in Table 5.1.

Table 5.1. *Assignment of species formed during CO pulse experiment on the unpromoted catalyst.*

Frequency, cm^{-1}	Species	Assignment
2143	CO on copper oxide	υ_{CO}
2112	CO on either $Cu^{\delta+}$ or on Cu^0 with Cu^{n+} as next-nearest neighbour	υ_{CO}
2102	CO on stepped plane of Cu^0	υ_{CO}
3620	bicarbonate on alumina	υ_{OH}
1650		$\upsilon_{COO}(a)$
1418		$\upsilon_{COO}(s)$
1227		δ_{OH}
≈1600	bidentate carbonate on zinc oxide	υ_{CO}
1323		$\upsilon_{COO}(a)$
1045		$\upsilon_{COO}(s)$

5.2.1.2 - Temperature Programmed Desorption

Results

Bands in the infra-red spectrum generally decreased in intensity as the sample temperature was raised. Fig. 5.10 shows the loss of the bands in the CO stretching region, while Fig. 5.11 shows those between 1700 and 1000 cm^{-1}. Spectra in Fig. 5.11 (which have not been baseline corrected) are grouped into three sets, thus minimising the problem of the sloping baseline and growing miscancellation features at higher temperatures, and allowing bands due to surface species to be seen more clearly.

In the CO stretching region, the shoulder at 2143 cm^{-1} was found to disappear first - it was no longer seen from 70 °C. The final traces of the main band now seen at 2114 cm^{-1} and the shoulder now at 2100 cm^{-1} disappeared by a temperature of 87 °C. The temperature of the maximum rate of desorption (T_{max}) for the main band was found to be 59 °C (determined by plotting the absorbance from more spectra than are shown in Fig. 5.10 as a function of temperature and differentiating to find the position of maximum gradient).

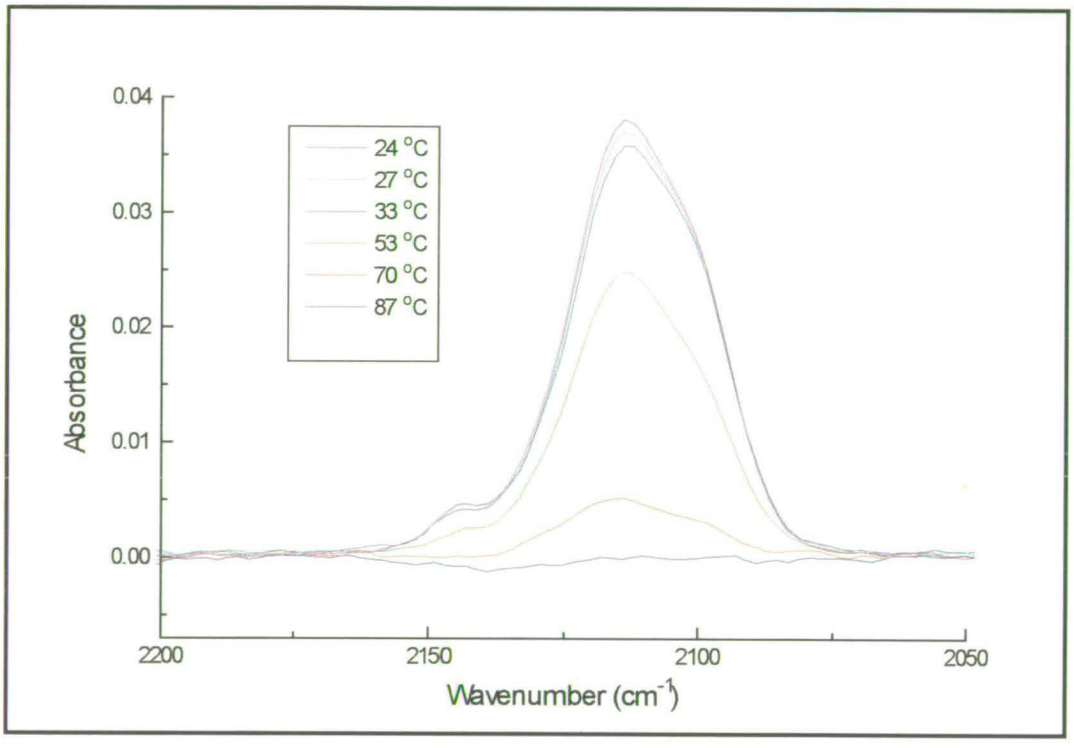

Fig. 5.10. *Temperature programmed desorption following CO pulse experiment for the unpromoted catalyst in the CO stretching region.*

The sharpest feature in the region between 1700 and 1000 cm^{-1} was that at 1227 cm^{-1}, and this was found to have disappeared by 125 °C. The band was not obscured by the miscancellation features, and this allowed T_{max} to be determined as 75 °C. The band at 1045 cm^{-1} appeared to exist until 180 °C, but the maximum temperature of existence for the bands at 1650 and 1323 cm^{-1} is unclear because of their positions relative to the developing miscancellation features.

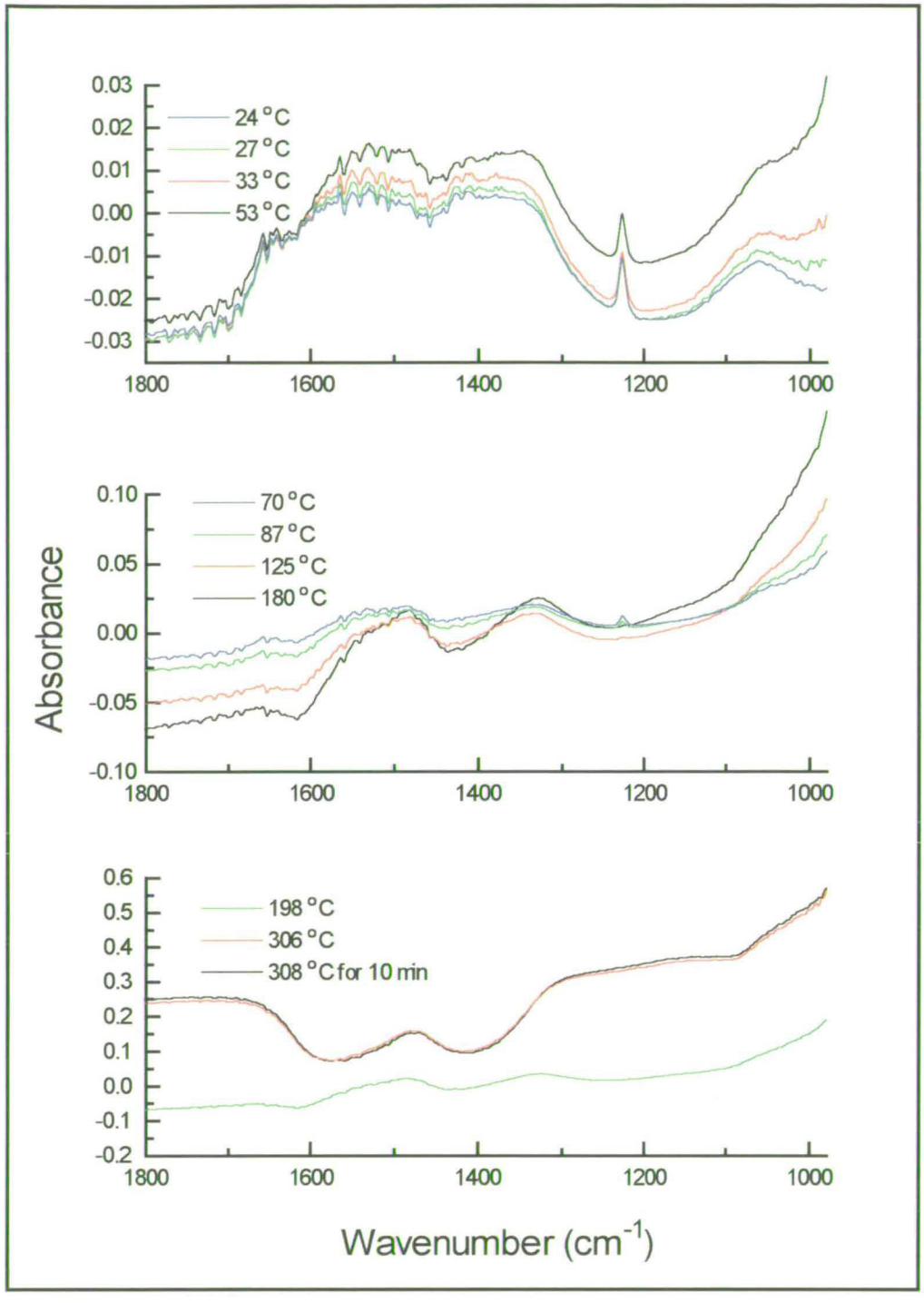

Fig. 5.11. *Temperature programmed desorption following CO pulse experiment for the unpromoted catalyst in the 1700 - 1000 cm^{-1} region (not baseline corrected).*

Additional information was recorded by the mass spectrometer. CO was evolved as the sample temperature was raised, and T_{max} (again, the temperature of the maximum rate of desorption) occurred at 51 °C (see Fig. 5.12). There is the

possibility of another feature at 79 °C, and presenting the original data along with the smoothed data in Fig 5.12 confirms that this is real, and has not been generated *via* the smoothing routine. There is also a slight increase in intensity of the trace between 250 and 300 °C. As in the case of the pulse experiment, the integrated area of the trace allows the amount of CO evolved ($CO_{(TPD)}$) to be evaluated, and is found to be 2.1 μmol.

CO_2 was also desorbed from the catalyst, as shown in Fig. 5.13. T_{max} occurred at 57 °C and there was a shoulder at higher temperature, 91 °C. A small desorption peak could also be seen at 289 °C. The total amount of CO_2 evolved ($CO_{2(TPD)}$) was found to be 27 μmol.

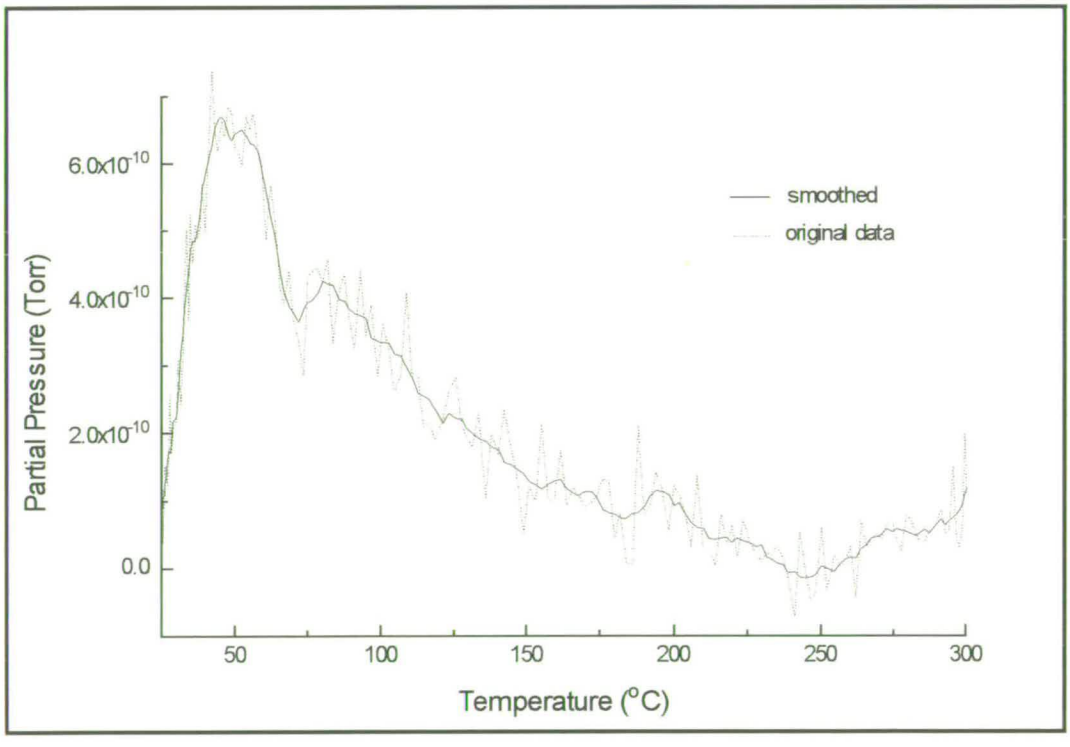

Fig. 5.12. *Temperature programmed desorption of CO from the unpromoted catalyst following CO pulse experiment (data has been corrected for CO_2 fragmentation).*

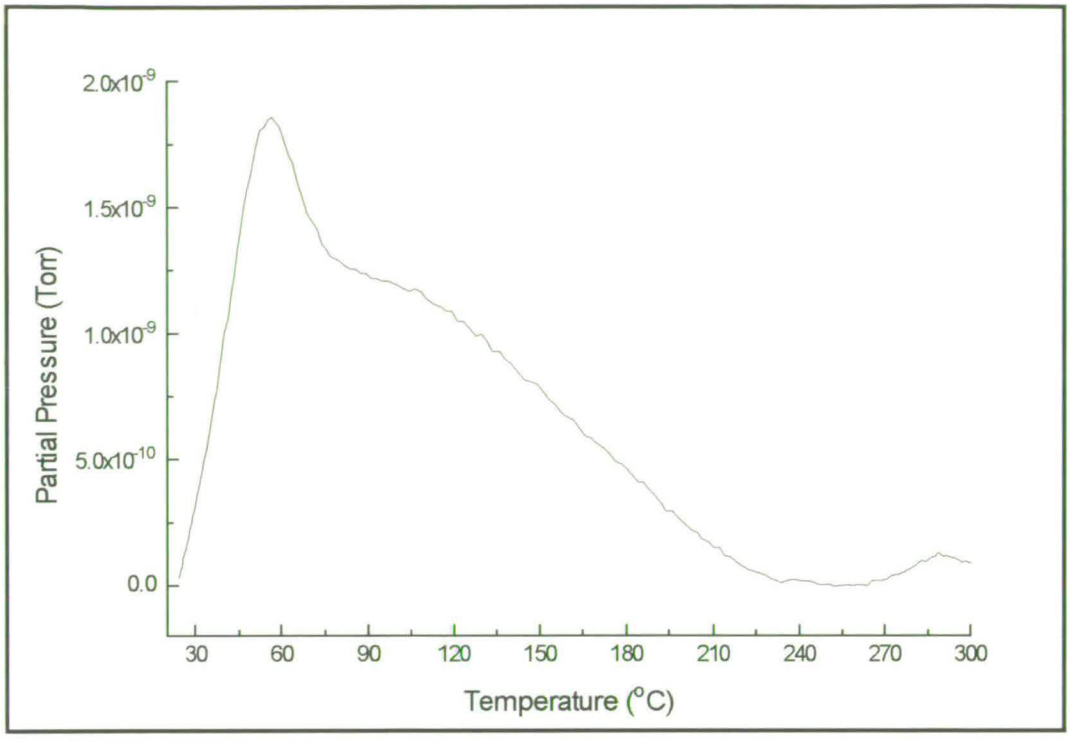

Fig. 5.13. *Temperature programmed desorption of CO_2 from the unpromoted catalyst following CO pulse experiment.*

Discussion

The infra-red desorption data allows further conclusions to be made on the nature of the surface species following adsorption of CO. T_{max} for the main CO stretching band was found to be 59 °C, and this correlates well with the value of 51 °C found by the mass spectrometer for CO. CO on copper oxide had disappeared from the spectrum at a lower temperature than the other two better-reduced copper species (Fig. 5.10), but its maximum rate of desorption occurred during the same temperature range (53 to 70 °C). The shoulder at 79 °C in the mass spectrometer CO trace is difficult to assign, since no more adsorbed CO is seen by the infra-red spectrum at this temperature. It is possible that the CO trace is influenced by CO_2, and perhaps the correction for CO_2 fragmentation has not compensated for the amount actually generated since there is a coinciding feature in the CO_2 trace.

The band at 1227 cm^{-1}, attributed to bicarbonate on alumina, was found from the infra-red spectra to desorb with a T_{max} of 75 °C. It is likely that bicarbonate, which is formed from the interaction of CO_2 and surface hydroxyl groups, will decompose to form CO_2. A peak is evident in the CO_2 mass spectrometer trace at 57 °C which could coincide with the bicarbonate desorption, although there is a 22 °C difference between the two T_{max} values. Another explanation for the peak at 57 °C is found when comparing the mass spectrometer traces for CO and CO_2. In spite of the CO trace having been corrected to take into account fragmentation of CO_2 in the mass spectrometer, its form still follows the trend of the CO_2 trace. Thus, it is possible that the peak at 57 °C could be due to adsorbed CO being oxidised as it desorbs from the copper surface, or CO desorbing from copper oxide as CO_2. If this is indeed the case, it is quite possible that any CO_2 desorbed as a result of bicarbonate decomposition (shown by the infra-red data to peak at 75 °C) could be obscured by the intense feature at 57 °C.

Another event recorded by the mass spectrometer is the shoulder in the CO_2 trace at 91 °C. It is difficult to attribute this with certainty to the remaining surface species identified during the pulse experiments - bidentate carbonate on zinc oxide - because of the worsening miscancellation at higher temperatures. However, the band at 1045 cm^{-1} did seem to have disappeared from the infra-red spectrum by a temperature of 180 °C, which would be consistent with it producing a higher temperature feature in the mass spectrometer trace than for the bicarbonate species. It has been observed [115] that bicarbonates generally only exist on alumina surfaces up to a temperature of 150 °C while at higher temperatures primarily carbonate species are present. Although the exact temperature values vary slightly between this study and that in the literature, the idea of bidentate carbonates existing at a higher temperature than bicarbonates is agreed upon. The disparity between this study and the literature value for the decomposition temperature of bicarbonate could be a result of a systematic error in the thermocouple reading. This is supported by evidence presented in later chapters. Alternatively, the disparity could be explained by physical

differences between pure alumina and an alumina component in a mixed oxide sample like the one under study.

Finally, the small amount of CO_2 recorded by the mass spectrometer at a temperature of 289 °C is attributed to its release from the bulk of the sample. Once again, the CO trace seems to mirror the form of the CO_2, and it is conceivable that CO could also have been released *via* decomposition of the bulk structure.

5.2.2 - Promoted Catalyst

5.2.2.1 - Pulse experiment

Results

The effect of pulsing the 1 wt% potassium-promoted catalyst ("1% K") with CO to successively higher pressures is seen in Fig. 5.14. Because of the weak intensity of the main band (maximum absorbance is only 0.00480) the signal to noise ratio of the spectra is low. However, there appear to be 2 frequencies - 2110 and 2100 cm^{-1} at low coverage - which are seen at 2111 and 2102 cm^{-1} respectively after the final pulse. The FWHM of the band envelope is 39 cm^{-1}.

Fig. 5.15 shows the build-up of bands in the region below 1700 cm^{-1} on pulsing with CO to successively higher pressure. The miscancellation features evident for the unpromoted catalyst shown in Fig. 5.5 were not so marked for the promoted catalyst, but atmospheric water did pose a problem as seen by the noisy region between about 1700 and 1400 cm^{-1}. Nevertheless, bands were seen at about 1600, 1323, 1227 and 1047 cm^{-1}, and these grew with increasing pressure of CO pulse. No band was observed in the 3600 cm^{-1} area, although the noise level was high so features could have been obscured (Fig. 5.16).

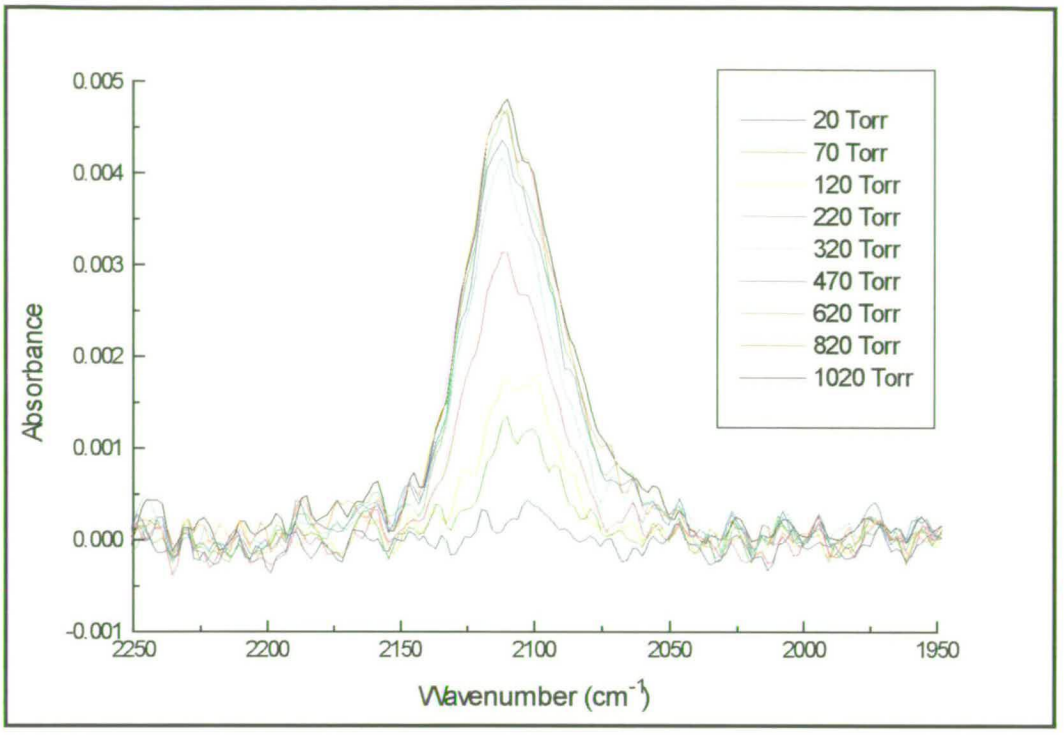

Fig. 5.14. *CO pulse experiment for the 1% K promoted catalyst.*

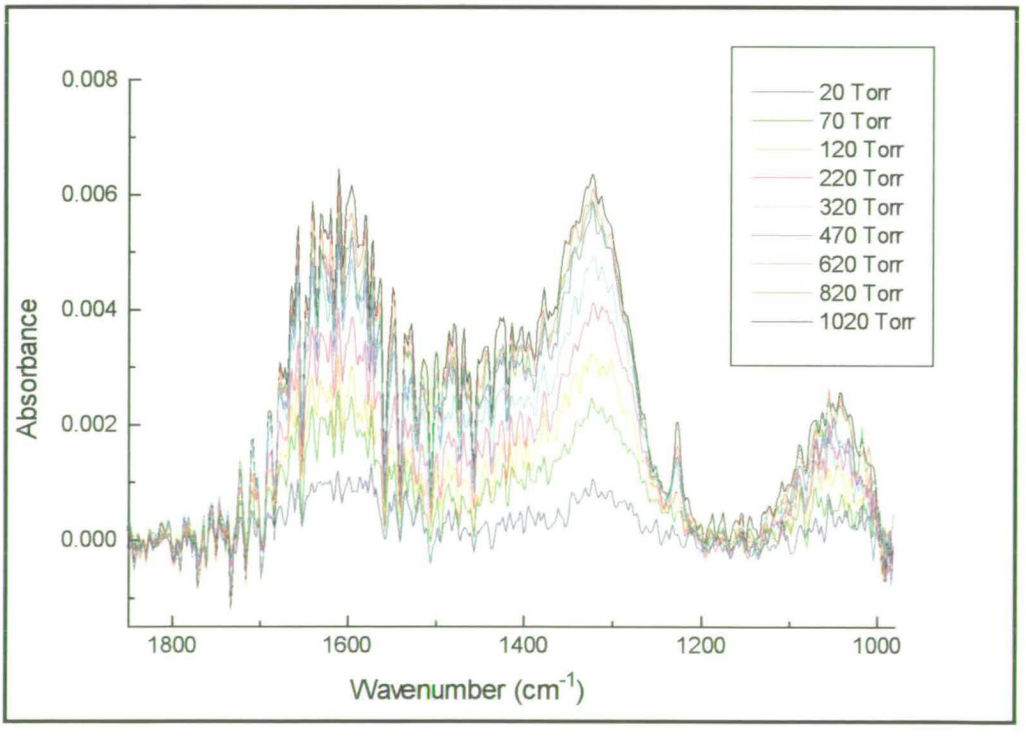

Fig. 5.15. *CO pulse experiment for the 1% K promoted catalyst - 1850-980 cm^{-1}*

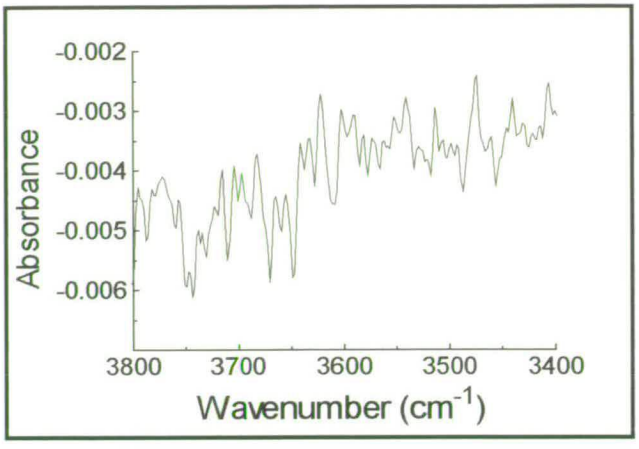

Fig. 5.15 *Spectrum taken after the final CO pulse on the 1% K promoted catalyst - absence of band at 3620 cm^{-1}.*

As for the unpromoted sample, both excess CO (i.e. that which had not adsorbed) and evolved CO_2 were observed by the mass spectrometer, as shown in Fig. 5.17. The quantities of unadsorbed CO ($CO_{(unadsorbed)}$) and CO_2 produced on exposure of the surface to CO ($CO_{2(reaction)}$) were calculated to be 12 and 3.7 μmol, respectively.

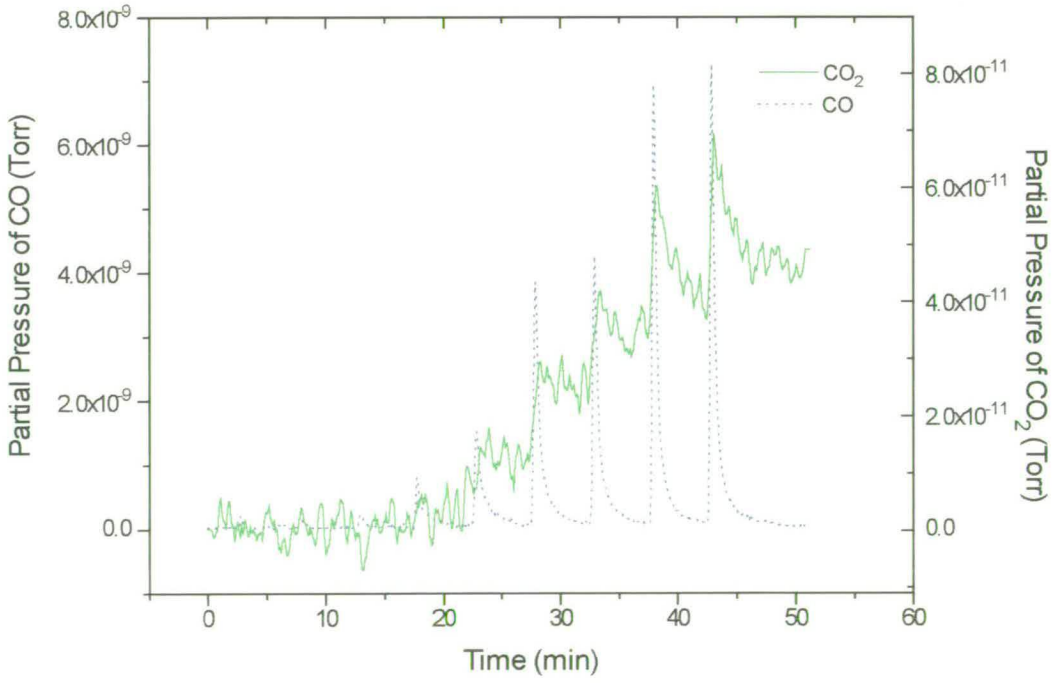

Fig. 5.17. *Gas phase CO and CO_2 observed by the mass spectrometer during the CO pulse experiment for the 1% K promoted sample*

Discussion

The band at 2102 cm^{-1} can be assigned, as for the unpromoted sample, to CO linearly adsorbed on a stepped plane of Cu^0, while that at 2111 cm^{-1} again suggests CO adsorbed on either $Cu^{\delta+}$ or copper with Cu^{n+} as its next nearest neighbour. There appears to be less contribution from the band at 2111 cm^{-1} than for the promoted sample, and the band at 2143 cm^{-1} is completely absent, suggesting that there is no copper oxide present. Overall it seems that the promoted sample is better reduced than the unpromoted.

The red shift in CO stretching frequency which has been observed previously for both copper [86] and other transition metal single crystals [85] and supported metals [50, 87] on promotion with alkali is absent. Fig. 5.18 shows this by comparing the spectra collected at saturation for the unpromoted and promoted samples and normalising their intensities.

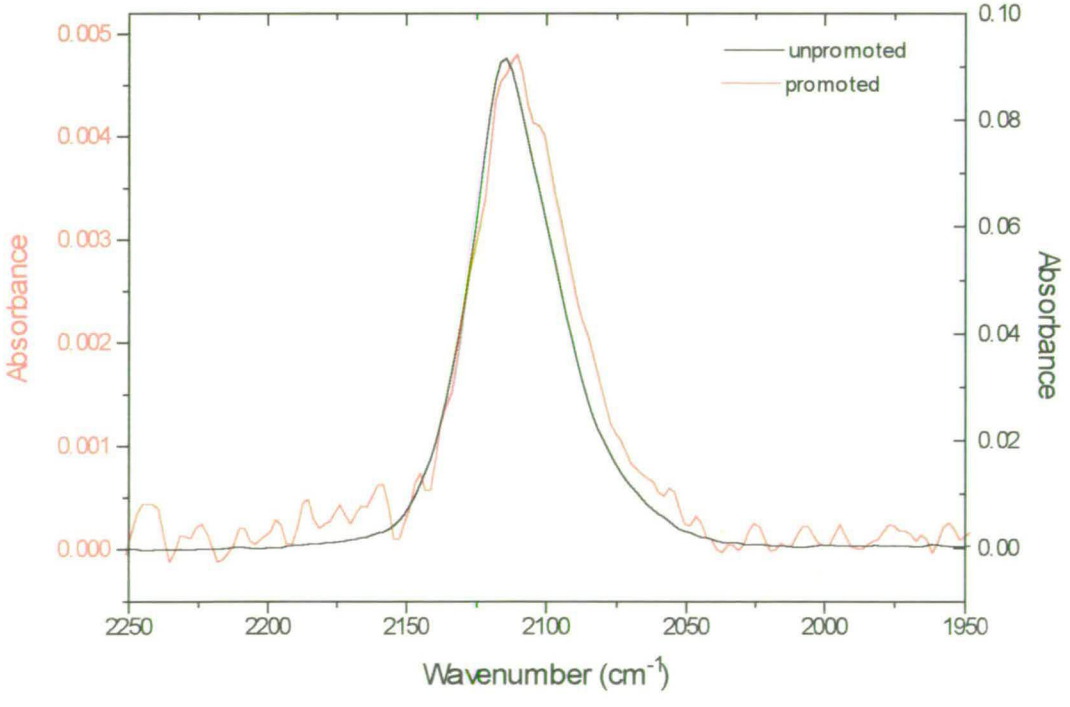

Fig. 5.18. *Comparison of unpromoted and 1% K promoted catalyst, showing negligible shift of CO stretching frequency on promotion.*

However, the most salient feature on promotion is an attenuation of the CO peak intensity from an absorbance of 0.0951 to 0.00480. One reason for this surprising result could be a *site blocking* action of the promoter, whereby the potassium covers the copper sites, resulting in a decreased quantity of adsorbed CO. In the study by Whitman and Ho [25] such a hypothesis was made for Ni(110) with coadsorbed CO and low coverages of potassium. LEED studies (Low Energy Electron Diffraction), in conjunction with HREELS, found evidence for islands of potassium where local, direct interactions occurred with CO molecules. Simultaneously, "blank" islands existed which were unaffected by the promoter, giving rise to CO stretching frequencies similar to those on the unpromoted surface. A similar situation might be expected to occur on Cu(110) and even on higher index planes of copper.

The study by Lackey *et al.* [83] of Cu(110) with coadsorbed potassium and CO, found that at 0.2 monolayer of potassium a band was seen at 2090 cm^{-1} which was identified as CO chemisorbed on copper sufficiently removed from alkali atoms to suffer no local interaction, and had a frequency unshifted from the value for the clean metal [41]. Increasing the alkali level to a full monolayer resulted in the disappearance of the band at 2090 cm^{-1} and increases in intensity in the region below 1600 cm^{-1}, which were attributed to the presence of K-CO complexes.

As an approximation, the alkali level in this study is expected to be about 1 monolayer for 1 wt% potassium assuming a 1:1 K:Cu ratio and that the alkali is not in islands or 3-dimensional clusters (Chapter 3). If comparisons are drawn with the work of Lackey *et al.* [83], the huge attenuation in CO stretching intensity is anticipated. The lack in red shift in the present study can be attributed to CO-Cu species which are unperturbed by local potassium interactions.

Finally, on the topic of the huge attenuation of CO stretching intensity, these findings are in agreement with the corresponding loss in copper surface area on promotion noted in Chapter 3. However, the loss in the CO stretching band goes far

beyond this; for the 1% K promoted catalyst a 95% loss in absorbance units is seen according to the infra-red data compared with a 40% loss found by the surface area measurements (neglecting any dipole-dipole coupling [79]). This suggests that the promotional effect of the alkali goes beyond being a simple surface area effect, perhaps preferentially preventing the adsorption of certain molecules.

If much of the copper surface area has been blocked by potassium, it is possible that the CO adsorbs and/or reacts with the potassium directly. The most striking effect of the alkali found by Lackey *et al.* [83] was the formation of K-CO complexes and these produced bands in the region of the spectrum below 1600 cm^{-1}. Therefore, it is worth looking now at the effect of the potassium promoter on this region.

To compare spectra for the unpromoted and the promoted samples in the 1700 - 1000 cm^{-1} region, Fig. 5.15 showed the existence of a sharp band at 1227 cm^{-1}, which was also seen in Fig. 5.5 for the unpromoted sample. This was attributed to a bicarbonate species on alumina. The promoted sample's spectrum was partly obscured by features due to atmospheric water making it difficult to observe the presence of the other characteristic bands of bicarbonate. However, on displaying the two samples' spectra together (Fig. 5.19) the possibility of a band at 1650 cm^{-1} becomes evident. Thus it is apparent that bicarbonate on alumina is also present for the promoted sample.

Fig. 5.19 also reveals that there is an overall decrease in intensity of the bands between 1700 and 1000 cm^{-1} on promotion. The maximum in the region (at 1323 cm^{-1}) is now only 0.006 absorbance units; 27 % of that for the corresponding measurement on the unpromoted sample. The total surface area for the promoted catalyst, determined by the BET method, was found to be 51 % of that for the unpromoted sample. The difference between this and the decrease in infra-red band intensities is probably partly because the sample was not subjected to any harsh pre-treatment before the BET measurements that could have induced catalyst

sintering. In agreement with the decrease in infra-red band intensities, it was found that proportionally less CO was adsorbed from the pulses of gas introduced to the promoted catalyst than the unpromoted catalyst. Expressing these values as a percentage of the total amount of gas detected by the spectrometer during the course of each experiment (to account for any variations in the performance of the mass spectrometer between experiments), it was found that for the unpromoted catalyst 21 % of the total gas detected was unadsorbed CO, while 41 % was unadsorbed for the promoted catalyst.

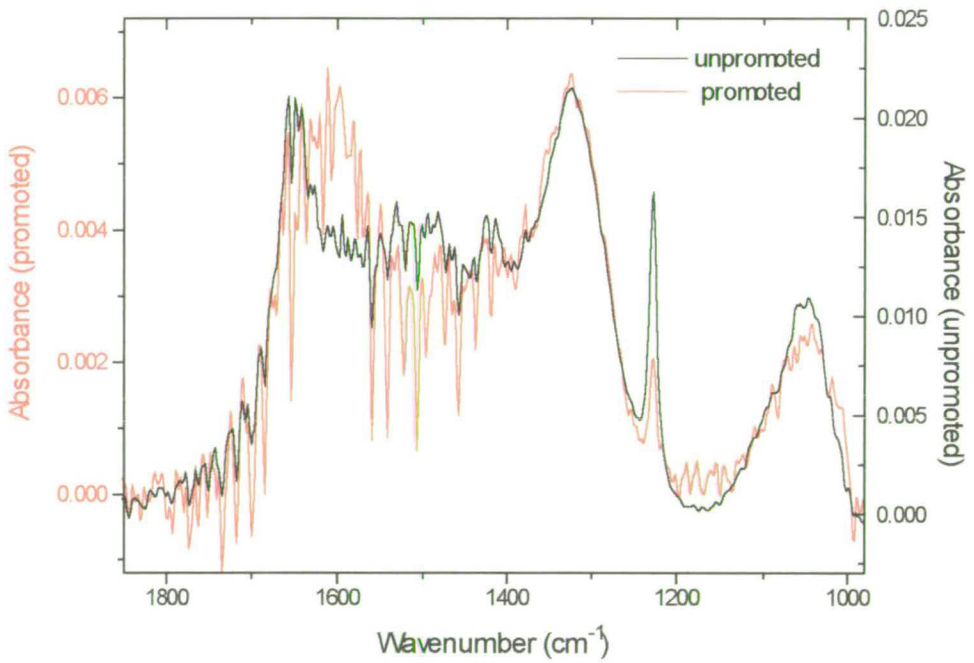

Fig. 5.19. *Comparison of unpromoted and 1% K promoted catalyst, showing 1700 - 1000 cm^{-1} region.*

On comparing the band at 1227 cm^{-1} for the two samples, the intensity for the promoted sample is only 11% of that for the unpromoted sample. In accordance with this, the band at 3620 cm^{-1}, attributed to the υ_{OH} of the bicarbonate species, is present on the unpromoted catalyst while being absent on the promoted sample. Thus, the level of bicarbonate species is decreased on the promoted catalyst surface more than other species with bands in the 1700 - 1000 cm^{-1} region.

An explanation for this behaviour can be found in Stork and Pott's work which was discussed in the introduction to this chapter [119]. They observed that alumina which had been promoted with potassium carbonate did not yield the formation of surface compounds such as potassium oxides or aluminates on calcination at temperatures up to 900 °C, but instead the formation of $-O^-K^+$ groups ocurred, according to reaction 5.7. The presence of these $-O^-K^+$ groups would be expected to hinder the formation of bicarbonate species from surface hydroxyl groups and CO_2.

$$K_2CO_3 + 2(-OH) \rightarrow CO_2 + H_2O + 2(-OK) \qquad \textit{reaction 5.7}$$

Another possible effect of the potassium can be suggested when considering the dominant bands in the spectrum for the promoted sample at 1600 and 1323 cm^{-1}. Previously, bands found on the unpromoted sample at 1323 and 1045 cm^{-1} and a feature suggested as existing at 1600 cm^{-1} were attributed to the presence of bidentate carbonate on the zinc oxide component of the catalyst. The dominance of these bands for the promoted sample could be simply attributed to the relative decrease in the amount of bicarbonate formed. However, it is also possible that a new potassium-related species has formed. The sort of complexes proposed by Lackey *et al.* must be ruled out. Identical bands were seen during this study in the spectra for the CO_2 reactions which will be discussed in detail in later in this chapter, meaning that the species is not likely to be of the formula $K_m(CO)_m$.

In another study, Krupay and Amenomiya [111] observed weak bands at 1590 and 1320 cm^{-1} at 150 °C on the adsorption of CO on potassium promoted alumina. Above 400 °C, bands at 1570 and 1320 cm^{-1} also developed. These bands were attributed to a CO_2^- ion chemisorbed on K^+, (1), and a bidentate carbonate, (2), respectively (Fig 5.20). Although no features were observed with CO at room temperature, on the adsorption of CO_2 at room temperature, the 1590 and 1320 cm^{-1} bands were seen, with the bands at 1570 and 1320 cm^{-1} growing in at 150 °C. Since CO_2 was observed by the mass spectrometer to be produced on contact of CO with

the catalyst during *this* study, it is possible that the bands observed could be due one of these species, which were thought by Krupay and Amenomiya to be intermediates in the exchange of oxygen between their alumina sample and both $C^{18}O_2$ and $C^{18}O$. Species (1) seems most likely as they observed this at room temperature. The bands at 1600 and 1323 cm^{-1} are not due to the formation of K_2CO_3, as this would be characterised by a band between 1500 and 1410 cm^{-1} [121].

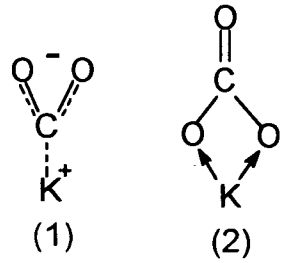

Fig. 5.20. *Carboxylate (1) and carbonate (2) observed by Krupay and Amenomiya [111] on potassium promoted alumina.*

The band at 1047 cm^{-1} could give some insight into whether species (1) or (2) is responsible for the bands in question; this would be present for a carbonate species, but not a carboxylate [32]. On plotting the absorbance against CO pulse pressure, the bands at 1600 and 1323 cm^{-1} would be expected to scale with one another, while that at 1047 cm^{-1} would act independently in consistency with all three bands having a contribution from the bidentate carbonate on zinc oxide and the bands at 1600 and 1323 cm^{-1} having an additional contribution from a species such as a potassium-associated carboxylate. On constructing this plot, within error limits the band at 1045 cm^{-1} acts in the same manner as the other two (Fig. 5.21, with intensities normalised to equal 1). However, this does not necessarily exclude there being a new species present - it could simply have formed at a similar rate to the bidentate carbonate on zinc oxide. This topic will be returned to in the discussion of the effect of promotion on CO_2 adsorption.

The temperature programmed desorption experiment might help to clarify this situation, but it seems certain from the pulse experiments that a bicarbonate species on alumina dominates the support of the unpromoted catalyst with a smaller quantity of a

bidentate carbonate on zinc oxide, while either the bidentate carbonate predominates on the 1% K promoted catalyst or, possibly, another species associated with the promoter has formed.

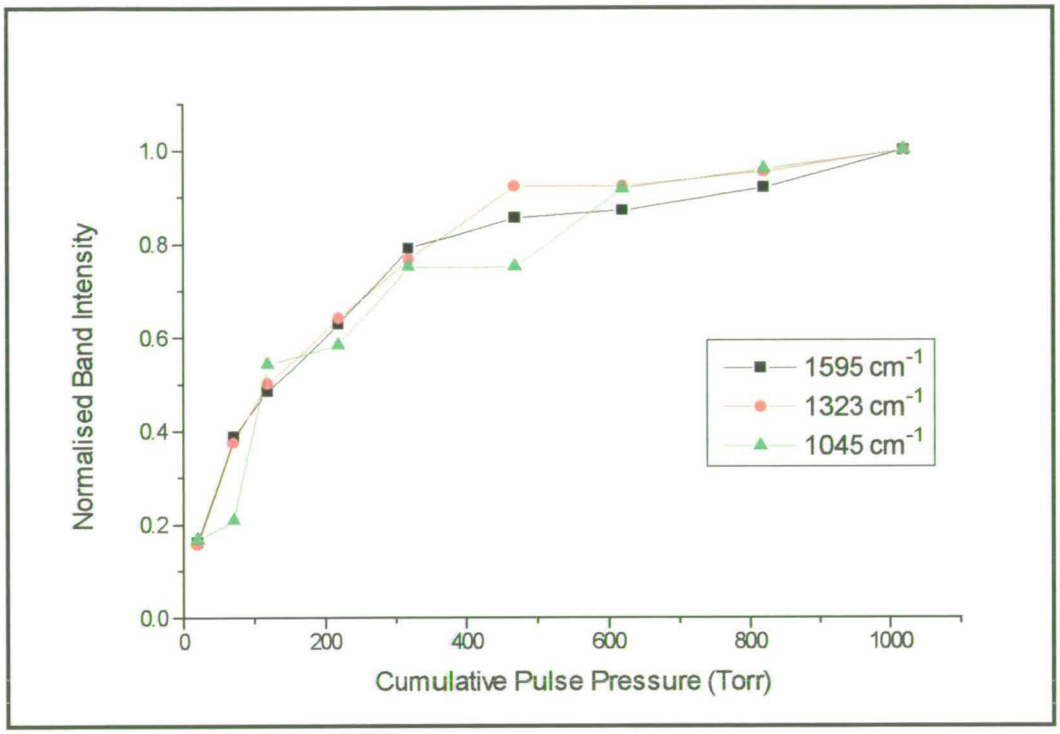

Fig. 5.21. *Variation in intensity of bands at 1600, 1323, and 1047 cm^{-1} vs cumulative CO pulse pressure for 1% K promoted catalyst (i.e. eventually 1020 Torr (11.0 μmol) have been pulsed). Band intensities have been normalised to equal 1.*

5.2.2.2 - Temperature Programmed Desorption

Results

As for the unpromoted sample, bands in the infra-red spectrum generally decrease in intensity as the sample temperature is raised. Fig. 5.23 illustrates these changes for the CO stretching region and Fig 5.24 for the region between 1700 and 1000 cm^{-1}. Once again, the data in the 1700 to 1000 cm^{-1} region have not been baseline corrected. The effect on the relative intensity of the single beam spectrum when heating a sample was

shown in Fig. 3.13 in Chapter 3. Fig. 5.22 justifies the use of raw data rather than baseline correcting by illustrating the type of misleading information that can arise in the presence of miscancellation features. The baseline corrected data shows two bands growing in with increasing temperature. One of these is at 1323 cm^{-1}, and actually coincides with a feature seen in the pulse experiment. However, the other (1480 cm^{-1}) is at the same position as the "well" between the two intense bands seen in the single beam spectrum at 1550 and 1400 cm^{-1}. Thus, these bands are assumed to be the result of the growing in of miscancellation as the temperature increases, and this is evident when noting their absence in the raw data of Fig. 5.24.

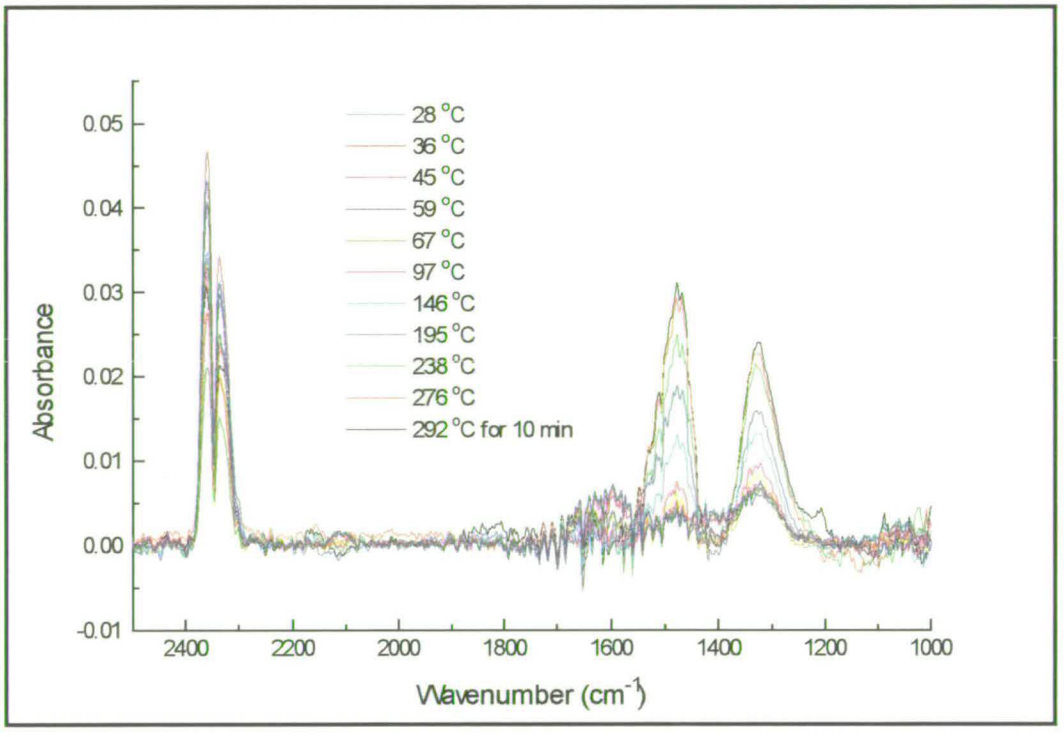

Fig. 5.22. *Temperature programmed desorption following CO pulse experiment for the 1% K promoted catalyst showing how baseline correction can generate misleading data.*

As for the unpromoted catalyst, the temperature at which species cease to exist on the surface will be stated. The most reliable features in the spectrum were again those which have been attributed to adsorbed CO and bicarbonate on alumina, which were found at 2111 (with a shoulder at 2102) and 1227 cm^{-1}, respectively.

Both CO and the bicarbonate species were found to have left the catalyst surface by 77 °C. The 1227 cm^{-1} is very weak, so cannot be easily seen in Fig 5.24. The temperature at which the rate of desorption was maximum - T_{max} - was determined by plotting the absorbance as a function of temperature and differentiating to find the position of maximum gradient. T_{max} was thus found to be 59 °C for both CO and the bicarbonate species. The CO stretching region has a poor signal to noise ratio owing to the low intensity of the bands.

The behaviour of the other bands in the spectrum was difficult to follow with increasing temperature, partly due to miscancellation problems, but also because of the high noise level. The band at 1600 cm^{-1} seemed to exist until around 121 °C, that at 1047 cm^{-1} which was a broad, weak band on a sharply sloping baseline appeared to desorb by 59 °C, while the feature at 1323 cm^{-1} seemed to grow until 146 °C and then had disappeared by about 195 °C.

Information recorded by the mass spectrometer shows that CO was evolved as the sample temperature was raised, and T_{max} occurred, as for the unpromoted sample, at 51 °C (Fig. 5.25). The integrated area of the trace allows the amount of CO evolved ($CO_{(TPD)}$) to be evaluated, and is found to be 0.52 μmol. CO_2 was also detected (Fig. 5.26). Overall, the trace is broad, but it is possible that it is composed of a broad maximum at 120 °C with an additional weak shoulder at 60 °C. The amount of $CO_{2(TPD)}$ evolved in this case was 13 μmol.

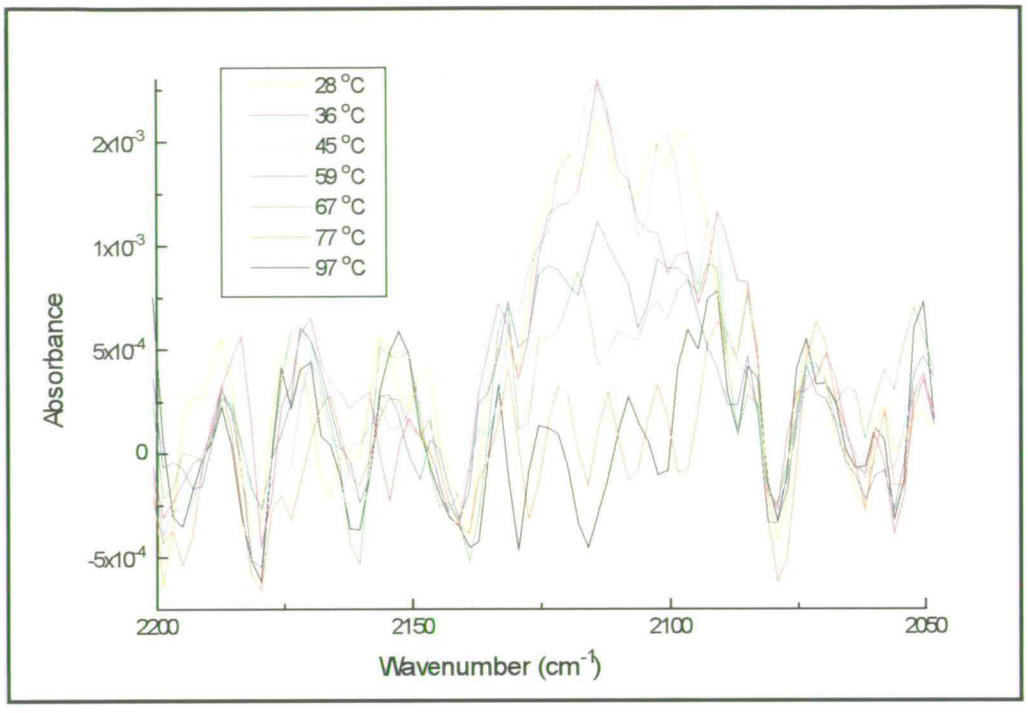

Fig. 5.23. *Temperature programmed desorption following CO pulse experiment for the 1% K promoted catalyst in the CO stretching region.*

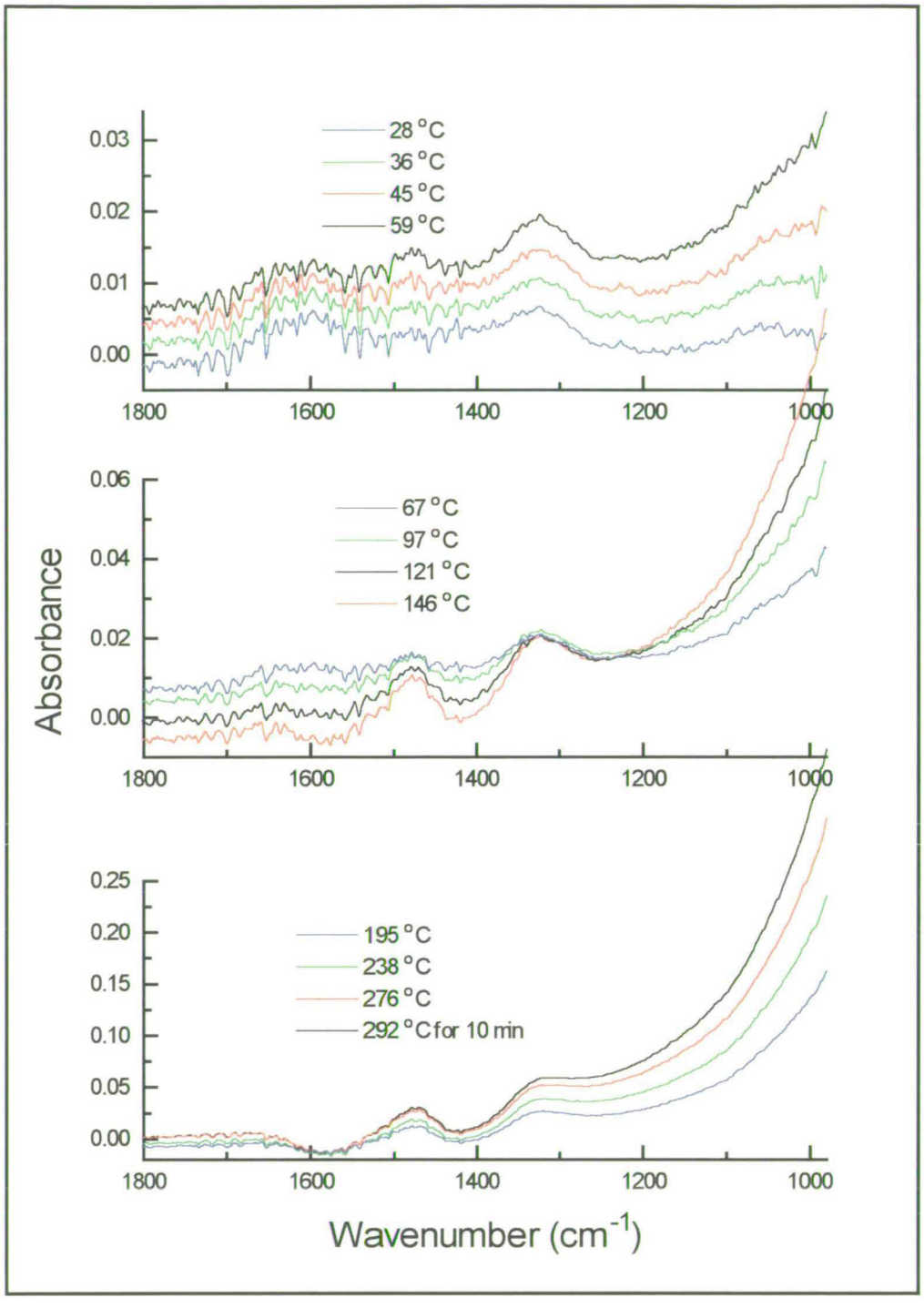

Fig. 5.24. *Temperature programmed desorption following CO pulse experiment for the 1% K promoted catalyst (not baseline corrected).*

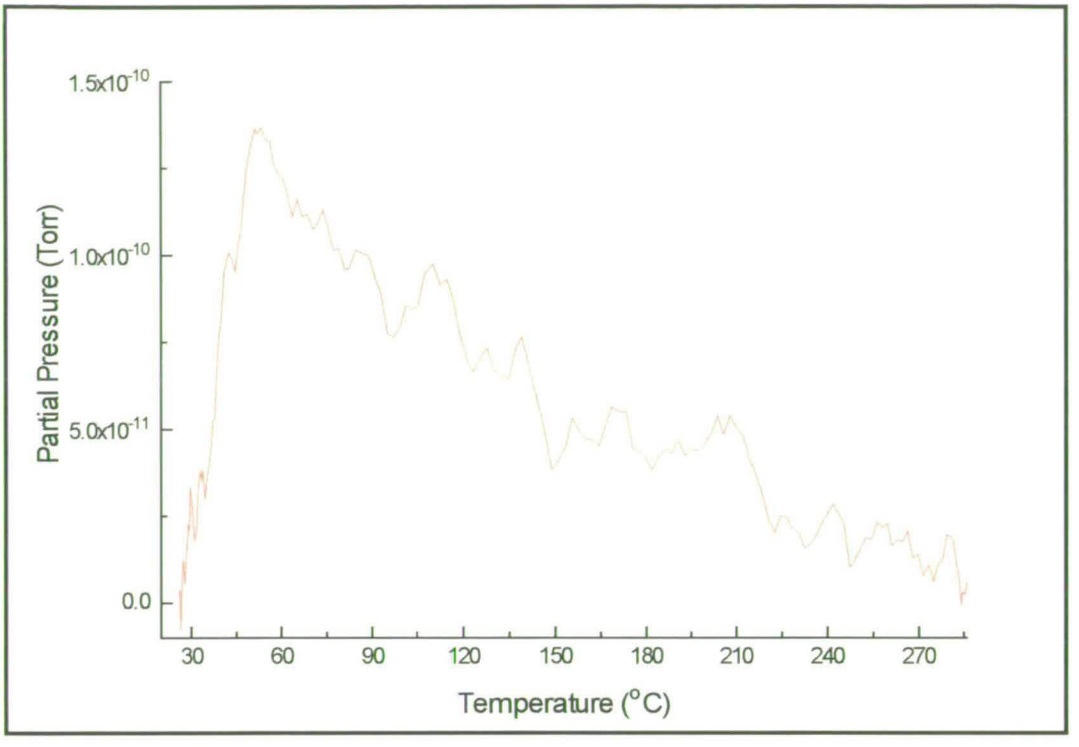

Fig. 5.25. *Temperature programmed desorption of CO from the 1%K promoted catalyst following CO pulse experiment.*

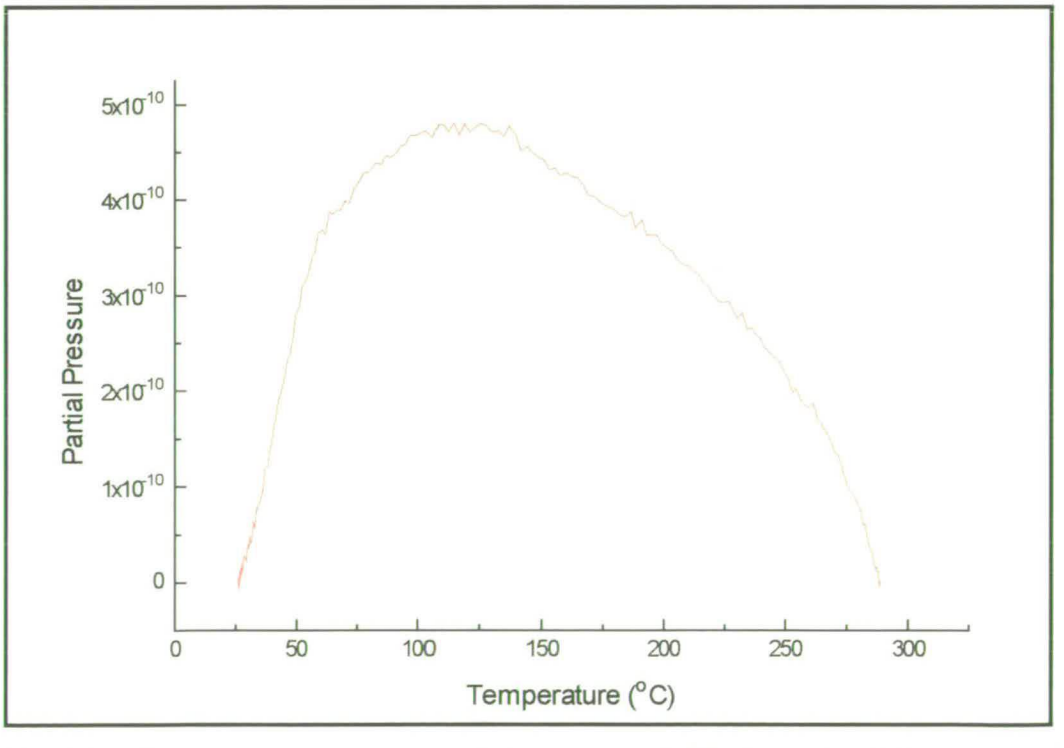

Fig. 5.26. *Temperature programmed desorption of CO_2 from the 1%K promoted sample following CO pulse experiment.*

Discussion

T_{max} for the CO stretching frequency was found to be 59 °C. This correlates well with T_{max} found for CO by the mass spectrometer, 51 °C. Comparing this information with the corresponding experiment for the unpromoted catalyst reveals no shift in T_{max} but an attenuation in the relative amount of CO desorbed such that (promoted $CO_{(TPD)}$) is 25% of (unpromoted $CO_{(TPD)}$). Although this finding is not as extreme as that from the pulse experiment where the CO stretching intensity was attenuated to 5% of the original value on promotion, the tendency is the same, and once again suggests a site blocking action of the promoter with no long range effects.

On considering the behaviour of the carbonate-type species during TPD, little may be said conclusively about the infra-red data, except that the band at 1227 cm^{-1}, attributed to bicarbonate on alumina, was found to have a T_{max} at 59 °C and was last seen on the surface at 77 °C. It is uncertain when exactly the other bands which have been attributed to bidentate carbonate on zinc oxide and possibly another species such as a carbonate/carboxylate associated with potassium left the surface, but the band at 1600 cm^{-1} was definitely present at temperatures greater than for the band at 1227 cm^{-1}, and was possibly last present at around 121 °C.

To compare this information with that found by the mass spectrometer, the CO_2 trace, shown in Fig. 5.26, is broad, indicating the possibility of a number of contributions. It is, however, possible that there is a weak shoulder at 60 °C and a broad maximum at 120 °C with a high temperature tail, and these could correspond to the desorption of bicarbonate, and bidentate carbonate or a carbonate/carboxylate associated with potassium, respectively. This suggestion once again reflects the finding in the literature [115] that bicarbonates decompose on alumina surfaces at lower temperatures than carbonate species.

On plotting together the CO_2 mass spectrometer traces for the unpromoted and 1% K promoted catalysts during TPD on different y axis scales (Fig. 5.27) it is

possible to highlight the differences. Firstly, the absence of the prominent peak found for the unpromoted sample at 57 °C is noted; it was suggested that the origin of this peak could be the oxidation of adsorbed CO to CO_2 by surface oxygen from copper during the TPD. The promoted catalyst's copper component was found to be better reduced, in support of this suggestion.

It is also clear that there is more of low temperature component in the mass spectrometer trace for the unpromoted catalyst (T_{max} between approximately 60 and 80 °C) which is, in addition to the suggestion made above, due to a greater quantity of bicarbonate on this surface. This is again consistent with the formation of an $-O^-K^+$ species which inhibits the formation of bicarbonate. The promoted catalyst appears to have more of a high temperature component (T_{max} between approximately 90 and 130 °C, and evolving CO_2 until about 300 °C) which could be due to a new, potassium-associated species.

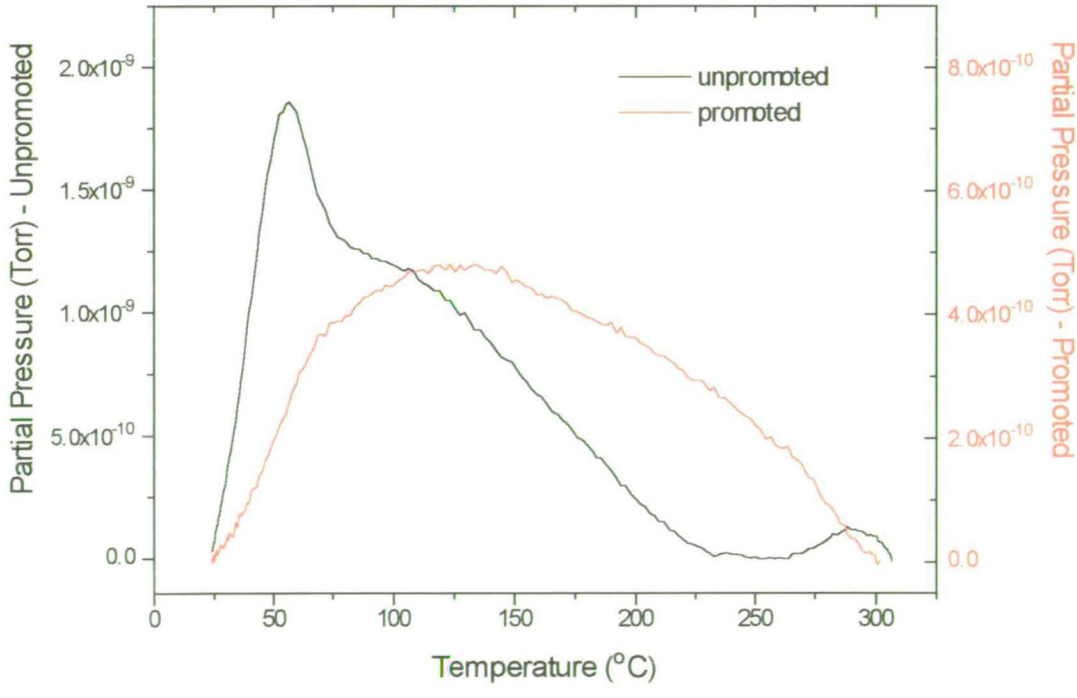

Fig. 5.27. *CO_2 evolved from the unpromoted and 1% K promoted catalysts during TPD - different scales for y axes*

5.2.3 - Effect of Varying the Level Of Promoter

In order to gain a broader picture of the action of the promoter, the effect of the potassium level on the CO band intensity and species desorbed during TPD were investigated. Catalysts promoted with from 0 to 1 wt% potassium were studied, in addition to a catalyst "promoted" with water so that effects due to the promotion method could be monitored.

Results

Fig. 5.28 shows a exponential-type decrease in absorbance with increasing promoter level. An initial decrease in CO uptake is noted even on "promotion" with water.

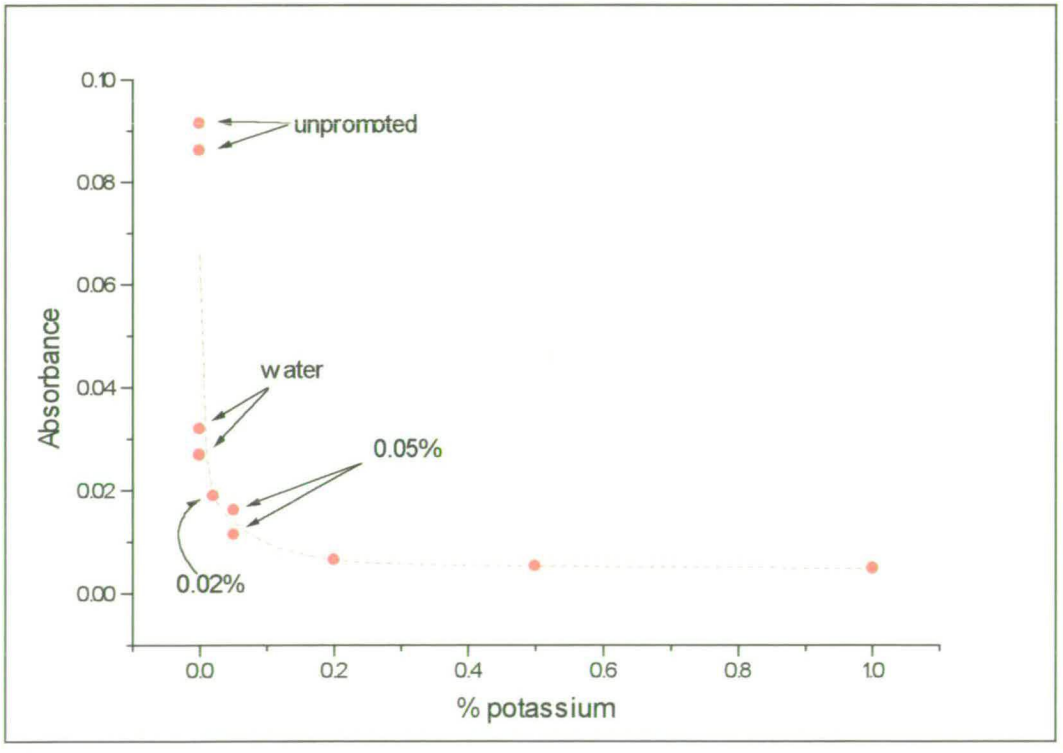

Fig. 5.28. *Variation of CO band intensity with potassium level, in wt%.*

The desorption of CO from the catalysts following the CO pulse experiment is illustrated in Fig. 5.29, as a function of alkali promoter level. T_{max}, 51 °C, is unchanged for each experiment, and a gradual decrease in the amount of CO desorbed with increasing promoter level is observed.

Fig. 5.30 shows the desorption of CO_2 from the catalysts following the CO pulse experiment as a function of alkali promoter level. Again, a gradual decrease in the amount of CO_2 desorbed from each catalyst on increasing promoter level is found, along with an increase in the relative importance of a high temperature component.

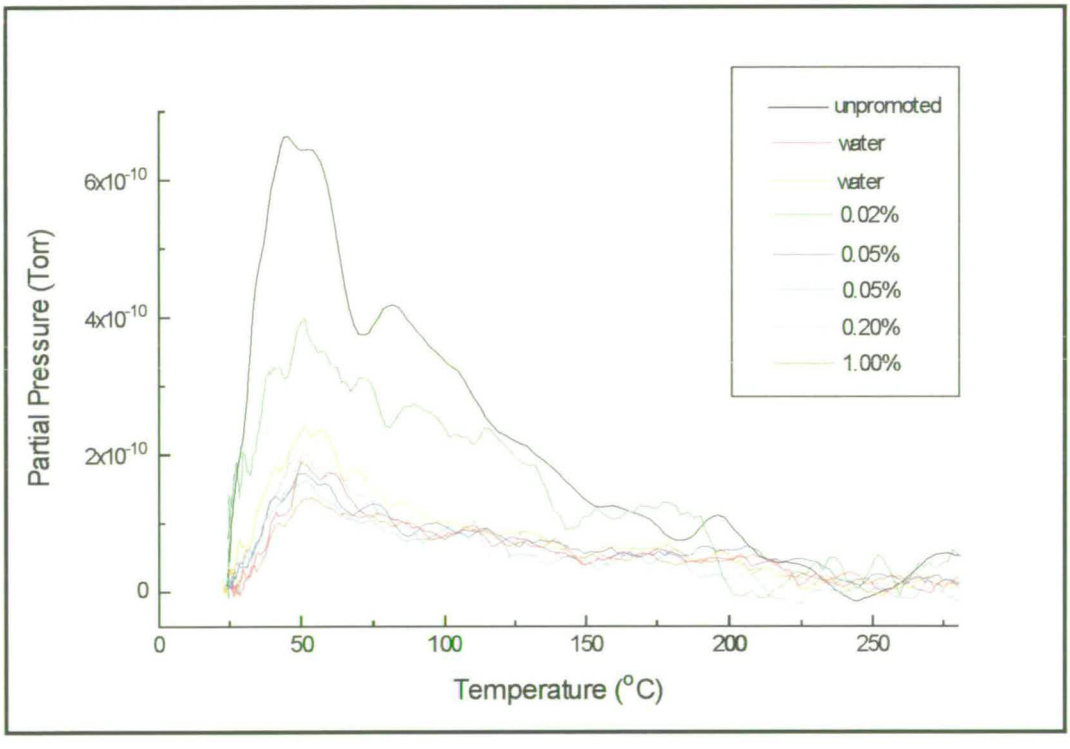

Fig. 5.29. *The variation in amount of CO evolved during TPD with the level of potassium (wt%).*

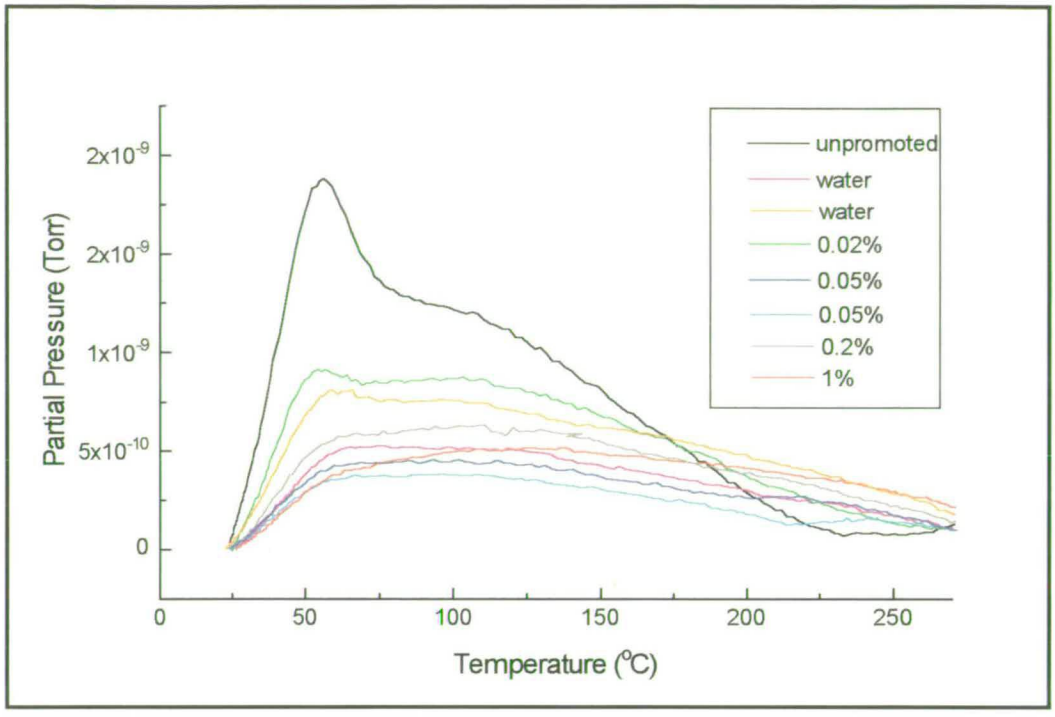

Fig. 5.30. *The variation in the amount of CO_2 evolved during TPD with the level of potassium (wt%).*

Discussion

The initial decrease in CO uptake on "promotion" with water alone suggests some change in morphology of the catalyst during the promotion procedure. Thereafter, a further decrease can be seen as the alkali level is increased, which is additional evidence for the existence of a site-blocking action of the promoter. The exponential-type nature of the curve in Fig. 5.28 suggests that after a potassium level of about 0.2 wt%, the alkali must have another destination, as no further attenuation in CO stretching frequency intensity is seen. It is possible that this destination is the support, and there is much evidence to substantiate this claim.

Fig. 5.29 shows that as the level of alkali increases, there is a decrease in the amount of CO desorbed during the TPD, which reflects the behaviour of the CO stretching frequency band. The lack of shift in T_{max} with increasing alkali level

reinforces the suggestion of the absence of long range effects of the alkali on the copper metal, even at low coverage, and the idea of "blank islands" of copper from Whitman and Ho can be invoked to explain this [25]. Another study of a supported metal system, Ru/SiO_2 catalysts promoted with a potassium salt, found agreement with this; Uner *et al.* [24] used proton NMR of hydrogen chemisorption to show that strong electronic interactions were not operable, and concluded that alkali atoms on single crystal surfaces were not good models for the behaviour of supported catalysts. They also found that the potassium promoter blocked adsorption sites.

In the case of desorbed CO_2 (Fig. 5.30), marked differences can be seen between the unpromoted and especially the 1 wt% K catalyst, with the other levels of promotion fitting in between. First, the prominent peak at about 57 °C was attributed to the oxidation of CO (which had been adsorbed on oxidised copper) as it left the surface. The gradual decrease of this peak with increasing level of promoter is consistent with a progressively more reduced surface, which was suggested by the absence of a shoulder at 2140 cm^{-1} (copper oxide) for the 1 wt% K promoted sample. An effect of the alkali on the support is also evident, which appears to be greatest for amounts of potassium above 0.2 wt%. The infra-red data taken during TPD has already shown that bicarbonate species on the support seem to leave the surface at temperatures lower than do other bands due to carbonate species. In accordance with this, two components seem to be present in the CO_2 mass spectrometer traces, peaking in the following approximate temperature ranges:

1) a "low temperature" desorption peaking between 60 to 80 °C, and
2) a "high temperature" desorption peaking between 90 and 130 °C.

A greater relative contribution from the high temperature component is seen even on "promoting" with water, which could be due to a morphological change. The effect continues with increasing level of promoter, once again suggesting either an enhanced amount of bidentate carbonate on zinc oxide or the formation of a new surface species associated with the potassium - perhaps a carboxylate or carbonate as shown in Fig.

5.20. This is at the expense of bicarbonate formation, which is thought to be hindered in the presence of potassium when hydroxyl groups are replaced by $-O^-K^+$ groups. In the study by Uner *et al.* [24], a similar effect was seen whereby the amount of surface silanol groups in silica was reduced by an exchange of potassium with Si(OH) groups to form Si(OK) species.

It has become clear during the various CO adsorption experiments that there are several paths which the CO can take when it comes into contact with the catalyst. The mass spectrometer has allowed the detection of "$CO_{2(reaction)}$" produced *via* the oxidation of CO by the catalyst surface at room temperature, "$CO_{(TPD)}$" during the desorption of CO from copper detected during TPD, and finally "$CO_{2(TPD)}$", evolved as a consequence of the decomposition of carbonates and possibly carboxylates, and also maybe produced reactively as CO leaves oxidised copper. The processes are represented by reaction 5.9.

$$CO_{(g)} \rightarrow CO_{2(reaction)} + CO_{(TPD)} + CO_{2(TPD)} \qquad \textit{reaction 5.9}$$

Table 5.2 shows the amount of each of these products from CO adsorption varying as a function of potassium level. It can be seen that the amount of all three species decreases with increasing promoter level, as was shown in the infra-red and mass spectrometer results, and this is expected, largely owing to the decrease in surface area on promotion. As a result, it is difficult to identify any trends within the data. To address this problem, an attempt has been made to normalise the data: each species has been expressed as percentage of the total species detected in each experiment. The situation is still not ideal - subtle effects are being investigated on data with large variations, and this is highlighted by looking at the experiments which have been repeated. Nevertheless, it appears tentatively that $CO_{2(reaction)}$ does decrease on promotion, while $CO_{(TPD)}$ is increased slightly and $CO_{2(TPD)}$ is increased to a greater extent. Plotting the information as bar graphs highlights the effects better (Fig. 5.31)

Table 5.2. *Variation in the relative amounts of products from CO adsorption with level of promotion, expressed both in μmol and as a percentage of the total.*

Promotion	$CO_{2(reaction)}$		$CO_{(TPD)}$		$CO_{2(TPD)}$		Total	
wt%	μmol	%	μmol	%	μmol	%	μmol	%
0	51	64	2.1	2.0	27	34	80	100
water	6.4	36	0.53	2.0	11	62	18	100
water	9.6	34	0.75	2.0	18	64	28	100
0.02	50	71	2.2	3.0	18	26	70	100
0.05	4.9	33	0.62	4.0	9.5	63	15	100
0.05	6.0	42	0.43	3.0	8.0	55	14	100
0.2	1.3	9.0	0.62	4.0	14	87	16	100
1	3.7	22	0.52	3.0	13	75	16	100

The reason for the decrease in $CO_{2(reaction)}$ with increasing alkali level could be explained by a decrease in the rate of reaction 5.10 because the sample is better reduced or, alternatively, it is possible that more of the CO_2 produced by oxidation is adsorbing on the catalyst.

$$CO_{(g)} + O_{(a)} \rightarrow CO_{2(g)} \qquad \textit{reaction 5.10}$$

This seems possible on looking at the relative increase in $CO_{2(TPD)}$ with increasing alkali level. Thus, it appears that the promoted catalyst is more effectively storing CO_2 in state to be released at high temperature. This state could be a new potassium-associated species, as suggested earlier. Whatever the identity, the tendency to convert CO to CO_2 has been increased, which has important implications for the use of the catalyst in the WGS reaction where the oxidation of CO to CO_2 is a proposed step in the redox-style mechanism [94], described in Chapter 7. The increase in $CO_{(TPD)}$, however, is small relative to the other changes, and might not be a real effect.

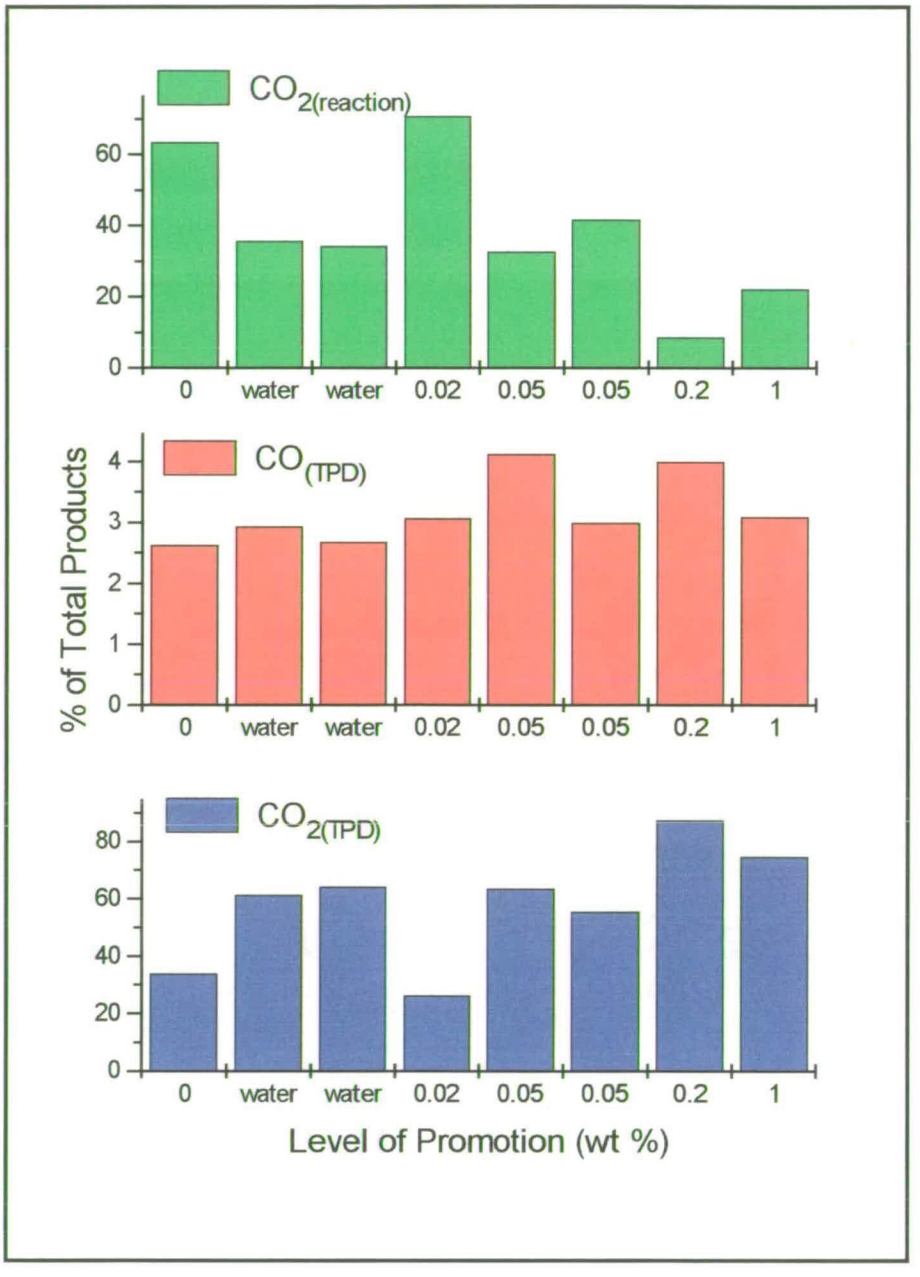

Fig. 5.31. *Variation in the relative amounts of products from CO adsorption with level of promotion, expressed as a percentage of the total.*

5.3 - The Adsorption of Carbon Dioxide

The CO_2 pulse experiments were carried out in the same way as for CO adsorption; CO_2 was pulsed with successively higher pressures in the sequence 20, 50, 50, 100, 100, 150, 150, 200, and 200 Torr, so that the total exposure was eventually 1020 Torr. Once again adsorbed species were monitored using DRIFTS, while gas phase species were detected using the mass spectrometer. Subsequently, a temperature programmed desorption was carried out.

As was discussed in Chapter 4, difficulty was encountered in maintaining consistency in the degree of catalyst reduction between sets of experiments. In order to characterise the catalyst surface and determine the state of the copper following pre-treatment, a CO pulse experiment was carried out. As detailed in Example 5 in Chapter 4, the surface was found to be better reduced; stepped planes of Cu^0 predominated, with a small amount of $Cu^{\delta+}$ or Cu^0 with Cu^{n+} as its next-nearest neighbour, and apparently no copper oxide. The state of the catalyst is the same for the remainder of this thesis.

5.3.1 - Unpromoted Catalyst

5.3.3.1 - Pulse Experiment

Results

Fig. 5.32 shows the effects of pulsing the unpromoted catalyst with CO_2 to successively higher pressures. The most intense features of the spectrum are in the region below 1700 cm^{-1}. After the first pulse (20 Torr), bands are clearly seen at 1655, 1427 and 1227 cm^{-1}, with a shoulder at 1331 and a weak band at 1038 cm^{-1}. There is the possibility of another shoulder at 1606 cm^{-1}, but the miscancellation at

about 1550 cm^{-1} makes it difficult to be certain. The sharpest bands continue to grow in intensity on increasing pressure of pulse, and on the final spectrum are found at 1650, 1425 and 1227 cm^{-1}. The band at 1038 cm^{-1} also becomes stronger and is shifted to 1053 cm^{-1} in the final spectrum, while the feature at 1331 cm^{-1} remains a weak shoulder.

Bands outwith the 1700 - 1000 cm^{-1} region include a very weak one at 3620 cm^{-1}, superimposed over a broad feature (Fig. 5.33) which develops as soon as CO_2 is admitted to the catalyst, and continues to grow with successive pulses. A very low intensity band is possibly present at 2194 cm^{-1}, but noise levels make it difficult to be certain. There is also the likelihood of one at 2339 cm^{-1}, although this is superimposed onto the bands of gaseous atmospheric CO_2 in the spectrometer (a doublet centred at 2347 cm^{-1}).

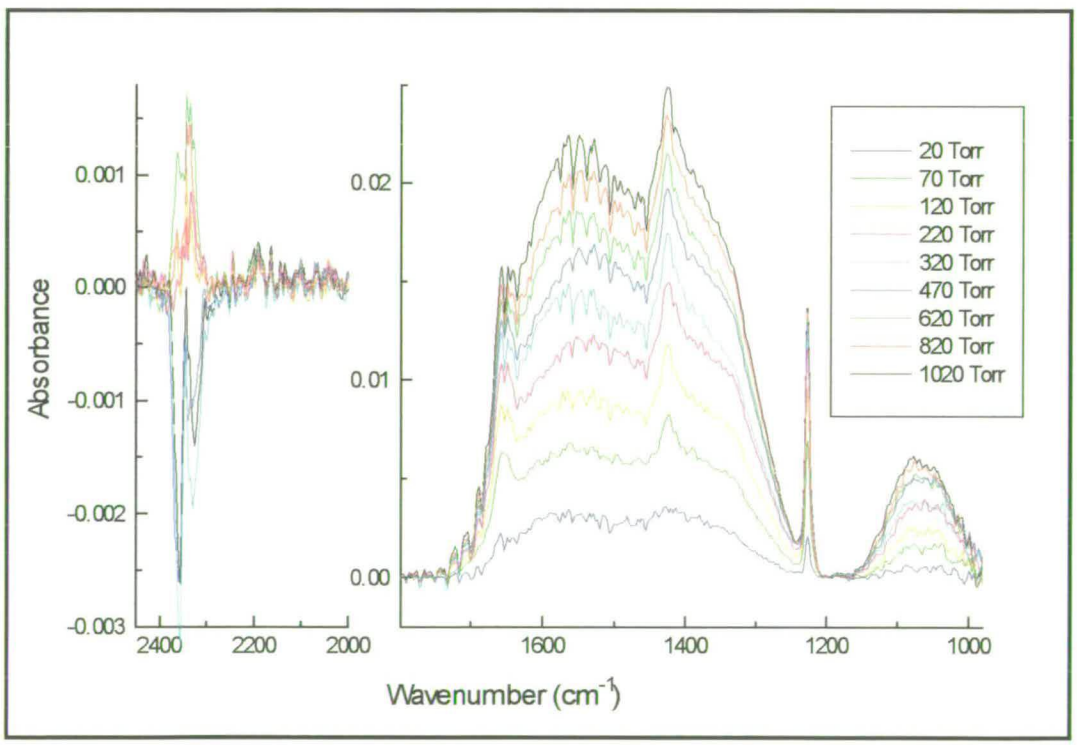

Fig. 5.32. *CO_2 pulse experiment for the unpromoted catalyst. Total exposure of CO_2 = 1020 Torr.*

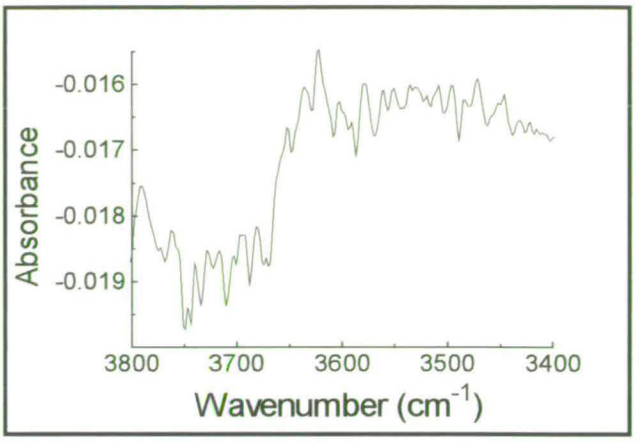

Fig. 5.33. *Band at 3620 cm^{-1}, shown following final pulse of CO_2 on unpromoted catalyst.*

In addition to observing gas phase CO_2 (i.e. that not adsorbed from the incoming pulse) with the mass spectrometer, some CO was also observed, as shown in Fig. 5.34. Following integration of the mass spectrometer traces, the amounts of unadsorbed CO_2 ($CO_{2(unadsorbed)}$) and CO produced on exposure of the surface to CO_2 ($CO_{(reaction)}$) were thus calculated to be 18 and 0.72 μmol, respectively.

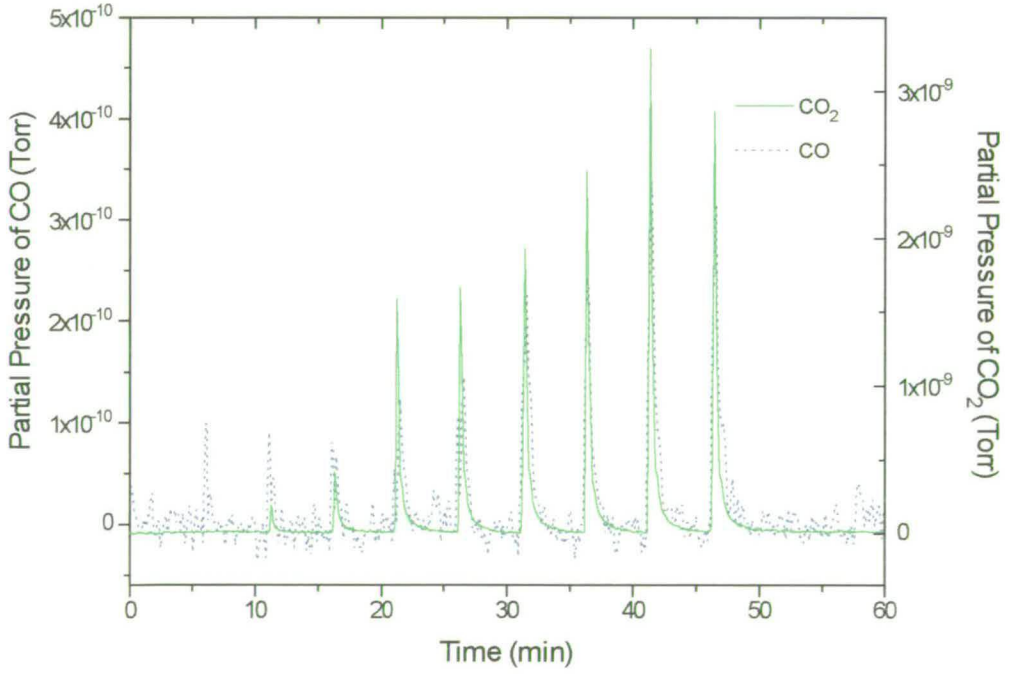

Fig. 5.34. *Gas phase CO and CO_2 observed by the mass spectrometer during the CO_2 pulse experiment for the unpromoted sample*

Discussion

As was mentioned in the introduction to this chapter, more pronounced and reproducible infra-red spectra are expected following adsorption with CO_2 compared with CO [111, 112]. This is due to the fact that no oxidation reaction is required to convert CO to CO_2 prior to adsorption (as discussed in the introduction). Certainly, it can be seen from Fig. 5.32 that overall the bands found at 1650, 1425 and 1227 cm^{-1}. are sharper than in the corresponding spectrum for CO adsorption (Fig. 5.5). Following the explanation for the adsorption of CO, these bands, along with that at 3620 cm^{-1}, are attributed to bicarbonate on alumina, which appears to be the dominant adsorbed species in the experiment. The band at 1053 and the shoulder at 1331 cm^{-1} in the final spectrum, suggest the existence of bidentate carbonate on zinc oxide, but this appears to be at a lower concentration than that in the corresponding CO experiment. Parkyns [112] has commented that when the level of hydroxylation of alumina is high enough, bicarbonate formation takes precedence over bidentate (or any other type of carbonate) formation from CO_2; in accordance with this, the broad feature over which the band at 3620 cm^{-1} is superimposed (assignable to hydrogen-bonded surface hydroxyl groups) is certainly more prominent during the CO_2 experiment. This could be due to either the surface being less thoroughly reduced, or, more likely, small amounts of moisture being introduced with the CO_2 gas.

The band seen in some spectra at 2339 cm^{-1} suggests the possibility of physisorbed CO_2. Parkyns [112] saw CO_2 physisorbed on alumina at 2346 cm^{-1}, Lavalley and co-workers [117] saw it on zinc oxide at 2358 cm^{-1} and Clarke *et al.* [102] saw it adsorbed on both SiO_2 and copper surfaces at 2340 cm^{-1}. The value observed during this study is therefore closest to that for copper, but uncertainty exists since spectra were only recorded at 4 cm^{-1} resolution. Hadden *et al.* [100] have shown that CO_2 is more strongly adsorbed in the presence of surface oxygen. The CO adsorption experiment in Example 5 of Chapter 4 which defined the state of the copper in this and the remaining experiments in this thesis showed that, although no copper oxide could be detected, the presence of partially oxidised copper was found.

In addition to unadsorbed CO_2 being detected by the mass spectrometer during the course of the pulse experiment, CO was also observed. This is evidence for the dissociation of CO_2 over the unpromoted catalyst, which, as highlighted in the introduction to this chapter, is known to occur over supported copper (reaction 5.8).

$$CO_2 \rightarrow CO_{(g)} + O_{(a)} \qquad \textit{reaction 5.8}$$

Other workers have reported the presence of adsorbed CO on copper following the dissociation of CO_2 over copper supported catalysts [101-103]. Surprisingly, in spite of the large amounts of gas-phase CO detected, none was observed to be adsorbed on copper in this study. However, it seemed likely that a small amount of adsorbed CO existed on the zinc oxide component of the catalyst, as suggested by the weak band at 2194 cm^{-1}. This band has been observed previously by Taylor and Amberg (at 2193 cm^{-1}) [109] and Ghiotti *et al.* (at 2187 cm^{-1} and shifting to 2193 cm^{-1} at low coverage) [122] following the adsorption of CO on zinc oxide. This finding could suggest that CO_2 is actually dissociating over the zinc oxide component of the catalyst, which seems unlikely. Otherwise, it is unclear why CO is found to be preferentially adsorbed on zinc oxide, when this was not suggested in the CO pulse experiment.

5.3.3.2 - Temperature Programmed Desorption

Results

Fig. 5.35 illustrates the decrease in intensity of bands in the 2500 - 2100 cm^{-1} region as the sample temperature is raised while Fig. 5.36 shows the 1700 - 1000 cm^{-1} region. The latter data has not been baseline corrected. The band at 1227 cm^{-1} attributed to bicarbonate has T_{max} at 103 °C. It disappeared at 187 °C, while other bands attributed to this species, 3630 and 1650 cm^{-1}, the former being weaker in intensity and the latter being obscured by miscancellation features, were no longer

seen after 158 °C. No information could be gleaned for the remaining bands, also owing to miscancellation problems.

A sharp band could be seen at 2340 cm^{-1} from room temperature to 46 °C, and especially at 28 °C. The weak feature at 2194 cm^{-1} observed during the pulse experiment was already within the level of noise at room temperature at the start of the TPD.

During the temperature programmed desorption, CO_2 was detected by the mass spectrometer. The resulting trace, which is shown in Fig. 5.37, is broad and could contain a number of contributions from different surface species. However, the main desorption feature seems to peak at around 114 °C. Another minor desorption can be seen at higher temperature with T_{max} at 272 °C. On integrating the area under the trace, it was found that 1.20 μmol CO_2 was desorbed during the course of the TPD. No CO was found to be desorbed from the sample.

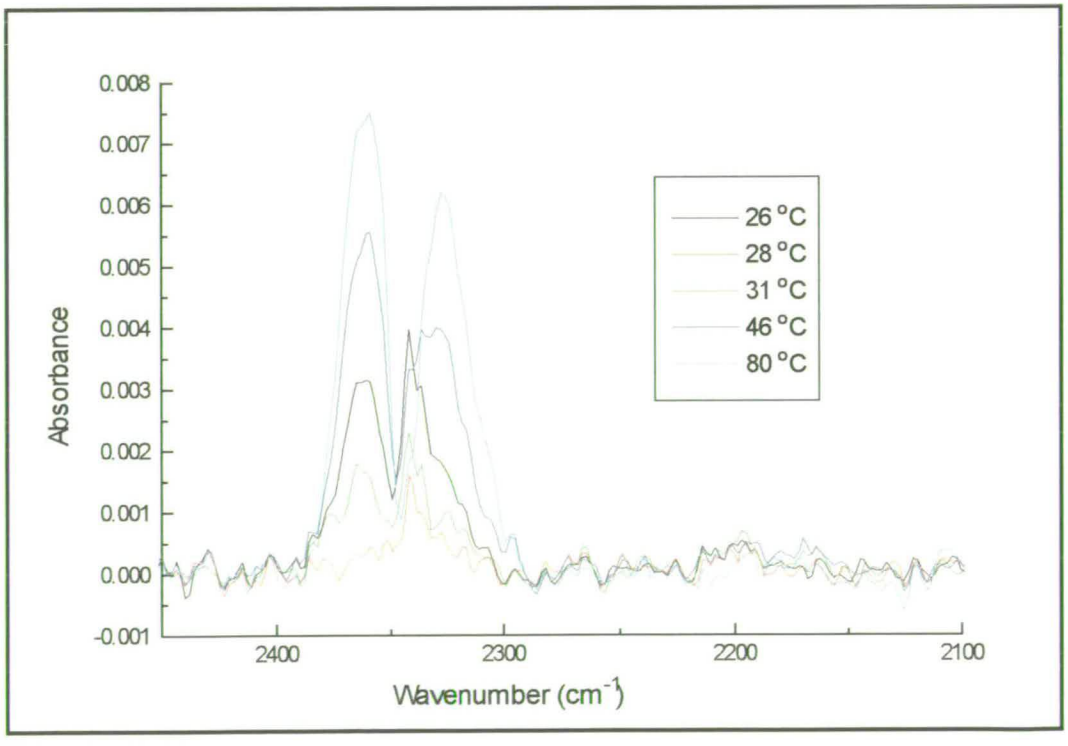

Fig. 5.35. *Temperature programmed desorption following CO_2 pulse experiment for the unpromoted catalyst - 2500 - 2100 cm^{-1}.*

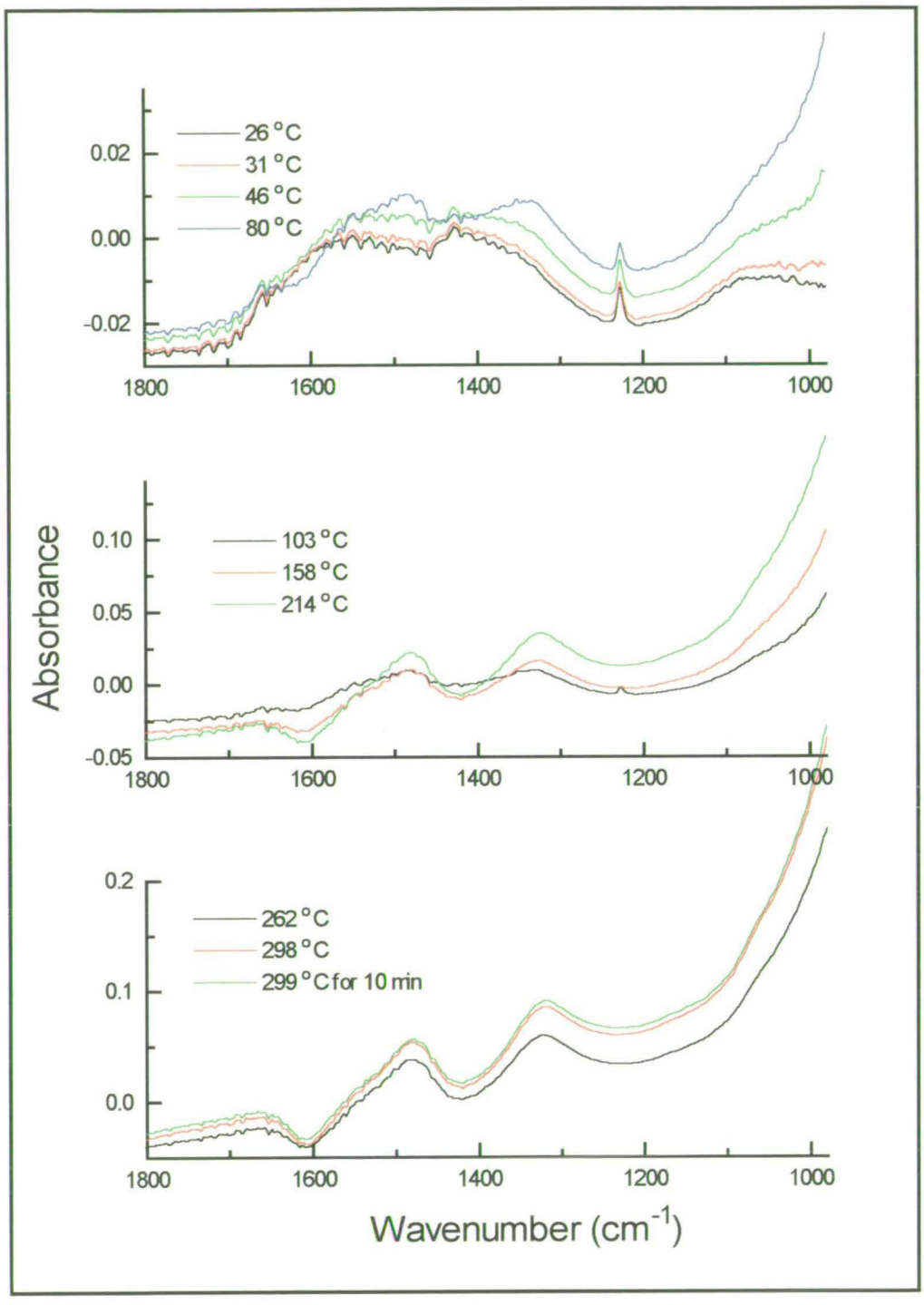

Fig. 5.36. *Temperature programmed desorption following CO_2 pulse experiment for the unpromoted catalyst in the 1700 - 1000 cm^{-1} region (not baseline corrected).*

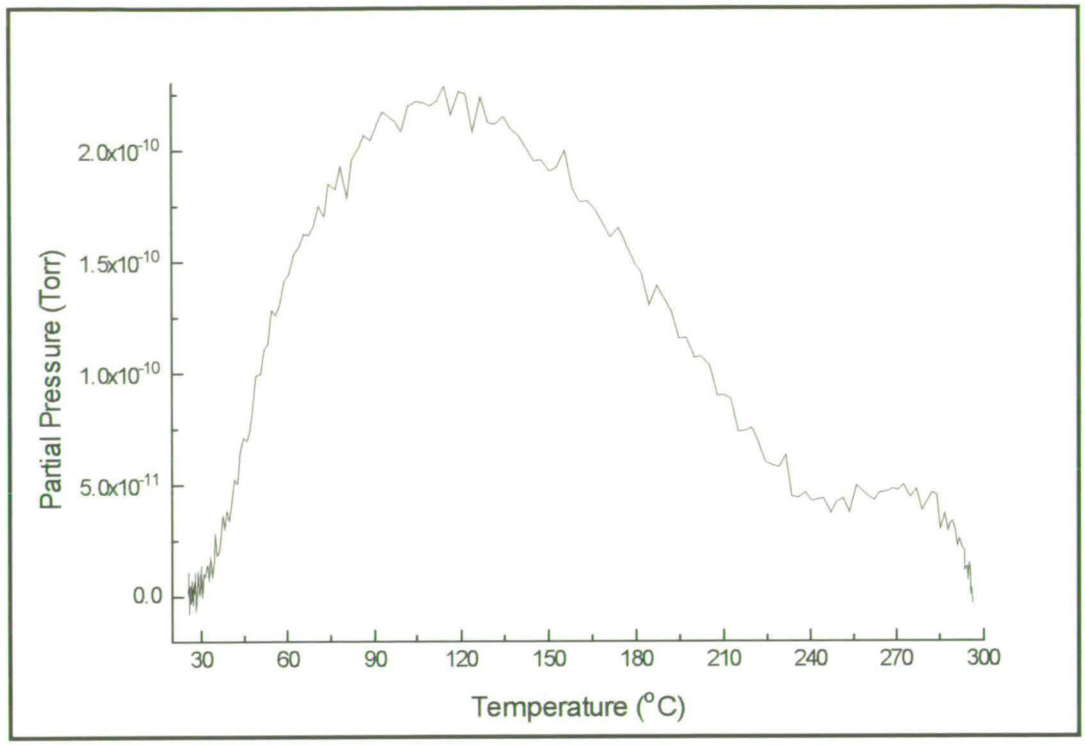

Fig. 5.37. *Temperature programmed desorption of CO_2 from the unpromoted sample following CO_2 pulse experiment.*

Discussion

The bicarbonate species has T_{max} at 103 °C and this is in good agreement with the main desorption feature found by the mass spectrometer which seemed to peak at around 114 °C. The weak band at 2194 cm^{-1} attributed to CO adsorbed on zinc oxide disappeared by 80 °C, suggesting weak adsorption. The sharp band at 2340 cm^{-1}, due to physisorbed CO_2, probably on copper, was seen convincingly at 28 °C. Otherwise, very little information can be gleaned form the infra-red spectra recorded during the TPD.

The minor desorption feature observed by the mass spectrometer at 272 °C is thought to be due to CO_2 being released from the bulk structure of the catalyst, as was also seen during the TPD following CO adsorption for the unpromoted catalyst (Fig. 5.13).

Unlike the TPD following the CO pulse experiment, no CO was found to desorb from the catalyst surface. This is consistent with the absence of a band in the infra-red spectrum due to adsorbed CO on copper. This also supports the argument that the pronounced peak at 57 °C in the CO_2-TPD trace following CO adsorption on the unpromoted catalyst (Fig. 5.13) must have been connected with the oxidation of adsorbed CO (reaction 5.11), as otherwise all other adsorbed species are identical in both experiments, according to the infra-red spectra. Comparison of the CO_2 desorption traces in Fig. 5.13 and Fig. 5.37 reveals that they are also very similar in shape, apart from the early feature at 57 °C

$$CO_{(a)} + O_{(a)} \rightarrow CO_{2(a)} \rightarrow CO_{2(g)} \qquad \textit{reaction 5.11}$$

5.3.2 - Promoted Catalyst

5.3.2.1 - Pulse Experiment

Results

As for the unpromoted sample, the most intense features of the spectrum are in the region below 1700 cm^{-1}, as shown in Fig. 5.38. After the first pulse (20 Torr) bands are seen at 1590 and 1320 cm^{-1}, with a shoulder at 1653 and the possibility of a weak band at 1040 cm^{-1}. After 70 Torr of CO_2, these bands continue to grow, along with a shift of the 1320 band to 1326 cm^{-1} and weak features appearing at 1412 and 1227 cm^{-1}. These features all grow on increasing pressure of CO_2 until in the last spectrum bands at 1592 and 1340 cm^{-1} dominate. The band at 1045 cm^{-1} is fairly intense, and weak features are seen at 1657, 1411 and 1227 cm^{-1}. Miscancellation features do not interfere with the observation of bands in this experiment.

The band seen for the unpromoted sample at 3620 cm^{-1} (Fig. 5.39) is not observed, although the noise level in this region is high, and could be obscuring bands. The possible feature at 2339 cm^{-1} in the unpromoted experiment is also not seen.

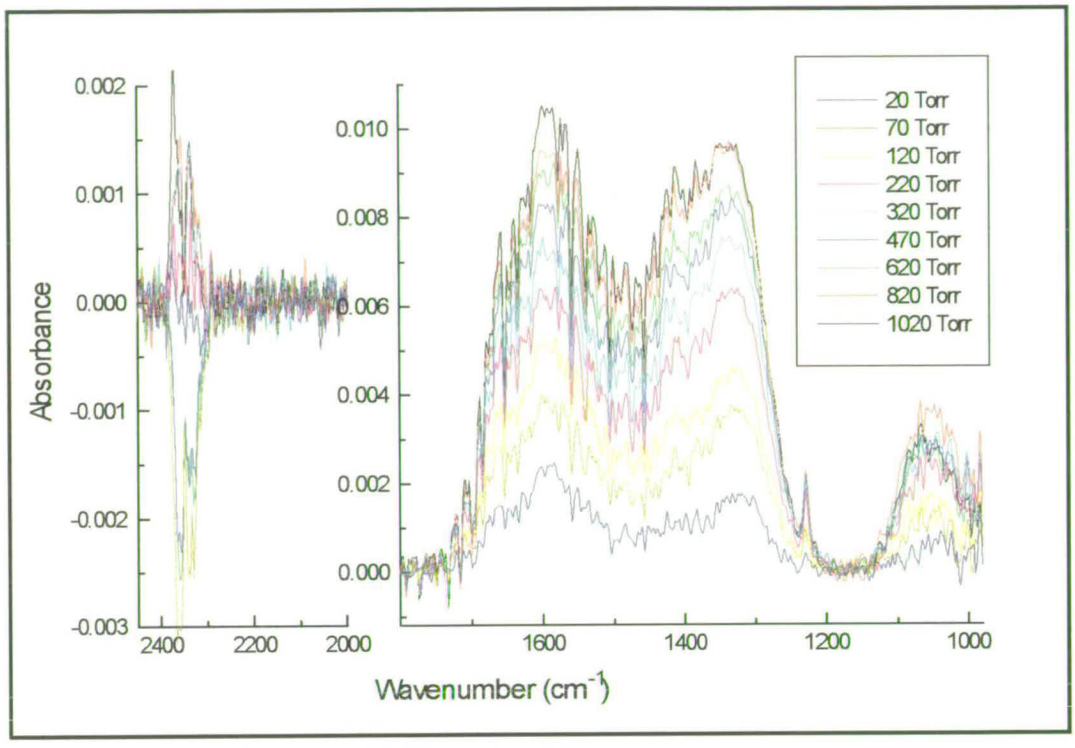

Fig. 5.38. *CO_2 pulse experiment for 1% K promoted catalyst*

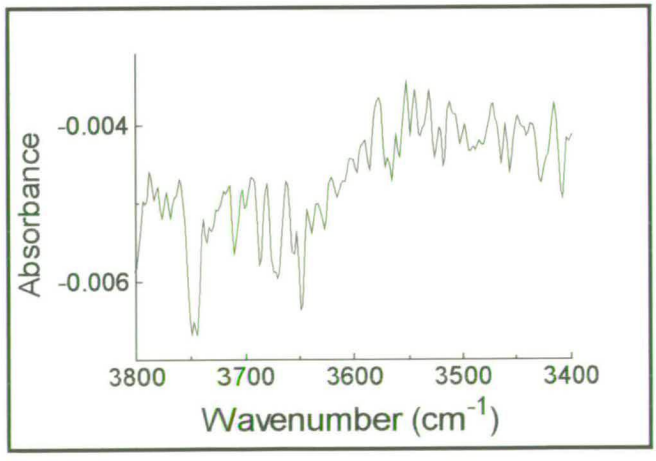

Fig. 5.39 *Spectrum taken after the final CO_2 pulse on the 1% K promoted catalyst - absence of band at 3620 cm^{-1}.*

Gas phase CO_2 and CO were once again detected by the mass spectrometer during the course of the pulse experiment; the amounts found on integration of the traces shown in Fig. 5.40 are 13 μmol ($CO_{2(unadsorbed)}$) and 1.2 μmol ($CO_{(reaction)}$).

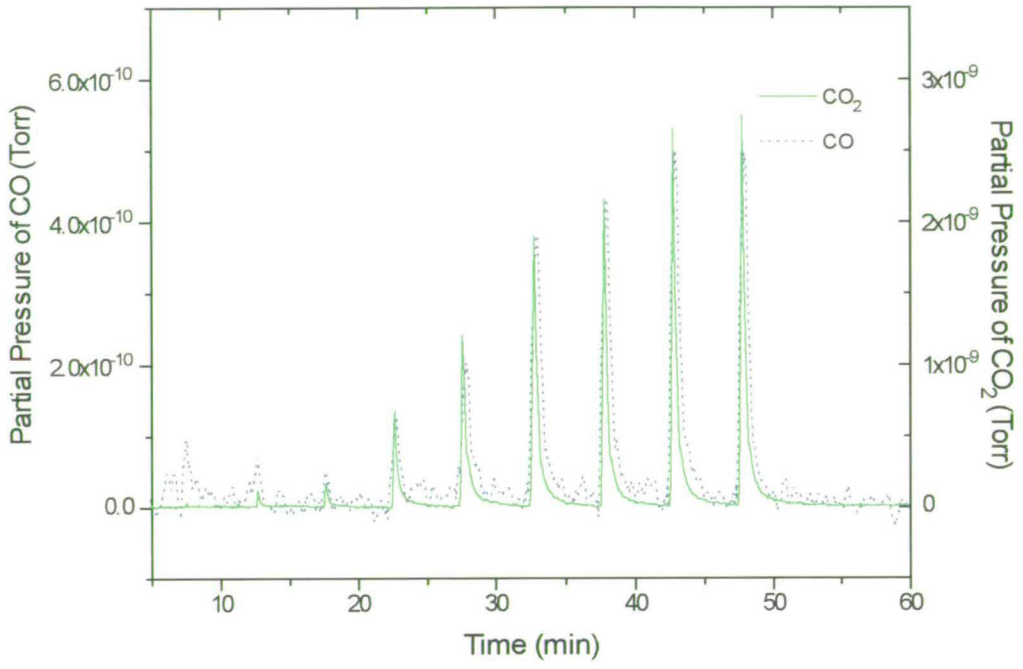

Fig. 5.40. *Gas phase CO and CO_2 observed by the mass spectrometer during the CO_2 pulse experiment for the 1% K promoted sample*

Discussion

Once again, the spectra following the adsorption of CO_2 reflect those found for CO adsorption, but are more pronounced. The bands at 1592 and 1340 and 1045 cm^{-1}, are similar to those found at 1600, 1323, and 1047 cm^{-1} during the CO adsorption experiment, and were previously attributed to bidentate carbonate adsorbed on zinc oxide with the possibility of a carbonate/carboxylate associated with potassium. These features again dominate the spectrum, but to an even greater extent than for the corresponding CO experiment. On plotting the absorbance against CO_2 pulse pressure (Fig. 5.41), the bands at 1592 and 1340 cm^{-1} appear to scale with one another, while that at 1045 cm^{-1} acts independently. Similarly for the CO pulse experiment, this

suggests all three bands having a contribution from the bidentate carbonate on zinc oxide, with the bands at 1592 and 1340 cm^{-1} having an additional contribution from a species such as a potassium-associated carboxylate. Moreover, the relative intensity of these two bands with respect to that at 1045 cm^{-1} is greater. Comparison with Fig. 5.21 for the analogous experiment with CO shows that the effect here is more convincing and gives more firm evidence for the presence of a carboxylate species.

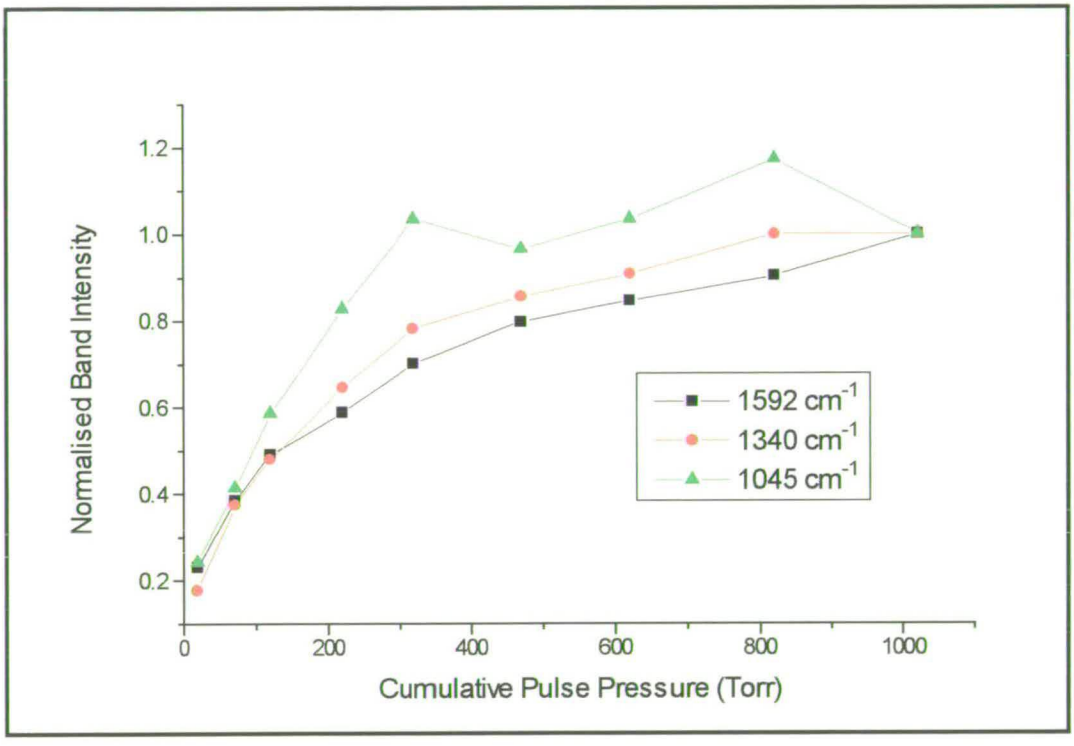

Fig. 5.41. *Variation in intensity of bands at 1592, 1340, and 1045 cm^{-1} vs cumulative CO_2 pulse pressure (i.e. eventually 1020 Torr(11.0 μmol) have been pulsed) for 1% K promoted catalyst.*

The features at 1657, 1411 and 1227 cm^{-1} attributed to bicarbonate on alumina are weaker than for the CO experiment and, in agreement, the band at 3620 cm^{-1} is absent. It appears again from this information that the alkali has the effect on the catalyst of changing the nature of species adsorbed on the support - probably partly through the exchange of the hydrogen on the alumina hydroxyl groups with K^+, and perhaps also through the stabilisation of a new carbonate/carboxylate species by K^+.

It can be tentatively suggested that no adsorbed CO_2 was present on the promoted sample, owing to the absence of a band at 2339 cm^{-1}. This is possibly due to the greater degree of reduction of the promoted catalyst, as suggested by the CO experiments. As discussed already, Hadden *et al.* [100] have shown that CO_2 is more strongly adsorbed in the presence of surface oxygen.

The quantities of gas phase CO_2 and CO detected by the mass spectrometer during the pulse experiments allow another effect of the promoter to be observed (Table 5.3). It can be seen that while the amount of $CO_{2(unadsorbed)}$ decreases on promotion, the amount of $CO_{(reaction)}$ actually increases. This suggests that more CO_2 has been either adsorbed or reacted on the promoted catalyst surface, and that more CO is produced over the promoted catalyst, in spite of its reduced surface area. The potassium promoter must be responsible for this difference.

Table 5.3. *Quantities of unadsorbed CO and CO_2 produced during the CO_2 pulse reactions.*

Catalyst	$CO_{2(unadsorbed)}$), μmol	$CO_{(reaction)}$, μmol
unpromoted	18	0.72
1% K promoted	13	1.2

The dissociation of CO_2 over copper was suggested as being responsible for the CO formed over the unpromoted catalyst. As was mentioned in the introduction to this chapter, addition of an alkali metal to a copper single crystal can enhance the rate of CO_2 dissociation. Rodriguez *et al.* [105] attributed this in a study of Cs/Cu(110) to the stabilisation of adsorbed CO_2 followed by its decomposition to produce CO and a carbonate species (reaction 5.2). Thomsen *et al.* [106] proposed a similar idea to explain how the low sticking probability of CO_2 on Cu(110) could be increased by the addition of potassium. After CO_2 adsorption at -163 °C, then heating the resulting adsorbed CO_2^- species at -73 °C, reaction 5.3 occurred.

$$2nCO_{2(g)} + Cs_{(a)} \rightarrow nCO_{(a)} + Cs.nCO_{3(a)} \qquad \textit{reaction 5.2}$$

$$2CO_2^- \rightarrow CO_3^{2-} + CO_{(a)} \qquad \textit{reaction 5.3}$$

However, these effects were attributed to the activation of the CO_2 molecule by charge transfer from the alkali-promoted metal substrate, which lowered the work function considerably. Since no electronic effects were found in the study with CO (i.e. no shift in the CO stretching frequency), this description seems unlikely in the present case. In addition, no adsorbed CO_2 was observed at any time on the promoted catalyst, and this could only be explained if the turnover for the reaction was very high, i.e. the reaction occurred quickly and adsorbed CO_2 did not exist long enough for detection. Solymosi and Bugyi [107] suggested that, alternatively, a direct interaction between potassium and CO_2 could exist in their study of K/Rh(111). As a result, a $K^+CO_2^-$ surface species was generated, which decomposed according to reaction.

$$K^+CO_2^- \rightarrow K^+O^- + CO_{(a)} \qquad \textit{reaction 5.12}$$

Although CO was only observed above 230 °C by Solymosi and Bugyi, this still seems like the most likely pathway for CO production. The potassium ions involved in such a reaction must reside on the support of the catalyst, owing to the absence of electronic effects discussed above. A potassium-carboxylate type species has already been proposed as existing on the support. Fig. 5.42 suggests two possible reaction paths for the CO_2, where the source of the potassium is suggested as being surface $-O^-K^+$ groups. It is possible that a surface carbonate species (2) associated with potassium could also be formed in the presence of additional surface oxygen and CO_2.

The enhanced bands in the infra-red spectra bear a resemblance to the broad, undefined carbonate bands seen on metal oxides. Therefore, based on this and the

absence of a shift in the CO stretching frequency, it appears that the enhancement of CO_2 dissociation must lie with a potassium-related species on the support.

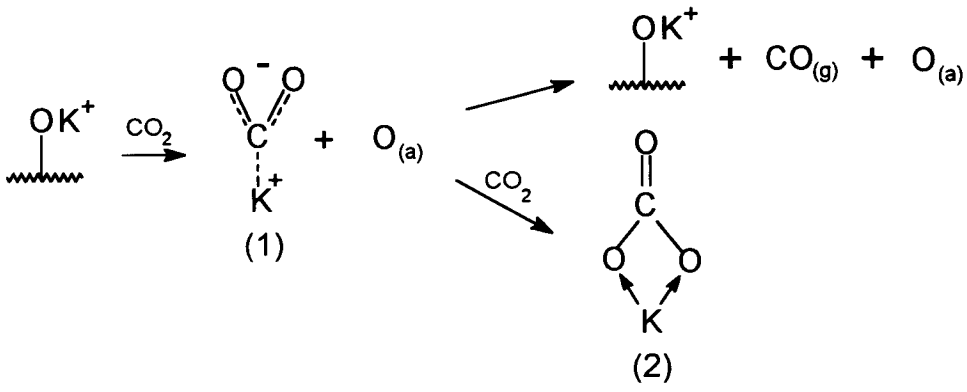

Fig. 5.42. *Possible reaction paths for CO_2 on the support of the promoted catalyst.*

5.3.2.2 - Temperature Programmed Desorption

Results

Fig. 5.43 illustrates the reduction in intensity of the infra-red bands between 1700 and 1000 cm^{-1} during the TPD. Traces of the band at 1227 cm^{-1} can be seen up to 75 °C. The band at 1592 cm^{-1} can be seen until about 206 °C, but at this point miscancellation features are growing in, making it difficult to be certain of the exact time of disappearance. Similarly, the bands at 1045 cm^{-1} and 1340 cm^{-1} are again difficult to follow but seem to have disappeared by 256 °C.

There is little of interest in the 2500 to 2100 cm^{-1} region as shown by Fig. 5.44.

As for the unpromoted catalyst, CO_2 was detected by the mass spectrometer during the TPD, but giving a trace which was even broader (Fig. 5.45). Cautiously, the main desorption feature could be said to peak at around 142 °C, but it is quite possible that there is at least one other feature at about 95 °C. Another minor

desorption shoulder can be seen at around 270 °C. On integrating the area under the trace, it was found that 1.6 μmol CO_2 was desorbed during the course of the TPD. Again, no CO was found to be desorbed from the sample.

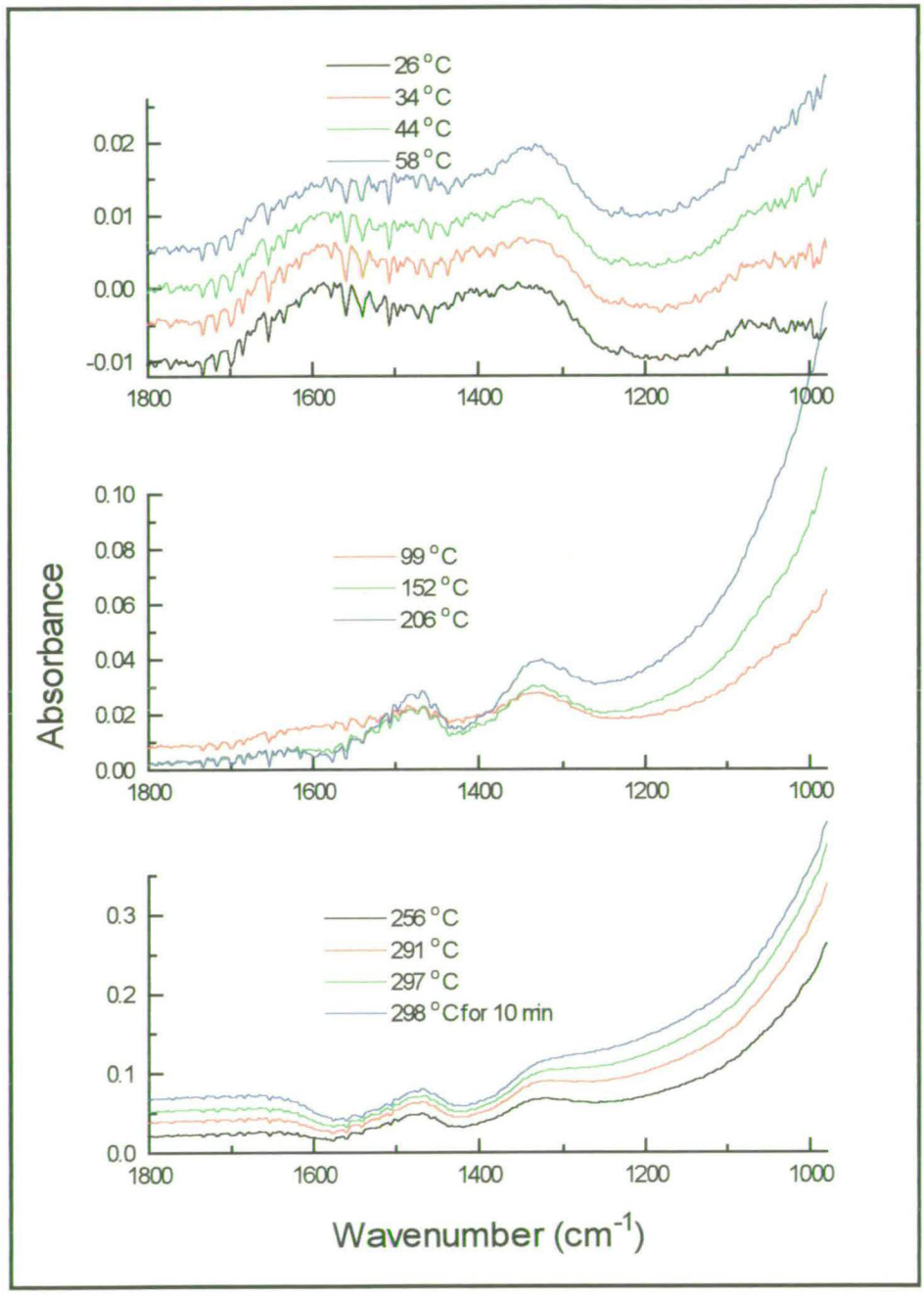

Fig. 5.43. *Temperature programmed desorption following CO_2 pulse experiment for the 1% K promoted catalyst in the 1700 - 1000 cm^{-1} (not baseline corrected).*

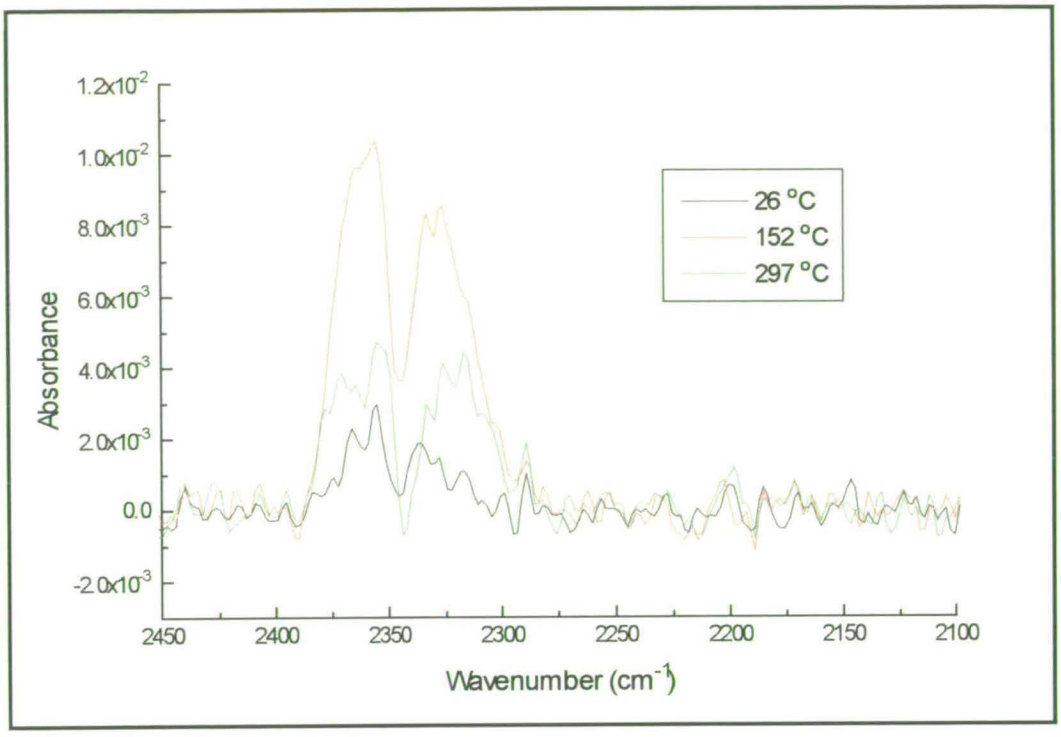

Fig. 5.44. *Temperature programmed desorption following CO_2 pulse experiment for the 1% K promoted catalyst in the CO stretching region.*

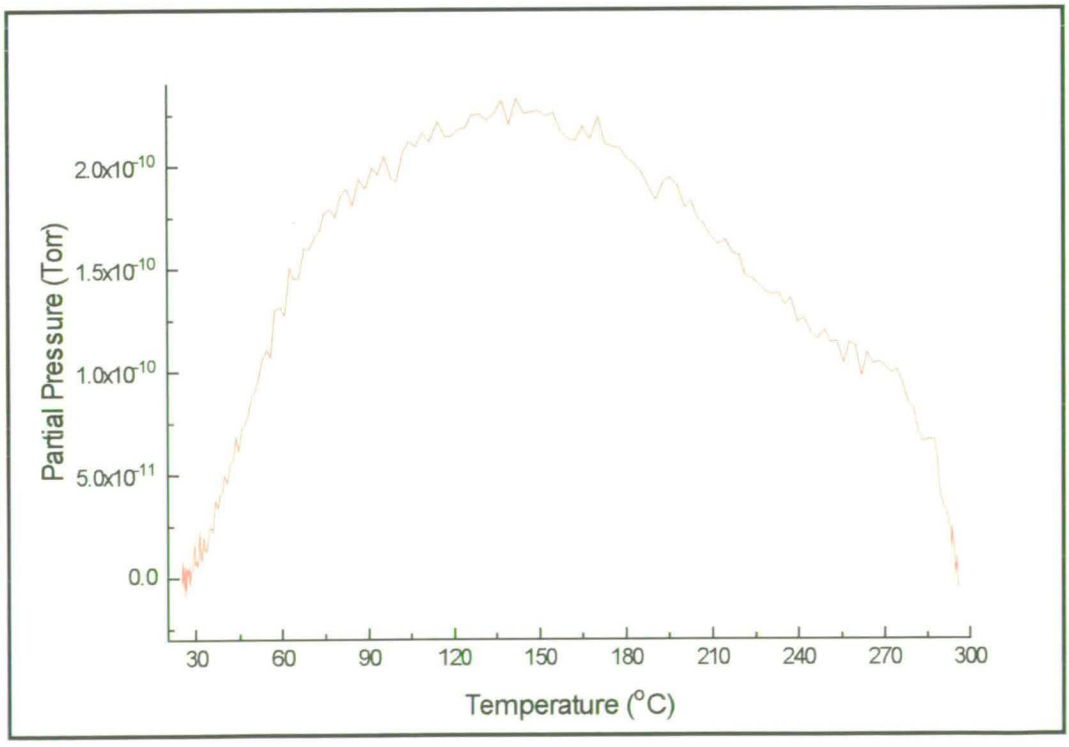

Fig. 5.45. *Temperature programmed desorption of CO_2 from the 1%K promoted sample following CO_2 pulse experiment.*

Discussion

The loss in intensity of the bicarbonate band at 1227 cm^{-1} occurred at a lower temperature than the loss of the features at 1592, 1340 and 1045 cm^{-1}, which are assigned to either bidentate carbonate on zinc oxide or a potassium-associated carboxylate or carbonate.

Table 5.4 shows that the amount of CO_2 evolved during the TPD, as found by the mass spectrometer, increased on promotion. The extent of this increase is substantial considering that the total surface area decreased on promotion by around 50 %. These results are illustrated by comparing the two mass spectrometer traces on the same scale, as in Fig. 5.46, below. The results show a greater amount of high temperature CO_2 desorption for the promoted sample than for the unpromoted, which could either be due to simply a higher relative concentration of bidentate carbonate on zinc oxide, or the presence of an additional, strongly adsorbed potassium-associated species. These TPD findings support those from the analogous CO experiments, and are also more clear-cut.

Table 5.4. *Quantities of CO_2 produced during the TPD experiments following CO_2 adsorption.*

Catalyst	$CO_{2(TPD)}$, Torr
unpromoted	1.2
1% K promoted	1.6

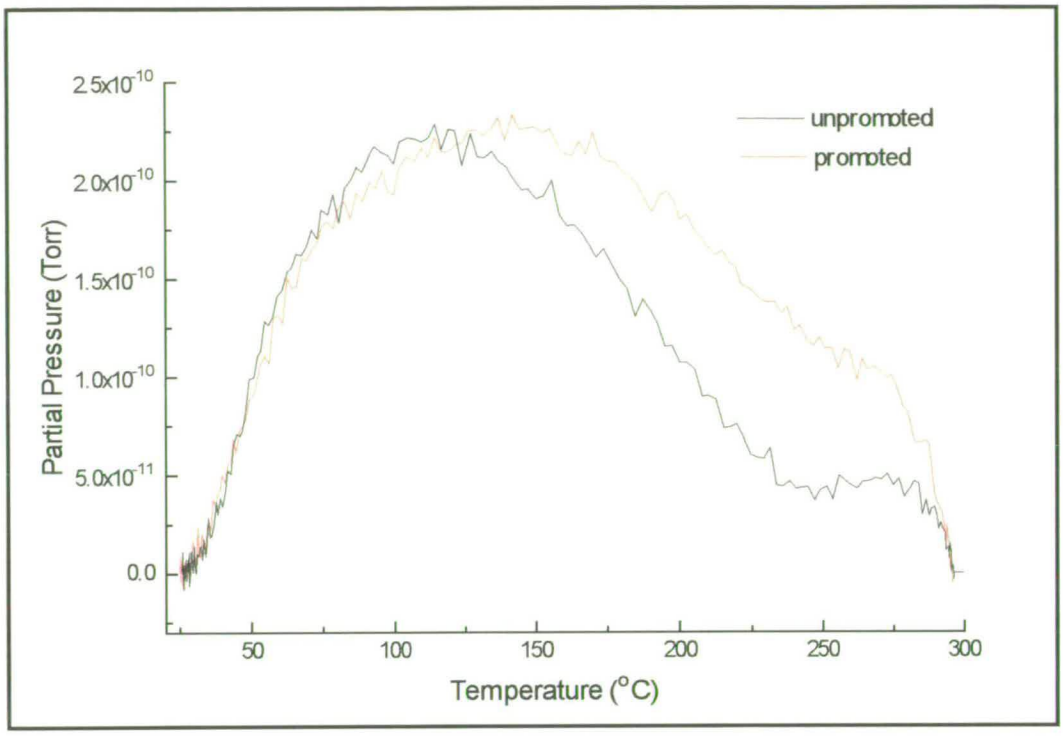

Fig. 5.46. *Comparison of temperature programmed desorption of CO_2 from the unpromoted and 1% K promoted sample following CO_2 pulse experiment.*

It is not possible to say with certainty what species is responsible for the enhancement in the high temperature CO_2 formation. To return to the infra-red pulse experiment evidence, an enhancement in bands was seen which was attributed to potassium-associated species on the support. From Fig. 5.41, it seemed possible that a carboxylate species could be responsible for the enhancement of the bands at 1592 and 1340 cm^{-1}. This species was also suggested as being responsible for the enhanced CO formation at room temperature from CO_2. Therefore, if the carboxylate species decomposes at room temperature to form CO, another species must be responsible for the enhancement of CO_2 formed at high temperature. This could quite simply be a higher relative concentration of bidentate carbonate on zinc oxide, but could alternatively be a potassium-carbonate type species such as K^+-CO_3^-, which was suggested in Fig. 5.42 as possibly existing on the support. Considering again the results by Rodriguez *et al.* [105] and Thomsen *et al.* [106], they both detected a high temperature desorption of CO_2 (at 230 - 430 °C and 180 - 280 °C, respectively), which they attributed to the decomposition of an alkali-carbonate species on the

copper metal (reactions 5.1 and 5.4, respectively). It is possible that a K^+-CO_3^- species on the support would also decompose in a similar manner at high temperature. In this case, it is quite possible that both a potassium carboxylate and carbonate reside on the support at room temperature (Fig 5.42). The carboxylate could then be responsible for the enhancement in CO formation from CO_2 during the pulse experiment, while the carbonate could be responsible for the enhancement in the amount of CO_2 evolved at high temperature from the promoted catalyst.

$$Cs.nCO_{3(a)} \rightarrow Cs_{(a)} + nCO_{2(g)} + nO_{(a)} \qquad \textit{reaction 5.1}$$

$$CO_3 \rightarrow CO_2 + O \qquad \textit{reaction 5.4}$$

Finally, the desorption shoulder in the CO_2 trace at 270 °C is once again put down to the loss of structural CO_2.

5.4 - Overall Effect of the Promoter on Carbon Monoxide and Carbon Dioxide Adsorption

A complex picture has been built up during this chapter of the effect of the promoter, and this can, in part, be attributed to the number of components in the catalyst and the reactivity of all of these towards the two adsorbates. Nevertheless, it has been possible to identify a number of effects.

The promoter hinders the adsorption of CO on the copper component of the catalyst, and a site-blocking mechanism has been invoked to explain this. The copper component also appears to be easier to reduce in the presence of the promoter. An effect on the support has been identified - infra-red bands due to bicarbonate species on alumina are decreased, and this has been attributed to a decrease in the number of surface hydroxyl groups, probably as a result of the exchange with K^+ ions to form $-O^-K^+$ species. The possibility of a new species is also apparent - either a carboxylate

or carbonate associated with potassium, as suggest by an enhancement in bands in the 1700 - 1000 cm^{-1} region. In accordance with these findings, TPD results have shown a relative decrease in the amount of CO_2 desorbed at low temperature (bicarbonate) and an accompanying dominance of the high temperature component of evolved CO_2 (attributed to the decomposition of bidentate carbonate on zinc oxide or one of the potassium-associated species).

CO adsorption studies carried out on catalysts with a varying level of alkali supported the above findings and also revealed that, as a proportion of the total products following CO adsorption, relatively less CO_2 was evolved from oxidation of CO at room temperature (reaction 5.13), but more was produced during TPD, suggesting that the CO_2 had been "stored" on the catalyst, perhaps in the form of a potassium-associated carbonate until decomposition at high temperature (reaction 5.14).

$$CO_{(g)} + O_{(a)} \rightarrow CO_{2(g)} \qquad \textit{reaction 5.13}$$

$$K^+CO_3^- \rightarrow CO_{2(g)} + (-O^-K^+) \qquad \textit{reaction 5.14}$$

The CO_2 adsorption studies reflected the CO studies but were more clear-cut. During the pulse experiments, the decrease in the level of bicarbonates on alumina and the relative increase in bidentate carbonates on zinc oxide or the potassium associated species were again revealed, and more convincing evidence was obtained for the presence of a potassium-carboxylate, according to the preferential enhancement of infra-red bands at 1595 and 1323 cm^{-1}. The formation of CO on exposure of the catalyst to CO_2 was enhanced in the presence of the promoter, owing to the activation of the CO_2 molecules by potassium. The exact mechanism of this effect is unclear, but it was suggested that the potassium carboxylate could be involved (reaction. 5.15).

$$CO_{2(g)} + (-O^-K^+) \rightarrow K^+CO_2^- \rightarrow (-O^-K^+) + CO_{(g)} + O_{(a)} \qquad \textit{reaction 5.15}$$

$$CO_{2(g)} + (-O^{-}K^{+}) \rightarrow K^{+}CO_2^{-} \rightarrow (-O^{-}K^{+}) + CO_{(g)} + O_{(a)} \qquad \textit{reaction 5.15}$$

To relate what is obviously a very complicated system to the WGS reaction is difficult, but two important points can be highlighted:

1) the formation of a potassium-associated carbonate during CO adsorption, with the subsequent decomposition of this compound to CO_2 during TPD could have implications for the forward WGS reaction, where the conversion of CO to CO_2 is an important step, (reaction 5.14) and
2) the enhanced conversion of CO_2 to CO during the pulse experiment, possibly *via* a potassium-associated carboxylate could also enhance the reverse WGS reaction. Presumably this reaction would also take place at higher temperatures, which are more relevant to WGS reaction conditions (reaction 5.15).

Chapter 6 - The Effect of Alkali Promotion on Methanol and Formic Acid Adsorption

6.1 - Introduction

The synthesis of methanol from $CO/CO_2/H_2$ mixtures over $Cu/ZnO/Al_2O_3$ is believed to take place [123] *via* a number of steps, where a formate species is the most stable and long-lived intermediate, and the hydrogenation of this species is thought to be the rate determining step of the reaction.

The pathway for methanol decomposition is closely related to that for methanol synthesis and, hence, much can be learned about the mechanism of methanol synthesis by studying its decomposition [124]. A similar situation exists for the adsorption of species which lead to a surface formate, such as formic acid [e.g. 125-127]. Such studies are interesting in the present case, since micro-reactor studies in Chapter 3 showed a decrease in by-product methanol synthesis on promotion - it would be desirable to know the effect of the alkali on oxygenate-type adsorbates.

6.1.1 - Methanol and Formic Acid Adsorption Studies

Vibrational methanol adsorption studies are reported in the literature for both copper single crystals [128-131] and supported copper catalysts [124, 132, 133]. For adsorption of methanol on copper at room temperature, the fundamental importance of pre-adsorbed oxygen has been demonstrated by Wachs and Madix [96]. They found that very little methanol chemisorbed on a clean Cu(110) surface, while chemisorption was greatly enhanced by surface oxygen. This was interpreted as the

oxygen acting as a "sink" for protons on the surface, thus leaving only methoxy species present above 0 °C, according to reaction 6.1.

$$2CH_3OH + O_{(a)} \rightarrow 2CH_3O_{(a)} + H_2O_{(g)} \qquad \textit{reaction 6.1}$$

These findings have been borne out in both RAIRS [128, 129] and EELS [130, 131] studies. Here, the adsorption of methanol on copper was shown to result in the formation of a stable methoxide species, where the -OH bond was replaced by a metal-oxygen bond. Very little alteration of the skeletal structure of the alcohol occurs on reaction [130], and C-O scission is unfavourable - thus the CH_3O-Cu system is ideal for model surface science studies, as the effect of surface contamination from decomposition products of the methoxy fragment are minimised. The methoxy structure is represented schematically in Fig. 6.1(A) [130], although debate as to its exact configuration exists [129, 130, 133].

As well as the presence of methoxy on copper, studies on supported catalysts report its existence on the support, such as silica [124, 132, 133] and zinc aluminate ($ZnAl_2O_4$) [134], while it has also been identified in studies on metal oxides, such as zinc oxide [135, 136] and alumina [137].

Like the adsorption of methanol, formic acid adsorption is also of interest both from a fundamental perspective - it is a simple organic molecule and the simplest carboxylic acid, which is capable of anchoring to the surface at two points on the molecule - and from an applied point of view as it allows the study of the formate intermediate in the methanol synthesis reaction. As anticipated, both copper single crystal and supported studies have revealed the presence of an adsorbed formate species on copper. Its exact configuration at low temperature is debated [125, 127, 138] but it is widely agreed that at about 27 °C it is found in the form of a bidentate species [124, 125, 127, 134, 138, 139]. Copper single crystal studies have concluded that the formate is "essentially upright" with its two oxygens in equivalent environments [125-127, 138], and this structure is shown schematically in Fig. 6.1(B).

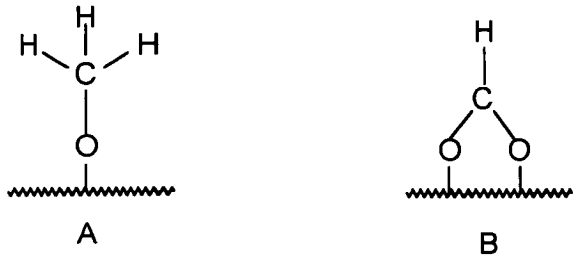

Fig. 6.1. *Schematic representation of (A) methoxy and (B) bidentate formate on copper.*

The reactivity of metal oxides to formic acid and the resulting formate formation makes the interpretation of studies on copper supported catalysts troublesome. Copper catalysts supported on zinc oxide [139] and zinc aluminate [134] have reported the presence of formate adsorbed on the support. The elucidation of these studies has been simplified by comparison with those concerning formates on metal oxides such as zinc oxide [134, 140] and alumina [141].

6.1.2 - Temperature Programmed Desorption of Methoxy and Formate Species

Many of the studies mentioned above have involved the heat treatment of the adsorbed species following methanol adsorption. It has been shown [96, 123, 132] that methoxy is thermally decomposed *via* oxidation to formaldehyde, which is subsequently oxidised to a formate species. The decomposition of methoxy according to reaction 6.2 has been discussed in a review by Waugh [123].

$$CH_3O_{(a)} \rightarrow H_2CO_{(g)} + H_{(a)} \qquad \textit{reaction 6.2}$$

This reaction occurred over both polycrystalline copper and zinc oxide at 110 °C to produce, in addition to formaldehyde and hydrogen, methanol, owing to the reaction of methoxy with surface hydrogen (reaction 6.3).

$$CH_3O_{(a)} + H_{(a)} \rightarrow CH_3OH_{(g)} \qquad \textit{reaction 6.3}$$

Waugh also summarised that the formate species was found to decompose over copper at 170 °C according to reaction 6.4. Meanwhile, formate was found to decompose over zinc oxide at 310 °C to produce *CO* and H_2 *via* $CO_{(a)}$ and $H_{(a)}$ (reaction 6.5).

$$HCOO_{(a)} \rightarrow \frac{1}{2}H_{2(g)} + CO_{2(g)} \qquad \textit{reaction 6.4}$$

$$HCOO_{(a)} \rightarrow H_{(a)} + CO_{(a)} + O_{(a)} \rightarrow \frac{1}{2}H_{2(g)} + CO_{(g)} + O_{(a)} \qquad \textit{reaction 6.5}$$

Individual studies have reinforced these findings, for instance methoxy on copper single crystals has been found to decompose to formaldehyde, hydrogen and methanol at between 70 and 100 °C [96, 129, 130]. The subsequent oxidation to formate, followed by its decomposition at 170 °C to CO_2 and H_2 has not been widely reported for copper single crystals [96]. However, some supported copper studies have seen, in addition to the presence of methoxy, the formation of formate on copper even at *room temperature* [132-134]. The amount of formate is found to increase on heating at 130 °C. The presence of adsorbed formaldehyde on copper has also been observed on a Cu/SiO_2 sample following methanol adsorption [124].

Studies on the heat treatment of formate species reflect the findings in the review by Waugh. The decomposition of formates resulting from formic acid adsorption on copper single crystal surfaces to CO_2 and H_2 is found to occur at 180 °C [126, 142]. Formate produced following the adsorption of methanol [124, 134] and the reaction of CO_2-H_2 mixtures [143] on the copper component of supported catalysts has also been found to decompose at about 180 °C to CO_2 and H_2. However, formate produced from the adsorption of formic acid has been found to

disappear by 130 °C on supported catalysts, forming CO_2, H_2 and CO. The CO was thought to be produced *via* the reaction of CO_2 with H_2 [134].

Waugh's general observation of formate decomposition over zinc oxide at 310 °C to produce CO and H_2 is supported [134, 140, 144], but CO_2 is frequently observed in addition [134, 140, 144]. There are also examples on supported zinc oxide where *only* CO_2 and H_2 are observed, e.g. by Millar *et al.* on ZnO/SiO_2 at 300 °C [145] and Burch *et al.*, again on ZnO/SiO_2 but at 360 °C [9].

The review by Waugh does not comment on any adsorbed species on, or species desorbed from, the alumina component of traditional $Cu/ZnO/Al_2O_3$ methanol synthesis catalysts during the aforementioned examples. In fact, in a study by Bowker *et al.* [61] it is commented that if the results from separate formaldehyde temperature programmed reaction spectroscopy experiments on a partially oxidised polycrystalline copper sample and a zinc oxide sample are superimposed, the resultant trace resembles that for the corresponding experiment on a $Cu/ZnO/Al_2O_3$ sample. Thus, it is implicit that the alumina component plays no part in the adsorption and decomposition of methoxy and formate species, and this is supported by an *in-situ* DRIFTS study of a $Cu/ZnO/Al_2O_3$ catalyst during methanol production, where no adsorbates were found on the alumina component [33].

6.1.3 - Effect of Alkali Promotion on the Adsorption of Methanol and Formic Acid

Unlike for CO adsorption, few studies exist in the literature for the adsorption of complex molecules such as methanol on alkali-promoted copper supported catalysts. Millar *et al.* have, however, investigated methanol adsorption on a potassium promoted Cu/SiO_2 sample [146]. They found evidence for the presence of a potassium methoxy species. A shift of 5 cm^{-1} to lower frequency was seen for the C-H stretching bands of a copper methoxy species at greater levels of potassium, which they explained by invoking a charge transfer mechanism. Finally, the appearance of adsorbed CO was given as evidence for the decomposition of methoxy, even at room temperature.

Millar *et al.* have also carried out a study on the adsorption of formic acid on a potassium promoted Cu/SiO_2 sample, where they found evidence for, in addition to a bidentate copper formate, a formate species on "potassium". Physisorbed formic acid on "potassium" was also identified [147].

6.2 - Methanol Adsorption

Pulse experiments were carried out as for CO and CO_2 in Chapter 5, except that in this case the adsorbate gas pressure was not increased with successive pulses. Instead, the maximum vapour pressure attainable at room temperature was pulsed over the catalyst (in the case of methanol, 100 Torr) nine times at 5 min intervals, so that eventually the catalyst had been exposed to 900 Torr. The subsequent temperature programmed desorption was also conducted in an analogous fashion to that for the CO and CO_2 experiments.

6.2.1 - Unpromoted Catalyst

6.2.1.1 - Pulse Experiment

Results

After the first 100 Torr pulse of methanol, bands were seen developing at 2943 and 2819 cm^{-1}, as shown in Fig. 6.2, with the possibility of shoulders at about 2914 and 2841 cm^{-1}. In parallel, two fairly intense features were seen at 1088 and 1034 cm^{-1}, with a weak band at 1185 cm^{-1}. A broad but weak feature was seen at 2625 cm^{-1}, and the presence of gas phase CO was shown by a weak doublet centred at about 2146 cm^{-1}. Once again, miscancellation features appeared at about 1550 and 1400 cm^{-1}.

After 200 Torr of methanol had been pulsed, the bands in the high frequency region of the spectrum were seen clearly at 2937 and 2820 cm^{-1}, while the shoulders were more pronounced at 2899 and 2838 cm^{-1}. The bands at low frequency were seen to grow - particularly that at 1188 cm^{-1}, which although weaker than the others was now prominent. A band at 2340 cm^{-1} was seen to be superimposed over the gaseous (atmospheric) CO_2 band envelope.

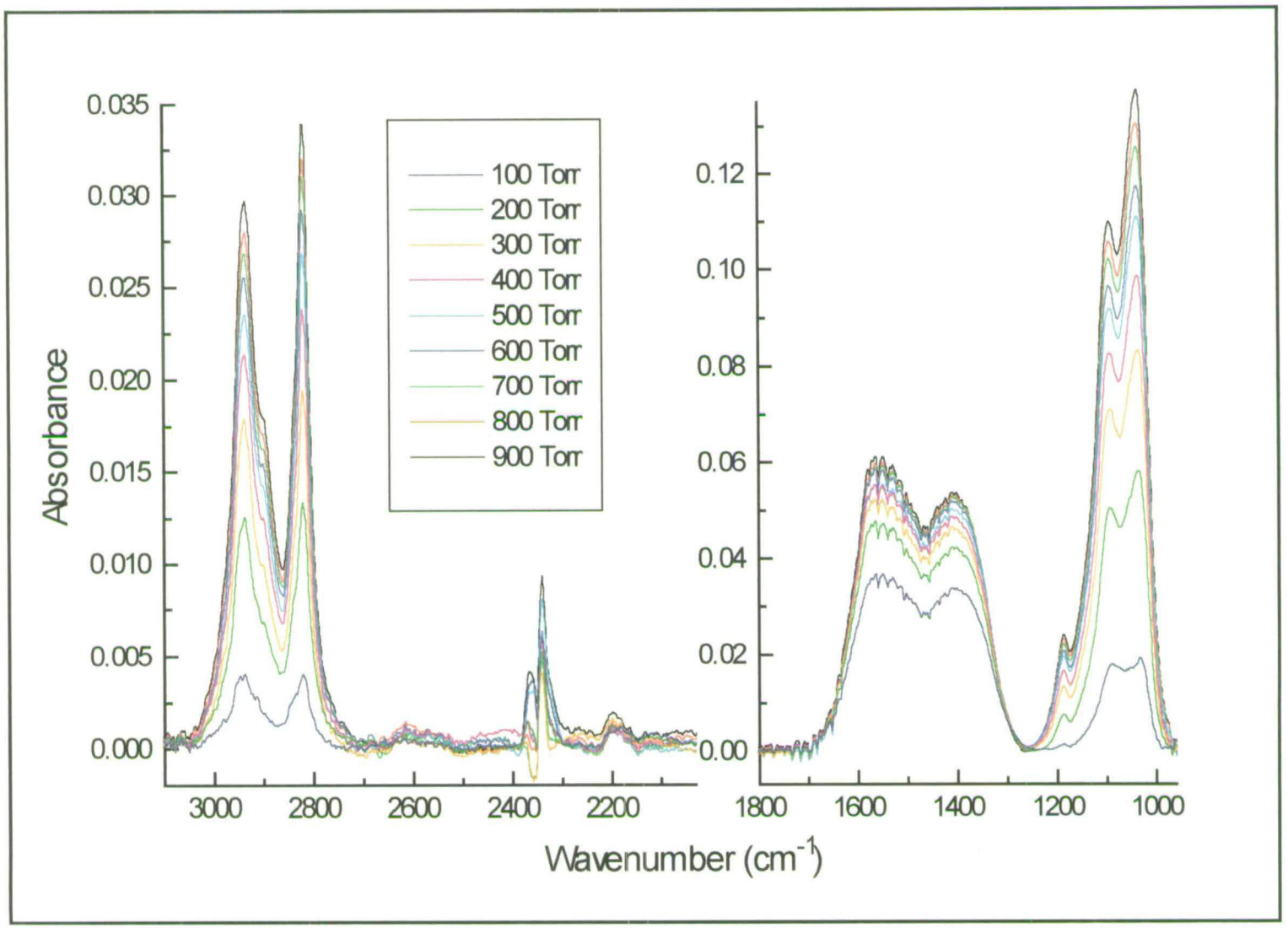

Fig. 6.2. *Methanol pulse experiment for the unpromoted catalyst. Total methanol exposure = 900 Torr.*

After the exposure of the catalyst to 300 Torr of methanol, all the bands continued to grow, but the shoulder now at 2841 cm^{-1} appeared to be becoming less obvious. This behaviour continued until the final pulse, where the main bands were seen at 2935, 2819, 1188, 1095 and 1036 cm^{-1}, with a shoulder at 2900 cm^{-1}. None of the bands had reached saturation, and it was clear that they would have increased in intensity had pulsing continued. The shoulder which was last observed at 2841 cm^{-1} was now no longer clearly seen, although an asymmetry could be seen in the 2819 cm^{-1} band at this position. A weak feature was still evident at about 2615 cm^{-1}, and the doublet centred at 2143 cm^{-1} appeared to have a band at 2197 cm^{-1} superimposed over it. The asymmetry at 2340 cm^{-1} in the band envelope of CO_2 remained.

Although the experiment was monitored throughout using the mass spectrometer, no gas phase species were detected.

Discussion

The areas of interest in the spectra collected during the pulse experiment are that around 2900 cm^{-1} (usually associated with the C-H stretching frequency) and that below about 1250 cm^{-1}. In order to aid assignment of the observed bands, it is useful to make a comparison with other studies of a similar nature. Some relevant band frequencies from investigations [128-131] of the adsorption of methanol on copper single crystals are listed in Table 6.1. It will be noted that there is disagreement between the assignments for the C-H stretching bands. It can also be seen, as commented by Sexton [130], that there is little difference between these bands for different planes of copper; that is, methanol appears to be relatively insensitive to different crystal planes.

Table 6.1. *Frequencies (in cm^{-1}) for bands assigned to a methoxy species on copper.*

Cu(100), EELS, [130]	Cu(110), EELS, [131]	Cu(111), RAIRS, [128]	Cu(100), RAIRS, [129]
2910, υ_{CH}(a)	2940, υ_{CH}(a)	2918, $2\delta_{CH}$(a)	2920, δ_{CH}(s) + δ_{CH}(a)
		2882, $2\delta_{CH}$(s)	2883, $2\delta_{CH}$(s)
2830, υ_{CH}(s)	2840, υ_{CH}(s)	2818, υ_{CH}(s)	2810, υ_{CH}(s)
1010, υ_{CO}		1036, υ_{CO}	984, υ_{CO}

On considering the bands seen in the C-H stretching region for the experiment under discussion - 2935, 2819 cm^{-1} in the final spectrum, with shoulders at 2900 and 2841 cm^{-1} - it is evident that they could easily be assigned to any of the above species. When considering the adsorption of methanol on the other components of the catalyst, zinc oxide and alumina, it is found that the situation becomes extremely complicated. The C-H stretching region for zinc oxide has been investigated by Nagao *et al.* [135], who found bands at 2930 and 2813 cm^{-1}, while Roberts and Griffin found values of 2936 and 2818 cm^{-1} [136]. Both of these studies correspond well with the frequencies found for the main bands in this study, and it is possible to suggest from this the presence of methoxy on zinc oxide. Busca *et al.* [137] reported the presence of three types of methoxy on alumina following methanol adsorption which depended on coverage and whose frequencies overlapped at certain points, making comparisons with this study difficult.

As a useful link between the single crystal studies and this study, and remembering the drawbacks with directly extrapolating the results from single crystal studies to supported catalysts (Chapter 1), it is pertinent to look at the work published on silica-supported copper. Millar *et al.* have studied this system extensively and have reported the presence of methoxy on copper found at 2926 and 2815 cm^{-1} on reduced samples, and 2930 and 2821 cm^{-1} on oxidised samples [132]. This result is interesting in itself - methoxy was not found on "reduced" copper single crystals - and suggests that the catalyst was incompletely reduced. The frequencies again fall within the range of those found in this study. Clarke and Bell have reported that methoxy bands were

only seen on their reduced Cu/SiO_2 sample at elevated temperature (at 2888 and 2822 cm^{-1}) but at room temperature when oxidised (2920 and 2824 cm^{-1}) [124].

None of the above supported catalyst studies discuss the region below 1200 cm^{-1}, owing to the 1300 cm^{-1} cut-off for silica. However, an infra-red investigation by Chauvin *et al.* of a $Cu/ZnAl_2O_4$ catalyst prepared by a similar route to the $Cu/ZnO/Al_2O_3$ sample under study here does look at the low frequency bands [134]. On first investigating the support ($ZnAl_2O_4$), they found strong bands in the C-H stretching region at 2940 and 2820 with shoulders at 2915 and 2895 cm^{-1}. These correlate very well with the main bands seen at 2935, 2819 and the shoulder at 2900 cm^{-1} in this study. Accompanying bands were also seen at 1185 and 1095, with a weak shoulder at 1040 cm^{-1}. Once again, these correlate well with those seen at 1188, 1095 and 1036 cm^{-1} on the $Cu/ZnO/Al_2O_3$ sample. They concluded from these results that two different methoxy species were in existence.

In the same investigation, on an unreduced 15% $Cu/ZnAl_2O_4$, similar results were seen as for the support, i.e. no new bands due to methoxy on the copper were observed. The only effect of the copper seemed to be a decrease in the thermal stability of the methoxy.

For the corresponding reduced sample however, the C-H stretching bands due to the support were obtained, but an additional shoulder was observed at 2840 cm^{-1}. This is probably due to methoxy on copper, which suggests that the shoulder found in this study at 2841 cm^{-1} can be attributed to the same. It is likely that an accompanying band in this region is obscured by support bands, at between 2940 and 2910 cm^{-1}, according to the single crystal data given above. This is again in spite of the suggestion from the single crystal data that preadsorbed oxygen is required for methoxy formation on copper. However, the evidence for some copper oxide was indeed seen during the CO pulse experiment for the sample under study.

Bands below 1200 cm^{-1} were found by Chauvin *et al.* at 1190 (weak), 1100 and 1035 cm^{-1}. Using $CH_3{}^{18}OH$ they demonstrated that the band at 1190 cm^{-1} was not due to the CO stretching band, unlike the other two, but due to a C-H stretch combination band. It was found that the intensity of the band at 1035 cm^{-1}, at a certain methanol pressure, preferentially increased relative to that at 1100 cm^{-1}, and was removed more easily on evacuation. It was thus suggested that this band was at least partly due to υ_{CO} of methoxy on copper.

From this information, it appears that following the methanol pulse experiment, the dominant species present on the catalyst surface was methoxy on the support, as shown by bands at 2935, 2819, 1188, 1095 and 1036 cm^{-1} in the final spectrum, with the shoulder seen in earlier spectra at 2900 cm^{-1}. It is not possible to be certain on which component of the support the species is adsorbed, but by comparison with the results of Nagao *et al.* [135] and Roberts and Griffin [136] for the C-H stretching region of the spectrum, it is more likely to be zinc oxide than alumina. However, as discussed by Chauvin *et al.*, the bands found at lower frequency show more resemblance to those found for alumina. Their sample was prepared by a co-precipitation technique similar to that used in this study and resulted in a $ZnAl_2O_4$ spinel phase in the support, so it is not surprising that infra-red bands have the character of methoxy adsorbed on both oxides. CO and CO_2 studies presented in Chapter 5 of this thesis have suggested that adsorption on both ZnO and Al_2O_3 can be detected separately for the $Cu/ZnO/Al_2O_3$ sample under study. Equally, spinel (a discrete compound) was not detected by XRD. It seems most likely that the methoxy is located on both components of the support in this study, the majority on the zinc oxide component (Chauvin attributes the band at about 1040 cm^{-1} to this) with less on the alumina (band at 1095 cm^{-1} [134]). Less alumina is present in the catalyst overall (2:1 $ZnO:Al_2O_3$) and this is in agreement with bands due to zinc oxide dominating the spectrum in the C-H region.

There is also evidence of a small amount of methoxy on copper, based on the presence of the shoulder at 2841 cm^{-1}, and a possible contribution to the band at

1036 cm^{-1}, which is the most intense in the υ_{CO} region. These assignments are summarised in Table 6.2.

Table 6.2. *Species present on $Cu/ZnO/Al_2O_3$ catalyst following methanol adsorption. (z) - located on ZnO, (a) - on alumina*

methoxy on copper (cm^{-1})	methoxy on support (cm^{-1})
	2935, υ_{CH} (z)
	2900, υ_{CH} (z)
2841, υ_{CH}	2819, υ_{CH} (z)
	1188, ρ_{CH} (z)
	1095, υ_{CO} (a)
1036, υ_{CO}	1036, υ_{CO} (z)

Finally, the remaining features seen during the pulse experiment include the weak feature at about 2615 cm^{-1}, a doublet centred at 2143 cm^{-1} over which a band at 2197 cm^{-1} was superimposed in later spectra and an asymmetry at 2340 cm^{-1} in the band envelope of CO_2. The doublet centred at 2143 cm^{-1} shows the presence of gas phase CO, the band at 2197 cm^{-1} reveals CO adsorbed on ZnO [109, 122], while the asymmetry at 2340 cm^{-1} in the band envelope of CO_2 suggests the presence of adsorbed CO_2, probably on copper or copper oxide [70, 102].

The presence of CO and CO_2 suggest the decomposition of methanol *via* formate over zinc oxide and copper, respectively (i.e. reactions 6.5 and 6.4, respectively). Although adsorbed formate was not detected during the infra-red data, its formation at room temperature from adsorbed methoxy on copper supported catalysts has been well-documented [132-134]. Chauvin *et al.* [134] attributed CO formation in a similar study to formate decomposition on copper. However, it can be suggested that in this case the CO originated on the zinc oxide because CO adsorbed on zinc oxide was not observed following CO pulse experiments. It is, therefore, likely that the CO has resulted from the decomposition of a species *in-situ*. The

decomposition of a species *in-situ*. The feature at 2615 cm^{-1} could be due to a combination band but the origin is uncertain. It does not correspond to any bands found for gas phase methanol [148].

6.2.1.2 - Temperature Programmed Desorption

Results

Figs. 6.3 - 6.6 show the variation of infra-red bands during the course of the TPD. Bands in the C-H stretching region are sharp and distinct (Fig 6.3), allowing a functional group chromatogram to be plotted, as shown in Fig. 6.4. Thus, T_{max} for the band at 2935 cm^{-1} was determined as being 164 °C, and this band along with that at 2819 cm^{-1} were no longer observed by 199 °C. The loss of the shoulder, now seen at 2835 cm^{-1}, correlated with the loss of the band at 2819 cm^{-1}. In parallel with these events, the main bands at 1095 and 1036 and the weak band at 1188 cm^{-1} had disappeared from the spectrum by 199 °C (Fig. 6.5). A new, weak, but sharp feature at 1032 cm^{-1} appeared in the spectrum between 92 and 174 °C, while another at 1347 cm^{-1} appeared at 174 °C and remained until 199 °C. As was experienced for the CO and CO_2 desorption experiments, miscancellation features posed a problem for the region below 1800 cm^{-1} during this experiment. Therefore, the spectra shown in Fig. 6.5 have not been baseline corrected.

Fig 6.6 shows how the band at 2340 cm^{-1} superimposed over the gaseous CO_2 band was especially prominent between 33 and 44 °C but then became obscured at higher temperatures. A complex behaviour was seen in the CO stretching region (also Fig 6.6) - a band was present at 2197 cm^{-1} which started to decrease in intensity at 71 °C, and was very weak by 119 °C. Thereafter, it appeared to become negative in intensity. Another negative band also appeared at about 2120 cm^{-1} from 71 °C, and continued to increase in intensity (negatively) throughout the remainder of the temperature ramp.

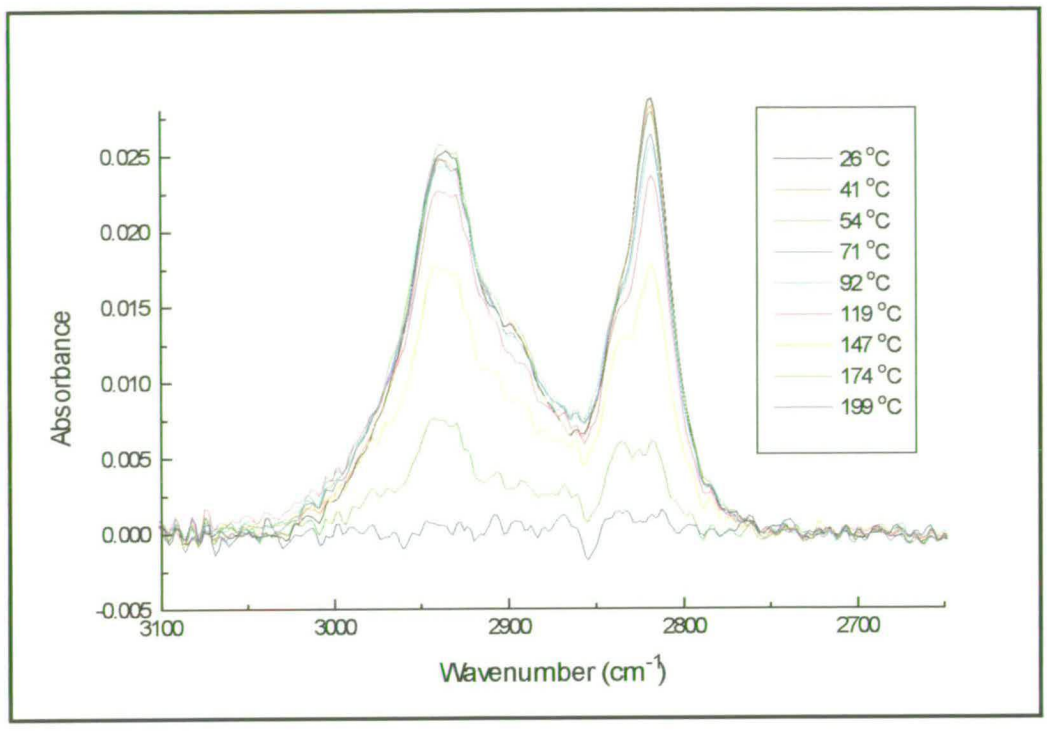

Fig. 6.3. *Temperature programmed desorption following methanol pulse experiment for the unpromoted catalyst in the 3100 - 2700 cm^{-1} region*

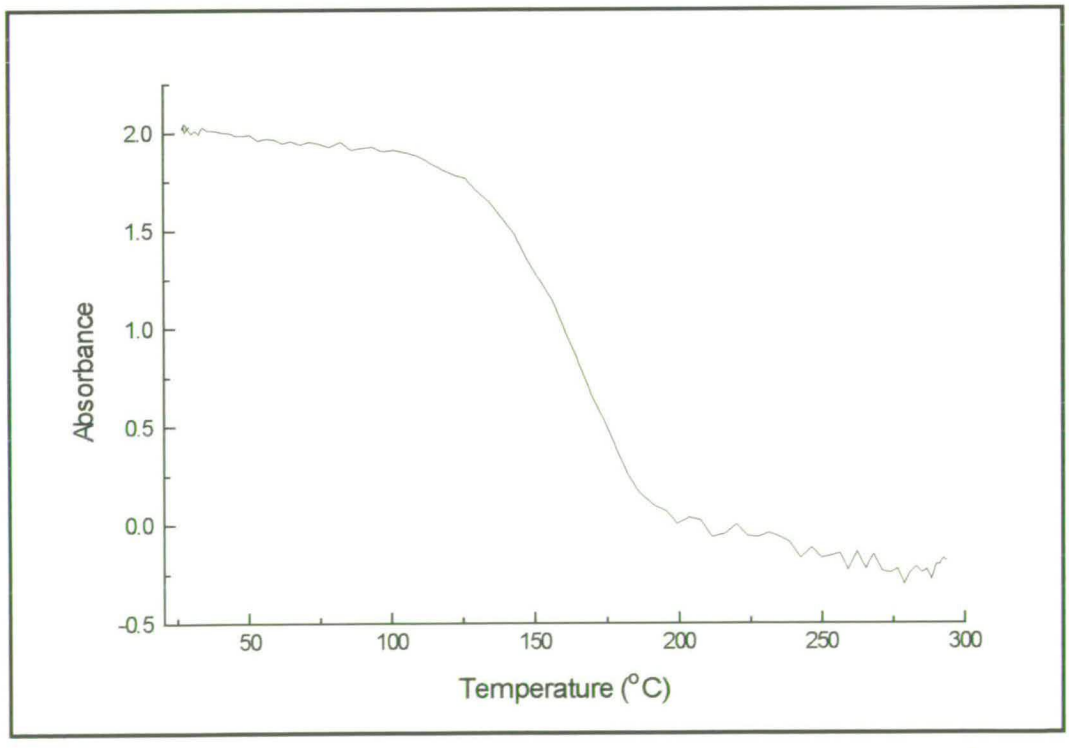

Fig. 6.4. *Functional Group Chromatogram, monitoring band at 2935 cm^{-1} during TPD*

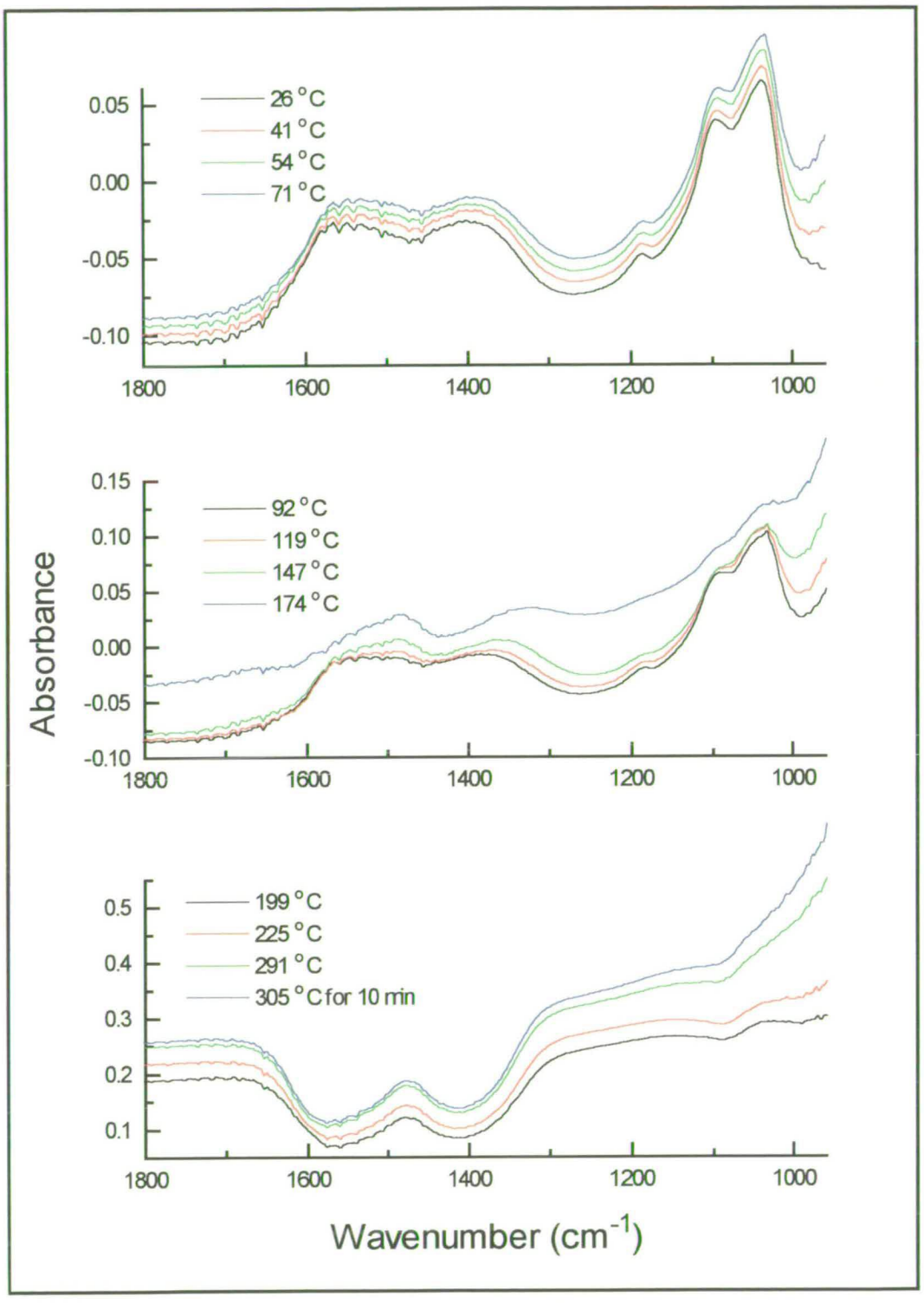

Fig. 6.5. *Temperature programmed desorption following methanol pulse experiment for the unpromoted catalyst in the 1800 - 1000 cm^{-1} region (not baseline corrected).*

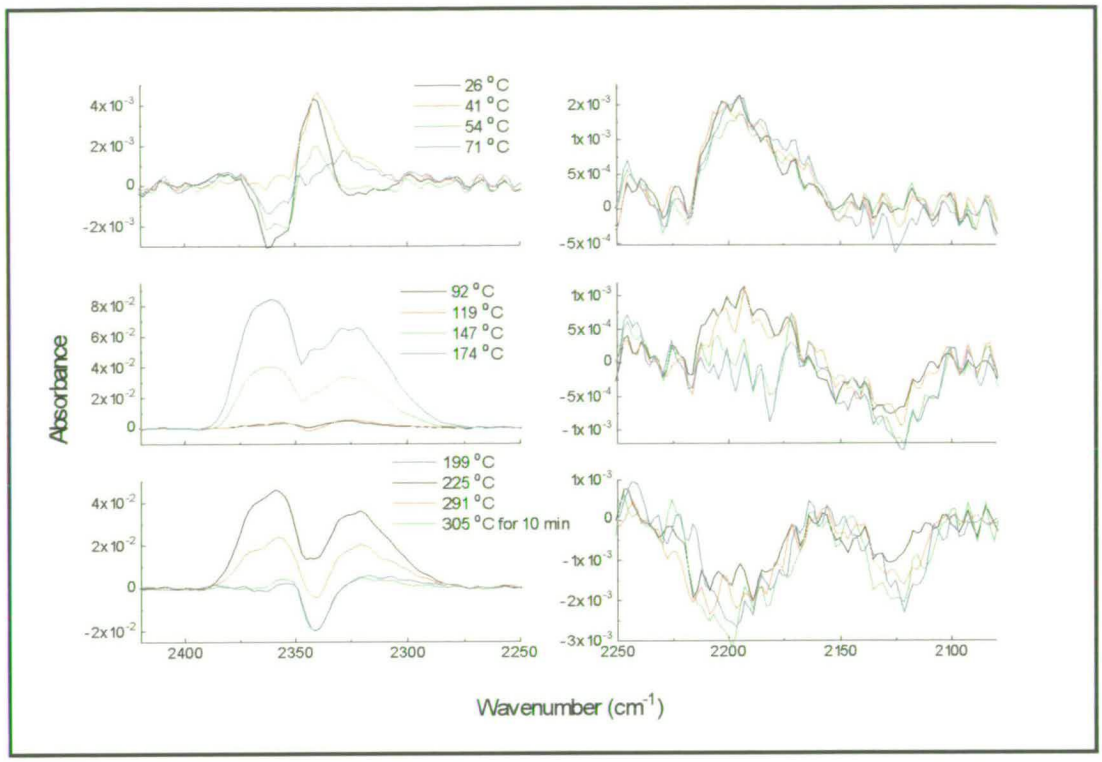

Fig. 6.6. *Temperature programmed desorption following methanol pulse experiment for the unpromoted catalyst in the 2500 - 2000 cm^{-1} region*

The gas phase species evolved during the TPD were monitored by mass spectrometry. Prior to this, a "blank" experiment was carried out by passing methanol pulses through the DRIFTS cell in the absence of a catalyst, in order to determine the major ionisation peaks expected due to the fragmentation of methanol in the mass spectrometer. This allowed the differentiation between these fragments and species due to the actual "reaction" with the surface during the experiments. The fragments which were identified as being important for the interpretation of the TPD results are listed with their relative abundances in Table 6.3. These values are intended as a guideline only, since calibration peaks were composed of only three data points owing to the instrument sampling rate. In addition, peaks due to CO^+ were already superimposed over a background of *m/e* 28, owing to small amounts of atmospheric nitrogen.

The fragment with *m/e* = 31 was designated as the base peak and thus arbitrarily given a relative abundance of 100%.

Table 6.3. *Fragments observed during methanol "blank" experiment*

m/e	Identity of Fragment Ion^+	Abundance/%
31	CH_2OH	100
30	H_2CO	57
28	CO	50

The mass spectrometer raw data from the methanol TPD experiment are shown in Fig. 6.7a. Fig 6.7b shows the results following correction for the fragmentation of methanol in the mass spectrometer, i.e. the traces for *m/e* 28 and 30 have been modified according to Table 6.3. From this figure, it can be seen that species with *m/e* 2, 28, 30, 31 and 44 were detected. Table 6.4 suggests the identity of the fragment ions responsible for these signals and the expected gas phase molecules from which the ions originated.

Table 6.4. *Ions detected by the mass spectrometer during the TPD following methanol adsorption, and the original molecules to which they correspond.*

m/e	Ion^+	Corresponding Species Evolved
2	H_2	H_2
28	CO	CO
30	H_2CO	H_2CO
31	CH_2OH	CH_3OH
44	CO_2	CO_2

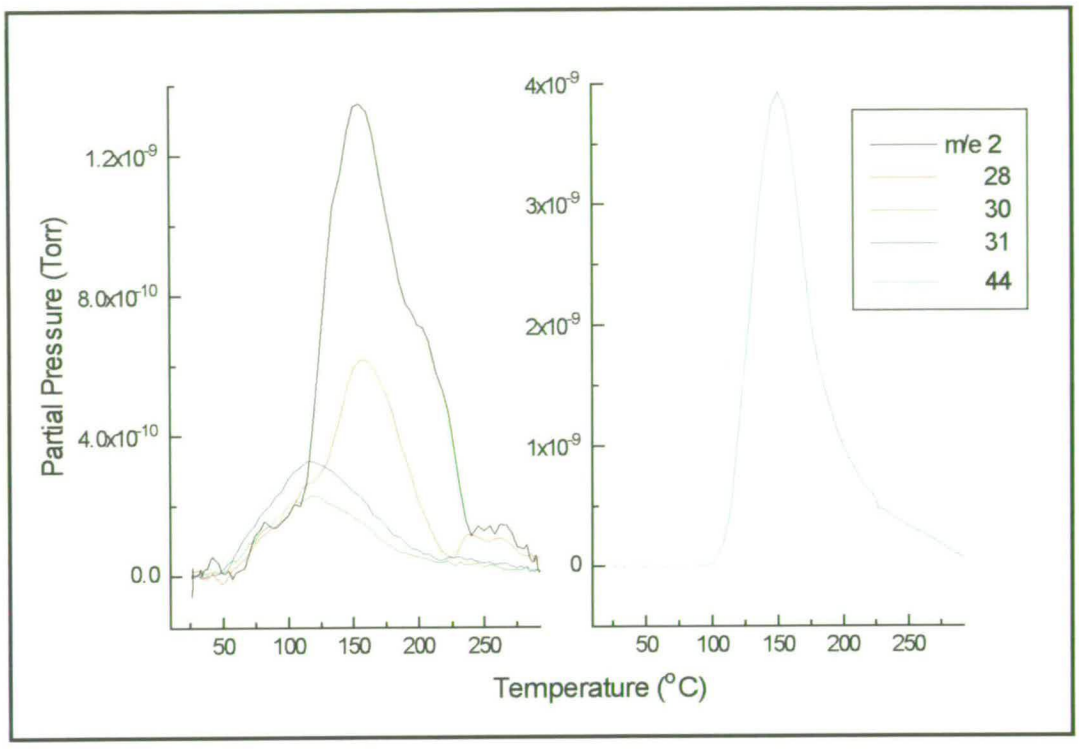

Fig. 6.7a. *TPD following the adsorption of methanol on the unpromoted catalyst - original data*

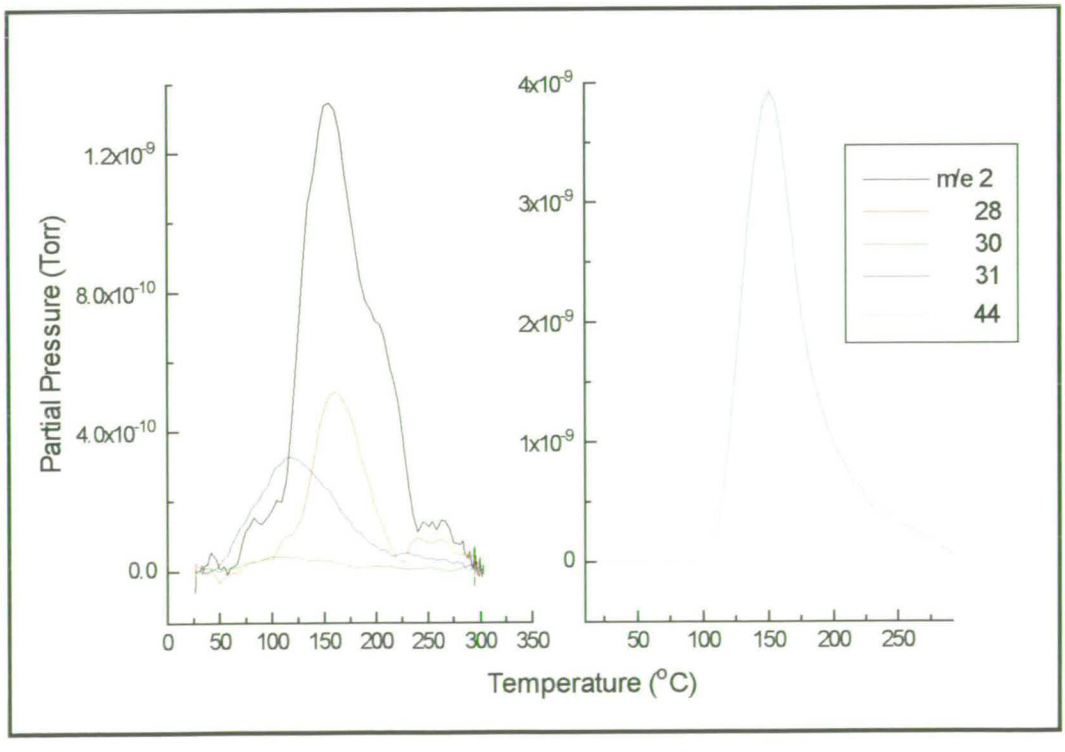

Fig. 6.7b. *TPD following the adsorption of methanol on the unpromoted catalyst - data corrected for fragmentation of methanol*

The corrected data in Fig. 6.7b shows traces corresponding to the evolution of CH_3OH and a very small amount of H_2CO (formaldehyde) starting at relatively low temperature and with T_{max}s at 117 and 112 °C respectively. Simultaneously H_2 was seen to be evolved slowly until 119 °C where a shoulder could be seen, and after which evolution took place at a greater rate, finally peaking at 156 °C. Once the fragmentation of methanol had been taken into account, it became clear that CO was not evolved at low temperature, unlike the other species mentioned thus far, and peaked at 161 °C. A small amount of CO was also seen at higher temperature (T_{max} = 250 °C) and it was possible that H_2 was desorbed in parallel. CO_2 was not evolved until a temperature of 95 °C, with T_{max} at 151 °C. These findings are summarised in Table 6.5, where the amount of each species produced is also given (in arbitrary units, a.u.) following integration of the peak areas.

Table 6.5. *Quantity of each species evolved during the TPD following methanol adsorption on the unpromoted catalyst, according to Fig. 6.7b.*

Species Evolved	T_{max} (°C)	Area of Peak (a.u)
H_2	156	2.8
CO (i)	161	0.72
(ii)	250	0.18
H_2CO	112	0.11
CH_3OH	117	0.80
CO_2	151	5.5

Discussion

The infra-red bands associated with methoxy on copper (2841 and 1036 cm^{-1}) and zinc oxide (2935, 2819, 1188, 1095 and 1036 cm^{-1}) have all died away by 199 °C and T_{max} was found for 2935 cm^{-1} by a functional group chromatogram to be at 164 °C. Bearing in mind the established result in the literature that methoxy species are expected to be decomposed on both copper and zinc oxide at 110 °C [123], the results obtained are peculiar. However, on closer inspection of the C-H region, a shoulder at 2930 cm^{-1} is evident, and it will be shown later in this chapter that this is due to a formate species on copper. This is accompanied at 174 °C by another feature at 1347 cm^{-1}, also due to formate on copper. Thus, it becomes clear that the functional group chromatogram was recording initially the decomposition of methoxy species, but at higher temperatures the decomposition of formate species. It has hence been shown that the functional group chromatogram was not of particular use in this application.

The sharp feature at 1032 cm^{-1} which exists between 92 and 174 °C appeared just below the temperature of maximum methoxy decomposition (found by the mass spectrometer as about 120 °C as discussed below). Since υ_{CO} for methanol (liquid) [148] is found at 1029 cm^{-1} and the band observed here is very sharp, it can be attributed to gas phase methanol.

Species assigned to adsorbed CO_2 on copper (the superposition of a band over the gaseous CO_2 band envelope) were prominent between 33 and 44 °C. Adsorbed CO_2 had already been observed at room temperature and was attributed to the decomposition over copper of small amounts of methoxy to formate and further to CO_2 and hydrogen. The band at 2197 cm^{-1}, which had again been seen at room temperature and attributed to CO adsorbed on zinc oxide following the decomposition of methoxy on the support *via* formate, was found to decrease in intensity slowly from about 71 °C. At higher temperatures (about 147 °C) the band started to become negative in intensity, suggesting that some preadsorbed CO existed

on the surface prior to the pulse experiment, when the background spectrum was recorded. Likewise, a negative band at 2120 cm^{-1} suggests that some preadsorbed CO on partially oxidised copper also existed.

The mass spectrometer results taken during TPD tie in with the infra-red data while offering more conclusive information. Interpretations will be of a qualitative nature, since the sensitivity of the mass spectrometer will vary depending on the species being detected. Formaldehyde and hydrogen were formed at low temperature (a peak at 112 °C and a shoulder at 119 °C respectively), indicative of the decomposition of methoxy on copper or zinc oxide. The evolution of the CH_2OH species, peaking at 117 °C, was evidence for the recombinative desorption of methoxy species with surface hydrogen to form methanol, as discussed in the introduction to this chapter (reaction 6.3) [96, 123, 129, 130].

At higher temperature, CO_2 and hydrogen were found to be evolved simultaneously, with T_{max} of 151 and 156 °C, respectively, and indicating the decomposition of formate on copper [123]. CO was also seen to be produced at this temperature, and it is assumed that this was either due to the decomposition of formate on zinc oxide or the reverse WGS reaction (RWGS). However, there are anomalies to both suggestions - the decomposition of formate on zinc oxide to produce CO and hydrogen is not expected until 310 °C [123], while the RWGS reaction should produce some water, yet none was detected by the mass spectrometer.

Finally, CO was again produced at a higher temperature still, peaking at 250 °C. In parallel, a small quantity of H_2 also appeared to be evolved, which once more suggests the decomposition of formate on zinc oxide [123] and is this time at a temperature more akin to those found in the literature. However, irregularities exist with this assignment also - no formate species are observable on the surface at these high temperatures according to the infra-red spectra (and indeed formate on zinc oxide was not observed at any point during the TPD). It also seems improbable that

so much more formate species would exist on copper than zinc oxide, bearing in mind that much more methoxy was positioned on the support at room temperature and, as will be shown subsequently, much more formate existed on the support than copper following the formic acid pulse experiment.

In summary, the infra-red data shows the gradual desorption of the room temperature decomposition products (CO_2 on copper and CO on zinc oxide) at fairly low temperature - these did not appear to be detected by the mass spectrometer and were presumably at too low a level. At higher temperature, methoxy species on copper and the support were observed to die away and bidentate formate on copper was seen. From the mass spectrometer data, it was revealed that methoxy species decomposed at 115 °C to produce formaldehyde, hydrogen and methanol in agreement with the literature discussed in the introduction, and CO_2 and hydrogen at a higher temperature proved the existence of bidentate formate on copper. The decomposition of formate on the support is more difficult to rationalise - CO peaking at 161 °C possibly also accompanied by a portion of the observed H_2 could have been due to this, but the temperature is much lower than that reported in the literature. Meanwhile, the CO produced at around 250 °C was in such a small quantity that it seems unlikely to have originated from what were the most intense features in the infra-red spectra.

6.2.2 - Promoted catalyst

6.2.2.1 - Pulse Experiment

Results

The results of the methanol pulse experiment are shown in Fig. 6.8. After the first pulse of methanol was introduced to the catalyst, only bands due to miscancellation were seen. The next spectrum had a high level of noise, but features were observed at about 2916, 2829, 1095 and 1038 cm^{-1}, with a very weak band at 1184 cm^{-1}. After the catalyst had been exposed to 300 Torr of methanol, bands could be seen more clearly at 2935 and 2822 cm^{-1}, with an asymmetry in the first band to the low frequency side. Bands at 1187, 1095 and 1038 cm^{-1} were then clearly seen. A significant amount of gas phase CO was observed, as indicated by a doublet centred at 2143 cm^{-1}, and its level at this point is the highest reached during the pulse experiment.

Following the final methanol pulse, bands were seen at 2935 and 2816 cm^{-1}, with the possibility of a shoulder at 2899 cm^{-1}, although the high level of noise in all the spectra makes it difficult to be certain. Other fairly strong bands included those at 1185, 1095 and 1038 cm^{-1}. The level of gas phase CO, which had diminished from the 5th pulse, was now negligible. At no point during the experiment was a feature observed at 2340 cm^{-1}, superimposed over the band envelope of CO_2.

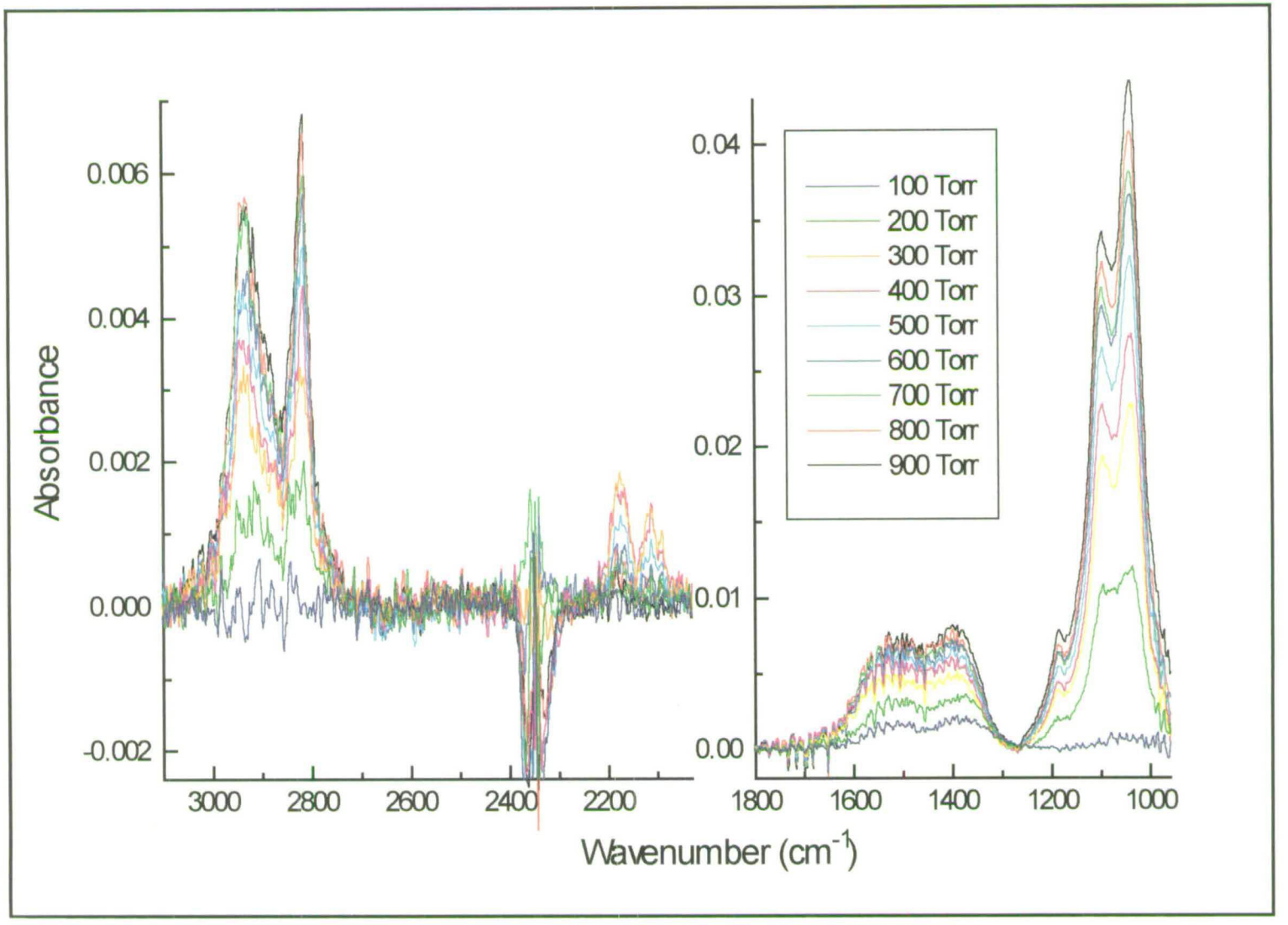

Fig. 6.8. *Methanol pulse experiment for the 1% K promoted catalyst. Total methanol exposure = 900 Torr.*

Discussion

The bands seen in the final spectrum subsequent to methanol adsorption at 2935, 2816, 1185, 1095 and 1038 cm^{-1}, with the possibility of a shoulder at 2899 cm^{-1}, resemble those found for the corresponding unpromoted experiment, apart from the absence of the shoulder at 2841 cm^{-1}. This suggests that either only methoxy on zinc oxide is present in this case, or that levels of methoxy on copper are too low to be detected. There is also an overall attenuation of the intensity of the main bands relative to the unpromoted sample's spectra, and the absorbances of the main bands in the final spectrum are displayed as a percentage of those for the unpromoted catalyst in Table 6.6. The greatest attenuation is seen for the bands in the C-H stretching region, where a contribution from the copper-methoxy species would have been made at approximately 2940-2910 and 2841 cm^{-1} - further evidence for a large decrease in the amount of copper-methoxy on promotion.

Table 6.6. *Absorbances of main bands for the 1% K catalyst as a percentage of those for the unpromoted catalyst*

Band (cm^{-1})	2935	2816	1185	1095	1036
%	19	2	33	31	32

The lack of bands due to copper-methoxy species in this case results partly from the decrease in copper surface area on promotion found by reactive frontal chromatography (to about 60 %), but the effect goes much further than this, as seen in the CO adsorption studies in Chapter 5 (an absorbance for the CO stretching band 5 % of the value on the unpromoted sample was found for the promoted). It is possible that this huge attenuation is once again due to a site blocking effect of the promoter, as suggested for the case of CO adsorption. Another possible explanation is that the copper in the promoted catalyst was better reduced than that of the unpromoted sample, as was suggested in the CO adsorption experiments in Chapter 5. As was discussed in the introduction to this chapter, Wachs and Madix [96] have

shown that chemisorption of methanol on copper as methoxy is greatly enhanced by surface oxygen.

As was mentioned in the introduction to this chapter, in a study of methanol adsorption on a potassium-promoted Cu/SiO_2 sample, evidence for a potassium methoxy species and a small red shift of 5 cm^{-1} for the copper-methoxy C-H stretching bands were seen [146]. Neither of these incidents were observed in the present study, although bands were relatively weak so either could conceivably have gone unobserved.

Gaseous CO was produced during the experiment, as shown by a doublet centred at 2143 cm^{-1}. It was produced at a higher level than for the unpromoted catalyst (1.8×10^{-3} absorbance units compared with 0.98×10^{-3}), especially considering the lower total surface area for the promoted sample (50 % of the unpromoted), but no adsorbed CO on zinc oxide was seen in this case. This increased $CO_{(g)}$ level could mean that methoxy is decomposing more easily *via* formate on zinc oxide in the presence of the alkali promoter, or that any decomposition products are simply desorbing, rather than remaining on the surface as for the unpromoted sample. The absence of adsorbed CO_2 on the promoted sample is consistent with the absence of (or low levels of) methoxy on copper which can be oxidised to formate.

In essence, the effect of the alkali promoter on methanol adsorption seems to be similar to its affect on CO adsorption in that the copper-methoxy bands are attenuated in size. The species adsorbed on the support are also affected - in this case methoxy appears to be oxidised to formate and decomposed to form $CO_{(g)}$, whereas on the unpromoted sample a lower level of $CO_{(g)}$ is observed but CO adsorbed on the support is seen.

6.2.2.2 - Temperature Programmed Desorption

Results

Figs. 6.9 - 6.11 show the variation in intensity of the bands due to adsorbed species on the catalyst surface during TPD. Once again, the spectra in the region below 1800 cm^{-1} (Fig. 6.11) have not been baseline corrected. A functional group chromatogram for the 2935 cm^{-1} band has not been plotted owing to problems highlighted for the unpromoted experiment. Fig 6.9 shows that features in the C-H stretching region were unchanged until 51 °C, at which point the band at 2935 cm^{-1} started to increase, along with an intensification to the high frequency side of the band which continued until 112 °C. Thereafter, a gradual decrease with increasing temperature occurred until the 2935 cm^{-1} band was no longer seen by a temperature of 166 °C. The band at 2818 cm^{-1} behaved similarly but appeared to exist for fractionally longer, and was last seen at 180 °C. It is difficult to comment on the shoulders in the spectra, owing to the poor signal to noise ratio. In parallel with the loss of the band at 2935 cm^{-1}, the main bands at 1095 and 1036 and the weak band at 1188 cm^{-1} had disappeared from the spectrum by 166 °C (Fig. 6.11).

The sharp feature seen for the unpromoted sample at 1032 cm^{-1} was also present during this experiment, and existed between 51 and 159 °C. That seen previously at 1347 cm^{-1} for the unpromoted catalyst was not, however, evident for the alkali promoted sample.

At no point during the TPD experiment was a band seen superimposed over the gaseous CO_2 band at 2340 cm^{-1} (Fig. 6.10). Similarly, no bands were seen in the CO stretching region.

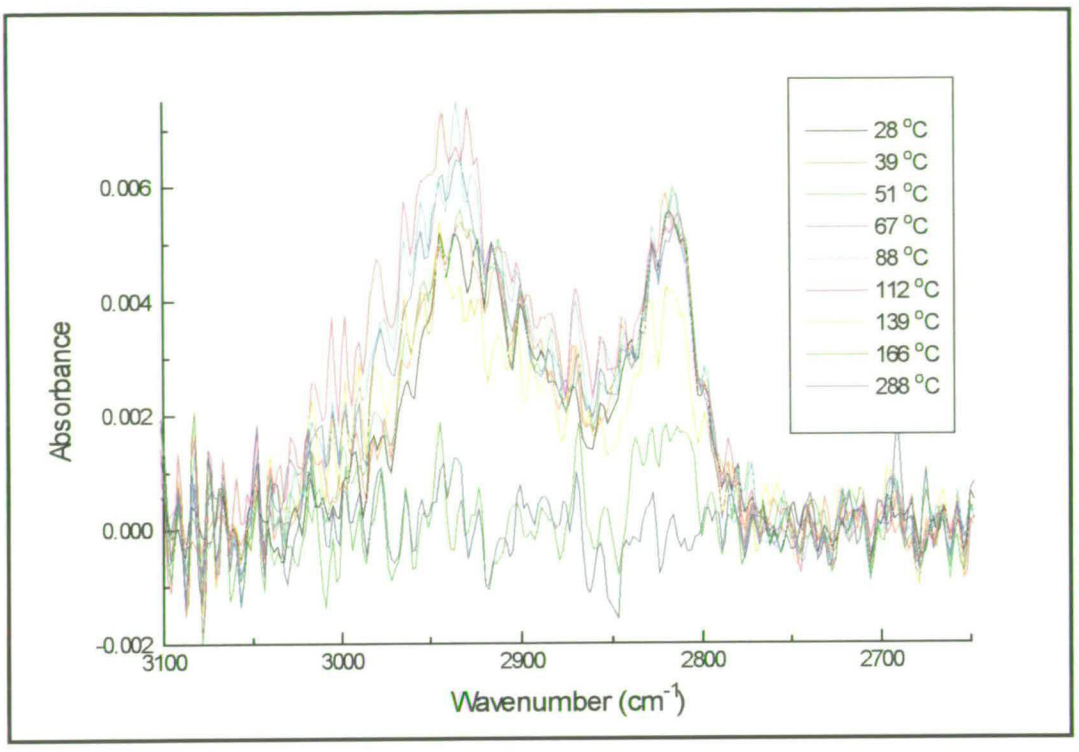

Fig. 6.9. *Temperature programmed desorption following methanol pulse experiment for the 1% K promoted catalyst in the 3100 - 2700 cm^{-1} region*

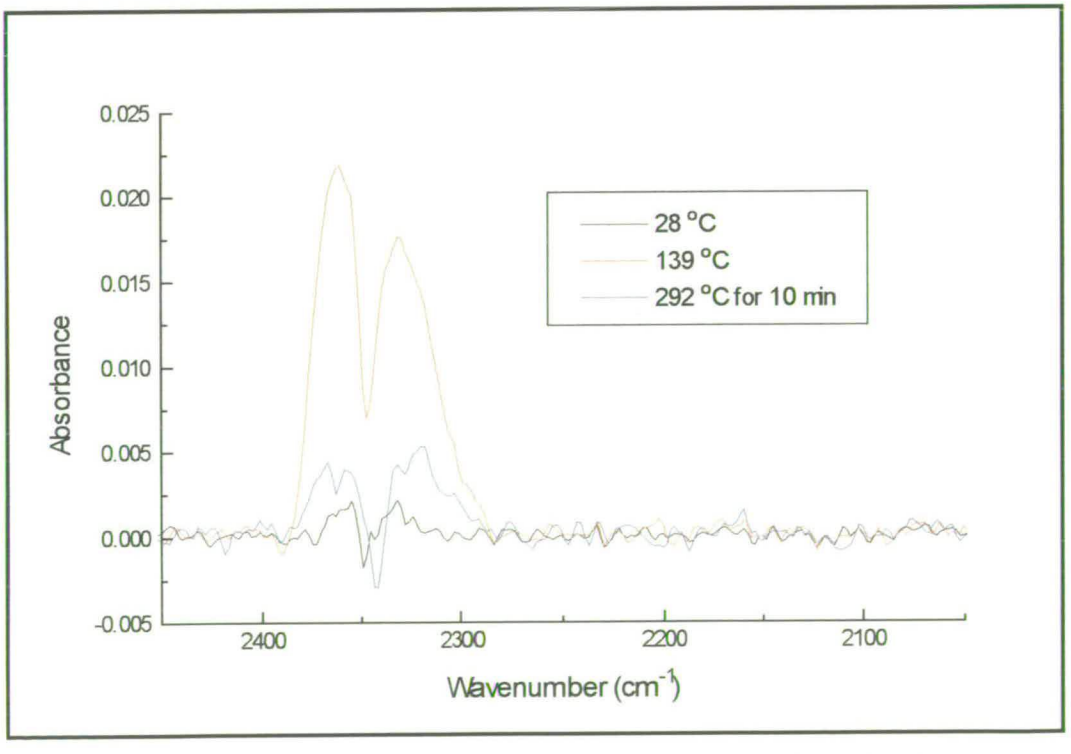

Fig. 6.10. *Temperature programmed desorption following methanol pulse experiment for the 1% K promoted catalyst in the 2500 - 2000 cm^{-1} region*

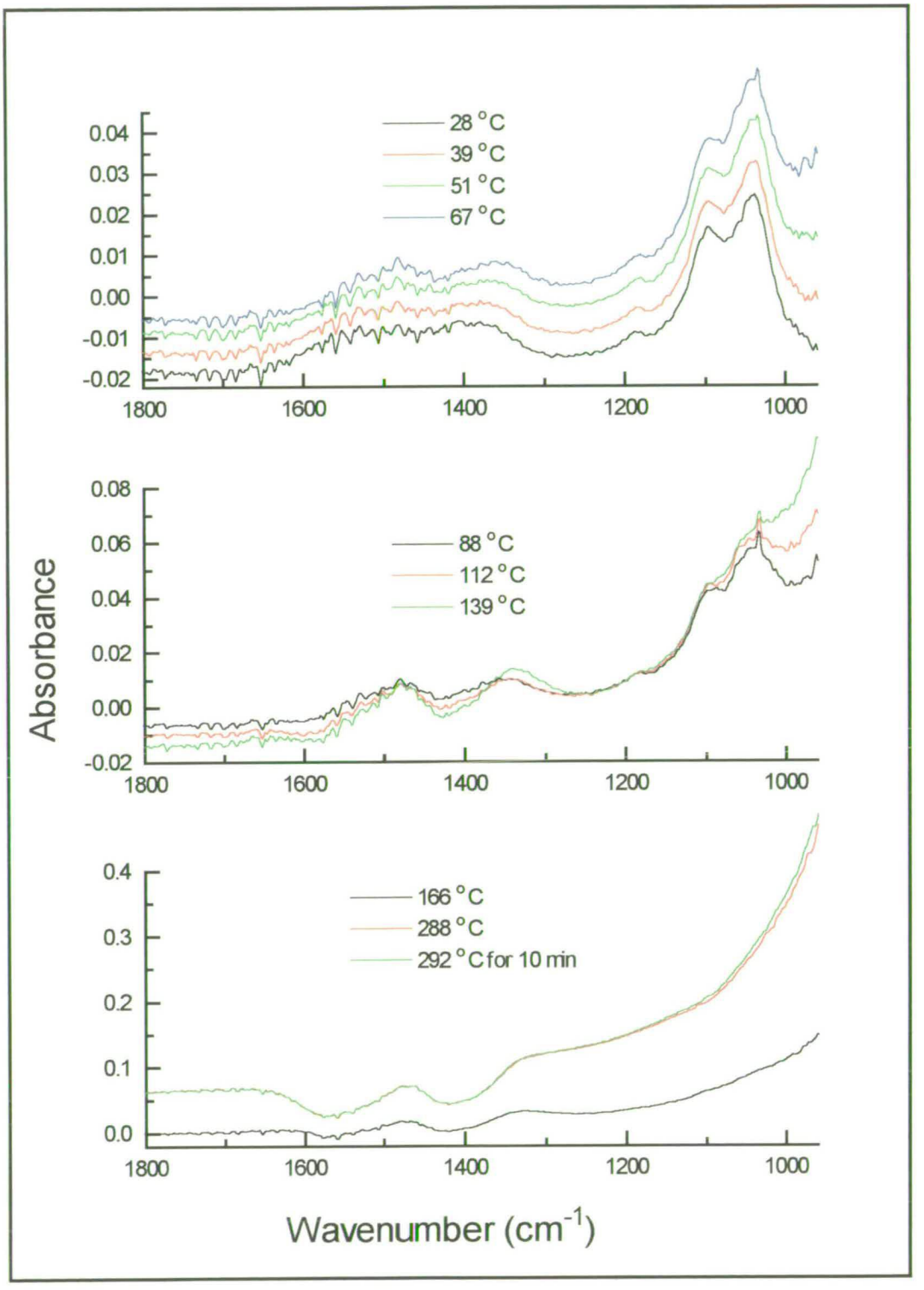

Fig. 6.11. *Temperature programmed desorption following methanol pulse experiment for the 1% K promoted catalyst (not baseline corrected).*

The mass spectrometer raw data from the methanol TPD experiment are shown for the promoted catalyst in Fig. 6.12a, while the results corrected for the fragmentation of methanol are presented in Fig. 6.12b.

Fig. 6.12b shows the evolution of CH_3OH (*m/e* 31) starting at a relatively low temperature and with T_{max} at 110 °C (refer to Table 6.4 for an explanation of the assignment of *m/e* values to gas phase molecules). It is assumed that no H_2CO (*m/e* 30) was formed; the negative trace is a result of the inaccuracy in the determination of the fragments' relative abundances (Table 6.3). H_2 was seen to evolve slowly until a possible inflexion at about 110 °C, after which evolution took place at a greater rate, finally peaking at 145 °C. CO was not produced at low temperatures, as the correction for methanol fragmentation illustrates (comparing Fig 6.12a with 6.12b). Its evolution was seen to peak at 166 °C. A small amount of CO was also detected at higher temperature (T_{max} = 257 °C) and was accompanied by H_2 with T_{max} at about 265 °C. As for the unpromoted sample, CO_2 was not evolved until a temperature of 101 °C, with T_{max} at 145 °C. Features seen at 230 °C in the CO_2 trace and at 222 °C in the H_2 trace are thought to be spuriously caused by the mass spectrometer. This information is summarised in Table 6.7, along with the integrated areas for the desorption peaks.

Table 6.7. *Quantity of each species evolved during the TPD following methanol adsorption on the 1% K promoted catalyst, according to Fig. 6.12b*

Species Evolved	T_{max} (°C)	Area of Peak (a.u.)
H_2	145	2.4
CO (i)	166	0.45
(ii)	257	0.24
H_2CO	-	0
CH_3OH	110	1.4
CO_2	151	4.9

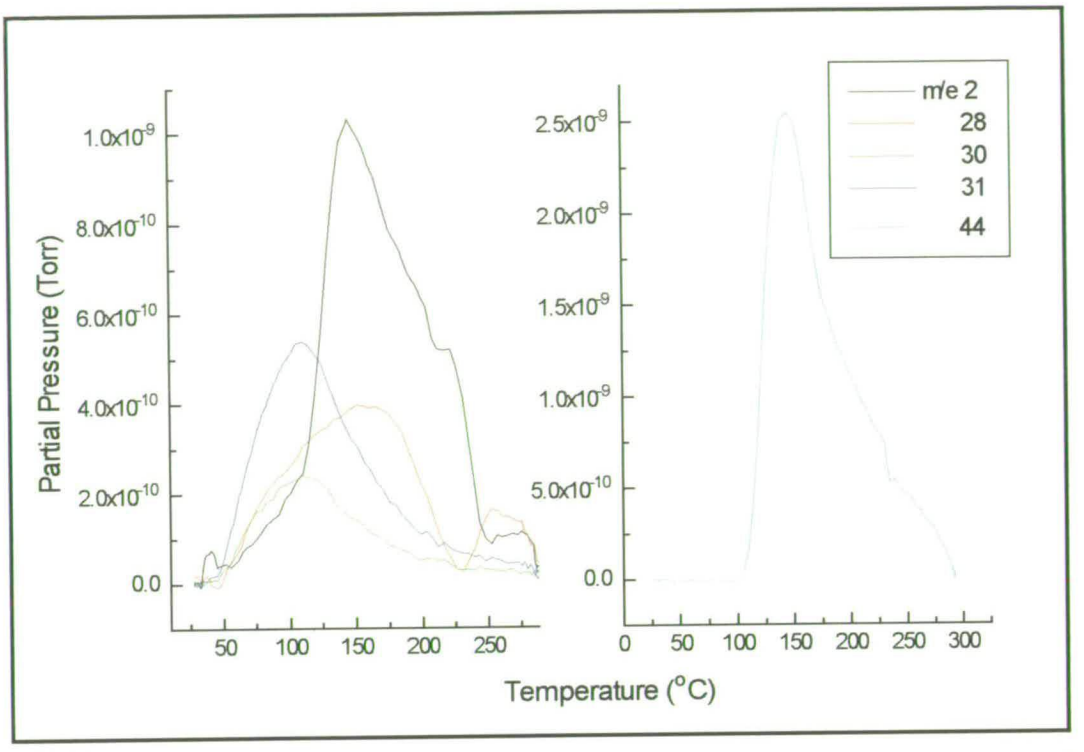

Fig. 6.12a. *TPD following the adsorption of methanol on the 1% K promoted catalyst - original data.*

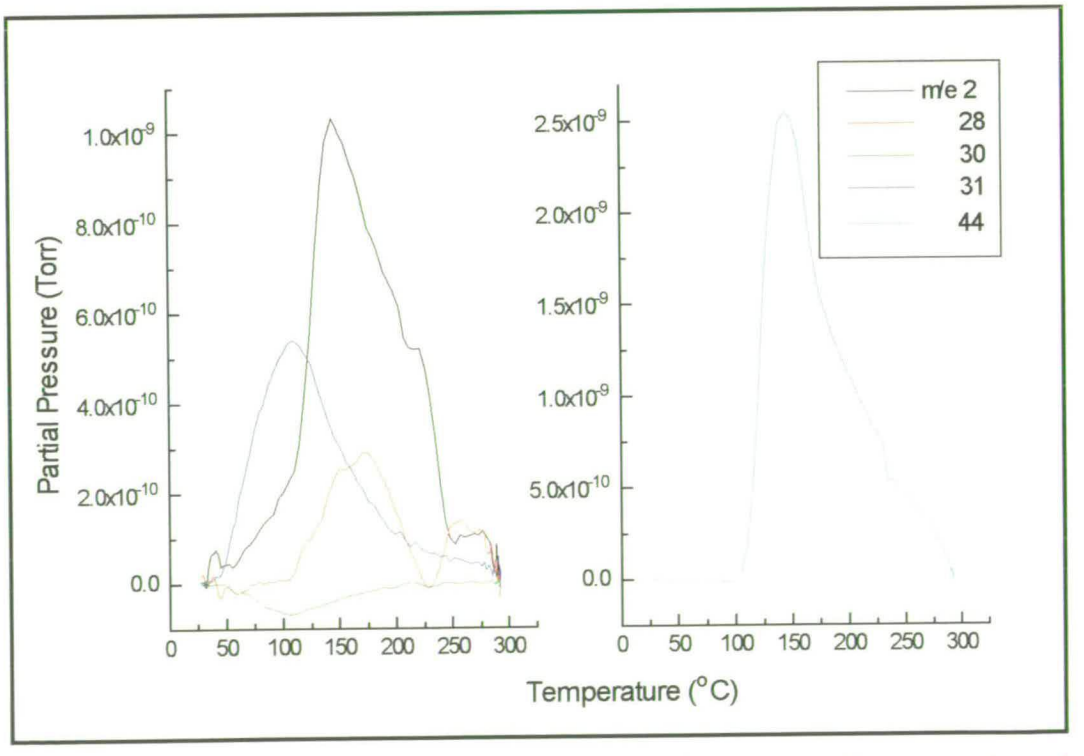

Fig. 6.12b. *TPD following the adsorption of methanol on the 1% K promoted catalyst - data corrected for fragmentation of methanol.*

Discussion

The bands associated with methoxy on zinc oxide were found to die away by 166 °C (2935, 1188, 1095 and 1036 cm^{-1}) and 180 °C (2819 cm^{-1}). These values are lower than the corresponding values for the unpromoted sample, suggesting that either there was less contribution from a formate species on copper (bands in the CH region), which would have the effect of increasing the overall desorption temperature, or/and that the adsorbed species is destabilised in the presence of the promoter (all bands). The absence of the band at 1347 cm^{-1} for the promoted catalyst, which was seen for the unpromoted and attributed to bidentate formate on copper, is in agreement with the former suggestion.

The sharp feature at 1032 cm^{-1} which was seen for the unpromoted sample between 92 and 174 °C was again observed, this time between 51 and 159 °C. This is again attributed to gas phase methanol from the recombinative desorption of methoxy with surface hydrogen (reaction 6.3 in the introduction).

Methanol was also seen by the mass spectrometer, peaking at 110 °C. This formation is usually accompanied by the evolution of formaldehyde [130]. The absence of this species during this experiment suggests a decrease in the amount of methoxy decomposed relative to the unpromoted catalyst. In addition, it was also found that in spite of the decreased total area of the promoted catalyst, more methanol species were observed than for the unpromoted catalyst (peak area 1.4 a.u. compared with 0.80 a.u.). It is thus postulated that more methanol is desorbed from the promoted sample intact while less C-H bond scission occurs to produce formaldehyde. This information, along with the finding by both infra-red and mass spectrometry that methanol was formed at a lower temperatures than for the unpromoted sample, suggests that the methoxy species was bonded less strongly to the surface in the presence of the promoter.

The formation of CO_2 and H_2 was seen at 145 and 151 °C in the same fashion as for the unpromoted catalyst and again is indicative of the decomposition of formate species on copper. However, no evidence was seen for this species at any time in the infra-red spectra. The quantity of each gas is slightly less than for the unpromoted catalyst in support of the suggestion that less methanol is decomposed over the promoted sample but there is still a substantial amount considering the absence of formate infra-red bands and the decrease in copper surface area on promotion. CO gas was also observed concomitant to these events and, as previously suggested for the unpromoted sample, decomposition of formate on zinc oxide or the RWGS reaction are implicated.

Finally, CO and H_2 were again observed at higher temperature still, with T_{max}s at 257 and 265 °C, possibly suggesting the decomposition of formate on zinc oxide [123], although no formate species were observable on the surface at this temperature.

In summary, during the TPD of adsorbed methoxy species from the promoted catalyst surface, there appears to be a lower level of decomposition species (H_2CO, CO, H_2, CO_2) compared with the unpromoted sample and a higher level of desorption products (i.e. methanol).

6.2.3 - Summary of the Effect of Promotion on Methanol Adsorption

In order to simplify the observations from the methanol adsorption experiments and the subsequent TPD, the range of reactions suggested to be occurring, with the effect of promotion on them, is illustrated in Fig. 6.13 (pulse experiment at room temperature) and Fig. 6.14 (TPD). Species in brackets were not actually observed in experiments.

During the pulse experiment, (Fig. 6.13), the promoter had the following impact:

- step (1) was decreased greatly and (by implication) step (3) was prevented,
- step (4) was decreased (but not to as great a degree as (1)) and step (6) was not observed, but step (7) was increased.

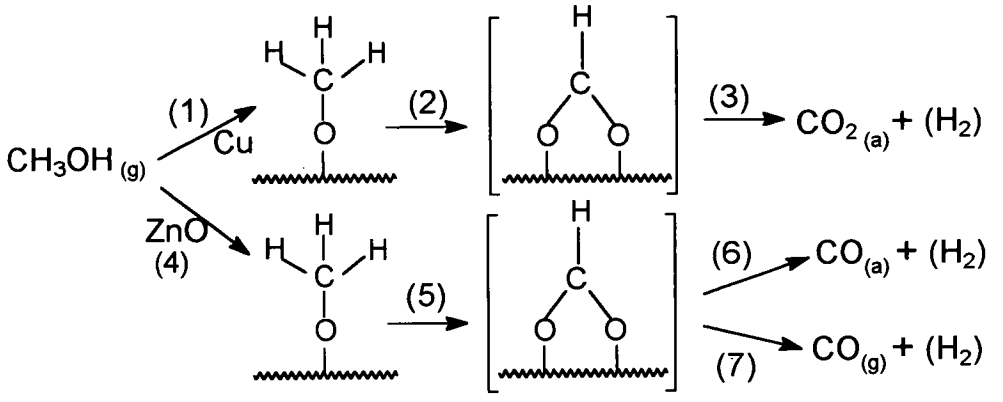

Fig. 6.13. *Proposed steps during the methanol pulse experiments*

During the TPD (Fig. 6.14) the promoter had the following impact:

- step (8) was increased, while step (9) was decreased,
- step (10) was decreased and step (11) was also decreased (by implication),
- step (13) was decreased.

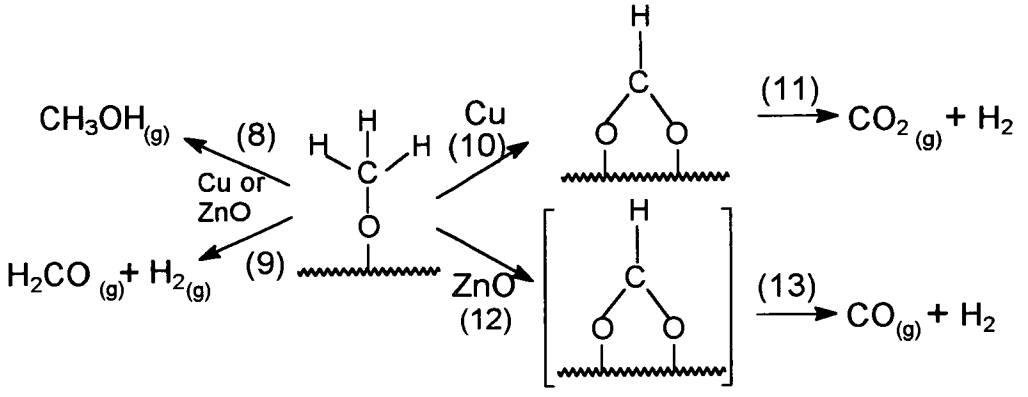

Fig. 6.14. *Proposed steps during the TPD following methanol adsorption*

6.3 - Formic Acid Adsorption

Experiments were carried out as for the methanol adsorption experiments. The maximum vapour pressure of formic acid attainable at room temperature was pulsed over the catalyst (in this case, 20 Torr) nine times at 5 min intervals, such that the catalyst was exposed to 180 Torr of formic acid in total. Following this, a temperature programmed desorption was carried out as usual.

6.3.1 - Unpromoted Catalyst

6.3.1.1 - Pulse Experiment

Results

As for the methanol experiment, bands were seen in the C-H stretching region, and these are shown in Fig. 6.15. Following the introduction of the first pulse, two main bands were observed at 2966 and 2886 cm^{-1}. These were accompanied by weak shoulders at 2930 and 2855 cm^{-1}. Intense features were also seen in the region of the spectrum below 1700 cm^{-1}. A broad, intense band was evident at 1609 cm^{-1} and another intense band appeared at 1367 cm^{-1}, with a shoulder at 1385 cm^{-1}. A very weak feature was observed at 1462 cm^{-1} and a broad feature was seen at 1047 cm^{-1}. In addition to these main regions of interest, a group of weak features was seen at 2731, 2622, 2191, and 2098 cm^{-1}. Finally, a broad band was found centred at about 3430 cm^{-1} (not shown here, but given in the TPD section following).

After an exposure of 40 Torr of formic acid, the bands in the C-H stretching region developed such that the main band was now found at 2880 cm^{-1}, with a small asymmetry at about 2855 cm^{-1}, a shoulder at 2962 and a small, sharp feature superimposed at 2933 cm^{-1}. The intense feature previously seen at 1609 cm^{-1} was now found at 1632 cm^{-1}, but with a possible asymmetry at the position where the band was

originally seen. The main band at lower frequency was now positioned at 1359 cm^{-1}, while the shoulder at 1385 was still evident and a new shoulder had also appeared at 1374 cm^{-1}. The weak features seen between 2800 and 2000 cm^{-1} continued to grow in intensity, as did those at 1462 and 1050 cm^{-1}.

By an exposure of 60 Torr, all features were seen to grow, but the bands at low intensity altered slightly, so that the main band was found at 1376 cm^{-1}, with a sharp feature superimposed onto this at 1352 and shoulders at 1385 and 1360 cm^{-1}. As pulsing continued, these features continued to grow except that at 1360 cm^{-1}, which was seen to gradually die away. Likewise, other bands also continued to grow and a new shoulder at 1323 cm^{-1} appeared after 100 Torr of formic acid had been pulsed. Features at 1774 and 1105 cm^{-1} appeared after 40 and 80 Torr, respectively, which possessed rotational fine structure - a sharp peak with broader bands either side. It was possible that an asymmetry existed at 2340 cm^{-1} in the gaseous CO_2 band but only following an exposure of 80 Torr of formic acid. Bands in the CO stretching region became more complex after an exposure of 60 Torr - that at 2191 cm^{-1} died away, while new features at 2178, 2135 and 2076 cm^{-1} grew in.

Following the introduction of the final pulse to the unpromoted catalyst, the main band in the C-H stretching region was found at 2885 cm^{-1}, while another at 2933 cm^{-1} was weaker, relatively. A weak shoulder was also seen at 2962 cm^{-1}. Bands at lower frequency were found at 1640 cm^{-1} (strong, with an asymmetry to the low frequency side), 1376 cm^{-1} (sharp), 1352 cm^{-1} (sharp), 1386 and 1323 cm^{-1} (both shoulders). Weak features were still evident at 2739, 2175, 2076 and 1465 cm^{-1}, as were broad bands at 3430 and 1050 cm^{-1}.

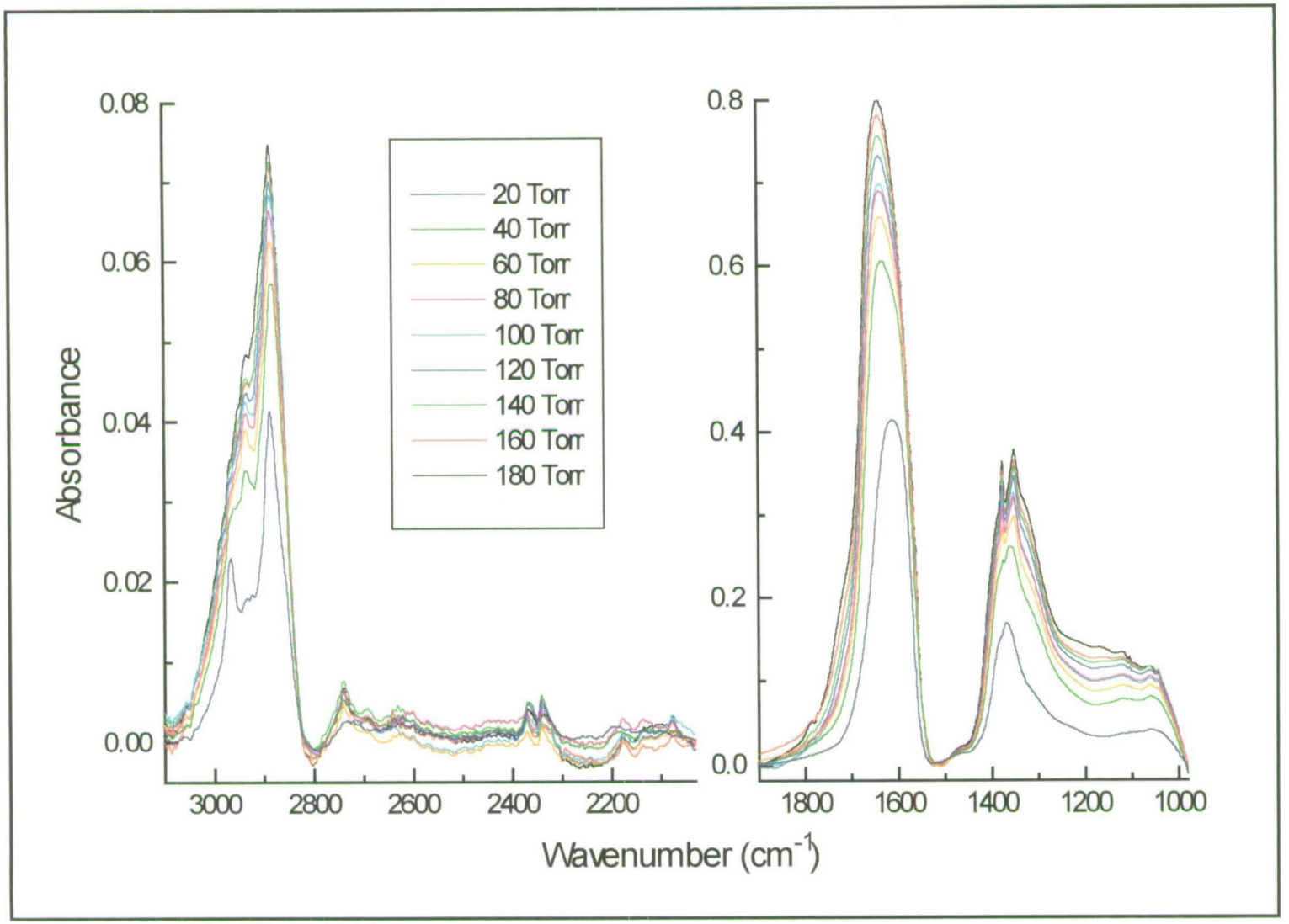

Fig. 6.15. *Formic acid pulse experiment for the unpromoted catalyst. Total formic acid exposure = 180 Torr.*

Discussion

The results listed above for the formic acid pulse experiment on the unpromoted catalyst are complex, so in order to aid band assignment, a comparison will be made with other studies of a similar nature and with the infra-red bands of formic acid itself (Tables 6.8, 6.9 and 6.10).

Table 6.8 shows that varying band frequencies have been reported for bidentate formate on copper single crystal surfaces, but in spite of this there is general agreement on the approximate region of the three main bands observed and their assignment. The highest frequency band in each case is due to the combination of the asymmetric (COO) stretch and the in-plane C-H deformation mode. No asymmetric stretch is seen owing to the metal-surface selection rule - since the adsorbed formate exists in an upright configuration, no dipole is generated perpendicular to the surface during this vibration.

There is better agreement in the position of the bands found for bidentate formate on copper in supported samples. Table 6.9 gives some examples from the literature. Shoulders were observed during this study after the first pulse at 2930 and 2855 cm^{-1}, and after an exposure of 60 Torr an accompanying band was also seen at 1352 cm^{-1}. By comparison with the literature values given in Table 6.9, it is evident that these features are due to bidentate formate on copper. Although the bands in the C-H stretching region are always weak, that at 1352 cm^{-1} is always prominent once it has appeared.

Assignment [138]	HCOOH monomer [138]	HCOOH dimer [138]	condensed HCOOH on Cu(110) [138]	m-HCOO on Cu(110) [138]	b-HCOO on Cu(110) [138]	b-HCOO on Cu(100) [125]	b-HCOO on Cu(100) [127]	b-HCOO on Cu(110) [126]
$\delta_{O-C=O}$	625	697	797	787				
δ_{O-C-O}					767	760	760	
δ_{OH}(oop)	642	917	960					
π_{CH}(oop)	1033	1050	1078					
υ_{C-O}	1104	1218	1235	1266				
υ_{COO}(s)					1355	1330	1325	1348 - 1358
δ_{CH}(ip)	1381	1365	1388	1381				
δ_{HOC}	1223	1450						
υ_{COO}(a)						1640		
$\upsilon_{C=O}$	1777	1754	1733	1640-1670				
$\delta_{HOC}+\upsilon_{C-O}$			2574					
$\upsilon_{C=O}+\pi_{CH}$(oop)			2757					
υ_{CH}	2942	2957	2937	2865	2849	2840	2870	2891 - 2900
υ_{COO}(a)+δ_{CH}(ip)				2945	2930	2910	2930	2948 - 2955
υ_{OH}	3569	3110	3100					

Table 6.8. *Reference data (in cm^{-1}) for formic acid, mondentate (m-HCOO) and bidentate (b-HCOOH) formate species, and condensed formic acid on copper single crystals. "ip" and "oop" denote in-plane and out of plane vibrations, respectively.*

Table 6.9. *Frequencies (in cm^{-1}) for bands assigned to a bidentate formate species on copper in supported samples. N.B. the values from reference [124] concerned formate formed from methanol decomposition*

Cu/SiO_2 [124]	Cu/SiO_2 [139]	$Cu/ZnAl_2O_4$ [134]	Assignment
2935	2938	2930	$\upsilon_{COO}(a) + \delta_{CH}(ip)$
2851	2857	2850	υ_{CH}
1351	1359	1352	$\upsilon_{COO}(s)$

The remaining bands are more difficult to assign. They were found at 2966, 2886, 1609, 1385, 1367 and 1047 cm^{-1} with weak features at 2731, 2622, 2191, 2098 and 1462 cm^{-1} after the first pulse, and 2962, 2885, 1640 (with an asymmetry at the low frequency side), 1323, 1386, 1376 and 1050 cm^{-1} with weak features at 2739, 2175, 2076 and 1465 cm^{-1} after an exposure of 180 Torr. When considering the results from the literature of formate species on zinc oxide [134, 139, 140], alumina [134, 141] and zinc aluminate [134], it seems most likely that in this case the bands at 2962, 2885, 2739, and 1386 cm^{-1} seen after the last formic acid pulse and that seen after the first at 1367 cm^{-1} are due to formate on zinc oxide. A comparison is made with the bands found by Chauvin *et al.* in Table 6.10.

Table 6.10. *Comparison of frequencies (in cm^{-1}) found in this study compared with those by Chauvin et al. [134] for formate on ZnO*

This Study	Chauvin *et al.*	Assignment
2962	2960	$\upsilon_{COO}(a) + \delta_{CH}$
2885	2882	υ_{CH}
2739	2740	$\upsilon_{COO}(s) + \delta_{CH}$
(1640)	1580	$\upsilon_{COO}(a)$
1386	1382	δ_{CH}
1367	1365	$\upsilon_{COO}(s)$

Presumably the band found by Chauvin *et al.* at 1580 cm^{-1} for the asymmetric (COO) stretch is present in this study but is obscured by the intense, broad band seen at 1640 cm^{-1} - this band possessed an asymmetry to the low wavenumber side and was actually positioned at 1609 cm^{-1} following the first pulse.

Evidence for the decomposition of bidentate formate on copper to CO_2 at room temperature is given by the presence of an asymmetry at 2340 cm^{-1} in the gaseous CO_2 band envelope after the sample had been exposed to 80 Torr of formic acid. Furthermore, the formation of small amounts of CO are indicated by the weak bands at 2098 cm^{-1} in the first spectrum, 2076 cm^{-1} in the final spectrum, and 2135 cm^{-1} in occasional spectra, suggesting the presence of CO on stepped and low index planes of copper, and copper oxide, respectively. This CO was probably produced from CO_2 either *via* the RWGS reaction (CO_2 and H_2 from copper-formate decomposition) or *via* CO_2 dissociation on copper. Presumably formate on copper decomposed first on stepped surfaces, followed by that on low index planes. The appearance of CO on low index planes is puzzling considering that CO adsorption experiments in Chapter 5 did not suggest their presence.

The decomposition of formate on zinc oxide has also apparently occurred - bands at 2190 and 2175 cm^{-1} are indicative of CO adsorption on zinc oxide, according to Ghiotti *et al.* [122] who found that the band shifted from the high to low frequency value with increasing coverage. Evidence for the presence of bidentate carbonate on zinc oxide is given by the bands at 1050 and 1325 cm^{-1} in the final spectrum. These features, along with another at 1590 cm^{-1}, were assigned in Chapter 5, following the interaction of CO_2 with the unpromoted catalyst. It is likely that the band at 1590 cm^{-1} is obscured by that at 1640 cm^{-1} in this particular case. The CO_2 for carbonate formation following formic acid adsorption could have formed either from copper-formate decomposition or from formate decomposition on the support to CO, followed by its subsequent oxidation to CO_2.

The broad band seen at 3430 cm^{-1} is due to surface OH groups, which could have several origins: water impurities introduced with the formic acid, the dissociative adsorption of formic acid to produce formate and a proton which goes on to form -OH with the surface, or water produced reactively from CO_2 and H_2 *via* the RWGS reaction. The broadness of the band suggests that the OH groups are hydrogen bonded.

Comparison of the position of several weak bands with frequencies in Table 6.8 allows their assignment. Those at 1774 and 1105 cm^{-1} are probably due to formic acid monomers in the gas phase [138], while that at 2739 cm^{-1} could be due to condensed formic acid. The weak band seen at 1462 cm^{-1} corresponds to δ_{HOC} in a formic acid dimer.

The most difficult band to assign is that at 1640 cm^{-1}. Several suggestions can be made as to its origin. In the study of formic acid adsorbed on alumina, a band was seen at 1625 cm^{-1} attributed to formate on alumina [141], but none of the other bands observed in that study were seen here. In an investigation of the adsorption of formic acid on a $Cu/ZnO/SiO_2$ catalyst, Millar *et al.* [139] looked at the region around 1600 cm^{-1} in detail and suggested the presence of three different formate species: a bidentate zinc formate formed on Zn-polar planes and giving rise to a band at 1582 cm^{-1}, an interfacial bidentate formate species associated with both the copper and zinc oxide components of the sample which gave rise to a band at 1600 cm^{-1} and finally a monodentate zinc formate species most probably produced on non-polar zinc oxide crystal planes with a band at 1626 cm^{-1}. It was suggested that the formic acid would interact most strongly with the zinc polar surfaces.

In another study, Edwards and Schrader [149] saw a band 1620 cm^{-1} following the adsorption of a CO_2-H_2 mixture on a Cu/ZnO sample and assigned it to adsorbed formaldehyde. It is unlikely that the band seen during this study at 1640 cm^{-1} can be attributed to this species since their 1620 cm^{-1} band was weak.

A band at around 1640 cm^{-1} has been reported by several authors following the adsorption of formic acid on copper single crystal surfaces, usually at low temperature, and has been attributed to various species: Sexton observed a strong band at this frequency at -173 °C and very weakly at 127 °C, and attributed it to the $\upsilon_{COO}(a)$ of a "low symmetry" bidentate formate species [125]. Dubois *et al.* attributed their band, seen at -153 °C, to the $\upsilon_{COO}(a)$ of a tilted formate, where the acidic proton remained associated with the acid and a certain degree of hydrogen bonding existed [127]. Bowker *et al.* assigned a band at 1657 cm^{-1} present at -273 °C to $\upsilon_{C=O}$ of monodentate formate [138]. They suggested that the carbonyl group was datively bonded to the surface, as in Fig. 6.16.

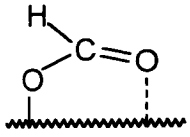

Fig. 6.16. *Model of monodentate formate, according to Bowker et al., [138].*

The suggestion from Bowker *et al.* seems plausible when considering that they also saw a band assigned to $\delta_{CH}(ip)$ at 1381 cm^{-1}. During this study, a band at 1376 cm^{-1} (as yet unassigned) was first seen when the band at 1640 cm^{-1} appeared and was much sharper that any of the bidentate formate on zinc oxide bands. However, it must be remembered that the species identified by Bowker *et al.* was only present below room temperature, and gradually converted to a symmetrical bidentate formate species on heating from -73 to 27 °C.

As a final suggestion, the band at 1640 cm^{-1} could be due to physisorbed water - Millar *et al.* [87] attributed a similar band at 1626 cm^{-1} on a Cu/SiO_2 catalyst to this. Considering this and the suggestions above, it becomes clear that it is not possible to assign the band to any one species with certainty. Conceivably there could be a mixture of different species present considering the large bandwidth.

In summary, the spectra recorded following formic acid adsorption on the unpromoted sample are clearly very complicated. Both bidentate formate on copper and on zinc oxide were identified. It was not possible to assign the intense, broad band at 1640 cm^{-1} with certainty. Formate decomposition on both copper and zinc oxide was identified by the adsorption of CO on both of these catalyst components, and the formation of bidentate carbonates from the interaction of CO_2 with the support.

6.3.1.2 - Temperature Programmed Desorption

Results

The spectra collected during the TPD are shown in Figs. 6.17 - 6.19. Bands in the C-H stretching region at the start of heating (Fig. 6.17) included a main band at 2885 cm^{-1} with a broad shoulder which now appeared to be at 2933 cm^{-1}. These were unchanged until 50 °C, when they started to decrease in size. By a temperature of 147 °C, the shoulder at 2933 cm^{-1} was diminishing more quickly than the main band, and at 173 °C three bands were clearly resolved in the region - at 2935, 2960 and 2875 cm^{-1}. The band at 2935 cm^{-1} continued to decrease in intensity until 243 °C, whereupon only that at 2875 cm^{-1} remained. This was finally no longer evident at 271 °C. The broad band centred at about 3430 cm^{-1} (not shown in the pulse experiment) was found to shift to 3490 cm^{-1} between 25 and 116 °C, before diminishing in intensity most rapidly between 116 and 147 °C. It was no longer present at 251 °C.

Considering the features at lower frequency (Fig. 6.19, not baseline corrected), the intense band at 1640 cm^{-1} appeared to initially grow in intensity from 30 to 90 °C. Thereafter, it decreased in intensity, but most at the high frequency side so that at 225 °C it was positioned at 1620 cm^{-1}, before finally disappearing at 275 °C.

It is hard to be definitive about this temperature, though, because the band was at the edge of the miscancellation features at 1550 and 1400 cm^{-1}.

The weak band at 1465 cm^{-1}, fairly sharp features at 1376 and 1352 cm^{-1} and shoulders at 1386 and 1323 cm^{-1} were unchanged by 74 °C. However, the 1376 and 1352 cm^{-1} features disappeared by 94 °C. At this temperature the shoulder at 1386 cm^{-1} had grown in intensity and sharpened in appearance while a new, also sharp, feature had appeared at 1361 cm^{-1}. By 116 °C another shoulder was evident at 1392 cm^{-1}, and the features at 1386, 1361 and 1323 cm^{-1} remained. Although the baseline was starting to slope by 147 °C features were seen at 1382, 1364 (weak) and 1307 cm^{-1}. At 202 °C only features at 1364 and 1346 cm^{-1} were seen, at 225 °C only that at 1364 remained and at 271 °C this had disappeared. It is difficult to determine at which temperature the bands at 1323 and 1050 cm^{-1} disappeared owing to the sloping baseline. Features at 1105 and 1774 cm^{-1} had disappeared by 173 °C, while that at 2739 cm^{-1} was no longer seen after 251 °C.

Fig. 6.18 shows the features in the CO_2 and CO region. The gas phase CO_2 band has a possible superposition of a weak feature at 2340 cm^{-1} from room temperature to 50 °C, but this is uncertain. Bands were observed at 2199 and 2174 cm^{-1} which were found to be stable until 68 °C, when they started to decrease in intensity until 90 °C. At this temperature, a doublet centred at 2143 cm^{-1} started to grow in, obscuring those at 2199 and 2174 cm^{-1}. This doublet remained until 251 °C, and thereafter decreased in size and was no longer seen at 291 °C - at this temperature, only a negative band at 2197 cm^{-1} could be observed. A band at 2137 cm^{-1} was seen to start decreasing in intensity from 38 °C, before disappearing at 90 °C, while one at 2075 cm^{-1} was seen to decrease at 68 °C before also disappearing at 90 °C.

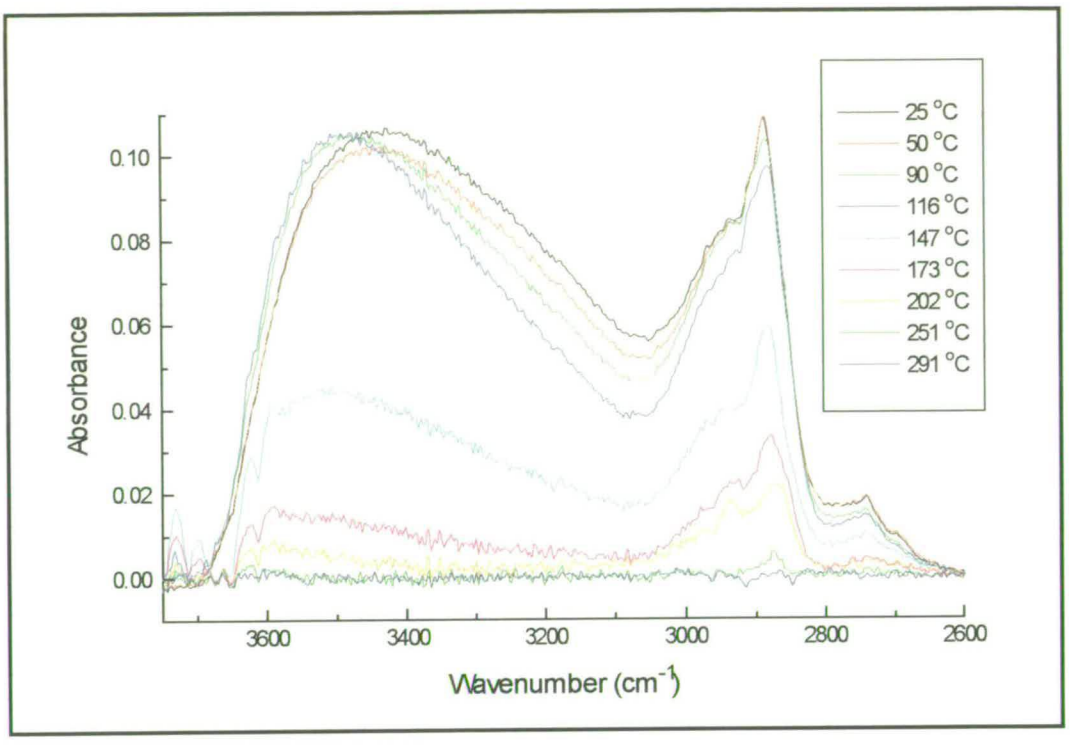

Fig. 6.17. *Temperature programmed desorption following formic acid pulse experiment for the unpromoted catalyst in the 3700 - 2600 cm^{-1} region*

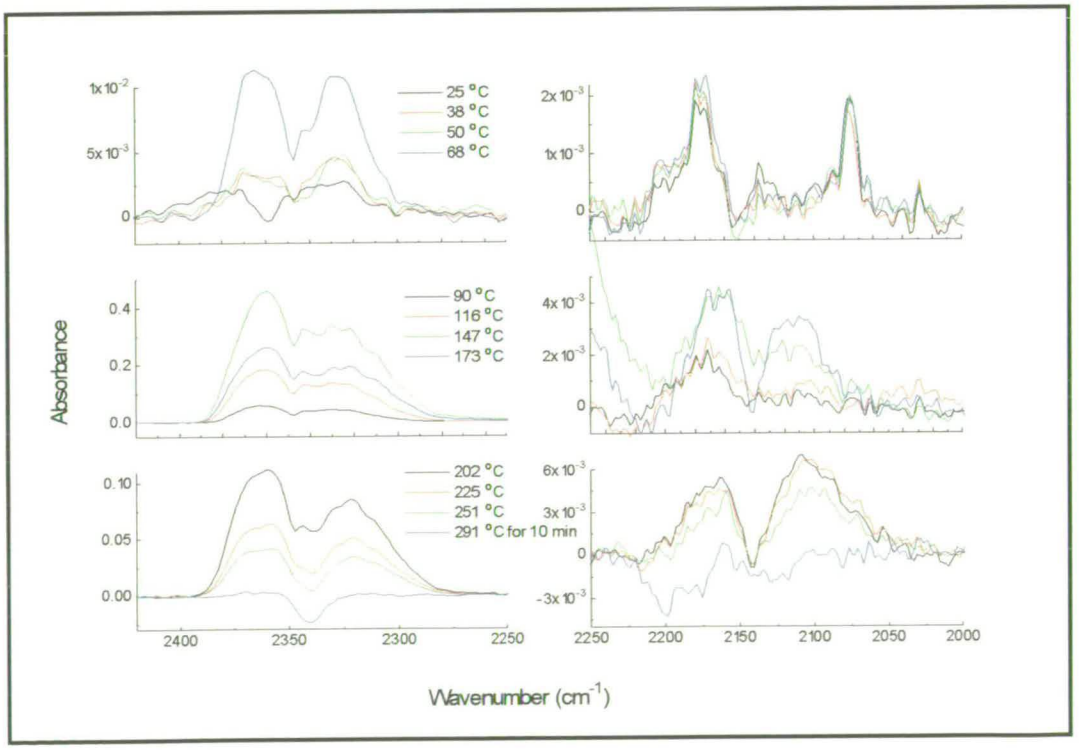

Fig. 6.18. *Temperature programmed desorption following formic acid pulse experiment for the unpromoted catalyst in the 2500 - 2000 cm^{-1} region*

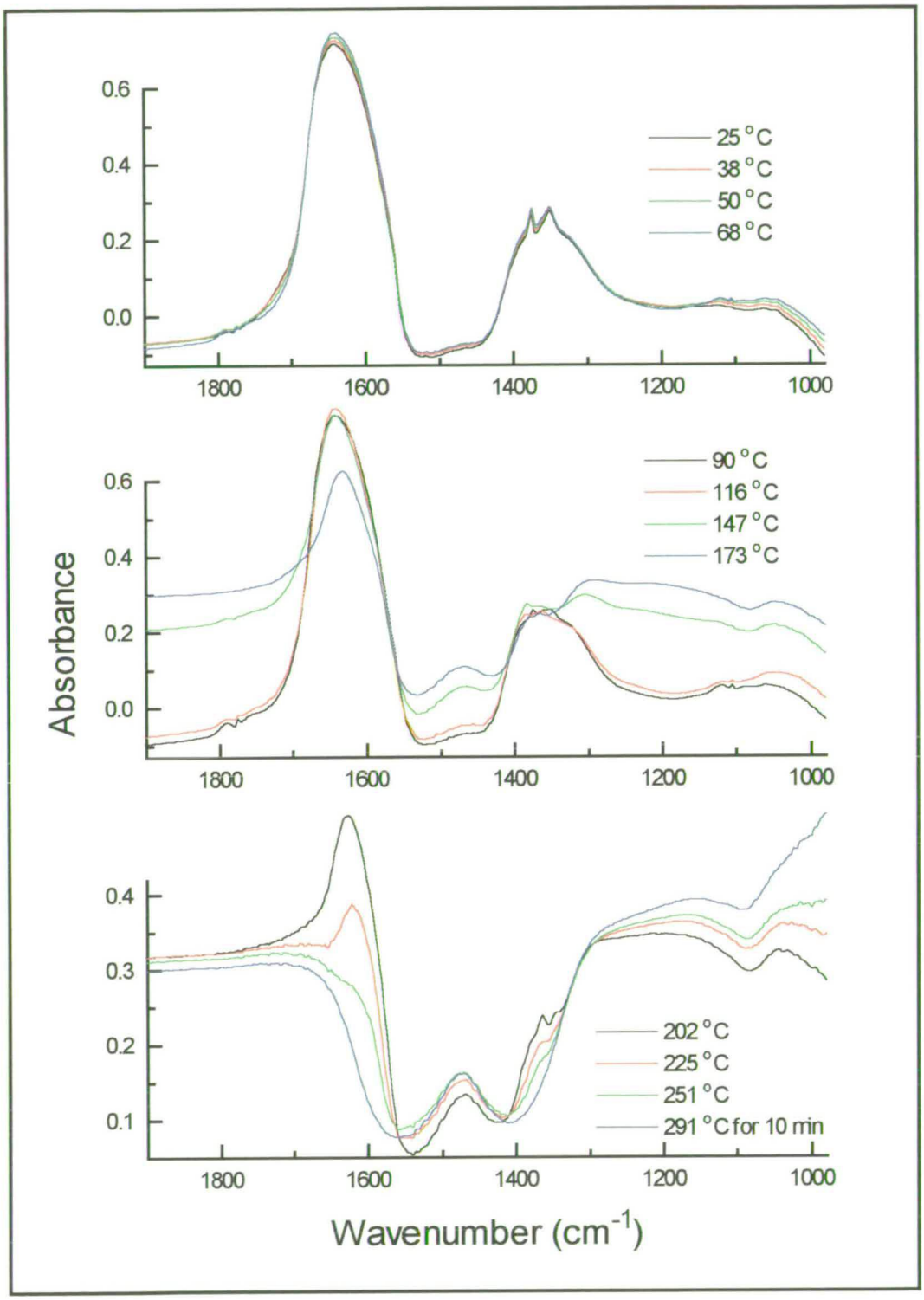

Fig. 6.19. *TPD following the formic acid pulse experiment on the unpromoted catalyst for the 1900 - 1000 cm^{-1} region (not baseline corrected).*

The gas phase species evolved during the TPD were monitored by mass spectrometry. Prior to this, a "blank" experiment was carried out in the same way as for the methanol experiments. Thus, determination of the major ionisation peaks expected due to the fragmentation of formic acid in the mass spectrometer was possible, allowing the differentiation between these fragments and species due to the actual "reaction" with the surface.

The fragments which were identified as being important for the interpretation of the TPD results are listed with their relative abundances in Table 6.11. The fragment with *m/e* = 29 was designated as the base peak and was arbitrarily given a relative abundance of 100%.

Table 6.11. *Fragments observed during formic acid "blank" experiment*

m/e	Identity of Fragment Ion$^+$	Abundance/%
29	HCO	100
28	CO	73
44	CO_2	53
18	H_2O	34
2	H_2	30

The mass spectrometer raw data from the formic acid TPD experiment are shown in Fig. 6.20. Only a small amount of HCO was detected during the TPD. Therefore, as an approximation, the other species have not been corrected for the contribution from the fragmentation of formic acid, and are assumed as being real "reaction" products. It can be seen that species with *m/e* 2, 18, 28, 29, 31 and 44 were detected. Table 6.12 suggests the identity of the fragment ions responsible for these signals and the expected gas phase molecules from which the ions originated.

Table 6.12. *Ions detected by the mass spectrometer during TPD following formic acid adsorption on unpromoted catalyst, and the original molecules to which they correspond.*

m/e	Ion^+	Corresponding Species Evolved
2	H_2	H_2
18	H_2O	H_2O
28	CO	CO
29	HCO	HCOOH
31	CH_2OH	CH_3OH
44	CO_2	CO_2

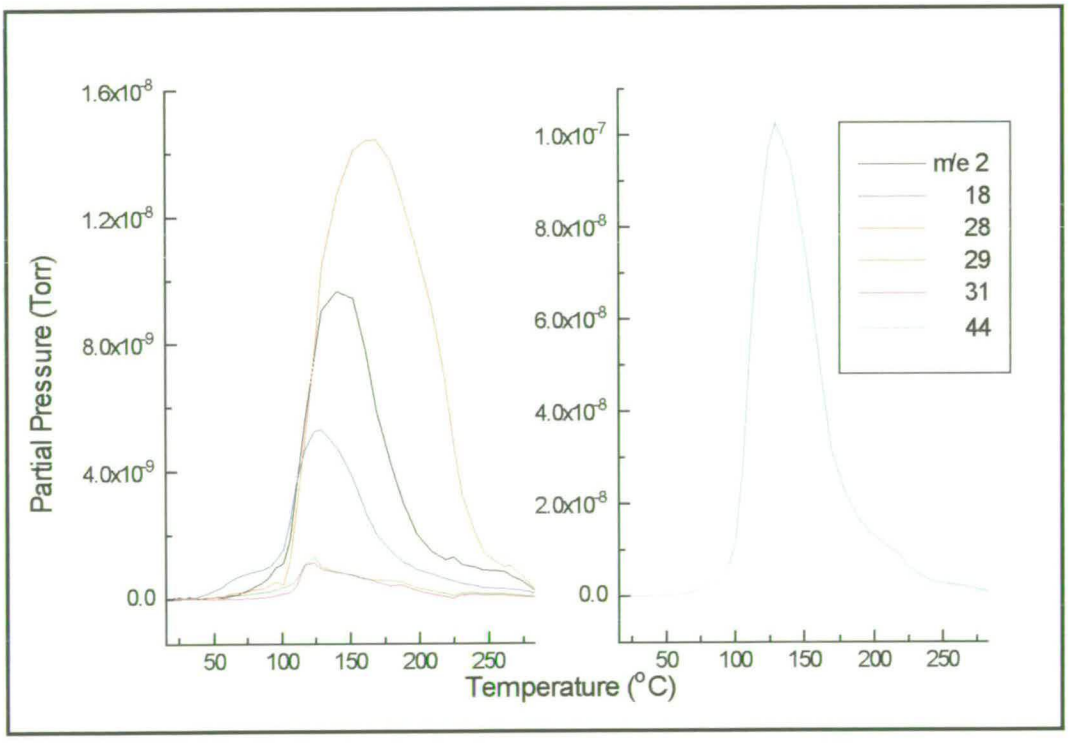

Fig. 6.20. *TPD following the adsorption of formic acid on the unpromoted catalyst.*

Fig 6.20 shows the evolution of a small amount of H_2O at low temperature, peaking at 75 °C. After this, H_2, H_2O, CO and CO_2 were seen to increase in pressure simultaneously. At this point, small amounts of formic acid and methanol were also seen. All of the species, and particularly CO, have very broad peaks, indicative of

formation over a wide temperature range. However, T_{max}s can be given as follows: methanol at 122 °C, formic acid at 124 °C, H_2O at 127 °C, CO_2 at 129 °C, H_2 at 140 °C, and CO at 161 °C. There is the possibility of a contribution at higher temperature to some of the traces, as suggested by an asymmetry to the CO trace at about 200 °C, and small shoulders in the H_2 and CO_2 traces at about 220 °C and to the CO trace at 250 °C. However, this cannot be said with certainty, and they could have been introduced spuriously by smoothing of noise in the original data. Table 6.13 summarises this information and gives the integrated peak area for each species.

Table 6.13. *Quantity of each species evolved during the TPD following formic adsorption on the unpromoted catalyst.*

Species Evolved	T_{max} (°C)	Area of Peak (a.u.)
H_2	140	17
H_2O	127	10
CO	161	32
HCOOH	124	2.4
CH_3OH	122	1.8
CO_2	129	150

Discussion

The bands found at the start of the TPD in the C-H stretching region at 2933 and 2885 cm^{-1} correspond to bidentate formate adsorbed on copper and zinc oxide respectively. The accompanying bands found at 2855 and 2962 cm^{-1} respectively for the two species can be noted on close inspection of the spectrum. Once the bands have started to decrease in intensity, that at 2933 cm^{-1} due to formate on copper decreases in intensity more quickly than the one at 2885 cm^{-1}. This is consistent with the literature discussed in the introduction to this chapter where it was shown that bidentate formate on copper decomposes at a lower temperature than that on zinc oxide [123]. Eventually, formate on copper disappears at 243 °C, while the main band

due to formate on the support remains until 271 °C (2875 cm^{-1}). Confusingly, the band at 1352 cm^{-1} which is also due to bidentate formate on copper was lost by 94 °C.

The loss of the band at 1352 cm^{-1} was accompanied by the disappearance of the band at 1376 cm^{-1}, also at 94 °C, which suggests it could be associated with copper. The behaviour of the intense band at 1640 cm^{-1} was such that intensity was lost first at the high frequency side so that it was positioned at 1620 cm^{-1} at 225 °C, which reflects the decrease with temperature of bidentate formate on copper. It was suggested in the discussion following the formic acid pulse experiment that the bands at 1640 and 1376 cm^{-1} could be due to a monodentate formate species, and their thermal behaviour certainly supports the suggestion of their being associated with copper. Complete loss of the band at 1620 cm^{-1} occurs by 275 °C, which is consistent with the species responsible for the band being associated with the support.

The other bands found at low frequency are difficult to follow with increasing temperature owing to the growing miscancellation features. The initial increase in intensity of the shoulder at 1386 cm^{-1} and improvement in clarity of the band at 1361 cm^{-1} (seen during the pulse experiment at 1367 cm^{-1}) suggest an increase in formate on zinc oxide, although a similar effect was not seen in the C-H stretching region. The increase can perhaps be attributed to the desorption of formic acid from the walls of the DRIFTS cell as it warmed up. The shoulder at 1386 cm^{-1} had disappeared by 202 °C but the other band was finally seen at 1364 cm^{-1} at 271 °C, in accordance with its accompanying bands at around 2900 cm^{-1}. A new feature was observed briefly at around 202 °C at 1346 cm^{-1}, and its origin is unclear - it was possibly associated with gas phase formic acid.

Infra-red results also show the presence of physisorbed CO_2 (an asymmetry in the atmospheric gaseous CO_2 band) from room temperature to 50 °C which results from the decomposition of bidentate formate on copper. Bands due to CO on copper - 2075 and 2135 cm^{-1} - and CO on zinc oxide - 2174 and 2199 cm^{-1} - also suggested the decomposition of formate (*via* CO_2 in the case of copper), and these left the

catalyst surface at a characteristically low temperature (90 °C). Formate decomposition continued at higher temperature, as indicated by the formation of gas phase CO (a doublet centred at 2143 cm^{-1}) from 90 °C. This doublet was observed until 291 °C, at which point no infra-red bands due to either formate species remained, suggesting their complete decomposition.

Gas phase species detected during the TPD by the mass spectrometer are more difficult to interpret than those for the methanol experiment. Fig. 6.20 shows that desorption peaks are broad, especially that for CO, which could suggest the contribution from a number of species.

The evolution of a small amount of H_2O at low temperature was seen, peaking at 75 °C, and this was probably simply due to the desorption of weakly bound molecular species from the catalyst surface. A shifting and narrowing of the broad infra-red band due to the O-H stretch from 3430 to 3490 cm^{-1} was seen between 25 and 116 °C which could correspond to the loss of a weakly bound species. The formation at low temperature (T_{max} = 123 °C) of formic acid coincided with the loss of infra-red features at 1105 and 1774 cm^{-1} which were attributed to formic acid monomers, and were completely removed from the surface by 173 °C. The simultaneous detection of desorbing methanol could possibly indicate that surface hydrogen from formate species are becoming mobile and hydrogenating other formates, possibly *via* formaldehyde, to methanol.

H_2, H_2O, CO and CO_2 were evolved in significant quantities from about 100 °C simultaneously, although they did not share common T_{max}s. It appears that CO_2 (T_{max} at 129 °C) was desorbed coincidentally with H_2 (T_{max} at 140 °C), although the latter probably also desorbed coincidentally with another species as indicated by its higher T_{max}. The decomposition of bidentate formate on copper is implicated as being responsible for these two species. An anomaly to this assignment is that the T_{max} expected as predicted by the literature is higher than that observed here [123] but not only that, the value obtained for bidentate formate decomposition following methanol

adsorption was also higher. The reason for this is unclear - perhaps the reaction is more facile because formate need not be formed from methoxy first, before it is decomposed, or perhaps formate is formed from methoxy on different sites from those it is adsorbed on following contact with formic acid. Indeed, Chauvin *et al.* [134] found that formate produced from the adsorption of formic acid on the copper component of a $Cu/ZnAl_2O_4$ catalyst disappeared by 130 °C, forming CO_2, H_2 and CO, while Clarke *et al.* [124] found that formate produced on the copper component of a Cu/SiO_2 following the adsorption of methanol decomposed at about 180 °C to CO_2 and H_2

CO was produced at the same time as the CO_2 and H_2 from copper-formate decomposition, and it is likely that these events are linked. The dissociation of CO_2 to CO and surface oxygen has already been shown to take place (Chapter 5), so this is one contender. Alternatively, the RWGS reaction could be occurring. This would also explain the coincident production of water with T_{max} at 127 °C, according to reaction 6.6. Another source of water at this temperature would be the simple desorption from the surface - the largest decrease in O-H stretching band intensity took place between 116 and 147 °C, which encompasses the mass spectrometer T_{max}.

$$HCOO \rightarrow \frac{1}{2}H_2 + CO_2 \leftrightarrow H_2O + CO \qquad \textit{reaction 6.6}$$

The large peak-width of the CO mass spectrometer trace has already been commented on, and it is likely that more than one contribution was involved - that discussed above, and at least one other. Formate on zinc oxide has been reported in the literature to decompose at around 300 °C [123] to form CO and H_2. The CO seen during this experiment could have been evolved from such a reaction, but it is not clear why T_{max} is so much lower (161 °C) than the literature value. It is anticipated that there are two likely reasons for this: first, as discussed in Chapter 4, difficulty was experienced in the measurement of the catalyst temperature, and it is possible that a systematic thermocouple error exists, and second, the value of 161 °C for T_{max} is an

average one, and is distorted by the formation of CO from CO_2 - T_{max} for formate decomposition may occur later (indeed, CO is still being produced in significant quantities up to 250 °C). Another confusing point, is that there appears to be very little H_2 accompanying CO formed at high temperature. This is thought to be a result of the decreased sensitivity of the mass spectrometer for H_2, as compared with, say CO.

The final uncertainty with this data is that the amount of CO_2 produced from supposed bidentate formate decomposition on copper is far in excess of CO produced from formate on zinc oxide, while the level of formate species on copper was always much lower than that on zinc oxide, as determined by infra-red spectroscopy. This reflects the uncertainties in the methanol adsorption experiments. Another possible source of CO_2 is the decomposition of formate on zinc oxide itself - CO_2 production has been reported in addition to CO production in the literature [130, 140, 144]. There are also other examples of supported zinc oxide where *only* CO_2 and H_2 are observed, as mentioned in the introduction to this chapter [9, 145].

To summarise the information gleaned from the TPD experiment, it has been shown that bidentate formate on copper is decomposed at a lower temperature than that on zinc oxide. The band at 1640 cm^{-1} decreased in intensity as the catalyst temperature was raised until the main band was found at 1620 cm^{-1} at 225 °C, suggesting a substantial loss in the species responsible for this band. The identity of this species is still uncertain, although its desorption temperature is similar to bidentate formate copper. Likewise, the band at 1376 cm^{-1} is also unassigned although it too desorbs in parallel with bidentate formate on copper. Thus, it seems possible that these bands could be due to some other formate species on copper, e.g. a monodentate formate. Mass spectrometer results are complex, but the decomposition of bidentate formate on copper (and possibly also zinc oxide) can be recognised by the simultaneous formation of CO_2 and H_2. CO was also observed by the mass spectrometer, and various sources were suggested for its production, including CO_2

dissociation, the RWGS reaction and, at a slightly higher temperature formate decomposition on zinc oxide.

6.3.2 - Promoted Catalyst

6.3.2.1 - Pulse Experiment

Results

Following the introduction of the first formic acid pulse to the promoted catalyst, as shown in Fig. 6.21, a main band was seen to form in the C-H stretching region at 2883 cm^{-1}, with an accompanying broad shoulder to the high frequency side, upon which a sharp feature was superimposed at 2961 cm^{-1}. Other intense features included a band at 1606 cm^{-1} and one at 1367 cm^{-1}. A prominent shoulder could be seen at 1322 cm^{-1}, as well as a broad feature centred at about 1038 cm^{-1}. Additionally, weak bands were seen at 2735 and 1460 cm^{-1}.

The main band at 2883 cm^{-1} was found to shift to 2878 cm^{-1} after the catalyst had been exposed to 40 Torr of formic acid and was again accompanied by a broad shoulder at 2961 cm^{-1}, although this time the additional sharp feature was absent. The intense bands at lower frequency were now seen at 1604 and 1360 cm^{-1} and were accompanied by a new shoulder at 1380 as well as that at 1322 cm^{-1}, which had become more pronounced. The broad band at 1038 cm^{-1} continued to grow, as did those at 2735 and 1460 cm^{-1}.

After a formic acid exposure of 60 Torr, all bands were seen to intensify, but it also seemed possible that an asymmetry to the high frequency side of the band at 1604 cm^{-1} was present. This was definite 80 Torr, and was positioned at 1635 cm^{-1}. At this point, all the other bands had continued to grow except those in the C-H stretching region. Other features which appeared to have rotational-fine structure also became

visible, centred at 1775 and 1105 cm^{-1}. After the 100 Torr, a small feature at 2940 cm^{-1} appeared.

After a formic acid exposure of 120 Torr, the broad shoulder at 2961 cm^{-1} seemed to be growing slightly relative to the main band at 2874 cm^{-1} which appeared to have reached saturation. There were contributions to the C-H region in the form of weak shoulders at 2940, 2902, 2933 and 2855 cm^{-1}. From 140 Torr, additional weak shoulders could be seen at 1718 and 1209 cm^{-1}. In the final spectrum, the main features included the band at 2874 cm^{-1} with a shoulder at 2855 cm^{-1} and its asymmetry to the high frequency side, over which features at 2972, 2940, 2902, and 2933 cm^{-1} were superimposed, the intense band at 1609 cm^{-1}, that at 1360 cm^{-1} with its shoulder at 1382 cm^{-1} and the broad band centred at about 1032 cm^{-1}. Weak features remained at 2734 and 1469 cm^{-1} with another at 1209 cm^{-1}.

A broad feature centred at 3450 cm^{-1} was seen throughout the pulse experiment, and, although the CO stretching region was largely obscured by noise, a weak band could be observed at 2175 cm^{-1} from the second pulse onwards.

Discussion

The presence of a formate species on zinc oxide is indicated by bands in the spectrum recorded following the first formic acid pulse - the main band in the C-H stretching region at 2883 cm^{-1}, an accompanying broad shoulder at 2961 cm^{-1} and intense bands at 1606 and 1367 cm^{-1} - and following the final pulse - 2874, 2961, 1609, 1360 and 1380 cm^{-1}. The shoulders attributed to bidentate formate on copper for the unpromoted sample in the C-H stretching region were not immediately present for the promoted sample, but very weak shoulders at 2933 and 2855 cm^{-1} were observed after a formic acid exposure of 120 Torr. An accompanying band at 1352 cm^{-1} was not observed but this was found to be weak for the unpromoted sample.

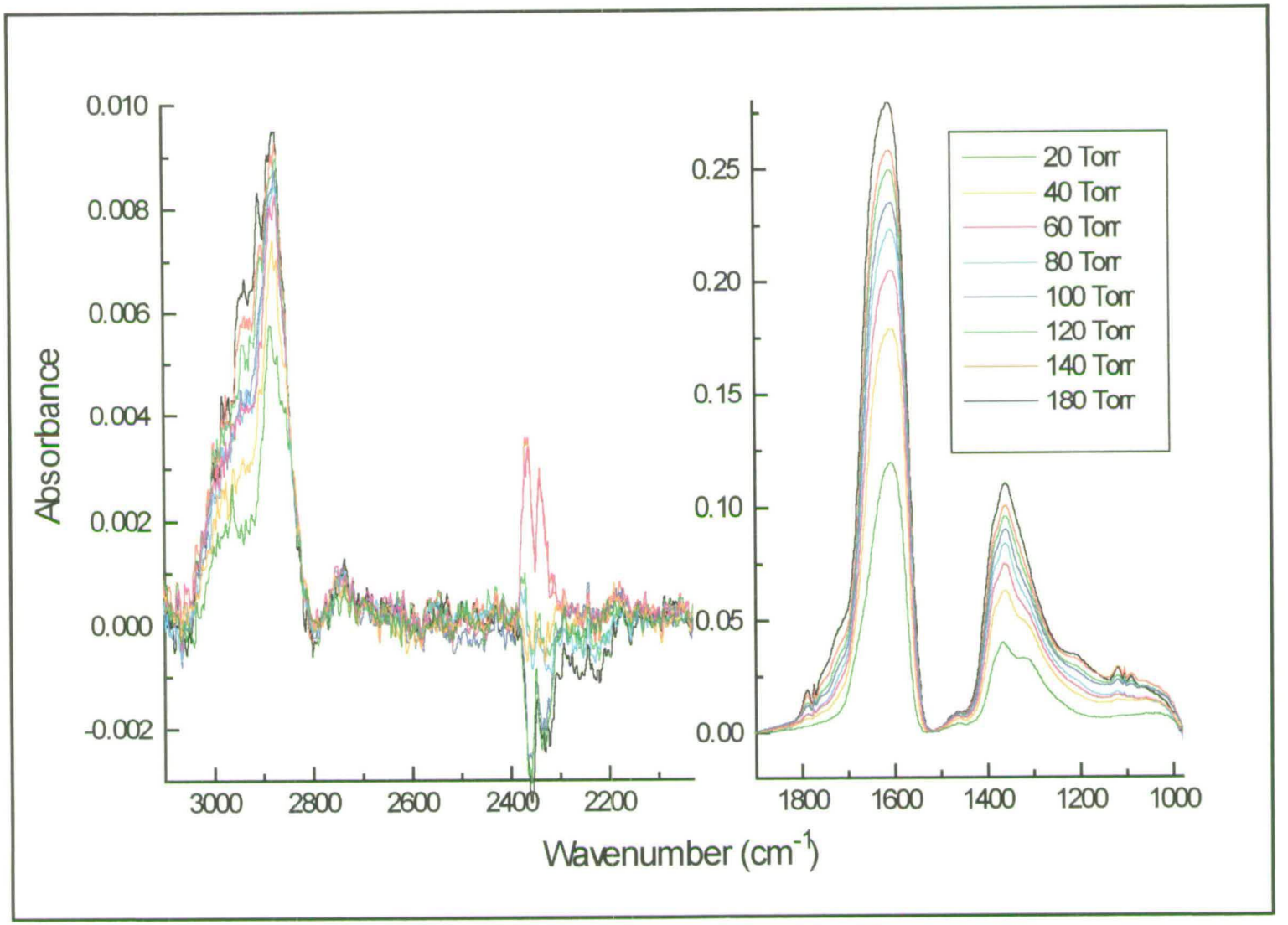

Fig. 6.21. *Formic acid pulse experiment for the 1% K promoted catalyst. Total formic acid exposure = 180 Torr.*

It is clear, however, that the amount of bidentate formate on copper has been significantly decreased relative to that on the unpromoted sample, and to a much greater extent than the corresponding species on the support. This result is once again reminiscent of that in Chapter 5, where promotion of the catalyst resulted in a decreased uptake of CO on copper owing to a proposed site blocking mechanism of the alkali. A similar effect was also seen for the methoxy species on copper.

Other similarities between the spectra for the unpromoted and promoted samples include the presence of a shoulder at 1322 cm^{-1} and a broad band at 1038 cm^{-1}, which are thought to be possibly accompanied by another which is obscured, at 1590 cm^{-1}. These are due to the interaction of CO_2 with zinc oxide or the alkali promoter to form a bidentate carbonate or a potassium ion-associated carbonate or carboxylate, respectively. The CO_2 was either produced from the decomposition of formate on copper, or from the oxidation of CO which had been produced by the decomposition of formate on zinc oxide. However, the bands are already evident after an exposure of 20 Torr of formic acid for the promoted sample, whereas they did not appear until a total exposure of 100 Torr for the unpromoted sample.

A band at 2175 cm^{-1}, which was seen for the unpromoted sample, was seen in the second spectrum and is suggested as being due to CO adsorbed on zinc oxide, giving evidence for the decomposition of formate species on zinc oxide. No adsorbed CO_2 on copper was seen at any stage during the experiment, probably as a result of the low level of formate on copper, or an increased rate of dissociation of CO_2 to CO over the promoted copper, as suggested in Chapter 5. On the unpromoted sample, evidence was found for higher concentrations of adsorbed decomposition products: adsorbed CO_2 on copper, and CO on copper and zinc oxide. Therefore, it appears that, as in the case of methanol adsorption, decomposition products remain adsorbed where they were formed on the unpromoted catalyst, but on promotion, they preferentially desorb at room temperature or go on to form a carbonate/carboxylate species on the support. This species could be formed as a result of stabilisation by the alkali ion.

Other minor differences found on promotion include the appearance of the feature at 2940 cm^{-1} accompanying those at 1775 and 1105 cm^{-1} after the third pulse, which were both seen for the unpromoted sample. This new band can also be attributed to gaseous formic acid monomers, according to Table 6.8. The higher level of all these bands on promotion could be explained by less species being adsorbed on the sample owing to its lower total surface area. New, weak features are also observed from the seventh pulse onwards at 1718 and 1209 cm^{-1}. The first band has been observed previously on potassium promoted silica [147] and assigned to formic acid physisorbed on "potassium". Alternatively, a band at 1733 cm^{-1} has previously been assigned to condensed formic acid on copper (Table 6.8). The band at 1209 cm^{-1} could be due to a formic acid dimer, again by comparison with the values in Table 6.8. Likewise, the band at 1460 cm^{-1}, which was seen for the unpromoted catalyst, can also be attributed to formic acid dimers. The feature at 2735 cm^{-1} is once again assumed as being due to condensed formic acid on copper. From this information it seems that, overall, more formic acid is physisorbed on or weakly associated with the promoted catalyst as compared with the unpromoted.

The most noticeable effect on promotion of the catalyst can be seen on inspection of the spectrum following the second pulse. Whereas for the unpromoted sample the intense band at 1609 cm^{-1} had shifted to 1632 cm^{-1} by the second pulse and a sharp feature at 1374 cm^{-1} had appeared, neither of these events were seen for the promoted. In later spectra for the promoted catalyst, there was an asymmetry to the band at 1609 cm^{-1} at about 1630 cm^{-1}, but the band at 1374 cm^{-1} was never seen. It is clear that the alkali promoter has had some effect to decrease the intensity of the higher frequency band and prevent the formation of the other altogether. There was confusion over the assignment of both of these bands for the unpromoted sample, but their sharp attenuation on promotion does suggest that they could be assignable to an species adsorbed on copper, such as monodentate formate. It was also suggested that the band seen for the unpromoted sample at 1640 cm^{-1} could be due to adsorbed water. In line with the decrease of this band on promotion, there is an attenuation of the broad band in the O-H stretching region of the spectrum (centred at 3450 cm^{-1}) to

about 10 % of the band intensity of the unpromoted sample. Therefore, it is also possible that the promoter prevents the adsorption of water or encourages its dissociation over promoted copper - certainly, surface science studies on caesium-promoted copper single crystals have suggested that the rate of the WGS reaction is enhanced by the acceleration of water dissociation [150]. However, this theory does not account for the absence of the band at 1374 cm^{-1}.

In summary, formate on zinc oxide was seen on the surface of the promoted catalyst at a lower level than for the unpromoted sample. The effect of promotion on formate bands associated with copper was more severe - only a small amount was found, as indicated by weak shoulders in the C-H stretching region after 120 Torr of formic acid had been passed over the catalyst. Clearly, the effect of the promoter goes further than a decrease in copper surface area, which was only about 40 % less than the unpromoted sample. The formation of carbonate-type species occurred earlier on in the pulse experiment than for the unpromoted catalyst. This formation immediately the formic acid was in contact with the catalyst, along with a lower concentration of adsorbed CO_2 and CO as compared with the unpromoted sample could be explained if potassium's presence destabilised the adsorbed CO_2 and CO, encouraging their desorption. They would then be available to go on to form carbonate-type species on the support, which are possibly associated with potassium. Promotion was also found to decrease the band at 1640 cm^{-1} in intensity relative to the unpromoted sample.

6.3.2.2 - Temperature Programmed Desorption

Results

The spectra collected during the TPD are shown in Figs. 6.22 - 6.24. Bands in the C-H stretching region at the start of heating (main band at 2874 cm^{-1} with an asymmetry to the high frequency side) decreased in size gradually with temperature, but first from the high frequency side (Fig. 6.22). At 206 °C only the band at

2868 cm^{-1} remained, and this was no longer seen at 233 °C. The broad band at 3450 cm^{-1} shifted to 3560 cm^{-1} with increasing temperature and gradually decreased in intensity until it was no longer visible at 206 °C.

Considering the bands at lower frequency (Fig. 6.24, not baseline corrected), that at 1609 cm^{-1} appeared to initially grow in intensity from 56 to 122 °C, before then narrowing first at the low frequency side such that between 122 and 152 °C it was positioned at 1620 cm^{-1}, and then returning to 1609 cm^{-1} where it remained until finally disappearing at 275 °C.

The other bands seen at low frequency maintained their intensity until 122 °C, whereupon a general decrease was seen leaving only the band at 1323 cm^{-1} unchanged. At 152 °C the baseline had begun to slope severely but it was possible that features existed at 1310 and 1347 cm^{-1}, with a shoulder at 1383 cm^{-1}. All features had disappeared by 206 °C, but again the sloping baseline made it difficult to be certain, which was true for the broad band between 1040 and 1030 cm^{-1}.

Bands at 1105 and 1775 cm^{-1} with rotational-fine structure started to form at 26 °C, reaching a maximum at 74 °C before finally disappearing at 152 °C.

Finally, little of interest occurred in the 2500 - 2000 cm^{-1} region (Fig. 6.23) - only the doublet due to gas phase CO_2 was seen.

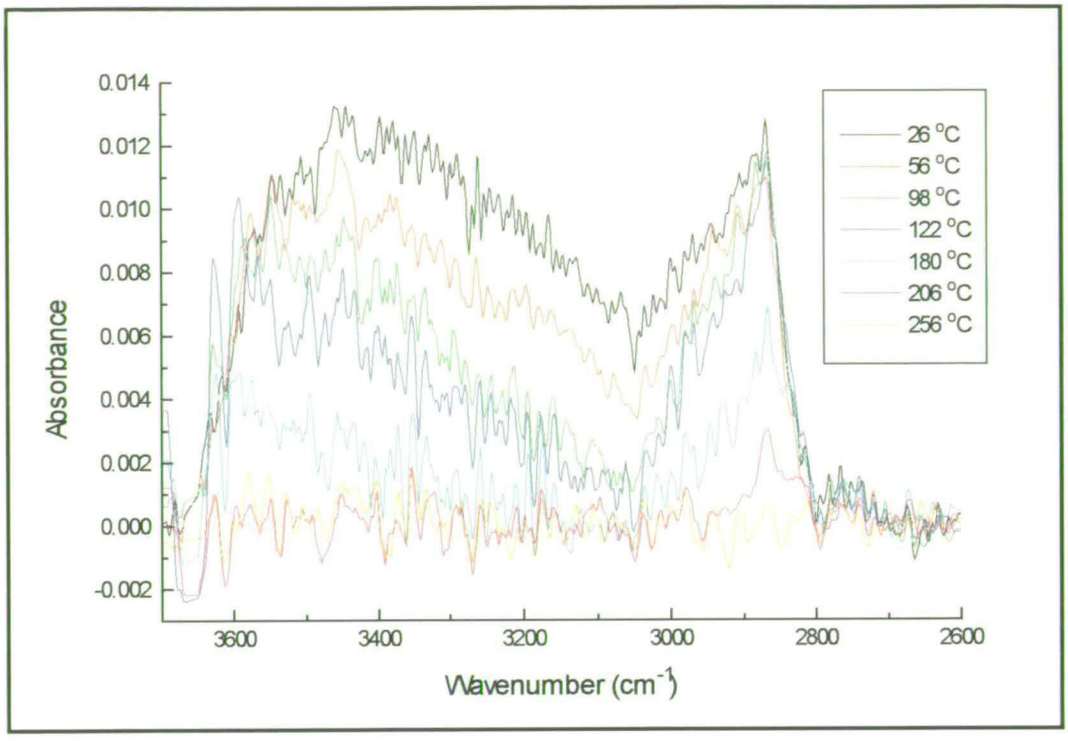

Fig. 6.22. *Temperature programmed desorption following formic acid pulse experiment for the 1% K promoted catalyst in the 3700 - 2600 cm^{-1} region*

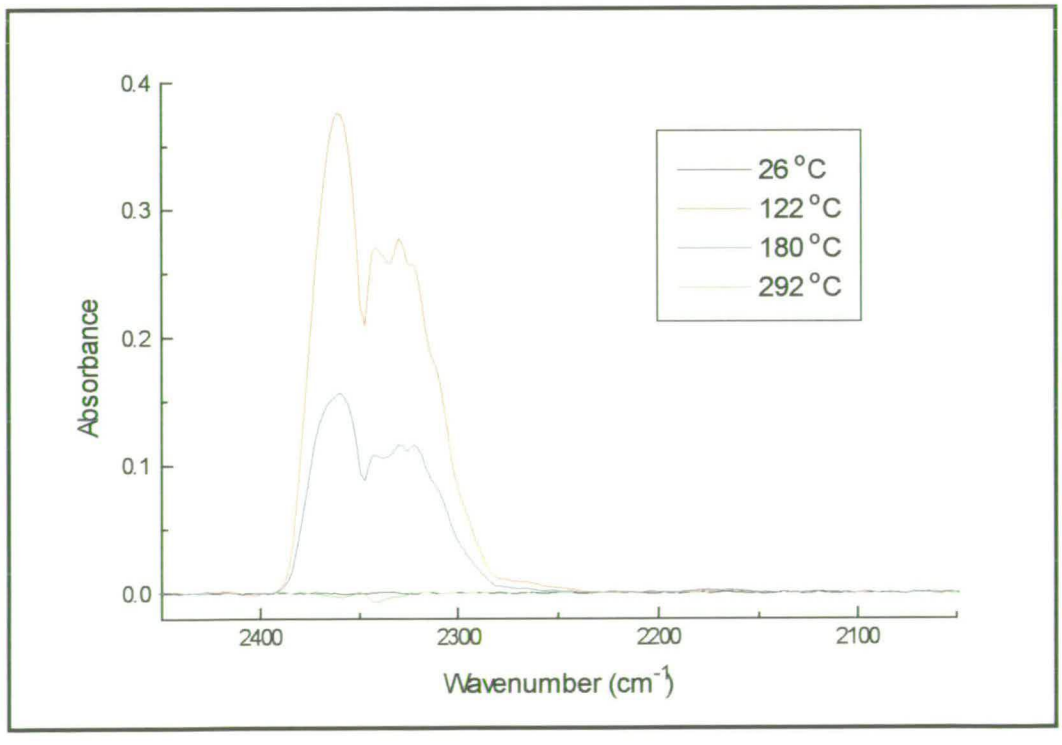

Fig. 6.23. *Temperature programmed desorption following formic acid pulse experiment for the 1% K promoted catalyst in the 2500 - 2000 cm^{-1} region*

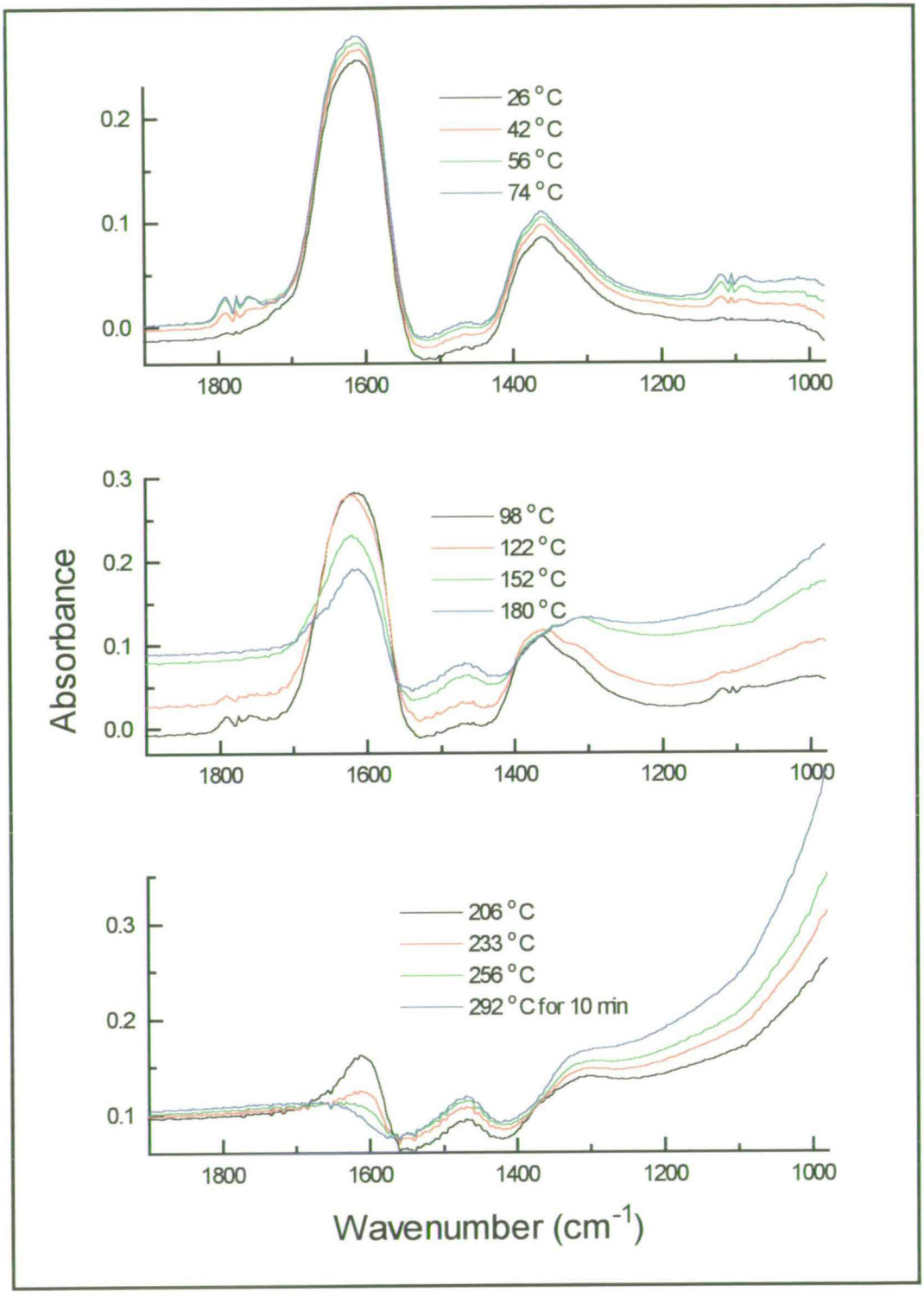

Fig. 6.24. *TPD following formic acid adsorption on 1% K promoted catalyst for the 1900 - 1000 cm^{-1} region (not baseline corrected).*

The mass spectrometer results show the species desorbed from the catalyst surface in Fig. 6.25 (refer to Table 6.12 for an explanation of the assignment of *m/e* values to gas phase molecules). Once again, since inspection of Fig. 6.25 shows that only a small amount of *m/e* 29 (HCO^+) was detected during the TPD experiment for the promoted catalyst, the other species have not been corrected for the contribution from the fragmentation of formic acid, and are assumed as being real "reaction" products. The evolution of a small amount of H_2O was seen at low temperature, as was the case for the unpromoted sample, peaking at 76 °C. It also appears that a small amount of CO was desorbed at low temperature. At fairly low temperature, H_2, H_2O, CO and CO_2 were seen to increase in pressure simultaneously, while small amounts of formic acid and methanol were also detected. As for the unpromoted sample, all of the species, and particularly CO, have very broad peaks, indicative of formation over a wide temperature range. However, T_{max}s of the desorption peaks can be given as follows: CH_3OH at 127 °C, HCOOH at 120 °C, H_2O at 123 °C, CO_2 at 123 °C, H_2 at 134 °C, and CO at 143 °C. As for the unpromoted sample, there is the possibility of a contribution at higher temperature to some of the traces, as suggested by an asymmetry to the CO trace at about 200 °C, and shoulders in the H_2 and CO traces at about 250 °C. Table 6.14 summarises this information and gives the integrated peak area for each species.

Table 6.14. *Quantity of each species evolved during the TPD following formic adsorption on the 1% K promoted catalyst.*

Species Evolved	T_{max} (°C)	Area of Peak (a.u.)
H_2	134	19
H_2O	123	6.4
CO	143	22
HCOOH	120	2.3
CH_3OH	127	1.4
CO_2	123	110

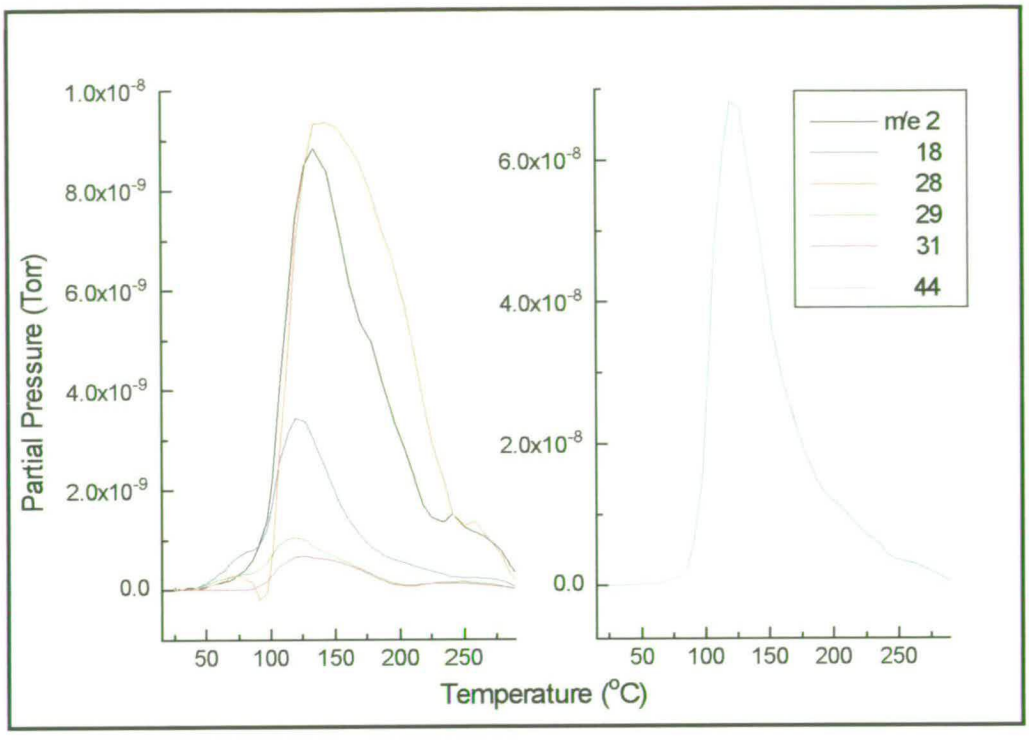

Fig. 6.25. *TPD following formic acid adsorption on 1% K promoted catalyst.*

Discussion

A gradual decrease in intensity was seen in the C-H stretching region of the infra-red spectra such that only the band at 2868 cm^{-1} remained at 206 °C, and even this was no longer present at 233 °C. These events occur about 40 °C lower than for the corresponding unpromoted experiment, which could point to the destabilisation of the formate species on zinc oxide in the presence of potassium.

The band at 1609 cm^{-1} appeared to grow in intensity before starting to decrease from 122 °C, and this behaviour can be attributed to the desorption of formic acid from the walls of the DRIFTS cell. Surprisingly, a shift took place to 1620 cm^{-1} until 152 °C, where it returned to 1609 cm^{-1}, and the reason behind this behaviour is unclear. If the feature at the high frequency side (around 1640 cm^{-1} in the case of the unpromoted sample) was due to water, it is possible that water was being formed, e.g. by the RWGS reaction - certainly, it was seen from the mass spectrometer results that

T_{max} for CO_2 and H_2 occurred between 122 and 152 °C. The final temperature of observation for this band on the promoted sample is at 275 °C - identical to that for the unpromoted sample.

Bands at 1105 and 1775 cm^{-1} which possessed rotational-fine structure and were seen at a maximum at 74 °C can be attributed to gaseous formic acid monomers. This increase with temperature could either be explained by the desorption of formic acid from the walls of the DRIFTS cell, or the release into the gas phase of weakly physisorbed formic acid dimers.

Bands in the low frequency region of the spectrum are once again difficult to follow with increasing temperature owing to the growing miscancellation features and sloping baseline. However, once again it appears that features are lost at a lower temperature than for the unpromoted sample - at 202 °C for those attributed to formate on zinc oxide. At 152 °C, features seen at 1347 and 1310 cm^{-1} are difficult to assign, and it is possible that their existence could be an artefact of the sloping baseline.

The mass spectrometer results show the formation of water at low temperature, peaking at 76 °C, again being indicative simply of desorption from the sample. A slight shift in the broad band at 3450 cm^{-1} due to the O-H stretching frequency occurred in coincidence with this between 26 and 98 °C. Formic acid and methanol desorption was detected with T_{max}s at 120 and 127 °C, respectively. The amount of each species is shown in Table 6.14, and on comparison with Table 6.13 it is evident that similar amounts were evolved, in spite of the lower total surface area of the promoted catalyst. This result reflects that found for methanol, where it was suggested that the methoxy species must be more weakly bound in the presence of the promoter, such that it desorbed intact at a lower temperature rather than remaining on the surface and being decomposed at high temperature. In the case of formic acid, bands due to gaseous monomers and dimers of formic acid were certainly more prevalent during the TPD for the promoted sample, in agreement with this.

H_2, H_2O, CO and CO_2 were, as for the unpromoted catalyst, evolved from around 100 °C simultaneously at an appreciable rate. It appeared again that CO_2 (T_{max} at 123 °C) was desorbed coincidentally with H_2 (T_{max} at 134 °C), with a possible additional contribution for H_2 as indicated by its higher T_{max}, and a similar result was seen for the unpromoted catalyst. The two species are again thought to be due to bidentate formate decomposition on copper but their desorption temperatures are slightly lower than for the unpromoted sample, suggesting the formate species has been destabilised by promotion. Surprisingly, though, by comparing Table 6.14 with Table 6.13 for the unpromoted catalyst, the amount of CO_2 evolved from the promoted catalyst is about 75 % of that from the unpromoted. This result is unexpected, considering that copper formate features were only weakly seen in the infra-red spectra. Thus, this result could be seen as evidence for the contribution from formate on zinc oxide to the CO_2 produced.

For the promoted sample, CO was seen to be desorbed with T_{max} at 143 °C. Comparing this with the value of 161 °C for the unpromoted catalyst, it has been shifted to a lower temperature and this is consistent with the infra-red result, where bands due to formate on both copper and zinc oxide were lost at a lower temperature on promotion.

Water was also seen to be evolved with a T_{max} at 123 °C (compared with 127 °C for the unpromoted) and it is possible that this, along with a contribution in the CO trace at this temperature, is due to the RWGS reaction. On expressing the amount of CO and H_2O for the promoted catalyst as a percentage of that for the unpromoted, values of 64% and 68% are found - this could reflect a surface area decrease on promotion, but it is hard to draw conclusions from this since several reactions could be occurring at this point.

Ultimately, it must be concluded that while suggestions can be made as to the effect of the alkali promoter on formic acid adsorption and formate decomposition, the situation is clearly complex and there may be many reaction pathways occurring

simultaneously. From this discussion it is evident that the main difference in the infra-red data on promotion is an apparent decrease in the temperature to which formate species on both copper and zinc oxide remain, while the mass spectrometer has indicated a decrease in T_{max} for CO_2, CO and H_2 in agreement with this. Approximately the same amount of formic acid and methanol was produced in the presence of the promoter, in spite of a decrease in total surface area, so overall it seems that formate species on the promoted catalyst desorb intact at relatively low temperatures, while on the unpromoted sample the formate is bound more strongly, and therefore remains adsorbed to become decomposed at a higher temperature.

6.3.3 - Summary of the Effect of Promotion on Formic Acid Adsorption

The range of reactions suggested to be occurring following formic acid adsorption with the effect of promotion on them is illustrated in Fig. 6.26 (pulse experiment at room temperature) and Fig. 6.27 (TPD). Species not actually observed are given in brackets.

During the pulse experiment (Fig. 6.26), the promoter had following impact:

- step (14) was encouraged while step (15) was decreased greatly. Step (18) was also decreased but to a lesser degree.
- step (20) (and possibly also (17)) was encouraged, possibly first *via* the desorption of adsorbed CO. In the case of the promoted catalyst, a potassium-associated carboxylate or carbonate might take the place of the bidentate carbonate shown.

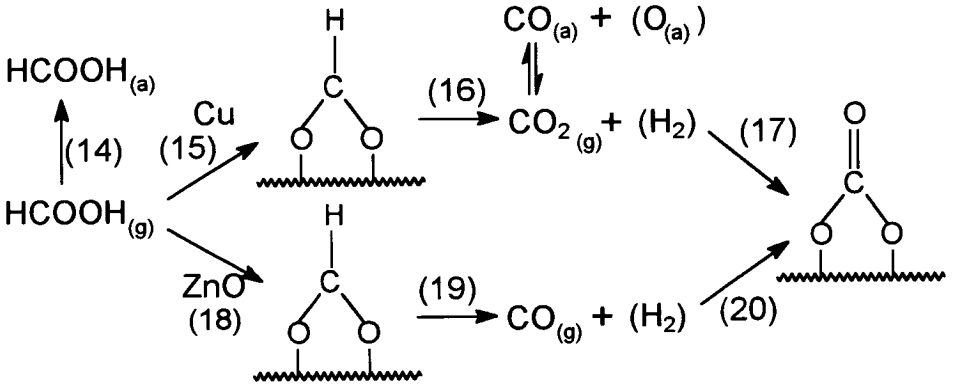

Fig. 6.26. *Proposed steps during the formic acid pulse experiments*

During the TPD (Fig. 6.27), the promoter had the following impact:

- steps (21) and (22) were unchanged, in spite of the lower surface area on promotion.
- steps (23) and (25) occurred at a slightly lower temperature, but whether a change in the reaction probability occurred is difficult to determine owing to the likelihood of several reactions occurring simultaneously.

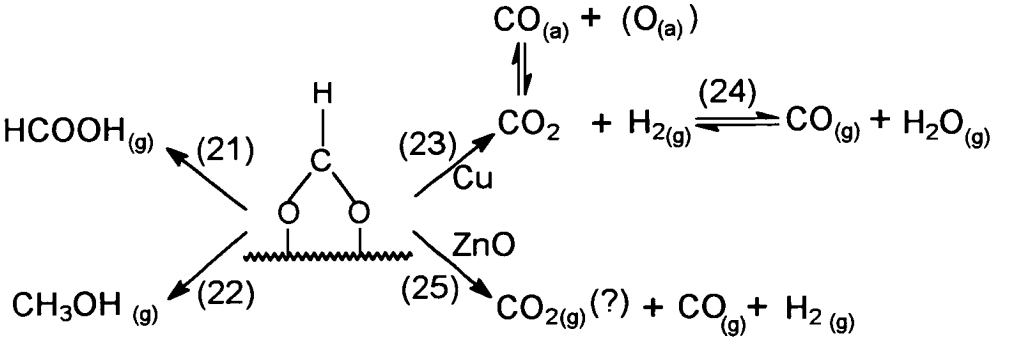

Fig. 6.27. *Proposed steps during the TPD following formic acid adsorption*

6.4 - Overall Effect of the Promoter on Methanol and Formic Acid Adsorption

A complicated picture has been built up during this chapter as to the effect of promotion on oxygenate adsorption. Moreover, it has been demonstrated that the interpretation of results even in the *absence* of the promoter is complex. Overlapping bands, especially in the C-H stretching region, have made it difficult to identify adsorbates. Difficulty was also encountered when analysing the mass spectrometer results from the formic acid TPD experiment, where it was suggested that the RWGS reaction might be in operation, thus leading to an even more confusing situation. Nevertheless, several species have been identified during the decomposition of both methanol and formic acid which correspond well with results in the literature. For instance, Clarke *et al.* [124] have summarised their findings for methanol decomposition on Cu/SiO_2, and their proposed reaction scheme is reproduced in Fig. 6.28.

Firm evidence has been seen during this study for the presence of methoxy on copper and bidentate formate on copper and on zinc oxide. The decomposition fragments of bidentate formate on copper (CO_2 and H_2) and zinc oxide (CO and H_2 and possibly also CO_2) have been identified during TPD in the gas phase, but also at room temperature on the surface in the form of CO_2 adsorbed on copper, CO adsorbed on copper and zinc oxide and carbonates from the interaction of CO_2 with the support. However, no evidence has also been found for formaldehyde and methylenebis(oxy) groups ($CH_2(O)_2$) on copper.

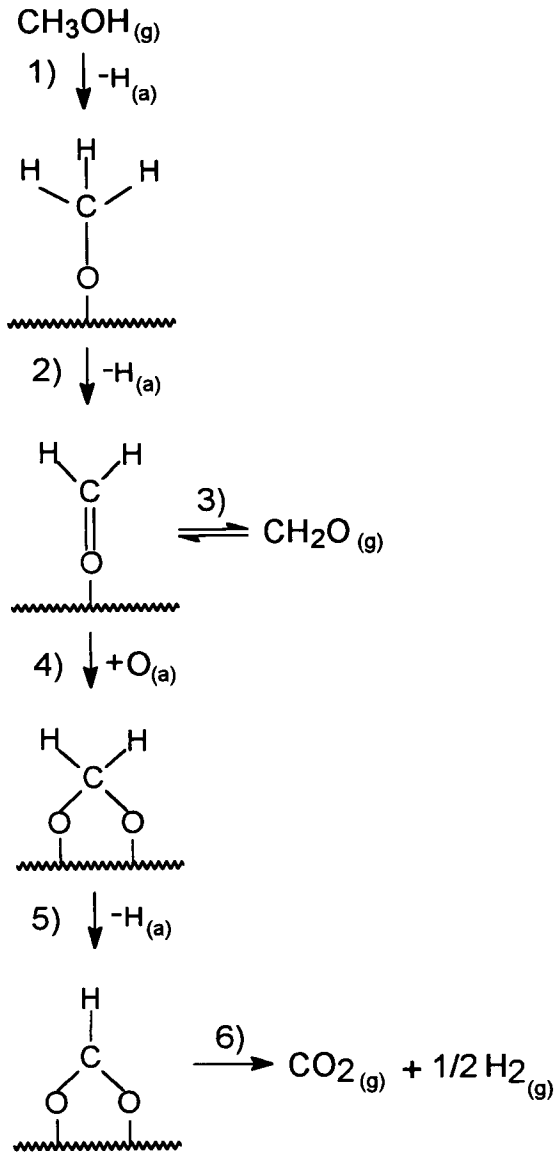

Fig. 6.28. *Decomposition of methanol on the copper component of Cu/SiO_2 [124]*

To briefly summarise the effects of the alkali promoter which have been elucidated for the two adsorbates:

1) *for methanol* - the formation of methoxy species on copper was hindered (possibly as a result of the copper component being better reduced). Adsorbed CO and CO_2 from the decomposition of methoxy at room temperature (possibly *via* a formate species) were not observed on promotion, but more gas phase CO was seen, suggesting a destabilisation of adsorbed species. There was less decomposition of methoxy overall during TPD, and more desorption of the molecule intact, on alkali promotion.
2) *for formic acid* - the promoter again hindered the formation of bidentate formate on copper. A lower concentration of formate decomposition products was seen (adsorbed CO and CO_2) but carbonate-type species were formed at a lower exposure of formic acid than the unpromoted catalyst. This could have been as a result of decomposition products (CO and CO_2) desorbing then interacting further with the support. The desorption intact of formic acid at slightly lower temperatures in the presence of the promoter and in quantities comparable with the unpromoted sample despite its lower surface area suggests that, as for the case of methoxy, formate was bound less strongly.

On looking at the mechanism in Fig. 6.28, it can be envisaged that under reaction conditions (i.e. at high temperature) the alkali has the effect of discouraging step (1) from taking place following methanol adsorption as methoxy, by encouraging desorption, while the formate species is discouraged from taking the step (6) pathway, by again being preferentially desorbed. This idea has more meaning in the context of methanol synthesis when considering the reverse process - by the concept of microscopic reversibility, it is envisaged that after step(-6) had occurred, the formate would desorb as formic acid and thus step (-5) would not take place.

Chapter 7 - The Effect of Alkali Promotion on the Temperature Programmed Reaction of a CO_2/H_2 Mixture

7.1 - Introduction

In order to elucidate the effect of an alkali promoter on the methanol selectivity of a water-gas shift catalyst, both the mechanism of the methanol synthesis and low temperature water-gas shift reactions need to be considered. Neither of these systems is completely understood, and in addition it is known [81] that the WGS reaction plays an important mechanistic role in methanol synthesis, thus complicating matters further.

It is generally accepted [123] that the methanol synthesis reaction takes place *via* a formate intermediate on copper, as previously discussed in Chapter 6. It has also been established that in a $CO/CO_2/H_2$ mixture the CO_2 is the source of carbon in the methanol synthesised [80]. CO in the gas mixture is thought to retard the RWGS and enhance the maximum rate of methanol synthesis by encouraging the WGS reaction [131]. Copper has been shown to be the active component for methanol formation [61, 152, 153] . The role of surface oxygen in the methanol synthesis has also been discussed, with most authors concluding that this species plays an important part in the mechanism [81, 134, 154].

The situation for the WGS reaction is far less clear, with much argument surrounding the mechanism [94]. Some authors suggest an associative mechanism taking place, again, *via* a formate intermediate (reaction 7.1) while others suggest a

redox mechanism in which the surface is constantly regenerated by the reactants (reaction 7.2).

$$CO + H_2O \rightarrow (\text{intermediate}) \rightarrow CO_2 + H_2 \qquad \textit{reaction 7.1}$$

$$H_2O + Red \rightarrow H_2 + Ox$$
$$CO + Ox \rightarrow CO_2 + Red \qquad \textit{reaction 7.2}$$

These disagreements arise, in part, owing to the large variation in experimental conditions between studies and also because of the variety of different catalysts under study, from single crystals to real industrial catalysts. Nevertheless, some investigations have found a good parallel between the kinetics seen on both Cu(111) [155] and Cu(110) [93, 155] single crystals and Cu/ZnO catalysts for the WGS reaction.

Both reactions have been studied with respect to alkali promotion. The WGS reaction has been found to be strongly accelerated over copper single crystals in the presence of a caesium metal promoter (30, 150, 156, 157) and supported catalysts in the presence of alkali salts [151, 158]. Single crystal studies have shown that the promoter causes an acceleration in water dissociation on the surface [30].

The situation for the impact of alkali promoters on methanol synthesis is more complicated. The rate of methanol synthesis from CO/H_2 is found to increase on promotion while conversely, CO_2/H_2 mixtures produce more methanol over unpromoted catalysts [59, 159-161]. Lui *et al.* [162] have explained this by showing that CO and CO_2 are converted to methanol on different catalytic sites.

Clarke and Bell [151] have investigated the synthesis of methanol from $H_2/CO_2/Ar$ and $H_2/CO_2/CO/Ar$ mixtures over a potassium-promoted Cu/SiO_2 catalyst, using transmission infra-red spectroscopy and temperature programmed reaction (TPR) experiments. They found that promotion had the effect of enhancing the

RWGS reaction, while suppressing methanol synthesis. Accordingly, an associative-type of mechanism was proposed for the RWGS reaction on the basis of an enhanced level of formate being detected on promotion. The intention of the work in this chapter was to simulate some of the experiments carried out by Clarke and Bell using DRIFTS and the $Cu/ZnO/Al_2O_3$ catalyst, which is more closely related to those used in industry than the model Cu/SiO_2 sample in their study. In addition, it was anticipated that this work would compliment the pulse experiments discussed so far.

A CO_2/H_2 mixture was chosen so that the RWGS reaction could be investigated, while also encouraging methanol synthesis, as suggested by Clarke and Bell by using a ratio of 3:1 H_2:CO_2 according to reaction 7.3.

$$3H_2 + CO_2 \rightarrow CH_3OH + H_2O \qquad \textit{reaction 7.3}$$

7.2 - Experimental Procedure

The experimental set-up has been described for the TPR experiment in Chapter 2 and was represented schematically in Fig. 2.5. Subsequent to pre-treatment, a CO_2/H_2 mixture with flowrates in an approximately 1:3 ratio (1:3.4 for the unpromoted catalyst and 1:3.6 for the 1% K promoted catalyst) was passed over the sample at 30 cm^3/min. After an isothermal period of 40 min at room temperature (25 ± 3 °C), a temperature ramp of +10 °C/min from room temperature to 100 °C then +1.6 °C/min to 300 °C was applied while the gas mixture was flowing continuously (shown in Fig. 7.1). A more gentle ramp was chosen from 100 °C to resolve better the more interesting effects which were anticipated from there.

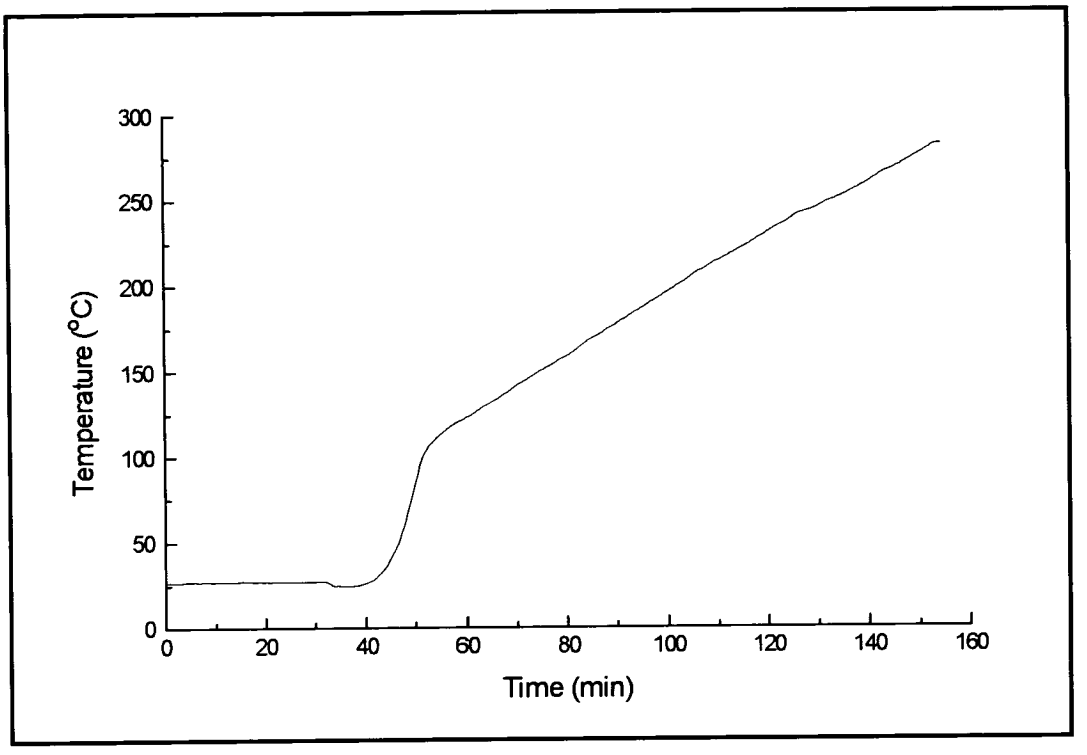

Fig. 7.1. *Temperature ramp for the TPR experiments.*

While the TPR experiment was being carried out, adsorbed species were detected by scanning infra-red spectra continuously in "kinetics" mode, as discussed in Chapter 2. A time resolution of 10 s was chosen (as in the TPD experiments) which corresponds to collecting spectra for 10 s periods and averaging these as one "scanset". During the first 5 minutes of 1% K catalyst's experiment, however, 5 s time resolution was used for better clarity, and as expected this produced spectra with a lower signal to noise ratio. Throughout the experiments, data was collected in parallel on the mass spectrometer, allowing gas phase species to be detected. Events will be quoted as a function of time during the isothermal period and thereafter as a function of temperature.

7.3 - Unpromoted Catalyst

Results

Infra-red bands in the region below 1700 cm^{-1} at 1653, 1424, 1309, 1227 and 1044 cm^{-1} were observed from 9 s after the CO_2/H_2 mixture was introduced into the DRIFTS cell, and while the sample was still at room temperature (25 °C). Fig. 7.2, showing spectra extracted from the kinetics file, illustrates the development of these species during the course of the experiment. The following changes can be observed: the sharp band at 1227 cm^{-1} intensified until about 3 min when a new shoulder at 1471 cm^{-1} formed. At this point, the peak at 1227 cm^{-1} started to diminish very gradually in intensity and continued to do so for the remainder of the experiment until it disappeared altogether. The other features, at 1653, 1424, 1309, 1100 and 1044 cm^{-1} grew in intensity until about 15 minutes, at which point they remained approximately the same height until 43 °C, when they decreased slowly in intensity. By 60 °C, miscancellation features grew in at 1500 and 1450 cm^{-1} and genuine peaks were obscured. At this point it seemed clear that the shoulder at 1471 cm^{-1} was a miscancellation feature.

Another feature observed in this region of the spectrum was that at 1215 cm^{-1}, which can also be seen in Fig. 7.2. This band grew in at 51 °C, and also remained until a temperature of 98 °C.

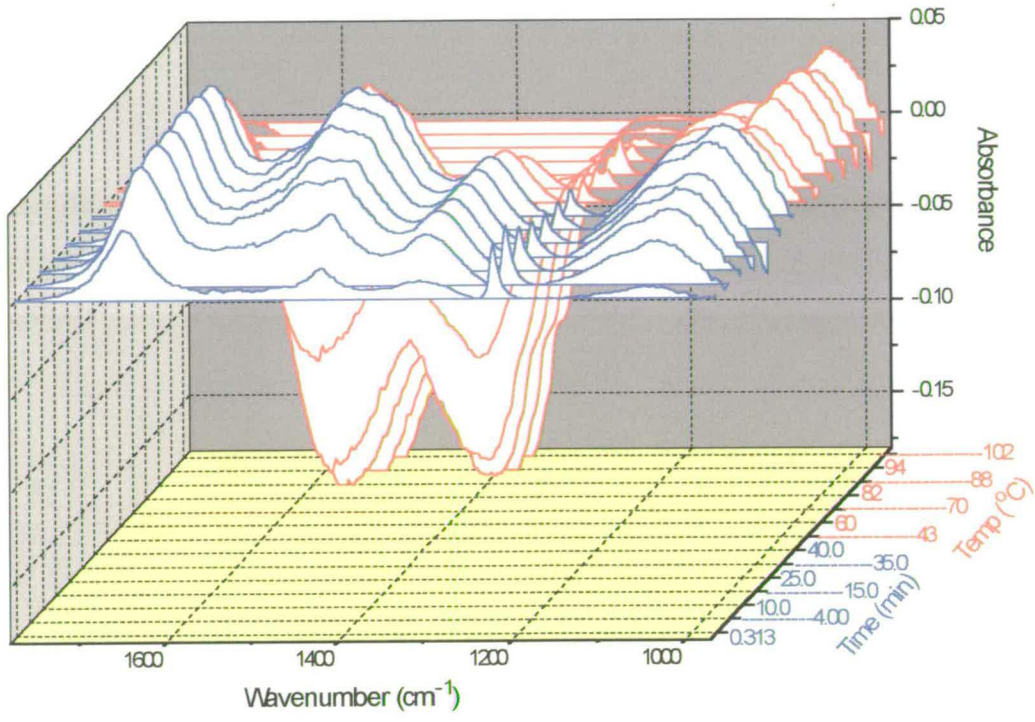

Fig. 7.2. *Extracted spectra showing development of the species in the region below 1700 cm^{-1} for the unpromoted catalyst.*

In order to gain more information on this region, a functional group chromatogram for the band at 1227 cm^{-1} was constructed, as shown in Fig. 7.3 as a function of time during the isothermal period at room temperature, and then as a function of temperature once the temperature ramp had commenced. This band was chosen because it was the sharpest and because it was deemed more reliable than those in the miscancellation area between 1400 and 1550 cm^{-1}. Thus, it is reiterated that there was an immediate gradual decrease in intensity of this band at room temperature, and then, as the temperature was raised, the remaining intensity decreased at a maximum rate at 76 °C, ceasing to exist altogether at 107 °C.

A functional group chromatogram for the band at 1215 cm^{-1} was also constructed (Fig. 7.4) showing that it reached a maximum intensity at 60 °C.

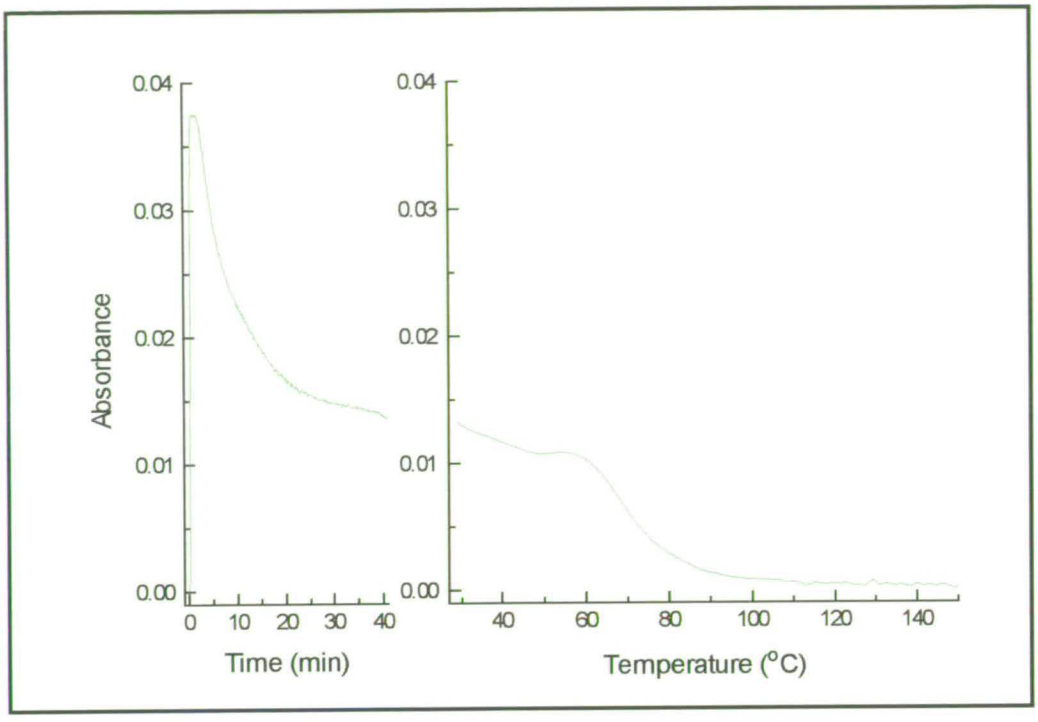

Fig. 7.3. *Variation in intensity of the band at 1227 cm^{-1} for the unpromoted catalyst, expressed first as a function of time during the isothermal period, and then as a function of temperature.*

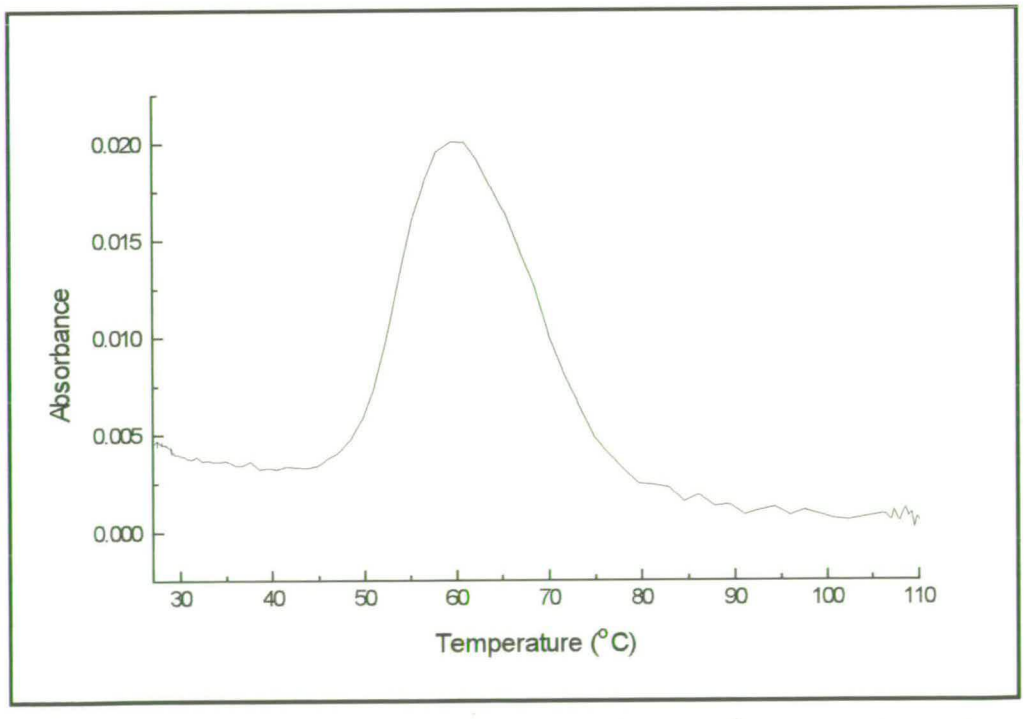

Fig. 7.4. *Variation in the intensity of the band at 1215 cm^{-1}, expressed as a function of temperature for the unpromoted catalyst.*

Outside of the region below 1700 cm^{-1}, a sharp band at 2077 cm^{-1} was also observed from 9 s after the CO_2/H_2 mixture was introduced into the DRIFTS cell (Fig. 7.5). Although this feature was weak, it was found to persist until around a temperature of 107 °C. A doublet centred at 2143 cm^{-1} was also observed in this region from about 140 °C.

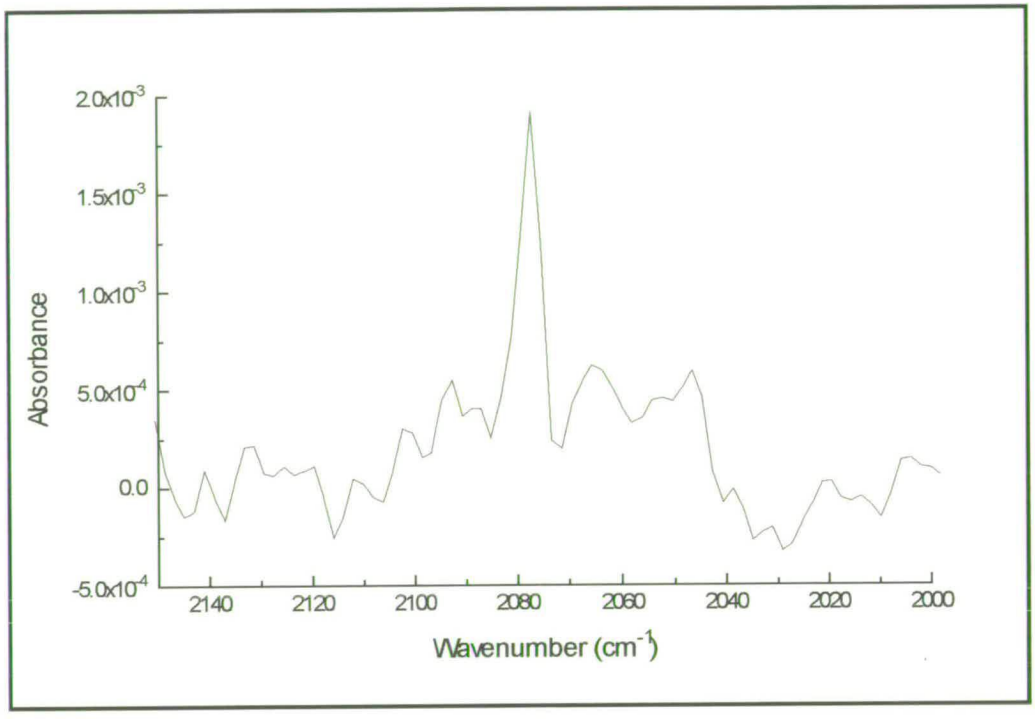

Fig. 7.5. *Extracted spectrum at 1.2 min showing the presence of the adsorbed CO species on the unpromoted catalyst.*

The final region of interest in the infra-red spectrum is that at around 2900 cm^{-1}, usually associated with C-H stretching bands. At about 50 °C, small bands at 2931 and 2852 cm^{-1} were evident. By a temperature of 94 °C, well defined bands at 2930 and 2850 cm^{-1} could be seen, and in addition a weak band could be discerned at 1351 cm^{-1} which was superimposed onto miscancellation features. The intensity of these features reached a maximum 126 °C, and thereafter decreased until their existence ceased at 239 °C. A weak shoulder at the high frequency side of the band at 2850 cm^{-1} appeared at 126 °C, and by 190 °C was more obvious as being at 2871 cm^{-1}. It died away in parallel with the main bands in this region. Fig. 7.6

illustrates development of the bands in the C-H stretching region over the course of the experiment, while Fig. 7.7 gives an example of a spectrum extracted at 126 °C, also showing the feature at 1351 cm^{-1}.

A functional group chromatogram was obtained by monitoring the band at 2930 cm^{-1} over time, and this information is expressed in Fig. 7.8 as a function of temperature. The precise time of formation was thus determined; onset 54 °C, maximum rate of production at 77 °C, and intensity levelling off at 126 °C. However, it looks from this plot as if the band at 2930 cm^{-1} never completely disappears, when, as stated above it was found to have done so by 239 °C. Therefore, this effect is assumed to be an artefact of the functional group chromatogram.

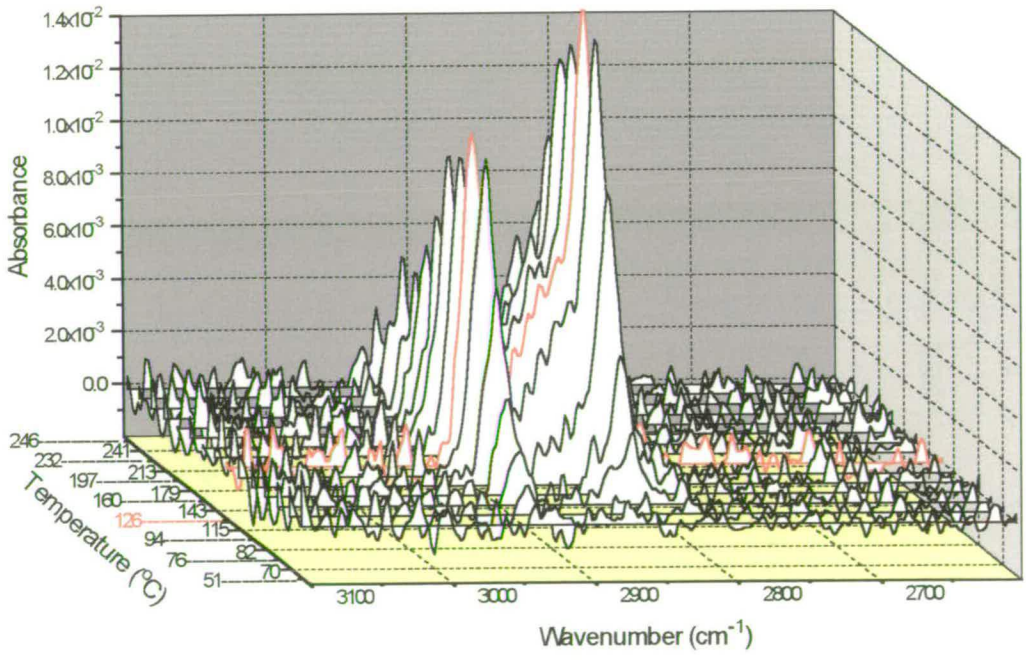

Fig. 7.6. *Extracted spectra showing development of the bands in the region around 2900 cm^{-1} for the unpromoted catalyst.*

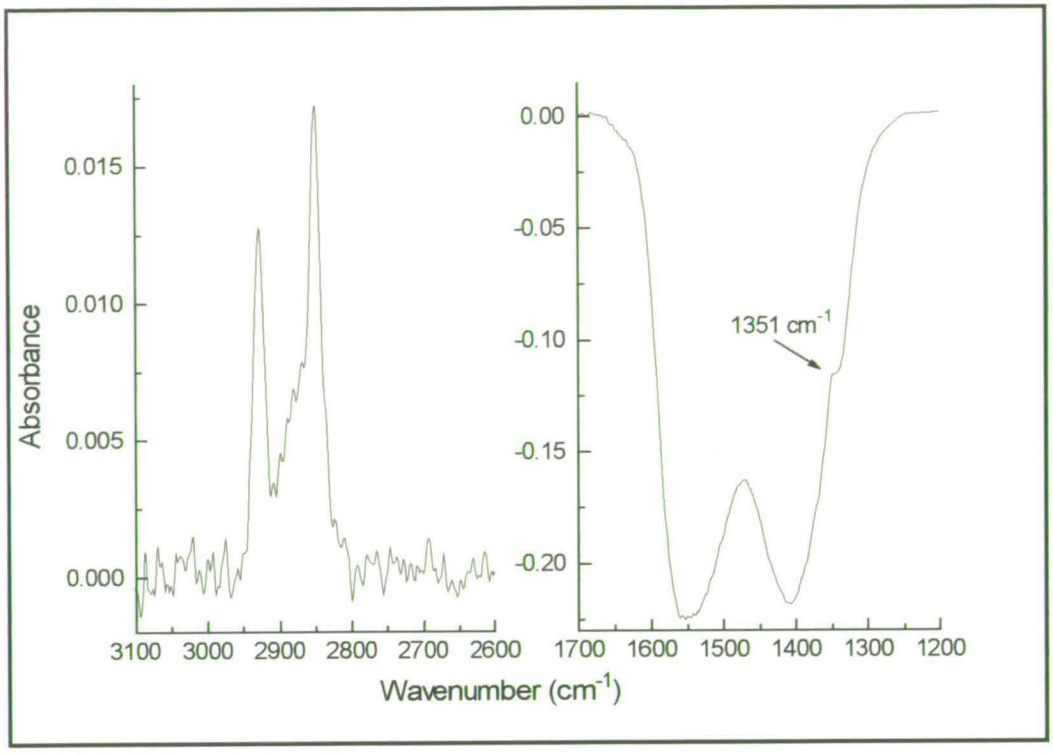

Fig. 7.7. *Example of a spectrum showing bands in C-H stretching region with accompanying feature at 1351 cm^{-1}, extracted at 126 °C for the unpromoted catalyst.*

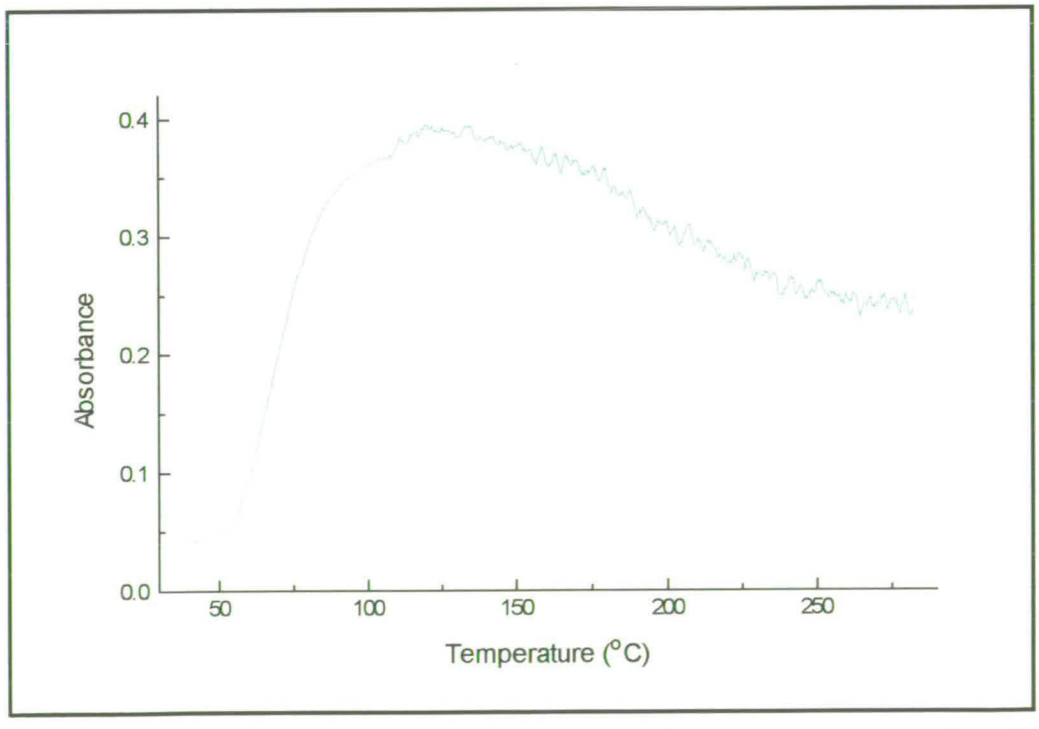

Fig. 7.8. *Functional group chromatogram obtained by monitoring the peak at 2930 cm^{-1} as a function of temperature for the unpromoted catalyst.*

Species detected by the mass spectrometer in the gas phase will now be considered. H_2O was observed by the mass spectrometer to start forming at room temperature at the end of the isothermal period (40.8 min and 25 °C). T_{max} occurred at a temperature of 80 °C and the signal returned to the baseline level at 132 °C. Integration of the peak showed that, in total, 38 a.u. (arbitrary units) of H_2O was produced in this temperature range. H_2O was again observed to increase at 152 °C, from where its presence remained until the end of the experiment (Fig. 7.9).

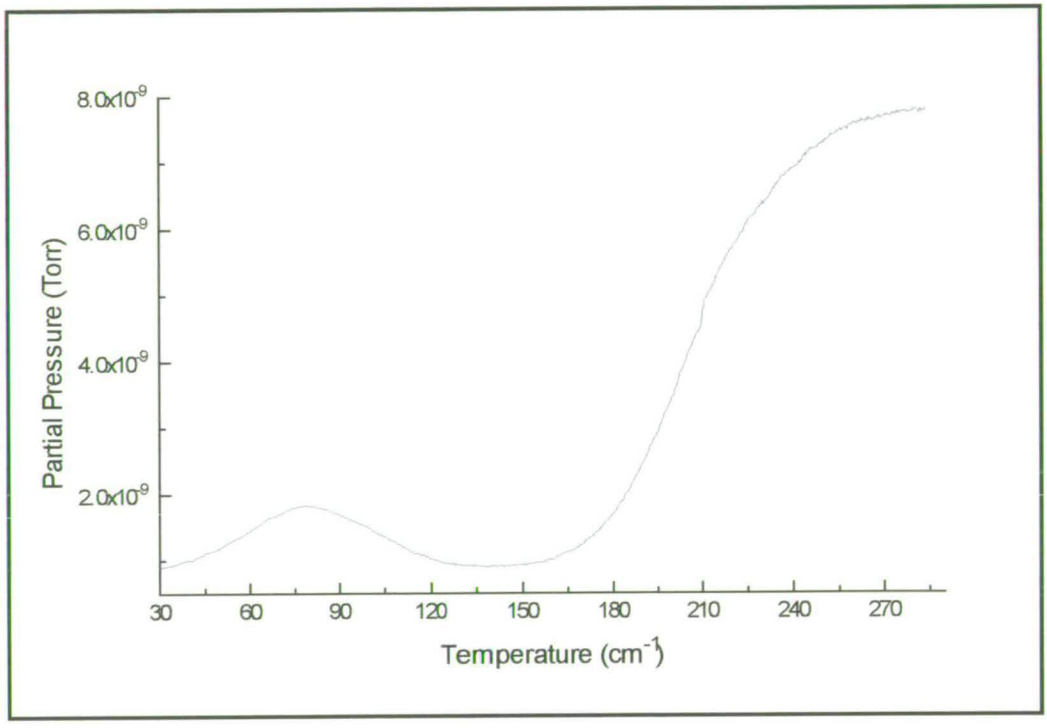

Fig. 7.9. *The formation of H_2O over the unpromoted catalyst during TPR.*

The onset of CO production was seen by the mass spectrometer at a temperature of 160 °C and persisted past the end of the experiment (Fig 7.10). Finally, the mass spectrometer detected the production of a species with *m/e* 31, indicative of methanol, from 144 °C until 202 °C. T_{max} occurred at 173 °C as shown in Fig. 7.11.

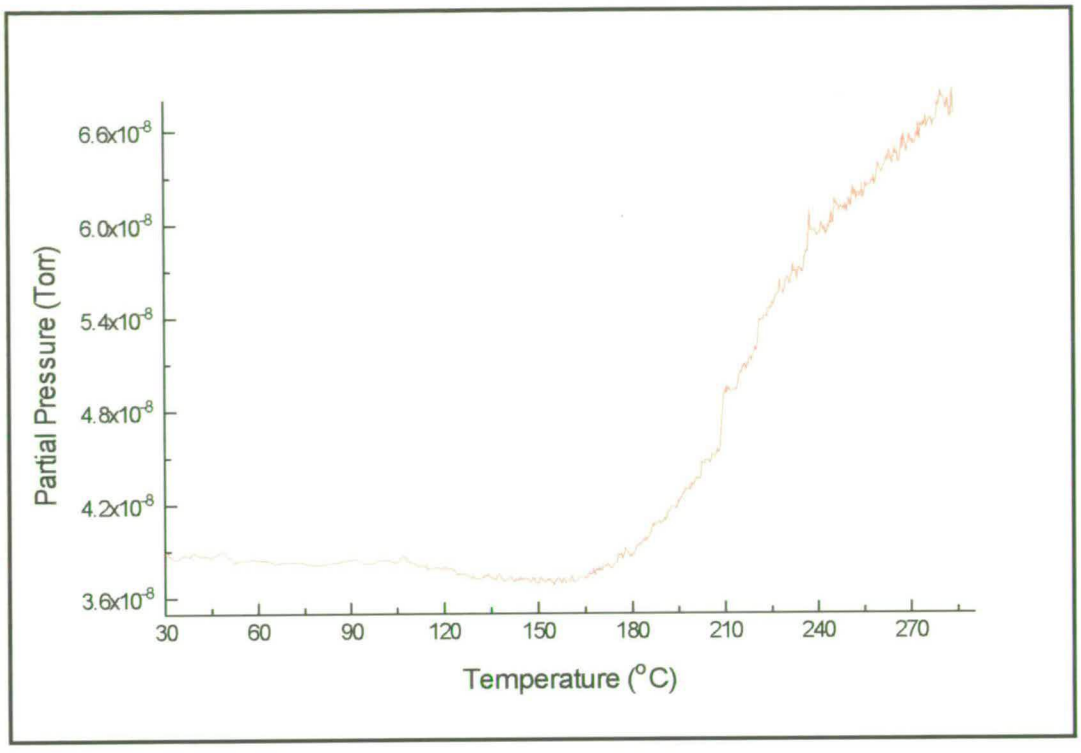

Fig. 7.10. *The formation of CO over the unpromoted catalyst during TPR.*

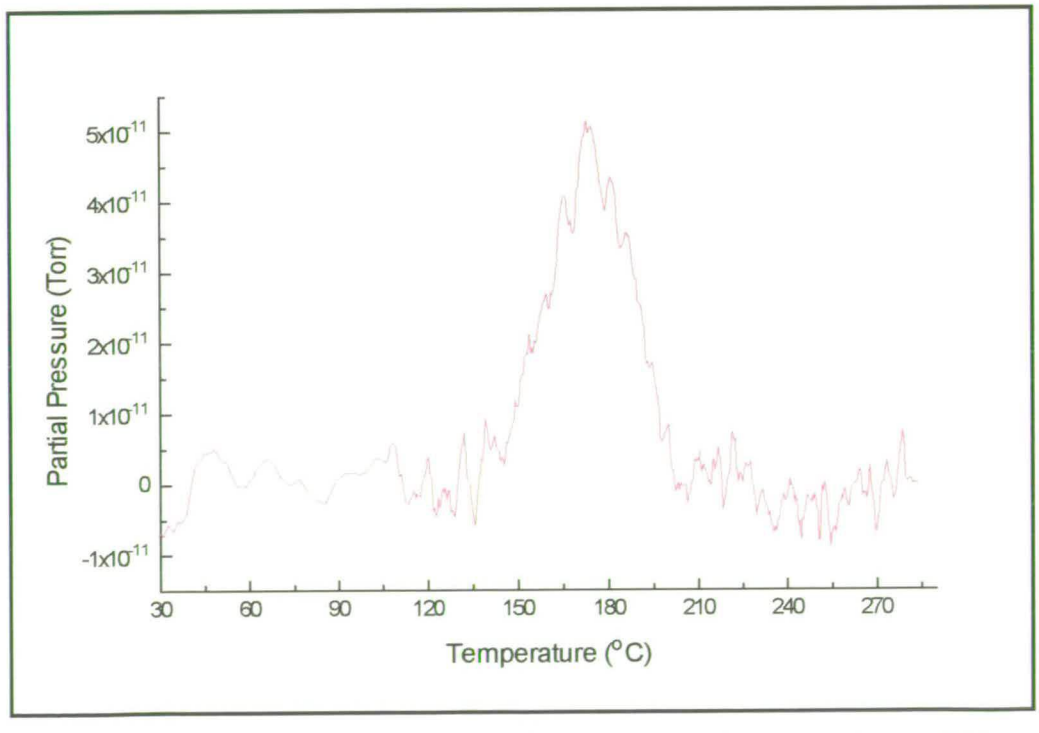

Fig. 7.11. *Methanol formation over the unpromoted catalyst during TPR.*

A summary of the important events occurring during the temperature programmed part of the experiment is shown in Fig. 7.12.

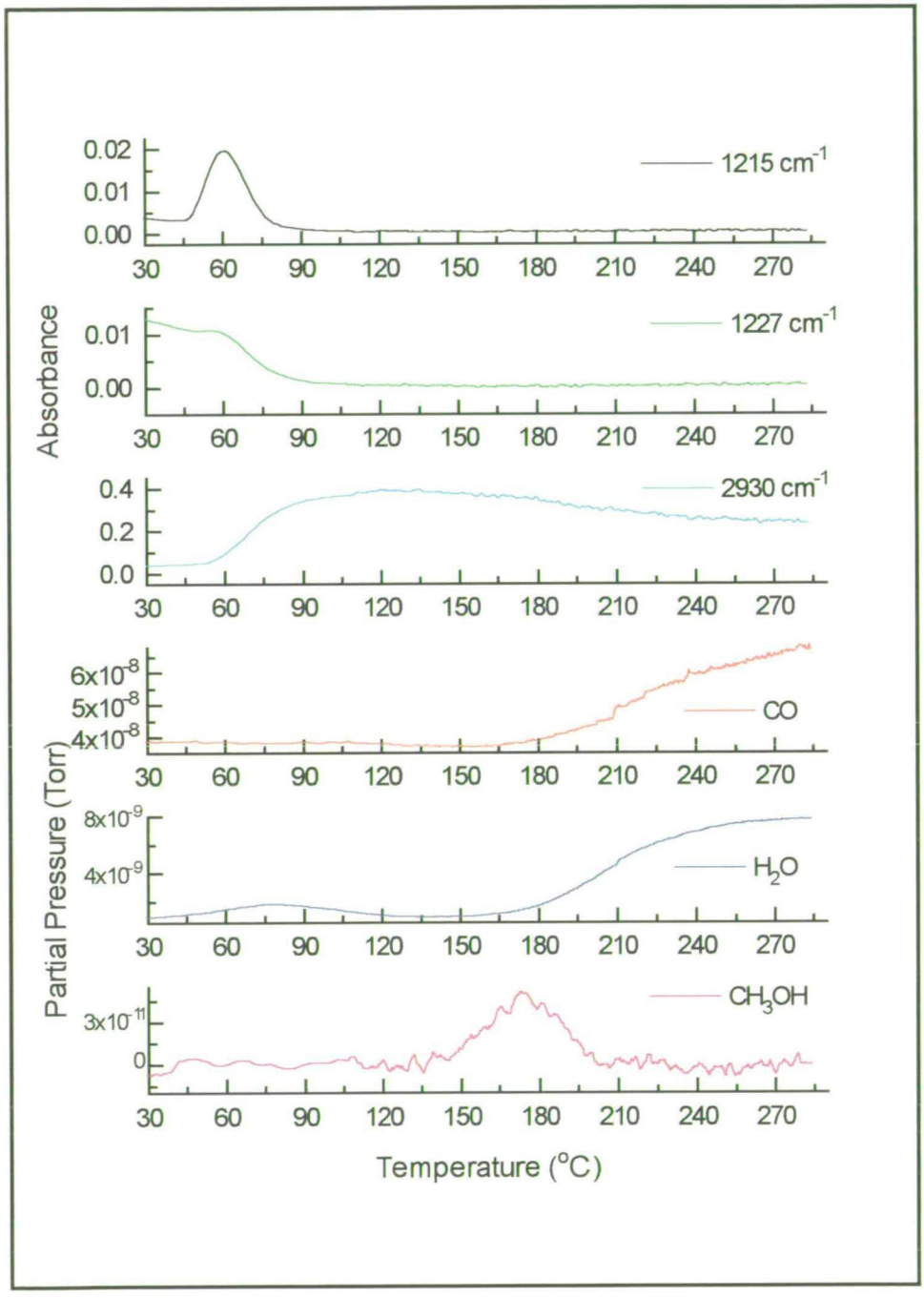

Fig. 7.12. *Summary of results for the unpromoted catalyst during the CO_2/H_2 TPR experiment.*

Discussion

Bands seen from room temperature in the infra-red spectra at 1653, 1424 and 1227 cm^{-1} are representative of bicarbonate species on alumina, as established in Chapter 5. These are formed as a result of the interaction between surface -OH groups and CO_2. Overall, these bands are more intense than those for the corresponding CO and CO_2 pulse experiments, which is anticipated owing to the larger quantities of adsorbate passing over the sample. Bands seen at 1309 and 1044 cm^{-1} suggest a bidentate carbonate species on zinc oxide, as was also discussed in Chapter 5, which results from the interaction of CO_2 with the oxide surface. No contribution was seen from a band at 1600 cm^{-1}, so it is suggested that levels of this species were simply very low, resulting in a very weak band.

As the experiment proceeded, miscancellation features were again found to be a problem in this region, but the use of a functional group chromatogram allowed the behaviour of the sharp band at 1227 cm^{-1} to be followed as a function of temperature: the greatest loss in intensity during the temperature ramp occurred at 76 °C, while the band was no longer present by 107 °C.

Other features below 1700 cm^{-1} included the shoulder at 1100 cm^{-1}. A band was seen in Chapter 6, at 1095 cm^{-1} which was attributed to υ_{CO} for methoxy on the support, while a band at 1107 cm^{-1} has been seen by Idriss *et al.* [163] and assigned to dioxymethylene (CH_2O_2) on zinc aluminate, but none of the accompanying bands were seen for either of these species in this case. The sharp band at 1215 cm^{-1} is also difficult to assign, which first appeared at 51 °C, reaching a maximum at 61 °C, and remaining until 98 °C.

Outwith this region, another feature was observed immediately the CO_2/H_2 mixture had been passed over the unpromoted catalyst, found at 2077 cm^{-1}, which remained until a temperature of 107 °C. As already discussed in Chapter 4, a band at this frequency is indicative of low index planes of copper, specifically Cu(111) [41].

The CO pulse experiments have suggested the absence of such planes for this catalyst, although a similar band was seen following the adsorption of formic acid in Chapter 6. There, it was proposed that bidentate formate on copper had decomposed to form CO_2 on copper which had then formed CO either simply by dissociation or *via* the RWGS reaction. Either of these suggestions is possible in this case. However, one anomaly is that the bandwidth found for this band during the CO_2/H_2 flow experiment is very narrow compared with that from the formic acid pulse experiment - FWHM of 6 cm^{-1} for a band of absorbance of 1.92×10^{-3} compared with FWHM of 9 cm^{-1} with an absorbance of 1.49×10^{-3}, and the reason for this is uncertain. The invariance in the intensity of the band at 2077 cm^{-1} suggests that the CO species could have reached a steady state; that is, CO was being constantly formed from CO_2 and desorbing. Presumably, the fact that no gas phase CO was observed until a higher temperature was due to the amount produced being below the detectability level of the mass spectrometer.

A similar sharp band has been reported several times previously [33, 151, 164] following the contact of supported copper catalysts with CO_2. Elliot *et al.* [164] stated from their study that the Cu(111) plane was inactive for CO_2 dissociation, postulating that highly stepped surfaces such as Cu(110) were necessary for the reaction, and observing that even Cu(211) was inactive. In agreement with the result from this study, Elliot *et al.* found that the intensity of the sharp band was invariant with time, but they did not give any suggestion as to its origin.

An alternative explanation for the origin of the band at 2077 cm^{-1} can be found in the work of Eischens and Pliskin [165]. They reported that the band due to CO adsorbed on platinum was shifted downwards by 30 cm^{-1} after treatment with hydrogen. A theory by Blyholder [166] was invoked in explanation: that the foreign gas (hydrogen) has an effect on the electronic structure of the metal. In this case, hydrogen would contribute electrons to the d-orbitals of the metal, which would in turn increase back-bonding to the CO molecule and the CO stretching frequency would fall. In the present study, this would imply that the band seen at 2077 cm^{-1}

could in fact be due to CO adsorbed on a stepped surface of copper - perhaps that which would usually produce a band at 2094 cm^{-1}.

One other event to occur from room temperature was detected by the mass spectrometer which recorded the evolution of water starting at the end of the isothermal period (25 °C), peaking at 80 °C, before then decreasing. Similar behaviour was seen during the TPD following formic acid adsorption on the unpromoted catalyst, and was thought most likely to be due to the desorption of water from the sample surface. This explanation also seems likely here, and in support, a broad band was seen in the infra-red spectrum between 3750 and 2750 cm^{-1}, centred at 3350 cm^{-1}, which could be due to water adsorbed on the support. This feature was found to increase in intensity until the end of the isothermal period, whereupon it decreased gradually with increasing temperature until it disappeared at 126 °C.

Other possibilities include a suggestion by Clarke and Bell [151] who observed a plateau in water production at 130 °C during the TPR of $CO_2/H_2/Ar$ over Cu/SiO_2 which they attributed to the reduction of surface oxygen produced during the dissociation of CO_2 on copper. A similar plateau has also been seen by Chinchen *et al.* [81] previously (although again at 130 °C) and they also attributed this to the reduction of surface oxygen, but that from incomplete reduction of the catalyst. Either of these suggestions is possible, although in both cases the formation was at a higher temperature than that found during this study. As a final suggestion, the RWGS reaction could have been responsible for the water production, although no CO was detected by the mass spectrometer at this time. However, the small amount of adsorbed CO suggested above could have been involved.

The remaining bands in the infra-red spectra to be observed were those at 2930 and 2850 cm^{-1} and the weak feature at 1351 cm^{-1}. These started to form at 54 °C, the majority being produced at 77 °C, with the intensity peaking at 126 °C. Comparison with the results from formic acid adsorption in Chapter 5 allows these features to be attributed to bidentate formate adsorbed on copper. The shoulder at

2871 cm^{-1} which first appeared at 127 °C can be assigned to bidentate formate on zinc oxide. Bearing in mind the results from formic acid adsorption on this catalyst where the features due to formate on copper were weak shoulders, it is surprising to find that during the TPR experiment the species on the copper is the predominant formate. In explanation of this, it has been found [123] that the formation of formate over copper is a lower energy pathway than that over zinc oxide. Moreover, Burch *et al.* [9] have suggested that zinc oxide can become inactivated towards formate synthesis during the course of the reaction, owing to the loss of the active centres (oxide anion vacancies).

In order to elucidate the route for formate formation, it is worth considering the key temperatures during the experiment mentioned so far:

1) *at room temperature*, after an initial induction period, water formed
2) *from about 51 °C*, the band at 1215 cm^{-1} grew in (51 °C) and bidentate formate on copper started to form (54 °C)
3) *from about 61 °C*, maximum intensity of the band at 1215 cm^{-1} (61 °C), large decrease in intensity of the band at 1227 cm^{-1} (76 °C), T_{max} for water (80 °C), and maximum rate of bidentate formate production (77 °C),
4) *from about 98 °C*, 1215 and 1227 cm^{-1} disappeared completely (98 and 107 °C respectively), $CO_{(a)}$ disappeared (107 °C) and formate production started to slowly decrease (126 °C).

The disappearance of the bicarbonates (and possibly also the bidentate carbonates on zinc oxide), the majority at 76 °C but finally at 107 °C, could be due to their rapid decomposition. These values are in fairly close agreement to those for the TPD of bicarbonate following formation from CO and CO_2 (Chapter 5); 75 and 125 °C, and 103 and 187 °C, respectively. Thus, evidence is provided for the simple decomposition of the bicarbonate species, although the TPD experiments were carried out under a helium carrier gas. Alternatively, it is possible that as the sample temperature was raised, the surface became increasingly reduced, such that no more hydroxyl or oxide centres remained to interact with CO_2 and produce carbonates.

From the key temperatures given above, it can be seen that the maximum rate of bicarbonate on alumina decomposition (band at 1227 cm^{-1}) coincided with the maximum rate of formate on copper production. This coincident disappearance of the bicarbonate (and possibly also bidentate carbonate) species along with the appearance of bands due to the bidentate formate on copper suggests another option: the involvement of the decomposition of bicarbonates/carbonates in formate formation. Millar *et al.* [101] have found evidence for the formation of bidentate formate on copper *via* a symmetrical carbonate on copper and Clarke and Bell [151] have suggested the scheme in Fig. 7.13 as being responsible. However, the fact that their carbonate was on *copper*, and not the support, indicates limited relevance to the study under question since bands due to copper-carbonate were not found in this case. This theory would become more likely if migration of CO_2 could occur from the support to copper as carbonate species decomposed.

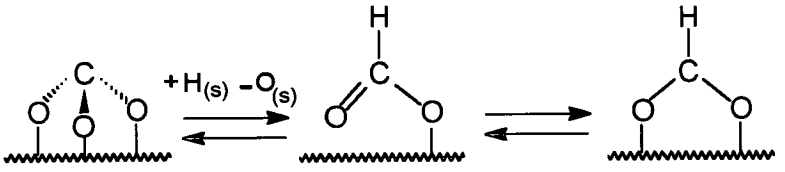

Fig 7.13. *Conversion of a symmetric carbonate on copper into bidentate formate on copper [151].*

The existence of some sort of interfacial formate species or synergy between copper and zinc oxide has been speculated as existing during methanol synthesis [9]. It is possible that the decomposition of bicarbonate/carbonate on the support (and in particular zinc oxide) could have initiated formate formation on copper in some way, if such a synergy exists. If carbonate decomposition was linked to formate formation, it is expected that some carbonate would always be observed in parallel with formate. A maximum was seen in the level of formate at 126 °C, after which the level decreased but no bicarbonate was seen after 107 °C. It is difficult to comment on the maximum temperature of existence of the bidentate carbonate, owing to the problems of growing miscancellation features at high temperature, but the CO_2 pulse

experiment suggested a maximum temperature of 187 °C. Even if this temperature were relevant to the TPR, bidentate formate on copper was found to remain until a far higher temperature - over 200 °C.

The hypothesis of carbonate conversion into formate on copper is not supported by Clarke and Bell who favour the direct hydrogenation of CO_2 (Fig. 7.14) on the basis that carbonate levels reach a steady state within 3 minutes in their study, while formate levels are small at room temperature and even after 20 minutes' exposure at 1 bar. As the temperature is raised to 80 °C, the carbonates decrease rapidly while formate levels still remain small, and do not become significant until after 80 °C.

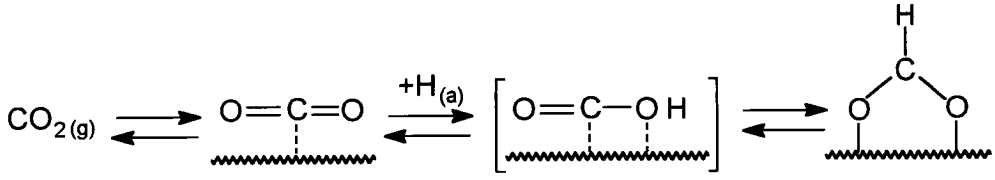

Fig. 7.14. *Direct hydrogenation of CO_2 to form formate species [151].*

Bearing in mind the lack of carbonate at high temperatures, the direct hydrogenation of CO_2 is a possibility for the formation of formate in this study, and the peak at 1215 cm^{-1} could then be due to the δ_{OH} mode of an intermediate such as O=C-OH adsorbed on copper (see Fig. 7.14). If this mechanism was in operation, it would suggest that the carbonates had simply decomposed at a temperature which was coincidentally the same as the formate formation temperature.

Finally, to discuss events at high temperature, it appears that the RWGS reaction is in operation; water was seen by the mass spectrometer to be produced from 152 °C onwards and CO production was also observed - from 140 °C from the infra-red data (gas phase doublet centred at 2143 cm^{-1}) and from 160 °C by the mass spectrometer. The disparity between the values for CO is assumed to be partly due to CO being a very strong infra-red chromophore and also because of high levels of

nitrogen in the mass spectrometer, which also has an *m/e* of 28. Waugh [167] has reported the forward WGS reaction to acquire a significant rate at 120 °C.

The mass spectrometer signals for both water and CO increased sharply with increasing temperature although the water signal started to level off at about 200 °C. Methanol formation started at 144 °C, peaking at 173 °C and decreasing thereafter. Similar findings were reported by Clarke and Bell who found that the turnover frequency for RWGS increased more rapidly than the rate of methanol synthesis above 230 °C. They also noted that selectivity of the reaction to methanol was increased on increasing the pressure from 1 bar to 7 bar. The rate limiting step for methanol synthesis is widely agreed to involve the hydrogenation of formate or some subsequent intermediate (e.g. formaldehyde) [123]. Thus it could be expected that on increasing the pressure in the present study, the rate limiting step could occur more easily and a more substantial amount of methanol would be produced.

7.4 - Promoted Catalyst

Results

Bands were evident at room temperature in the region below 1700 cm^{-1} at 1653, 1422, 1312, 1227 and 1034 cm^{-1} shortly after the CO_2/H_2 mixture was introduced into the DRIFTS cell - this time from 9.5 s. The development of these species is illustrated in Fig. 7.15, which shows spectra extracted from the kinetics file.

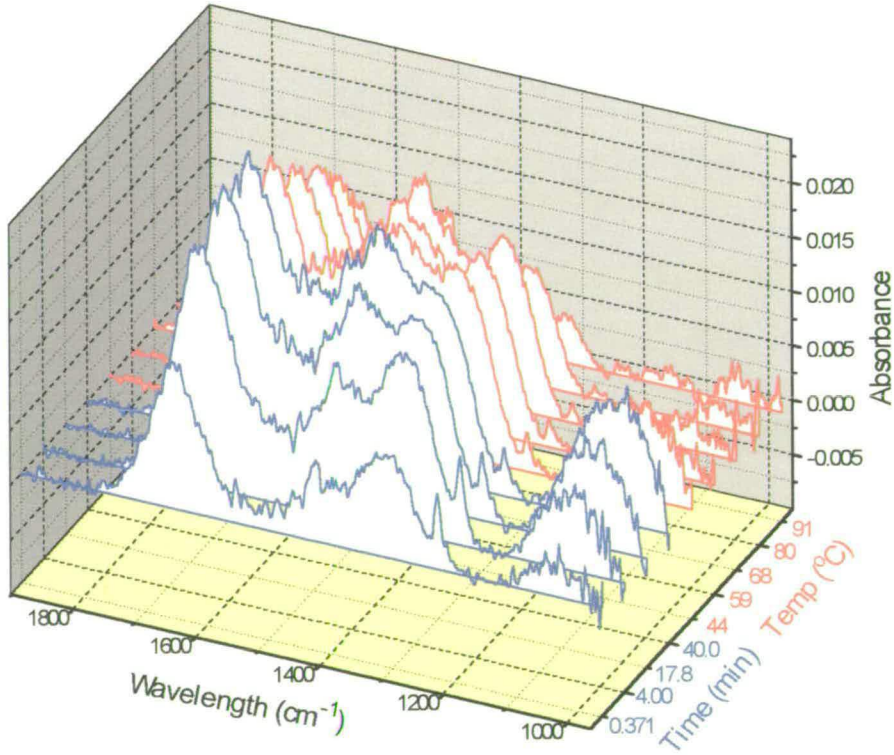

Fig. 7.15. *Extracted spectra showing development of bands in the region below 1700 cm^{-1} for the promoted catalyst.*

In detail, at 4 min all the peaks had intensified, but by 17.83 min, when spectra were next scanned, slight shifts had taken place (now 1644, 1426, 1333, 1045 cm^{-1}). Although at this point most of the peaks had continued to grow, the peak at 1227 cm^{-1} had decreased in intensity, as it continued to do until disappearing at a

temperature of 110 °C. At 40 min, 27 °C, slight shifts in frequency were again evident (1638, 1427, 1329, 1227 and 1047 cm^{-1}) while a shoulder at 1479 cm^{-1} started to grow in. At 44 °C, the features started to decrease in intensity apart from the shoulder at 1470 cm^{-1} which continued to grow. At 80 °C, all the peaks, even that at 1470 cm^{-1}, continued to decrease and at 91 °C, it was obvious that miscancellation was dominating the spectrum and no more information could be gleaned at this point.

The build-up and later disappearance of the peak at 1227 cm^{-1} (again, seen as the most reliable feature in the region) is shown by the functional group chromatogram in Fig. 7.16, which shows the information initially as a function of time during the isothermal period at room temperature, and then as a function of temperature. Thus it can be seen that there is a gradual decrease in the band intensity already at room temperature, which is followed at higher temperature by the complete removal of the species responsible for this band, in line with the behaviour of the unpromoted catalyst. The blue dashed line simply represents a period when data collection had ceased.

A sharp band at 2077 cm^{-1} was again observed to form early on in the experiment - at 9.5 s after the CO_2/H_2 mixture was introduced into the DRIFTS cell. This is shown in Fig. 7.17 and remained until 159 °C when a doublet centred at 2143 cm^{-1} appeared which persisted past the end of the experiment (9910 s, 165 minutes, 283 °C). No other infra-red bands were observed for the promoted catalyst.

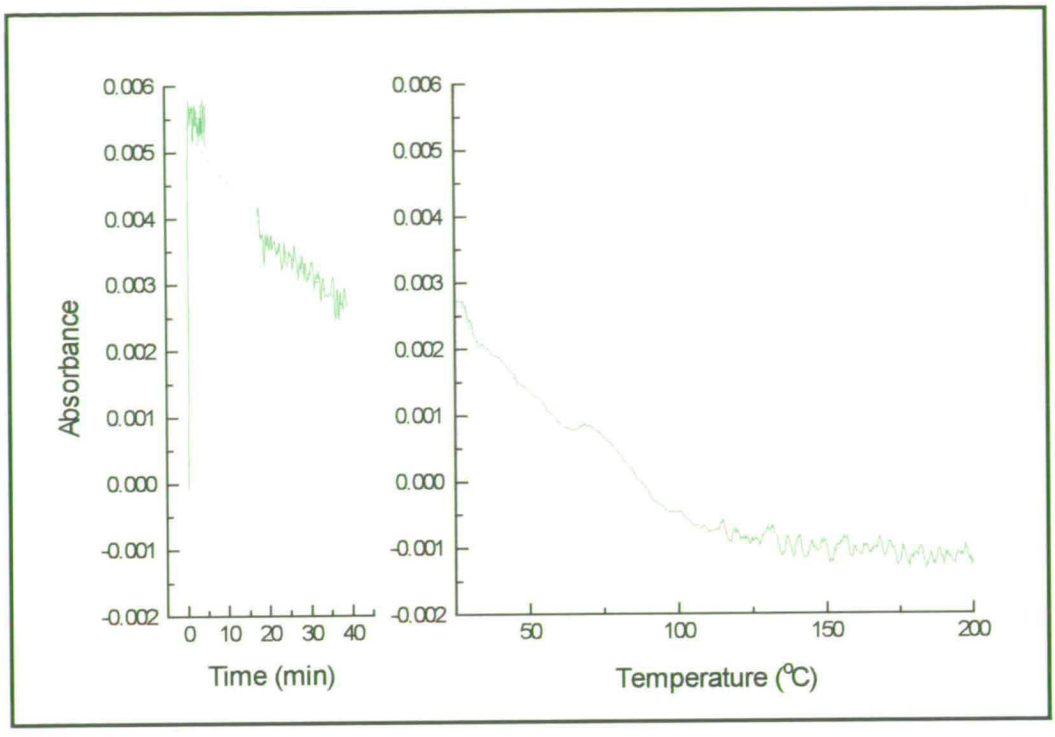

Fig. 7.16. *Variation of intensity of the band at 1227 cm^{-1} for the promoted catalyst, expressed initially as a function of time during the isothermal period at room temperature, and then as a function of temperature.*

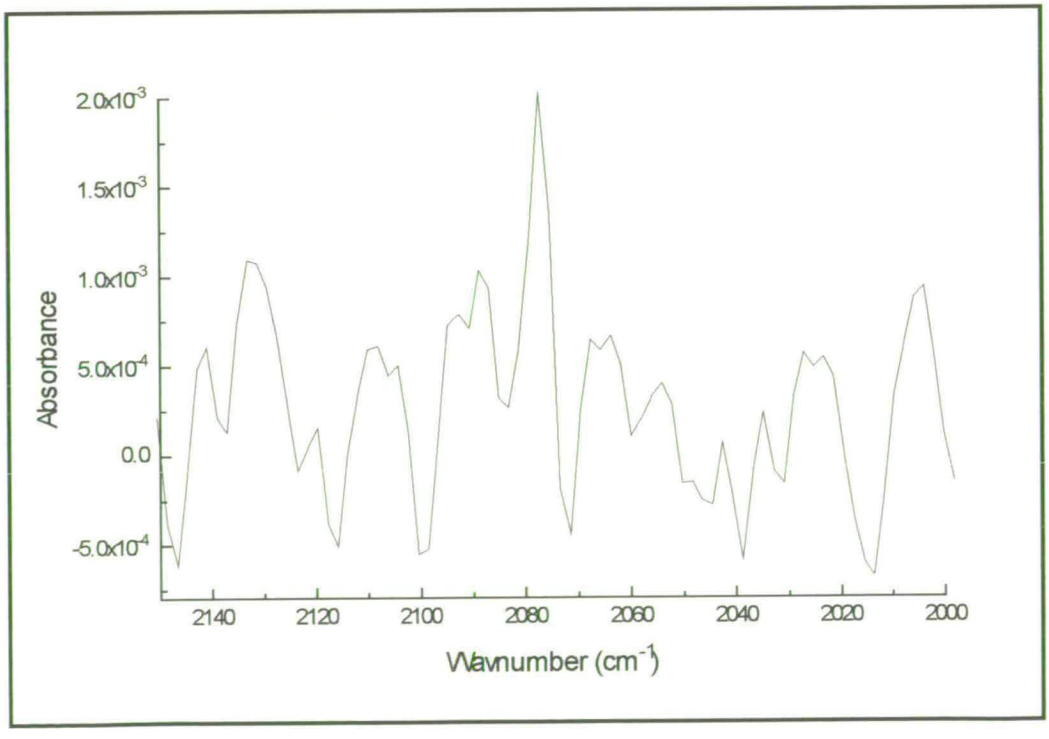

Fig. 7.17. *Band at 2077 cm^{-1} extracted at 1.2 min for the promoted catalyst*

Gas phase species detected by the mass spectrometer included H_2O from 48 °C. T_{max} for this species occurred at 98 °C. The signal returned to background levels by 135 °C. In total, 26 a.u. of H_2O was produced in this temperature range. H_2O was observed by the mass spectrometer to be produced again from a temperature of 148 °C and its presence remained until the end of the experiment. Gas phase CO was also detected by the mass spectrometer at 151 °C. Figs. 7.18 and 7.19 illustrate the formation of H_2O and CO respectively during the experiment.

Finally, a contribution was seen for the mass spectrometer at *m/e* 31, again indicative of the formation of methanol from 120 °C with T_{max} at 181 °C. It was produced until 243 °C, as shown in Fig. 7.20.

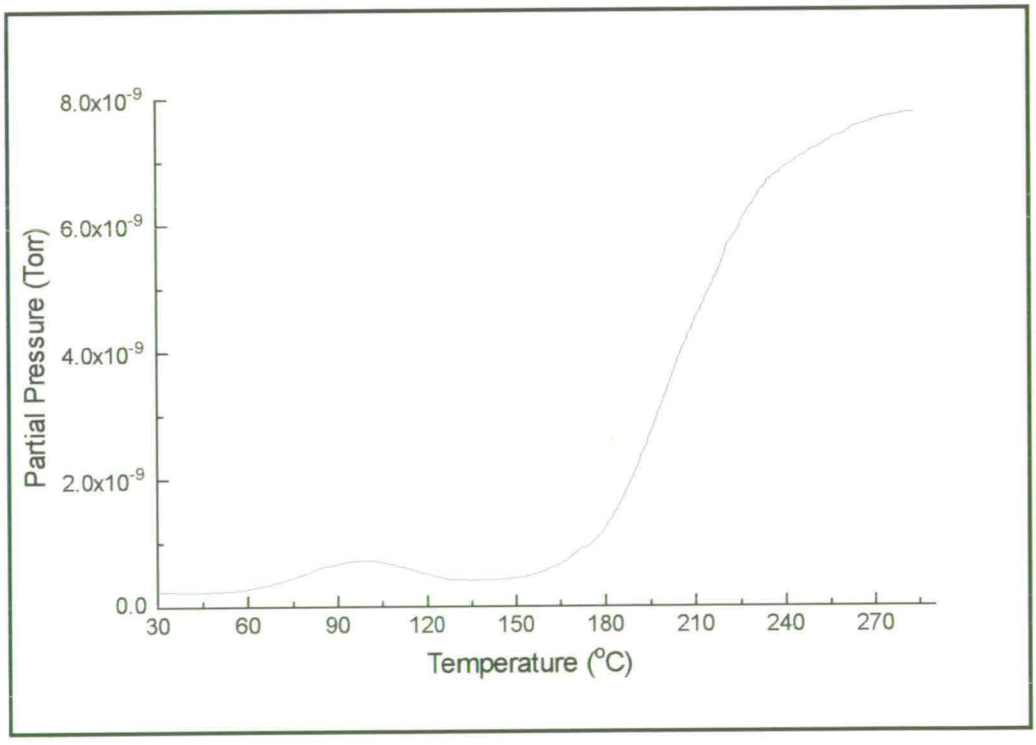

Fig. 7.18. *The formation of H_2O over the promoted catalyst during TPR.*

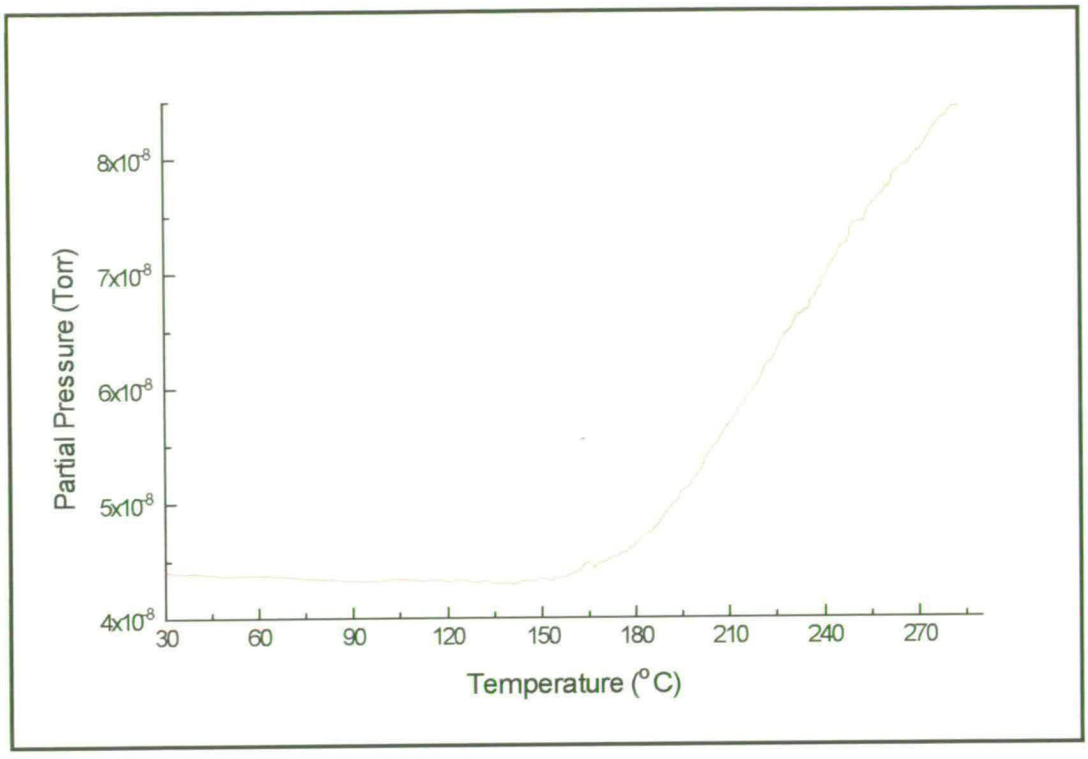

Fig. 7.19. *The formation of CO over the promoted catalyst during TPR.*

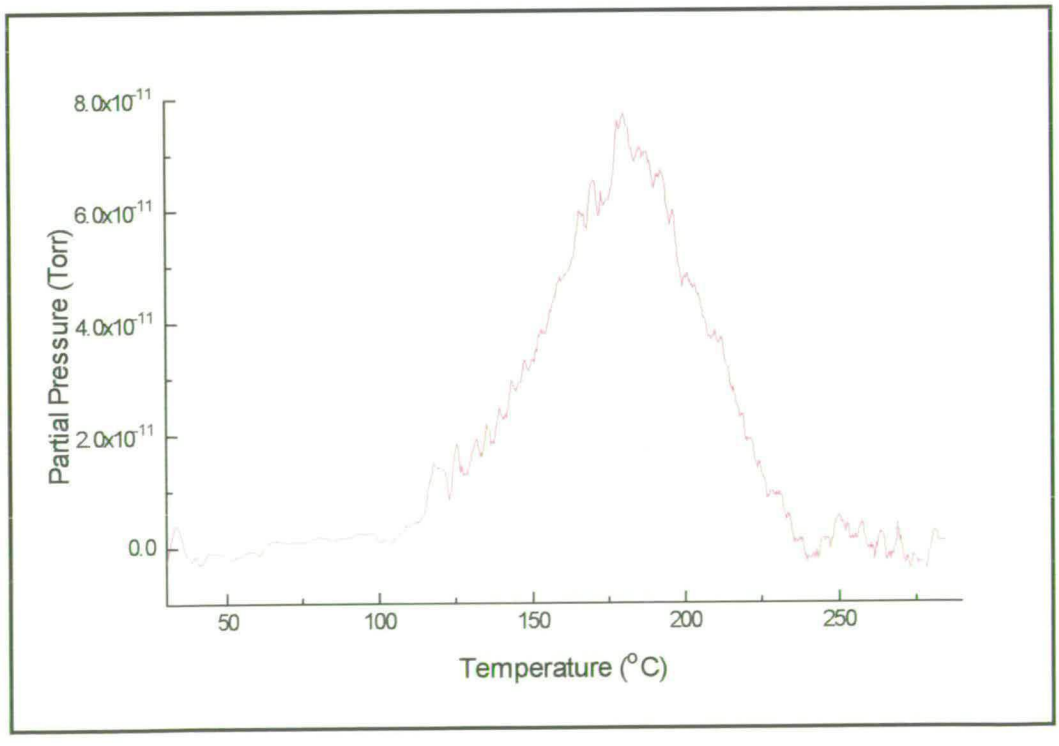

Fig. 7.20. *The formation of methanol over the promoted catalyst during TPR*

A summary of the important events recorded during the temperature programmed part of the experiment is shown in Fig. 7.21.

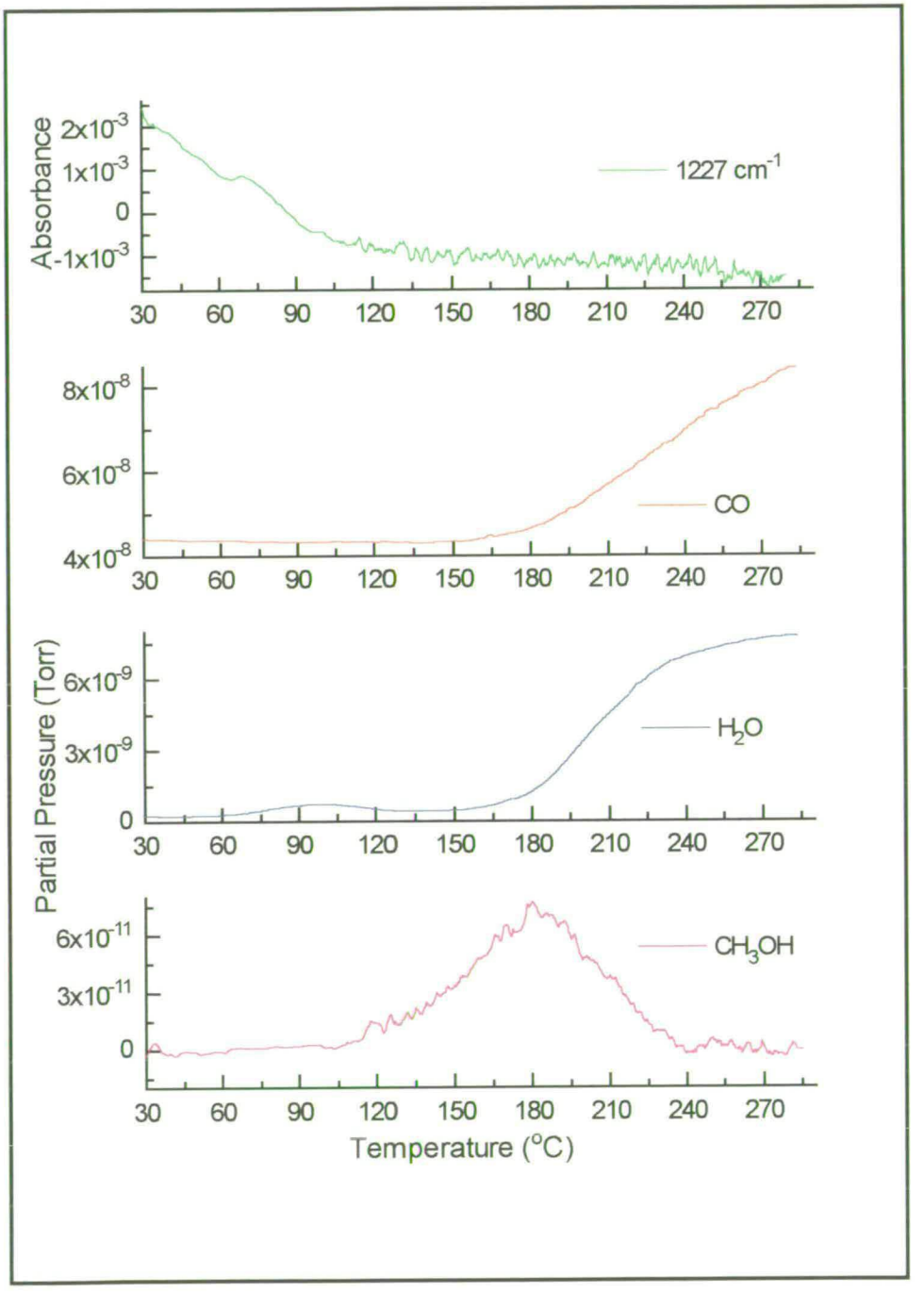

Fig. 7.21. *Summary of results for the promoted catalyst during the CO_2/H_2 TPR experiment.*

Discussion

As was found for the unpromoted catalyst, bicarbonates on alumina (1638, 1427 and 1227 cm^{-1}) were observed as soon as the CO_2/H_2 mixture was passed over the sample. Bands which were attributed previously to bidentate carbonates on zinc oxide at 1329 and 1047 cm^{-1} were observed, and on closer inspection of the spectra it was deemed likely that a contribution at 1600 cm^{-1} was also present, as expected.

Comparison of the thermal dependence of the carbonate-type bands with those seen for the unpromoted sample shows that in both experiments bands started to decrease in temperature from about 44 °C, while the band at 1227 cm^{-1} was last seen at 110 °C in this case, and 107 °C in the case of the unpromoted catalyst. However, a comparative plot for each catalyst at 4 min (Fig. 7.22) shows that, as seen for the CO and CO_2 pulse experiments, there is relatively more of the bicarbonate on alumina for the unpromoted catalyst, and more of either bidentate carbonate on zinc oxide or a carbonate/carboxylate associated with the potassium on the promoted catalyst.

The corresponding spectra for the CO and CO_2 pulse experiments showed a more marked contrast between the unpromoted and promoted catalysts in this region (e.g. Fig. 5.19 in Chapter 5). This is assumed as being due to the dynamic conditions in this example; in the presence of H^+ or H_2 from the CO_2/H_2 mixture, bicarbonate and carbonate would probably interconvert, for instance as in reaction 7.4.

$$CO_3^{2-} + H^+ \leftrightarrow HCO_3^- \qquad \textit{reaction 7.4}$$

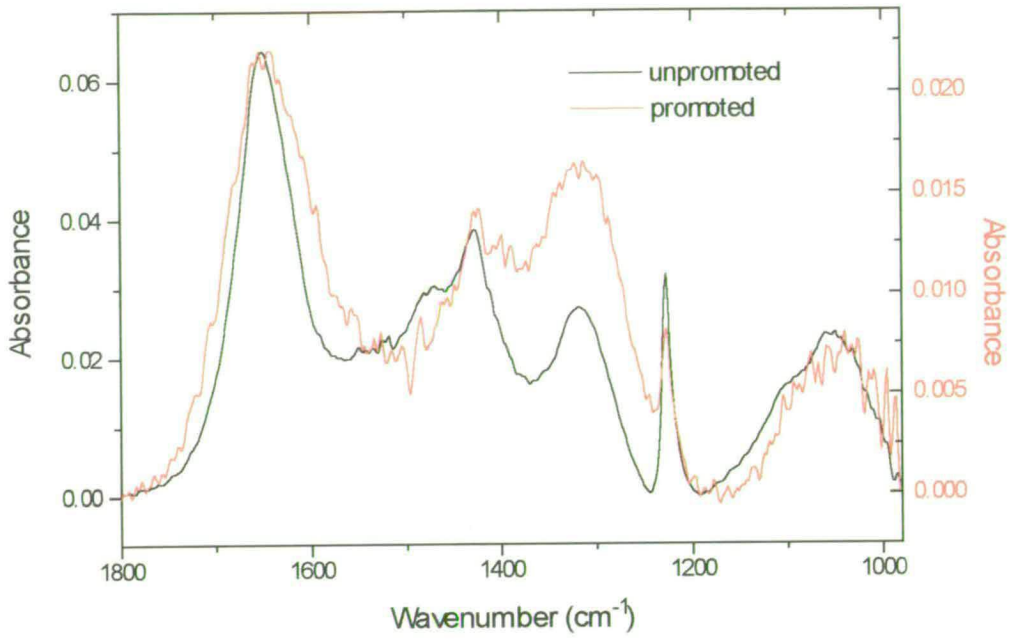

Fig. 7.22. *Comparison of the region below 1700 cm^{-1} for the unpromoted and promoted catalysts.*

The only remaining infra-red feature to be observed for the promoted catalyst was that at 2077 cm^{-1}, which was assigned for the unpromoted sample as possibly being due to CO adsorbed on low index planes of copper, or CO on stepped planes of copper that have been influenced by the coadsorption of hydrogen. A comparison is made in Fig. 7.23 between adsorbed CO on the unpromoted catalyst and the promoted catalyst. Interestingly, the two bands are of approximately the same size, in spite of the relatively smaller copper surface area of the promoted catalyst, and the site-blocking effect of the alkali promoter towards CO molecules suggested in Chapter 5. The band was found to persist until gas phase CO grew in at 159 °C (a doublet centred at 2143 cm^{-1}), which supports the assignment of the sharp band to adsorbed CO.

Whether the band at 2077 cm^{-1} is due to a hydrogen-influenced CO species on a stepped copper plane, or due to CO formed on a stepped plane which has

subsequently migrated onto the low index planes, it seems that the reaction of $CO_2 \rightarrow CO$ has not been hindered by alkali promotion, and could even support the suggestion of a direct promotion of the copper metal. However, this seems unlikely based on the absence of any shift in the CO stretching frequency both here and in Chapter 5.

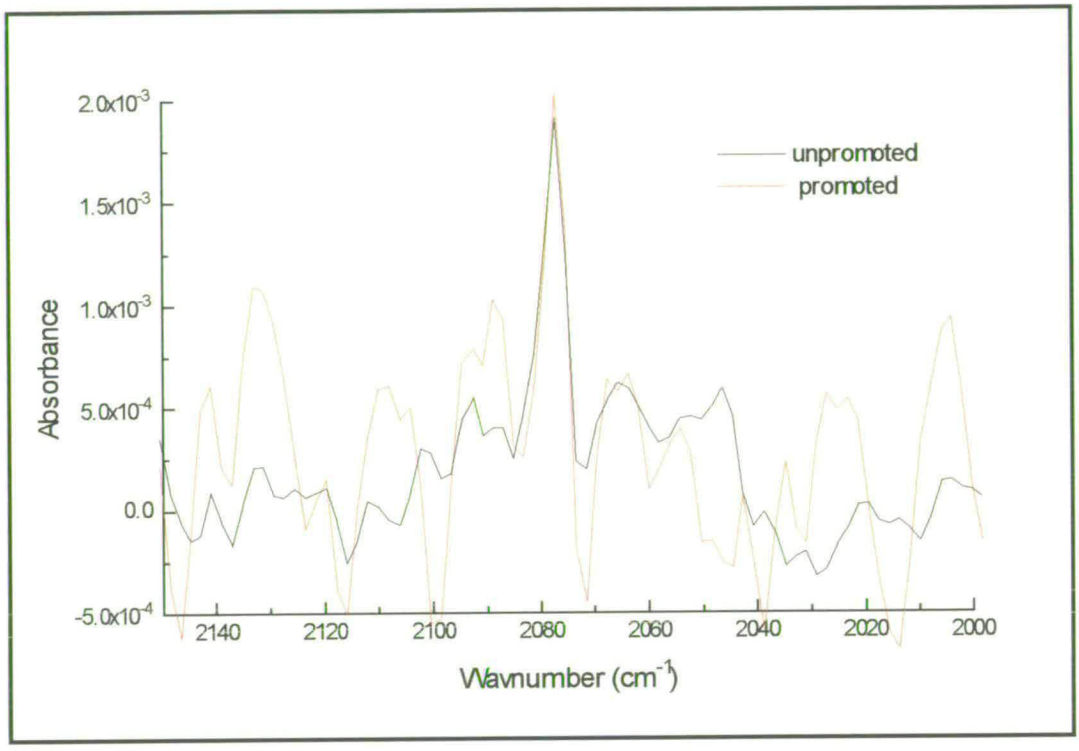

Fig. 7.23. *A comparison of adsorbed CO found on the unpromoted and promoted catalysts, both at 1.2 min (lower signal to noise ratio of promoted catalyst spectrum is due to a different time resolution being used, as discussed in section 7.2).*

The remaining event to occur at relatively low temperature was the formation of water. The most likely source for this water formation was assumed to be desorption from the support for the unpromoted sample, indicated by the loss of a broad band at around 3400 cm^{-1}. However, this band was not seen for the promoted sample. The amount of water produced at low temperature for the promoted catalyst was found to be 69 % of the value for the unpromoted sample, while the decrease in total surface area for the promoted sample was 50 % (BET). Therefore, the decrease in the amount of water formed could be explained in terms of the surface area

difference. However, its formation commenced at 48 °C, unlike that for the unpromoted sample which was already seen at room temperature, towards the end of the isothermal period. T_{max} was also found to occur at a higher temperature - 98 °C for the promoted catalyst whereas it was seen at 80 °C for the unpromoted. The shift in T_{max} on promotion possibly suggests an additional source of water, and perhaps the idea proposed by Clarke and Bell [151] of the reduction of surface oxygen produced during the dissociation of CO_2 on copper could explain this; certainly, the dissociation of CO_2 was found to occur more over the promoted catalyst in Chapter 5.

The most important absences in the infra-red data which were seen for the unpromoted catalyst are the bands due to bidentate formate on copper and formate on zinc oxide, and Fig. 7.24 shows this absence compared with the bands seen for the unpromoted catalyst. This complete loss is remarkable, and as a result, it can be definitively stated that the effect of the alkali in reducing the selectivity of the catalyst to methanol is to prevent formate formation; the precursor to methanol. Other absences are the bands at 1215 and 1100 cm^{-1}, and it could be speculated that these were related to formate formation, possibly as an intermediate between CO_2 and bidentate formate and an intermediate between formate and methanol, respectively.

The most straight-forward explanation for the absence of bidentate formate on copper would be the loss in copper surface area. Very intense, sharp bands were found for the unpromoted sample. The loss in copper surface area on promotion was about 40 %, so based on surface area arguments alone, bands would be expected. Thus, it seems that a real promotional effect is in existence.

Beyond the obvious suggestion of a decrease in copper area, it becomes necessary to speculate on what could be the impact of the promoter on formate formation. First, the CO adsorption studies in Chapter 5 suggested that the promoted catalyst seemed to be better reduced following pre-treatment than did the unpromoted. It has been shown that surface oxygen promotes the chemisorption of CO_2 and hence eventual CO_2 hydrogenation to methanol, *via* formate [81]. Thus, if

less surface oxygen was present initially on the promoted catalyst, less CO_2 would have been adsorbed and less formate seen. Certainly, physisorbed CO_2 was seen as a band at 2340 cm^{-1} following the CO_2, methanol and formic acid pulse experiments on the unpromoted catalyst, while it was never observed on the promoted. This could have been a combination of a decreased copper surface area and a more completely reduced surface. Other results from the literature which correspond with these suggestions include that from Chauvin *et al.* [134] who also claimed that surface oxygen participated in the formation of formate at room temperature, and that from Calvery and Smith [161], who noted in a study of methanol synthesis on a potassium carbonate-promoted $Cu/ZnO/Cr_2O_3$ catalyst that CO_2 hydrogenation only took place on unpromoted copper sites.

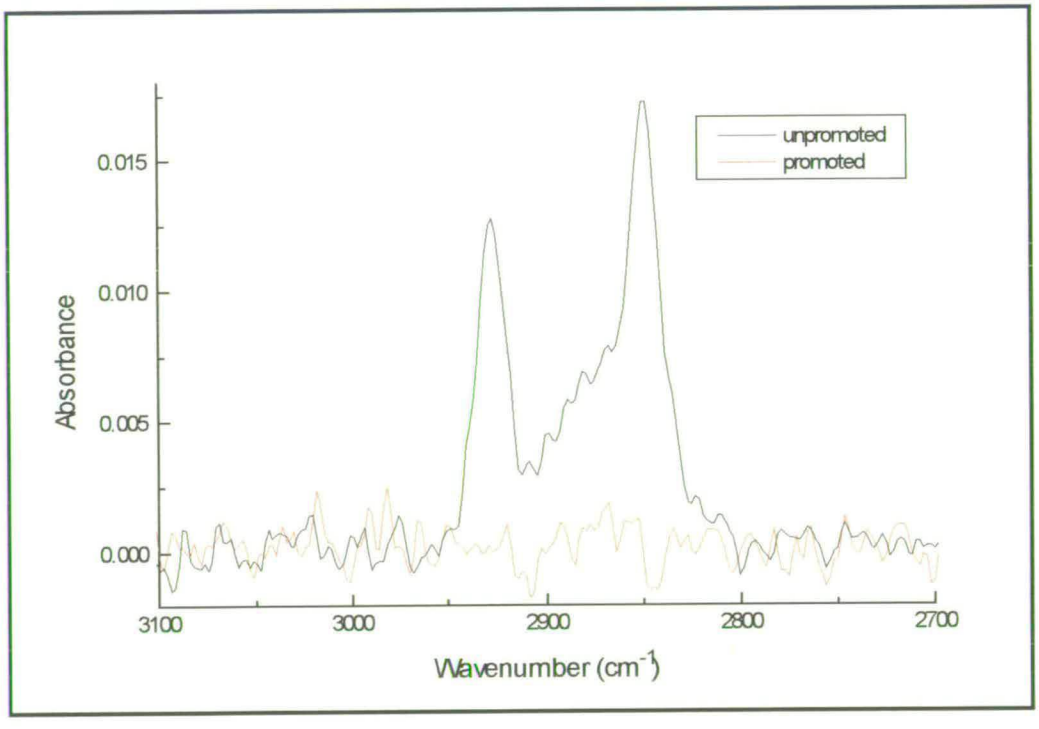

Fig. 7.24. *The absence of bands in the C-H stretching region for the promoted catalyst compared with those seen for the unpromoted catalyst at 126 °C.*

Having considered the effect of promotion on CO_2, it is worth speculating upon the effect on the hydrogen component of the gas mixture. Two possible routes to the bidentate formate were discussed for the unpromoted sample, one involving the

conversion of carbonates to formates (Fig. 7.13) and one involving the direct hydrogenation of CO_2 (Fig. 7.14). The latter suggestion seemed most plausible based on the assumption that a small amount of carbonate would always be present for formate to exist if the former suggestion were true. But regardless of this, for both mechanisms surface hydrogen was involved. Thus, where formate is not produced (or is at too low a level to be detected) the alkali promoter could be influencing the availability of surface hydrogen. Burch *et al.* [14] advocate the existence of a synergistic relationship between the copper and zinc oxide components of the catalyst; they believe that although the rate determining step of methanol synthesis (i.e. the hydrogenation of formate or some other similar intermediate) takes place on copper, the overall rate of the reaction can be enhanced by the presence of zinc oxide. This supposedly occurs by hydrogen dissociating on copper then spilling over to zinc oxide, where it is stored in readiness to hydrogenate intermediates. As a result, the zinc oxide surface becomes hydrided and hydroxylated. They also propose that, on heating, -OH groups may be transferred from zinc oxide in the same way and these encourage formate formation even more. Thus active sites may be generated on the copper by the transfer of oxygen in the form of -OH.

Since the findings by Burch *et al.* [14] were said to be particularly noticeable for co-precipitated catalysts like the one in this study, it therefore seems possible that one effect of the alkali on the support could be to prevent either the transfer or even formation of surface hydrogen and hydroxyl groups. In Chapter 5, it was suggested that the lower level of bicarbonate on the promoted sample was due to surface -OH groups being replaced by $-O^-K^+$ [119]. If this could also occur under reaction conditions, it is possible that hydrogenation of adsorbed CO_2 could be inhibited.

Finally, to discuss events occurring at high temperature, gas phase CO was detected by the mass spectrometer to be produced from 151 °C and by the infra-red spectrometer from 159 °C. Water was observed by the mass spectrometer from 148 °C. These are assumed to be due to the RWGS reaction, as was the case for the unpromoted sample. The fact that the reaction still proceeds at an appreciable rate in

spite no of bidentate formate on copper being detected implies that, in this case, a redox-style mechanism is in operation for the RWGS reaction, in agreement with other authors [8, 80].

In addition, on comparing the traces of the two species for the two samples (Fig. 7.25), it is found that, surprisingly, the amounts produced are not affected detrimentally by the promoter. It was shown in the CO_2 pulse experiment in Chapter 5 that, on promotion, the formation of CO from CO_2 was enhanced. Considering the redox-type mechanism for the RWGS reaction (reaction -(7.2)) the dissociation of CO_2 is the first step. If this is increased in rate, then the overall RWGS rate may be affected. The enhancement of dissociation activity of CO_2 in this case appears to more than compensate for the loss in copper surface area suggested from CO pulse experiments and attributed to a site blocking effect of the potassium promoter. In Chapter 5, it was unclear what exactly the mechanism of this enhancement could be attributed to, but evidence suggested that a potassium-associated species on the support could be involved, such as a carboxylate.

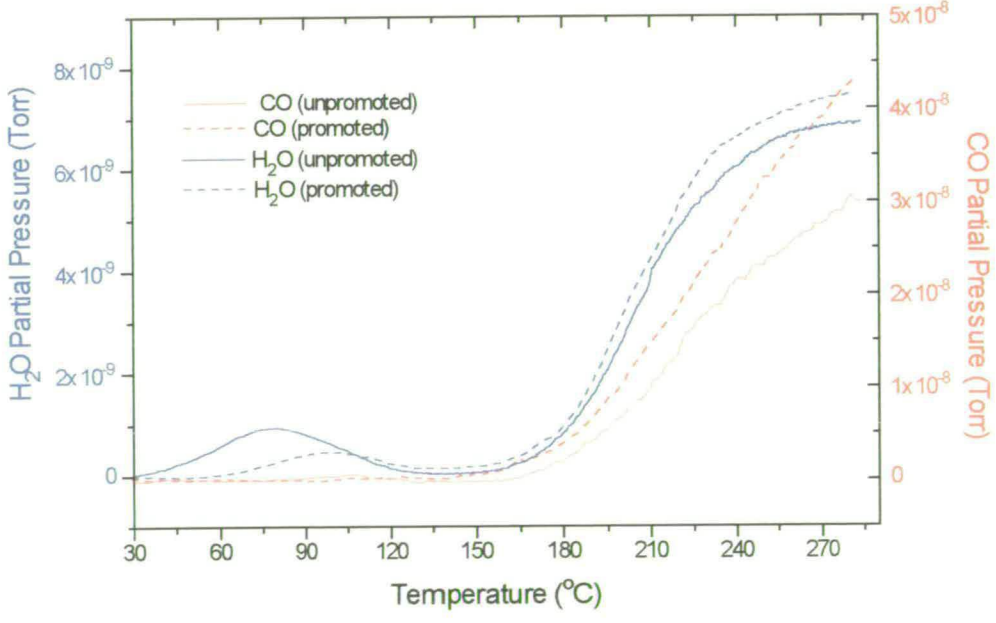

Fig. 7.25. *Comparison of CO and Water production at high temperature for the unpromoted and promoted samples.*

Amenomiya and Pleizier [168] have observed that the activity for the WGS reaction over alumina could be enhanced on potassium promotion. Clarke and Bell [151] also observed an enhancement of the RWGS on promotion in their study of the reaction of $CO_2/H_2/Ar$ over Cu/SiO_2. They attributed this to the hydrogenation of a potassium-associated carboxylate to formate with its subsequent transfer to copper i.e. an associative mechanism. Since no formate was observed in the present study, such a mechanism cannot in operation for the RWGS reaction. However, it is still possible that a potassium-carboxylate could be taking part in a redox-type mechanism.

Finally, the small amount of methanol produced during the reactions has not been commented on. It is not clear why methanol should be produced for the promoted catalyst, when no formate species was observed. Equally, it seems strange that the amount of methanol produced should be greater over the promoted catalyst and, moreover, that it should be produced over a wider temperature range, as shown in Fig. 7.26.

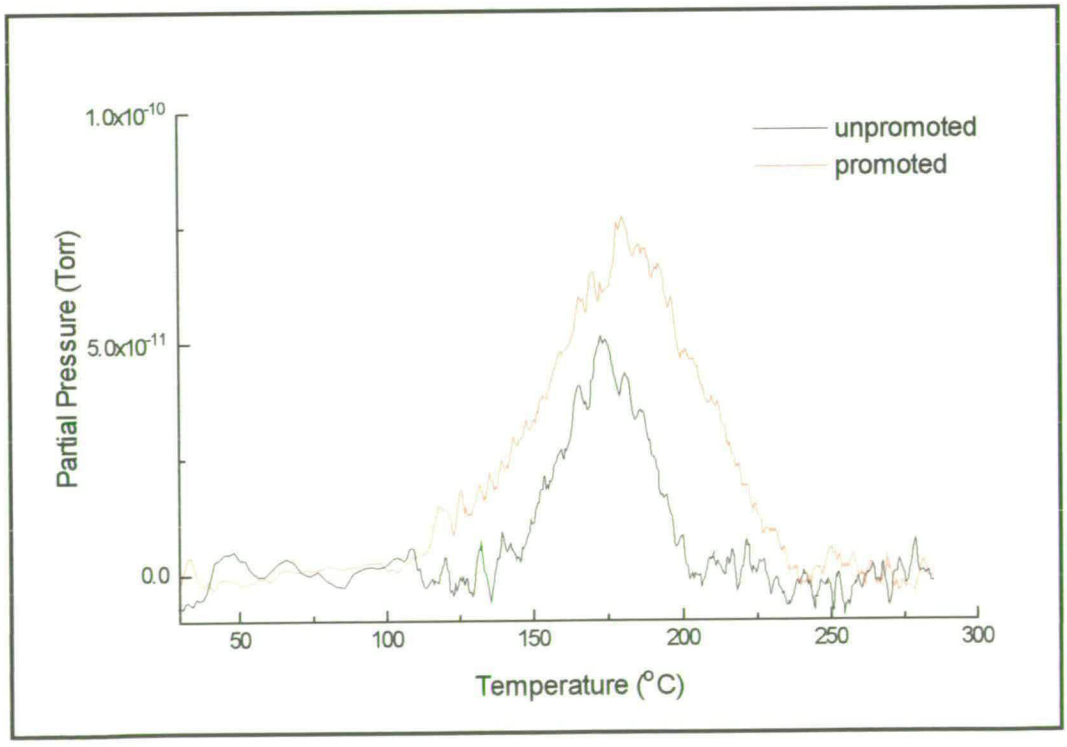

Fig. 7.26. *Comparison of methanol produced over the unpromoted and promoted catalysts.*

There are several possible reasons for this: 1) the amounts of methanol produced were at the detectability limit for the mass spectrometer, so readings were possibly inaccurate, 2) the baselines of the traces were sloping and uneven, meaning that the data required baseline correction - errors could have been introduced into what were already very small peaks, 3) methanol was monitored at *m/e* 31, so this could have been influenced by any molecular oxygen produced (*m/e* 32) if the mass spectrometer was unable to resolve the two species, and finally, 4) it is possible that the methanol observed was formed by another route, parallel to the one where formate was an intermediate.

In summary, it is difficult to clarify the real effect of the promoter in this experiment since the system is so complex, both in terms of the number of components in the catalyst and also the reactant gas mixture. Nevertheless, it can be concluded without a doubt that in this study the presence of the potassium promoter reduces the level of bidentate formate on copper, while leaving the RWGS reaction largely unaffected. The overall effect of the alkali has been suggested to be due to three factors:

1) a decrease in the amount of adsorbed CO_2 on copper in the presence of the promoter, probably as a result of the decrease in copper area (alkali site-blocking mechanism), and also possibly as a result of a decrease in surface oxygen on copper,
2) a decrease in the rate of hydrogenation of the adsorbed CO_2, owing to a reduction in the degree of hydroxylation of the support through the presence of $-O^-K^+$ species on the promoted catalyst, and
3) an enhanced CO_2 dissociation which compensates for the loss in copper surface area on promotion. As a result, the RWGS reaction still proceeds at level comparable with that on the unpromoted sample, in spite of a decrease in both copper and total areas.

Chapter 8 - Overall Impact of Alkali Promotion on $Cu/ZnO/Al_2O_3$ Catalysts in the Water-Gas Shift Reaction

Micro-reactor studies presented in Chapter 3 showed that the selectivity of the $Cu/ZnO/Al_2O_3$ catalysts for the WGS reaction was enhanced at the expense of the methanol synthesis reaction by promoting with alkali metal salts. The DRIFTS experiments in this study have sought to determine the mode of action of the promoter.

Chapter 5 dealt with the adsorption of CO and CO_2 on the unpromoted and promoted catalysts. It was found that the promoter hindered the adsorption of CO on the copper component of the catalyst, and a site-blocking mechanism was invoked to explain this. No evidence for an electronic effect of the promoter on copper was observed, since no shift in the CO stretching frequency occurred. CO adsorption also showed that the copper component was easier to reduce in the presence of the promoter. On the support, the formation of a bicarbonate species on alumina following the oxidation of CO to CO_2 was found to be discouraged. This was suggested as being due to a decrease in the number of surface hydroxyl groups, probably as a result of the exchange with K^+ ions to form $-O^-K^+$ species. TPD experiments showed an enhancement of a species which decomposed to produce CO_2 at a higher temperature than bicarbonate. Infra-red spectra suggested this to be due to either proportionally more of a bidentate carbonate on zinc oxide which was present for the unpromoted catalyst, or a new species such as a carboxylate or carbonate associated with potassium.

CO adsorption studies carried out on catalysts with varying alkali levels supported the above findings and also revealed that, as a proportion of the total

products following CO adsorption, relatively less CO_2 was evolved from oxidation of CO at room temperature, but more was produced during TPD, suggesting that the CO_2 had been "stored" on the catalyst, perhaps in the form of a potassium-associated carbonate or carboxylate until decomposition at high temperature.

CO_2 adsorption studies revealed a similar effect of the promoter on the support. The relative decrease in the level of bicarbonates on alumina and increase in bidentate carbonates on zinc oxide or the potassium-associated species were again observed by infra-red spectroscopy, and more convincing evidence was obtained for the presence of a potassium-carboxylate at room temperature. The formation of CO_2 at high temperatures owing to the decomposition of a surface species was even more pronounced. By drawing parallels with results from the literature [105-107] this species was postulated as being a carbonate; i.e. bidentate carbonate on zinc oxide or a potassium-associated carbonate, as opposed to potassium carboxylate.

The formation of CO on contact of the catalyst with CO_2 was enhanced in the presence of the promoter. No evidence was found which suggested this to be due to an effect of the promoter on the copper component. Other authors [105-107] have shown how CO_2 can be activated over single crystal surfaces to produce CO, but a workfunction change accompanies this. As discussed above, no shift in the CO stretching frequency was observed, so this mechanism is unlikely to operate in this case. The potassium carboxylate species on the support suggested above could act as an intermediate between CO_2 and CO.

Following the TPR of a CO_2/H_2 mixture (Chapter 7) it was concluded that the presence of the potassium promoter discouraged and possibly prevented the formation of bidentate formate on copper, while the RWGS reaction proceeded at a similar rate on both unpromoted and promoted catalysts. Fig 7.14 suggested how formate could be formed *via* the hydrogenation of adsorbed CO_2. It was found in Chapter 5, that physisorbed CO_2 could be observed on copper following the CO_2 adsorption on the unpromoted catalyst, but not on the promoted. This could simply be a result of the

decrease in copper surface area on promotion, but could also be related to the fact that the promoted catalyst was found to be more completely reduced than the unpromoted, according to the CO adsorption studies. CO_2 has been found to adsorb more strongly on copper in the presence of surface oxygen [100], which would increase the likelihood of the subsequent hydrogenation of the adsorbed species to formate. It was also speculated that the hydrogenation of adsorbed CO_2 could be discouraged on the promoted catalyst as a result of the replacement of -OH groups with $-O^-K^+$ species; Burch *et al.* [14] have reported that spillover of atomic hydrogen and hydroxyl groups from zinc oxide to copper can enhance formate formation.

The continuation of the RWGS reaction at a rate comparable to (and even possibly greater than) that on the unpromoted catalyst, in spite of the accompanying surface area decrease on promotion, can also be explained with reference to the results in Chapter 5. The enhanced conversion of CO_2 to CO during the pulse experiment, possibly *via* a potassium-associated carboxylate, would also be expected to enhance the RWGS reaction, where CO_2 dissociation is a necessary step in the redox-type mechanism. Although the pulse experiment was conducted at room temperature, this reaction would also take place at the higher temperatures more relevant to WGS reaction conditions.

To extend the ideas of Chapter 5 to the forward WGS reaction, it is possible that a potassium-associated carbonate proposed as forming during CO adsorption could be important. The decomposition of species on the support to CO_2 at high temperature (i.e. detected by the mass spectrometer as peaking between 90 and 130 °C but continuing until 300 °C) was found to be enhanced on promotion. The reverse WGS reaction was shown in Chapter 7 to occur at an appreciable rate from about 150 °C. If this were also true for the forward WGS reaction, it is possible that the conversion of CO to CO_2 could be enhanced *via* a potassium-carbonate species. This could be in addition to the effect suggested by copper single crystal studies that an increased rate of dissociation of water is responsible for the enhancement of the forward WGS reaction [30].

The investigation of methanol and formic acid adsorption in Chapter 6 allowed the effect of the alkali to be approached from a different angle; the impact on the adsorption of the undesired by-product. The most striking result from that study was the attenuation of both methoxy and bidentate formate species adsorbed on the copper component of the catalyst on promotion. This could have been a result of both the decrease in copper area but also the greater degree of reduction of the promoted catalyst. During TPD, there was less decomposition of methoxy overall on promotion and more desorption of the molecule intact, implying that other intermediates during the formation of methanol might be adsorbed less strongly on the catalyst surface, allowing them less chance of remaining on the surface long enough to form methanol. The desorption intact of formic acid at slightly lower temperatures in the presence of the promoter suggests that, as for the case of methoxy, formate was bound less strongly.

The results from Chapter 7 suggests that the most marked, and arguably most important, effect of the promoter observed is the prevention of bidentate formate formation on copper. Fig. 8.1 illustrates the two pathways which are proposed as being instrumental in the enhancement of the catalyst's selectivity for the WGS reaction. Pathway (1) is hindered in the presence of the promoter, while an alternative route for the RWGS reaction (pathway (2)) is suggested as operating to compensate for the decreased copper surface area.

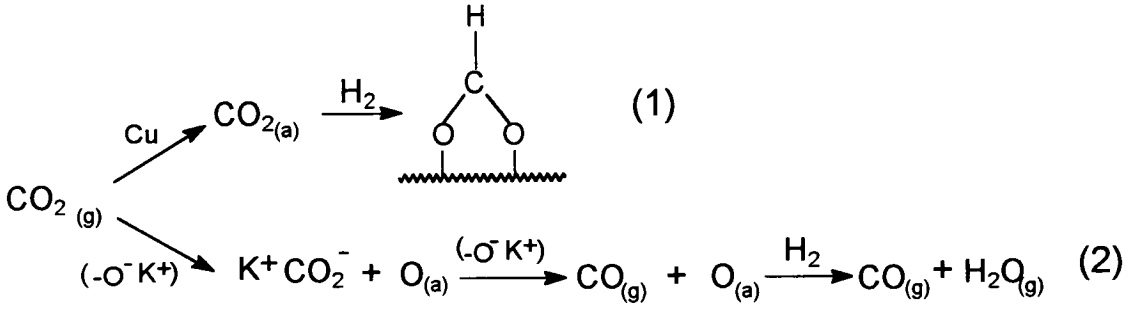

Fig. 8.1. *Suggested influence of the alkali promoter: pathway (1) is hindered and pathway (2) introduced.*

Chapter 8 - Overall Impact of Alkali Promotion on $Cu/ZnO/Al_2O_3$ Catalysts in the Water-Gas Shift Reaction

Micro-reactor studies presented in Chapter 3 showed that the selectivity of the $Cu/ZnO/Al_2O_3$ catalysts for the WGS reaction was enhanced at the expense of the methanol synthesis reaction by promoting with alkali metal salts. The DRIFTS experiments in this study have sought to determine the mode of action of the promoter.

Chapter 5 dealt with the adsorption of CO and CO_2 on the unpromoted and promoted catalysts. It was found that the promoter hindered the adsorption of CO on the copper component of the catalyst, and a site-blocking mechanism was invoked to explain this. No evidence for an electronic effect of the promoter on copper was observed, since no shift in the CO stretching frequency occurred. CO adsorption also showed that the copper component was easier to reduce in the presence of the promoter. On the support, the formation of a bicarbonate species on alumina following the oxidation of CO to CO_2 was found to be discouraged. This was suggested as being due to a decrease in the number of surface hydroxyl groups, probably as a result of the exchange with K^+ ions to form $-O^-K^+$ species. TPD experiments showed an enhancement of a species which decomposed to produce CO_2 at a higher temperature than bicarbonate. Infra-red spectra suggested this to be due to either proportionally more of a bidentate carbonate on zinc oxide which was present for the unpromoted catalyst, or a new species such as a carboxylate or carbonate associated with potassium.

CO adsorption studies carried out on catalysts with varying alkali levels supported the above findings and also revealed that, as a proportion of the total

products following CO adsorption, relatively less CO_2 was evolved from oxidation of CO at room temperature, but more was produced during TPD, suggesting that the CO_2 had been "stored" on the catalyst, perhaps in the form of a potassium-associated carbonate or carboxylate until decomposition at high temperature.

CO_2 adsorption studies revealed a similar effect of the promoter on the support. The relative decrease in the level of bicarbonates on alumina and increase in bidentate carbonates on zinc oxide or the potassium-associated species were again observed by infra-red spectroscopy, and more convincing evidence was obtained for the presence of a potassium-carboxylate at room temperature. The formation of CO_2 at high temperatures owing to the decomposition of a surface species was even more pronounced. By drawing parallels with results from the literature [105-107] this species was postulated as being a carbonate; i.e. bidentate carbonate on zinc oxide or a potassium-associated carbonate, as opposed to potassium carboxylate.

The formation of CO on contact of the catalyst with CO_2 was enhanced in the presence of the promoter. No evidence was found which suggested this to be due to an effect of the promoter on the copper component. Other authors [105-107] have shown how CO_2 can be activated over single crystal surfaces to produce CO, but a workfunction change accompanies this. As discussed above, no shift in the CO stretching frequency was observed, so this mechanism is unlikely to operate in this case. The potassium carboxylate species on the support suggested above could act as an intermediate between CO_2 and CO.

Following the TPR of a CO_2/H_2 mixture (Chapter 7) it was concluded that the presence of the potassium promoter discouraged and possibly prevented the formation of bidentate formate on copper, while the RWGS reaction proceeded at a similar rate on both unpromoted and promoted catalysts. Fig 7.14 suggested how formate could be formed *via* the hydrogenation of adsorbed CO_2. It was found in Chapter 5, that physisorbed CO_2 could be observed on copper following the CO_2 adsorption on the unpromoted catalyst, but not on the promoted. This could simply be a result of the

decrease in copper surface area on promotion, but could also be related to the fact that the promoted catalyst was found to be more completely reduced than the unpromoted, according to the CO adsorption studies. CO_2 has been found to adsorb more strongly on copper in the presence of surface oxygen [100], which would increase the likelihood of the subsequent hydrogenation of the adsorbed species to formate. It was also speculated that the hydrogenation of adsorbed CO_2 could be discouraged on the promoted catalyst as a result of the replacement of -OH groups with $-O^-K^+$ species; Burch *et al.* [14] have reported that spillover of atomic hydrogen and hydroxyl groups from zinc oxide to copper can enhance formate formation.

The continuation of the RWGS reaction at a rate comparable to (and even possibly greater than) that on the unpromoted catalyst, in spite of the accompanying surface area decrease on promotion, can also be explained with reference to the results in Chapter 5. The enhanced conversion of CO_2 to CO during the pulse experiment, possibly *via* a potassium-associated carboxylate, would also be expected to enhance the RWGS reaction, where CO_2 dissociation is a necessary step in the redox-type mechanism. Although the pulse experiment was conducted at room temperature, this reaction would also take place at the higher temperatures more relevant to WGS reaction conditions.

To extend the ideas of Chapter 5 to the forward WGS reaction, it is possible that a potassium-associated carbonate proposed as forming during CO adsorption could be important. The decomposition of species on the support to CO_2 at high temperature (i.e. detected by the mass spectrometer as peaking between 90 and 130 °C but continuing until 300 °C) was found to be enhanced on promotion. The reverse WGS reaction was shown in Chapter 7 to occur at an appreciable rate from about 150 °C. If this were also true for the forward WGS reaction, it is possible that the conversion of CO to CO_2 could be enhanced *via* a potassium-carbonate species. This could be in addition to the effect suggested by copper single crystal studies that an increased rate of dissociation of water is responsible for the enhancement of the forward WGS reaction [30].

The investigation of methanol and formic acid adsorption in Chapter 6 allowed the effect of the alkali to be approached from a different angle; the impact on the adsorption of the undesired by-product. The most striking result from that study was the attenuation of both methoxy and bidentate formate species adsorbed on the copper component of the catalyst on promotion. This could have been a result of both the decrease in copper area but also the greater degree of reduction of the promoted catalyst. During TPD, there was less decomposition of methoxy overall on promotion and more desorption of the molecule intact, implying that other intermediates during the formation of methanol might be adsorbed less strongly on the catalyst surface, allowing them less chance of remaining on the surface long enough to form methanol. The desorption intact of formic acid at slightly lower temperatures in the presence of the promoter suggests that, as for the case of methoxy, formate was bound less strongly.

The results from Chapter 7 suggests that the most marked, and arguably most important, effect of the promoter observed is the prevention of bidentate formate formation on copper. Fig. 8.1 illustrates the two pathways which are proposed as being instrumental in the enhancement of the catalyst's selectivity for the WGS reaction. Pathway (1) is hindered in the presence of the promoter, while an alternative route for the RWGS reaction (pathway (2)) is suggested as operating to compensate for the decreased copper surface area.

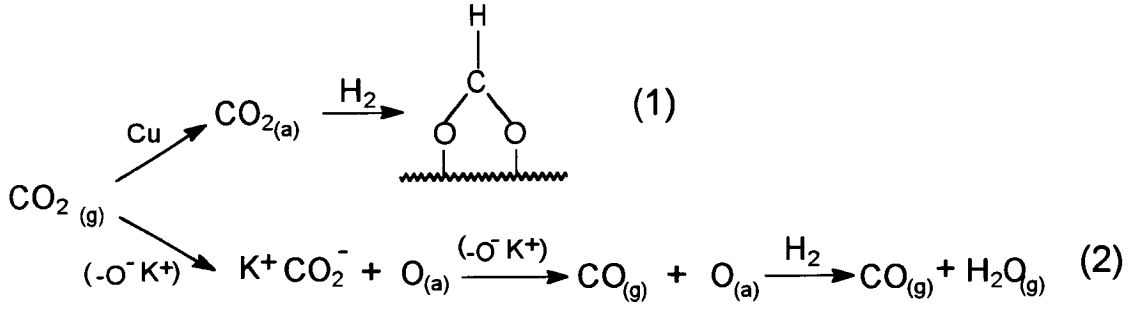

Fig. 8.1. *Suggested influence of the alkali promoter: pathway (1) is hindered and pathway (2) introduced.*

References

[1] M.V. Twigg, *Catalyst Handbook*, 2nd Edition, Wolfe Publishing, London, (1989).

[2] C.T. Campbell and K.A. Daube, *J. Catal.* **104**, 109, (1987).

[3] L. Mond and C. Langer, *British Patent* **12**, 608, (1888).

[4] C. Bosch and W. Wild, *Canadian Patent* **153**, 379, (1914).

[5] G.C. Chinchen, P.J Denny, J.R. Jennings, M.S. Spencer and K.C. Waugh, *Appl. Catal.* **36**, 1, (1988).

[6] R.G. Herman, K. Klier, G.W. Simmons, B.P. Finn and J.B. Bulko, *J. Catal.* **56**, 407, (1979).

[7] E.G.M. Kuijpers, R.B. Tjepkema, W.J.W. van der Wal, C.M.A.M. Mesters, S.F.G.M. Spronk and J.W. Geus, *Appl. Catal.* **25**, 139, (1986).

[8] E. Colbourn, R. A. Hadden, H. D. Vandervell, K. C. Waugh and G. Webb, *J. Catal.* **130**, 514, (1991).

[9] R. Burch, R.J. Chappell and S.E. Golunski, *J. Chem. Soc. Faraday Trans.1* **85**(10), 3569, (1989).

[10] G.C. Chinchen, K.C. Waugh and D.A. Whan, *Appl. Catal.* **25**, 101, (1986)

[11] K. Klier, *Adv. Catal.* **31**, 243, (1982).

[12] P.B. Himmelfarb, G.W. Simmons, K. Klier and R.G. Herman, *J. Catal.* **93**, 442, (1985).

[13] T.H. Fleisch and R.L. Mieville, *J. Catal.* **90**, 165, (1984).

[14] R. Burch, S.E. Golunski and M.S. Spencer, *Catal. Lett.* **5**, 55, (1990).

[15] K.C. Waugh, *Catal. Today* **15**, 51, (1992).

[16] G.D. Sizgek, H.E. Curry-Hyde and M.S. Wainwright, *Appl. Catal. A: General* **115**, 15, (1994).

[17] H.P. Bonzel, *Surface. Sci. Rep.* **8**, 43, (1987).

[18] W.D. Mross, *Catal. Rev -Sci. Eng.* **25**(4), 591, (1983).

[19] N.D. Lang, S. Holloway and J.K. Norskov, *Surface. Sci.* **150**, 24, (1985).

[20] R. Schloegl in *Physics and Chemistry of Alkali Metal Adsorption*, Eds. H.P. Bonzel, A.M. Bradshaw and G. Ertl, Elsevier, Amsterdam, p. 347, (1989).

[21] N.D. Lang in *Physics and Chemistry of Alkali Metal Adsorption*, Eds. H.P. Bonzel, A.M. Bradshaw and G. Ertl, Elsevier, Amsterdam, p. 11, (1989).

[22] J.E. Crowell and G.A. Somorjai, *Appl. Surface. Sci.* **19**, 73, (1984).

[23] T.V.W. Janssens, G.R. Castro, K. Wandelt and J.W. Niemantsverdriet, *Phys. Rev. B* **49**, 14599, (1994).

[24] D.O. Uner, M. Pruski, B.C. Gerstein and T.S. King, *J. Catal.* **146**, 530, (1994).

[25] L.J. Whitman and W. Ho, *J. Chem. Phys.* **83**(9), 4808, (1985).

[26] D. Lackey and D.A. King, *J. Chem. Soc., Faraday Trans. 1*, **83**(9), 2001, (1987).

[27] G.A. Somorjai and M.A. van Hove, *Prog. Surface. Sci.* **30**, 201, (1989).

[28] G.A. Somorjai and E.L. Garfunkel in *Physics and Chemistry of Alkali Metal Adsorption*, Eds. H.P. Bonzel, A.M. Bradshaw and G. Ertl, Elsevier, Amsterdam, p. 347, (1989).

[29] D.J. Dwyer in *Physics and Chemistry of Alkali Metal Adsorption*, Eds. H.P. Bonzel, A.M. Bradshaw and G. Ertl, Elsevier, Amsterdam, p. 307, (1989).

[30] C.T. Campbell in *The Chemical Physics of Solid Surfaces*, Eds. D.A. King and D. Woodruff, Elsevier, Amsterdam, Vol. 6, Chapter 9, p. 287.

[31] B.E. Hayden, K.C. Prince, P.J. Davie, G. Paolucci and A.M. Bradshaw, *Solid State Commun.* **48**(4), 325, (1983).

[32] A.A. Davydov, *Infra-red Spectroscopy of Adsorbed Species on the Surface of Transition Metal Oxides*, Ed. C.H. Rochester, John Wiley and Sons, Chichester, (1990).

[33] S. Bailey, G.F. Froment, J. W. Snoek and K.C. Waugh, *Catal. Lett.* **30**, 99, (1995).

[34] R.P. Eischens, W.A. Pliskin and S.A. Francis, *J. Chem. Phys.* **22**, 178, (1954).

[35] R.P. Eischens, S.A. Francis and W.A. Pliskin, *J. Chem. Phys.* **60**, 194, (1956).

[36] R.P. Eischens and W.A. Pliskin, *Adv. Catalysis* **10**, 1, (1958).

[37] P. R. Griffiths and M.P. Fuller, *Adv. Infra-red Raman Spect.*, **9**, 63, (1981).

[38] P.D. Holmes, G.S. McDougall, I.C. Wilcock and K.C. Waugh, *Catal. Today* **9**, 15, (1991).

[39] M.P. Fuller and P.R. Griffiths, *Anal.Chem.*, **50**, 1906, (1978).

[40] N. Sheppard and T.T. Nguyen, in *"Advances in Infrared and Raman Spectroscopy"*, Vol.5, Pg 67-148, Eds. R.J.H. Clark and R.E. Hester, Heyden, London, (1978).

[41] J. Pritchard, T. Catterick and R.J. Gupta, *Surface Sci.*, **53**, 1, (1975).

[42] R.G. Greenler, *J. Chem. Phys.* **44**, 310, (1966).

[43] R.G. Greenler, D.R. Snider, D. Witt and R.S. Sorbello, *Surface Sci.* **118**, 415, (1982).

[44] R.W. Judd, H.J. Allen, P. Hollins and J. Pritchard, *Spectrochimica Acta.* **43A**(12), 1607, (1987).

[45] A.O. Taylor and J. Pritchard, *J. Chem. Soc., Faraday Trans.* **86**(15), 2743, (1990).

[46] J.R. Rostrup-Nielsen, *Chem. Engng Sci.*, **50**(24), 4061, (1995).

[47] J.M. Hollas, *Modern Spectroscopy*, John Wiley and Sons, Chichester, (1992).

[48] Bio-Rad Digilab Division, Cambridge, MA, U.S.A.

[49] Spectra-Tech Diffuse Reflectance Accessory, Spectra-Tech, Stanford, CT, U.S.A.

[50] P. Marshall, *PhD Thesis*, University of Edinburgh, (1994).

[51] D. Tichit, M.H. Lhouty, A. Guida, B.H. Chiche, F. Figueras, A. Auroux, D. Bartalini and E. Garrone, *J. Catal.* **151**, 50, (1995).

[52] F. Trifiro, A. Vaccari and O. Clause, *Catal. Today* **21**, 185, (1994)

[53] P. Gheradi, O. Ruggeri, F. Trifiro and A. Vacari, in *Preparation of Catalysts III*, **21**, 723, Elsevier Science, (1983)

[54] H.P. Bonzel and H.J. Krebs, in *Physics and Chemistry of Alakli Metal Adsorption*, Eds. H.P. Bonzel, A.M. Bradshaw and G. Ertl, Elsevier, Amsterdam, p. 331, (1989).

[55] C. Busetti, G. Del Pierro, G. Manara, F. Trifiro and A. Vacari, *J. Catal.* **85**, 260, (1984).

[56] G. Sengupta, D.P. Das, M.L. Kundu, S. Dutta, S. K. Roy, R. N. Sahay, K. K. Mishra and S. V. Ketchik, *Appl. Catal.* **55**, 165, (1989).

[57] G.C. Chinchen, C.M. Hay, H.D. Vandervell, K.C. Waugh, *J. Catal.* **103**, 79, (1987).

[58] R.S. Houk and J.J. Thompson, *Mass Spectrometry Review,* **7**, 425, (1988).

[59] G. R. Sheffer and T. S. King, *J. Catal.* **116**, 488, (1989).

[60] I.M Hamadeh, D. King and P.R. Griffiths *J. Catal.* **88**, 264, (1984).

[61] M. Bowker, R.A. Hadden, H. Houghton, J.N.K. Hyland and K.C. Waugh, *J. Catal* **109**, 263, (1988).

[62] L.H. Little, *Infra-red Spectra of Adsorbed Species,* Academic Press, London (1966).

[63] G.A. Somorjai, *Introduction to Surface Chemistry and Catalysis,* John Wiley and Sons, New York, (1994).

[64] H.G. Tompkins and R.J. Greenler, *Surface Sci.*, **28**, 194, (1971).

[65] H.A. Pearce, *PhD Thesis*, University of East Anglia, (1974).

[66] K.P. de Jong, J.W. Geus and J. Joziasse, *Appl. Surface Sci.*, **6**, 273, (1980).

[67] M. Moskovits and J.E. Hulse, *J. Phys. Chem.*, **81**(21), 2004, (1977).

[68] F. Bocuzzi, G. Ghiotti and A. Chiorino, *Surface Sci.*,**156**, 933, (1985).

[69] M.A. Kohler, N.W. Cant, M.S. Wainwright and D.L. Trimm, *J. Catal.*, **117**, 188, (1989).

[70] J.W. London and A.T. Bell, *J. Catal*, **31**, 32, (1973).

[71] K.P. de Jong, J.W. Geus and J. Joziasse, *J. Catal.*, **65**, 437, (1980).

[72] R. Hierl, H. Knoezinger, H-P. Urbach, *J. Catal.*, **69**, 475, (1981).

[73] P. Hollins and J. Pritchard, *Surface Sci.*, **134**, 194, (1983).

[74] D.L. Roberts and G.L. Griffin, *J. Catal.*, **110**, 117, (1988).

[75] P. Hollins and J. Pritchard, *Surface Sci.*, **138**, 75, (1984).

[76] G.J. Millar, C.H. Rochester and K.C. Waugh, *J. Chem. Soc. Faraday Trans.* **87**(9), 1467, (1991).

[77] G.J. Millar, C.H. Rochester, S. Bailey and K.C. Waugh, *J. Chem. Soc. Faraday Trans.* **89**(7), 1109, (1993).

[78] P.W. Atkins, *Physical Chemistry*, Oxford University Press, Oxford, (1990).

[79] V.M. Browne, S.G. Fox and P. Hollins, *Catal. Today* **9**, 1, (1991).

[80] G.C. Chinchen, P.J. Denny, D.G Parker, M.S Spencer and D.A. Whan, *Appl.Catal.* **30**, 333, (1987).

[81] G.C. Chinchen, M.S Spencer, K.C. Waugh and D.A. Whan, *J. Chem. Soc. Faraday Trans. 1*, **83**, 2193, (1987).

[82] M. Bowker, R.A. Hadden, H. Houghton, J.N.K. Highland and K.C. Waugh, *J.Catal.* **109**, 263, (1988).

[83] D. Lackey, M. Surman, S. Jacobs, D. Grider and D. A. King, *Surface Sci.* **152/153**, 513, (1985).

[84] G. Pirug and H.P. Bonzel, *Surface Sci.* **199**, 371, (1988).

[85] K.J. Uram, L. Ng and Y.G. Yates Jr., *Surface Sci.* **177**, 253, (1986).

[86] L. H. Dubois, B. R. Zegarski and H. S. Luftman, *J. Chem. Phys.* **87**(2), 1367, (1987).

[87] G.J. Millar, C.H. Rochester and K.C. Waugh, *J. Chem. Soc. Faraday Trans.* **88**(10), 1477, (1992).

[88] D. Heskett, I. Strathy, E.W. Plummer and R.A. de Paola, *Phys. Rev. B.* **32**(10), 6222, (1985).

[89] L.H. Dubois and G. A. Somorjai, *Surface Sci.* **128**, L231, (1983).

[90] C.T. Au, S. Singh-Boparai and M.W. Roberts, *J. Chem. Soc. Faraday Trans.1* **79**, 1779, (1983).

[91] R.J. Behm and C.R. Brundle, *J. Vac. Sci. Technol.*, **A1**(2), 1223, (1983).

[92] G.C. Chinchen, K.C. Waugh and D.A. Whan, *Appl.Catal.* **25**, 101, (1986).

[93] J. Nakamura, J. A. Rodriguez and C.T. Campbell, *J. Phys.: Condens. Matt.* **1**, SB149, (1989).

[94] C. Rhodes, G.J. Hutchings and A.M. Ward, *Catal. Today.* **23**, 43, (1995).

[95] C.T. Campbell, K.A. Daube and J.M. White, *Surface Sci.* **182**, 458, (1987).

[96] I.E. Wachs and R.J. Madix, *J.Catal.* **53**, 208, (1978).

[97] T. Schneider and W. Hirschwald, *Catal. Lett.* **14**, 197, (1992).

[98] P.B. Rasmussen, P.A. Taylor and I. Chorkendorf, *Surface Sci.* **269/270**, 352, (1992).

[99] R.G. Copperthwaite, P.R. Davies, M.A. Morris, M.W. Roberts and R.A. Ryder, *Catal. Lett.* **1**, 11, (1988).

[100] R.A. Hadden, H.D. Vandervell, K.C. Waugh and G. Webb, *Catalysis Lett.* **1**, 27, (1988).

[101] G.J. Millar, C.H. Rochester, C.Howe and K.C. Waugh, *Mol. Phys.* **76**(4), 833, (1991).

[102] D.B. Clarke, I. Suzuki and A.T. Bell, *J.Catal.* **142**, 27, (1993).

[103] S-I. Fujita, M. Usui, N. Takezawa, *J.Catal.* **134**, 220, (1992).

[104] S.S. Fu and G.A. Somorjai, *Surface Sci.* **262**, 68, (1992).

[105] J.A. Rodriguez, W.D. Clendening, J.M. Campbell, W. Min and C.T. Campbell, *J. Vac. Sci. Technol.* **A7**(3), 2118, (1989).

[106] E.V. Thomsen, B. Jorgensen and J. Onsgaard, *Surface Sci.* **304**, 85, (1994).

[107] F. Solymosi and L. Bugyi, *J. Chem. Soc. Faraday Trans.1* **83**, 2015, (1987).

[108] F. Solymosi and A. Berko *J.Catal.* **101**, 458, (1986).

[109] J.H. Taylor and C.H. Amberg, *Can. J. Chem.* **39**, 535, (1961).

[110] N. D. Parkyns, *J. Chem. Soc. (A)*, 1910, (1967).

[111] B. W. Krupay and Y. Amenomiya, *J.Catal.* **67**, 362, (1988).

[112] N. D. Parkyns, *J. Chem. Soc. (A)*, 410, (1969).

[113] G. Busca and V. Lorenzelli, *Mater. Chem.* **7**, 89, (1982).

[114] N. D. Parkyns, *J. Phys. Chem.* **75**(4), 526, (1971).

[115] M. P. Rosynek, *J. Phys. Chem.* **79**(13), 1280, (1975).

[116] J.W. Hightower, *Prepr. Div. Petr. Chem., Am. Chem. Soc.*, **18**, 262, (1973).

[117] J. Saussey, J.C. Lavalley and C. Bovet, *J.Chem. Soc. Faraday Trans. 1,*. **78**, 1457, (1982).

[118] C. Chauvin, J. Saussey, J.C. Lavalley and G. Djega-Mariadassou, *Appl. Catal,*. **59**, 1457, (1986).

[119] W.H.J. Stork and G. T. Pott, *J. Phys. Chem.* **78**(24), 526, (1974).

[120] F. Bocuzzi, G. Ghiotti and A. Chiorini, *Surface Sci.* **162**, 361, (1985)

[121] F.A. Miller and C.H. Wilkins, *Anal. Chem.* **24**, 1253, (1952).

[122] G.Ghiotti, F. Bocuzzi and R. Scala, *J.Catal.* **92**, 79, (1985).

[123] K.C. Waugh, *Catal. Today* **15**, 51, (1992).

[124] D.B. Clarke, D.K. Lee, M.J. Sandoval and A.T. Bell, *J. Catal* **150**, 81, (1994).

[125] B.A. Sexton, *Surf. Sci.* **88**, 319, (1979).

[126] B.E. Hayden, K. Prince, D.P. Woodruff and Bradshaw, *Surf. Sci.* **133**, 589, (1983).

[127] L.H. Dubois, T.H. Ellis, B.R. Zegarski and S.D. Kevan, *Surf. Sci.* **172**, 385, (1986).

[128] M.A. Chesters and E.M. McCash, *Spectrochim. Acta.* **43A**, 1625, (1997).

[129] J.P. Camplin and E.M. McCash, *Surf. Sci.* **360**, 229, (1996).

[130] B.A. Sexton, *Surf. Sci.* **88**, 299, (1979).

[131] B.A. Sexton, A.E. Hughes and N.R. Avery, *Appl. Surf. Sci.* **22/23**, 404, (1985).

[132] G.J. Millar, C. H. Rochester and K.C. Waugh, *J. Chem. Soc. Faraday Trans.* **87**(17), 2795, (1991).

[133] G.J. Millar, C. H. Rochester and K.C. Waugh, *J. Chem. Soc. Faraday Trans.* **88**(15), 2257, (1992).

[134] C. Chauvin, J. Saussey, J-C. Lavalley, H. Idriss, J.P. Hindermann, A. Kiennemann, P. Chaumette and P. Courty, *J. Catal* **121**, 56, (1990).

[135] M. Nagao and T. Morimoto, *J. Phys. Chem.* **84**, 2054, (1980).

[136] D.L. Roberts and G.L. Griffin, *J. Catal* **95**, 617, (1985).

[137] G. Busca, P.F. Rossi, V. Lorenzelli, M. Benaissa, J. Travert and J-C. Lavalley, *J. Phys. Chem.* **89**, 5433, (1985).

[138] M. Bowker, S. Haq, R. Holroyd, P.M. Partlett, S. Poulston and N. Richardson, *J. Chem. Soc. Faraday Trans.* **92**(23), 4683, (1996).

[139] G.J. Millar, C. H. Rochester and K.C. Waugh, *J. Chem. Soc. Faraday Trans.* **88**(7), 1033, (1992).

[140] T. Shido and Y. Iwasawa, *J. Catal* **129**, 343, (1991).

[141] Y. Noto, K. Fukuda, T. Onishi and K. Tamaru, Trans. Faraday Soc. **63**, 2300, (1967).

[142] M. Bowker, E. Rowbotham, F.M. Leibsle and S. Haq, *Surf. Sci.* **349**, 97, (1996).

[143] G.J. Millar, C. H. Rochester, S. Bailey and K.C. Waugh, *J. Chem. Soc. Faraday Trans.* **88**(14), 2085, (1992).

[144] M. Bowker, H. Houghton and K.C. Waugh, *J. Chem. Soc. Faraday Trans. 1,* **77**, 3023, (1981).

[145] G.J. Millar, C.H. Rochester, S. Bailey, K.C. Waugh, *J. Chem. Soc. Faraday Trans.1* **88**(14), 2085, (1992).

[146] G.J. Millar, C. H. Rochester and K.C. Waugh, *J. Catal* **142**, 263, (1993).

[147] G.J. Millar, C. H. Rochester and K.C. Waugh, *J. Catal* **155**, 52, (1995).

[148] G. Herzberg, *Infra-red and Raman Spectra of Polyatomic Molecules*, D. Van Nostrand Company, Inc., New York, (1945).

[149] J.F. Edwards and G.L. Schrader, *J. Phys. Chem.* **88**(23), 5620, (1984).

[150] J.M. Campbell, J. Nakamura and C.T. Campbell, *J. Catal* **136**, 24, (1992).

[151] D.B. Clarke and A.T. Bell, *J. Catal.* **154**, 314, (1995).

[152] M. Muhler, E. Toernqvist, L.P. Nielsen, B.S. Clausen, and H. Topsoe, *Catal. Lett.* **25**,1, (1994).

[153] P.B. Rasmussen, P.M. Holmblad, T.Askaard, C.V. Ovesen, P. Stoltze, J.K. Norskov, I. Chorkendorff, *Catal. Lett.* **26**, 373, (1994).

[154] T. Fujitani, M. Saito, Y. Kanai, T. Kakumoto, T. Watanabe, J. Nakamura and T. Uchijima, *Catal. Lett.* **25**,271, (1994).

[155] C.T. Campbell and K-H. Ernst, *ACS Symp. Ser.* **482**, 130, (1992).

[156] C.T. Campbell and B.E. Koel, *Surface Sci.* **393**, 1, (1987).

[157] J. Nakamura, J. M. Campbell and C. T. Campbell, *J. Chem. Soc. Faraday Trans.1* **86**(15), 2725, (1990).

[158] K. Klier, C-W. Young and J. G. Nunan, *Ind. Eng. Chem. Fundam.*, **25**, 36, (1986).

[159] G. R. Sheffer and T. S. King, *J. Catal.* **115**, 376, (1989).

[160] J. Nunan, K. Klier, C-W. Young, P. B. Himmelfarb and R.G. Herman, *J. Chem. Soc. Chem. Commun.*, **1311**, 193, (1986).

[161] E. M. Calvery and K. J. Smith, *J. Catal.* **130**, 616, (1991).

[162] G. Lui, D. Willcox, M. Garland and H. H. Kung, *J. Catal.* **96**, 251, (1985).

[163] H. Idriss, J.P. Hindermann, R. Kieffer, A. Kiennemann, A. Vallet, C. Chauvin, J.C. Lavalley and P. Chaumette, *J. Mol. Catal.* **42**, 205, (1987).

[164] A.J. Elliot, R.A. Hadden, J. Tabatabaei, K.C. Waugh and F.W. Zemicael, *J. Catal.* **157**, 153, (1995).

[165] R.P. Eischens and W.A. Pliskin, in *Advances in Catalysis*, Vol. X, p. 1, Academic Press Inc., New York, (1958).

[166] G. Blyholder, *J. Phys. Chem.* **68**, 2772, (1964).

[167] K. C. Waugh, *Appl. Catal.* **43**, 315, (1988).

[168] Y. Amenomiya and G. Pleizier, *J. Catal.* **76**, 345, (1982).

Appendix - Purity and Suppliers of Gases

Gas	Purity (%)	Supplier
CO	99.95	Linde Gas
CO_2 (chapter 5)	99.995	Linde Gas
H_2	99.99	BOC
He	99.996	BOC
CH_3OH	99.9	Aldrich
HCOOH	96	Aldrich
CO_2 (chapter 7)	99.995	BOC